UNIVERSITY OF MARYLAND

ABSTRACT

Title of Dissertation: Stress Intensity Factors for Structural Steel I-beams

Daqing Feng, Doctor of Philosophy, 1996

Dissertation directed by: Pedro Albrecht

Professor, Department of Civil Engineering

Robert J. Sanford

Professor, Department of Mechanical Engineering

The application of fracture mechanics to highway steel bridges has been hampered by a lack of stress intensity factor (SIF) solutions for cracks in I-beams. Previous work cannot provide satisfactory solutions. In this study, the finite element analysis method was used to develop accurate SIFs for two-tip and three-tip cracks in I-beams under tension or bending.

Cracked I-beams were modeled with eight-node shell elements, with the web and flanges being fully joined along the junction lines. The region around the crack tips, singularity quarter-point elements were used. To ensure accurate and converging solutions, mesh patterns around the crack tips were studied. Also, different methods of extracting SIFs from FEA results were discussed based on benchmark problem studies.

Governing parameters for cracked I-beams were determined. For two-tip

web cracks, the SIFs are functions of applied stress, crack length, eccentricity, and flange-to-web cross-sectional area ratio. For three-tip cracks in web and flange, the SIFs are functions of applied stress, web and flange crack lengths, and flange-to-web cross-sectional area ratio. The flange-to-web area ratio describes the constraining effect of the flange on the web crack of a two-tip cracked I-beam; the interaction forces between web and flanges greatly affect SIFs for a three-tip cracked I-beam.

The SIFs were calculated based on a total of 2,106 FEAs performed for a wide range of the parameters. The results were fitted with equations for ready use by practicing engineers. An example illustrates the calculation of SIFs for a three-tip crack in a composite steel-concrete beam of a steel bridge.

UNIVERSITY OF MARYLAND

STRESS INTENSITY FACTORS

FOR STRUCTURAL STEEL I-BEAMS

by

Daqing Feng

Dissertation submitted to the Faculty of the Graduate School of the
University of Maryland at College Park in partial fulfillment
of the requirement for the degree of
Doctor of Philosophy
1996

C1 (VOL. I OF II)
MD
DEPT OF MECHANICAL ENGINEERING MARYLAND
LD
3231
.M70d
Feng, D.
Vol. 1

Advisory Committee:

Professor Robert J. Sanford, Chairman/Advisor
Professor Pedro Albrecht, Advisor
Professor William L. Fourney
Professor Donald W. Vannoy
Assistant Professor Ian Flood

DEDICATION

To my parents and wife!

ACKNOWLEDGMENT

The author would like to express his most grateful appreciation to Professor Pedro Albrecht and Professor Robert J. Sanford for their continuous encouragement, support and guidance during the time of this study.

The author would like to express his sincere gratitude to Mr. William Wright of Federal Highway Administration for his technical support and helpful discussions.

Thanks are extended to Dr. Ian Flood, Department of Civil Engineering, University of Maryland, Dr. Xiaoguang (Chester) Chen, ACTA Incorporation, and Dr. Phillip Yen, Federal Highway Administration, for their helpful discussions.

Many thanks for their help are extended to the staff and colleagues of the Mechanical and Civil Engineering Departments, University of Maryland; and the staff of the Structures Division, Federal Highway Administration, McLean, Virginia.

He also likes to acknowledge the Teaching and Research Assistantships from the Mechanical and Civil Engineering Departments as well as the Graduate Research Fellowship from the Federal Highway Administration.

Finally, he wishes to express his appreciation to his wife, Yingnan, and his parents for their constant support. Without them this work would not have been possible.

TABLE OF CONTENTS

LIST OF TABLES

Chapter 6:

Appendix A:

LIST OF FIGURES

Chapter 1:

Chapter 2:

Chapter 3:

Chapter 4:

Chapter 5:

Chapter 6:

Appendix A:

Chapter 1: Introduction

1.1 Problem

Fatigue and fracture have caused steel bridges to fail for many years. Over one-half of the 577,710 bridges in the federal highway system are more than 30 years old. Many of them are made of steel. Because of such factors as type of material, design details and quality of fabrication, initial cracks or crack-like flaws in structural components of steel bridges sometimes cannot be avoided. Cracks propagate as a result of stress ranges induced by trucks crossing the bridges. When a crack reaches the critical size, the girder may fracture.

Fatigue cracking of a steel bridge is costly. Besides the tangible repair cost, traffic delays when one or more lanes have to be closed inflict intangible cost that may greatly exceed the repair cost.

The discovery of a crack in a steel bridge immediately places the state engineer who is responsible for public safety in a dilemma. He must decide whether to close the entire bridge or just an individual lane while the bridge is being retrofitted. To help him decide, the engineer must determine if the calculated stress intensity factor (SIF), K, is smaller or greater than the fracture toughness, K_c, of the steel.

Fracture mechanics analysis of crack extension provides a systematic,

scientific approach to characterizing the severity of cracks and predicting when they may become unstable during the structure's service life. A complete fracture study involves both stress analysis to determine the SIF and material testing to determine the material's resistance to crack extension. This study focuses on the former, that is, the calculation of SIFs in cracked steel bridge girders.

Cracks in steel bridges can usually be analyzed with linear-elastic fracture mechanics (LEFM). The fundamental postulate is that crack extension is governed solely by the value of the SIF. Since bridges typically fracture during the winter months when the temperature is low, the critical value of the SIF, called the fracture toughness K_c, lies on the lower shelf and the lower portion of the transition region. Therefore, plastic deformation is limited to a small crack-tip region and the linear-elastic fracture mechanics approach is valid.

Knowing the SIF, one can determine the static strength of a cracked structure (residual strength) and the crack growth rate under cyclic loading (fatigue).

Type of loading and the size, shape and orientation of the crack play a major role in determining the applicable K values. Solutions for simple structural configurations and loadings are available in several handbooks (Tada, et al. 1973, Sih 1973, Rooke and Cartwright 1976, and Murakami 1986). But few, if any, solutions exist for cracks in rolled I-beams, welded I-beams and plate

girders that are commonly used in steel bridges. This has greatly hindered the application of fracture mechanics to fatigue and fracture analysis of steel highway bridges.

1.2 Crack Types

Previous studies on fatigue strength of steel bridge details, including stiffeners and attachments, showed that all cracks initiate from flaws at stress raisers, typically at weld toes on web or flange surfaces (Fisher, et al. 1970; Fisher, et al. 1974).

When a transverse stiffener is welded to the web alone, the crack propagates in three stages. After initiating at points along the toe of the stiffener to web weld, the crack grows first as a surface crack through the web thickness, then as a two-tip through crack with one front moving up and the other down the web. Finally it grows as a three-tip crack with one front moving further up the web and the other two fronts extending across the flange width (Figure 1.1).

When the stiffener is welded to the web and flanges, shown in Figure 1.2, the crack initiates at points along the toe of the fillet weld connecting the stiffener to the tension flange. In this case the crack grows in two or three stages depending on where the crack initiates across the flange width. During the first stage, one or more cracks propagate in a semi-elliptical shape and

coalesce. After this part-through crack breaks through the extreme fiber of the tension flange, it grows in the second stage as a two-tip crack across the tension flange. Upon further propagation, a three-tip crack forms if the inner tip enters the web before the outer tip reaches the flange edge. But if the tip closest to the flange edge breaks through, the crack then grows with one front moving up the web and the other across the flange width.

Cracks at attachments welded eccentrically to the flange grow like those at stiffeners. The attachment in Figure 1.3 is welded to the flange along its length but not the width. The crack initiates at the end of a weld and then propagates in two or three stages.

Cracks in welded beams, shown in Figure 1.4, initiate at a porosity, weld repair, tack weld, or stop-start position in the longitudinal flange to web fillet weld. When the crack initiates at an internal porosity, it grows approximately in a circular shape, with the initial defect at its center, until the crack front reaches the extreme fiber of the tension flange. The crack then changes into a three-tip crack with two fronts propagating across the flange and one front advancing upward into the web.

These examples illustrate that typical cracks in steel beams have either two tips or three tips. SIFs for such cracks under an applied moment or axial force are essential to the application of fracture mechanics in highway bridges.

1.3 Previous Work

1.3.1 Summary

Many methods for obtaining SIFs have been developed. Aliabadi and Rooke (1991) divided them into three categories depending on degree of sophistication and time required to obtain a solution (Table 1.1). For a simple geometrical configuration, or where a structural component can be easily modeled, SIF solutions may be obtained directly from handbooks (Tada, et al. 1973, Sih 1973, Rooke and Cartwright 1976, and Murakami 1986). When handbook solutions do not exist or only an estimate is required, a relatively simple method from category 2 may be adequate. Finally, when a highly accurate SIF is required, or the structural shape is complex, the numerical methods listed in category 3 must be used.

For a two-tip or three-tip cracked I-beam, the complex geometry and interaction between the web and flanges make it exceedingly difficult to calculate SIFs. An I-beam consists of one web plate and two flange plates in 3-D space. As the crack extends into both the web and flange, the crack opening displacements (CODs) must be equal at the flange-web junction. Likewise the web and flange displacements along the junction line away from the intersection of the two cracks must also be equal. These displacement continuity conditions induce interaction forces whose magnitude and distribution depend on the applied load, I-beam geometry, and crack lengths.

Greif and Sanders (1965), Isida (1973), Nishimura (1991) and others analyzed a cracked plate with stringers or edge stiffeners. This geometry is commonly found in both aircraft fuselages and ship hulls. Although the boundary conditions are different from those of an I-beam, the effect of edge stiffeners on the cracked plate is similar to that of flanges on a two-tip cracked web.

Chen (1992) obtained SIF solutions for two-tip central and eccentric cracks in the web with the weight function method (WFM). For three-tip symmetric or non-symmetric cracks, he used the energy release rate method.

Isida's (1973) solution for center-cracked plate with edge stiffener and Chen's (1992) solutions for two-tip and three-tip cracked I-beams are discussed in the following three subsections.

1.3.2 Center-cracked Plate with Stiffened Edges

The flanges in an I-beam with a two-tip web crack act like edge stiffeners that effectively restrain the CODs and thus reduce the SIF. Similar geometries exist in many other structures. For example, sheets in aircraft fuselages and ship hulls are usually reinforced with stiffeners that may arrest a crack or alleviate stresses. The effects of these stiffeners on the SIF have been studied by Greif and Sanders (1965), Isida (1973). In actual airplane fuselages and ship hulls, the stiffeners are usually riveted or bolted to the plate, but in the studies

of Greif and Sanders (1965) and Isida (1973) the stiffeners were assumed to be integral with the plate. In rolled or welded I-beams used in steel bridges, the flanges and web are also connected integrally.

Greif and Sanders (1965) were the first to study the problem of a plate with longitudinal stiffeners. The stiffener was assumed to have zero flexural stiffness. Isida (1973) studied the same problem by including both the axial and flexural rigidities. In his study, Isida used the method of Laurent expansion of the complex potentials and determined the expansion coefficients from the boundary conditions. He performed the numerical calculations with the perturbation technique and obtained the SIFs from the 36-term power series of λ^2, where λ is the ratio of crack length to plate width.

Stress Functions

Figure 1.5 shows a center-cracked plate reinforced with stiffeners along both edges. Only the plate is subjected to axial tension. The stress function χ of this problem can be expressed in terms of complex potentials $\varphi(\zeta)$ and $\psi(\zeta)$:

$$\chi = Tb^2 \, \mathrm{Re}\{\bar{\zeta}\varphi(\zeta) + \psi(\zeta)\} \tag{1.1}$$

where T is the applied tension stress and b is the half width of the web. The corresponding stress and displacement components for plane stress are given by:

$$\begin{aligned} \sigma_x &= T\,\mathrm{Re}\{2\varphi'(\zeta) - \bar{\zeta}\varphi''(\zeta) - \psi''(\zeta)\} \\ \sigma_y &= T\,\mathrm{Re}\{2\varphi'(\zeta) + \bar{\zeta}\varphi''(\zeta) + \psi''(\zeta)\} \\ \tau_{xy} &= T\,\mathrm{Im}\{\bar{\zeta}\varphi''(\zeta) + \psi''(\zeta)\} \\ E(u - iv) &= Tb[(3-\nu)\bar{\varphi}(\bar{\zeta}) - (1+\nu)\{\bar{\zeta}\varphi'(\zeta) + \psi'(\zeta)\}] \end{aligned} \tag{1.2}$$

where ξ and η are dimensionless coordinates, and v is Poisson's ratio. In the complex plane:

$$z = x + iy$$

$$\xi = \frac{x}{b},\ \eta = \frac{y}{b},\ \zeta = \xi + i\eta = \frac{z}{b} \tag{1.3}$$

the stress function can be rewritten in the more convenient form:

$$\chi = \chi_o + \chi_1 + \chi_2 \tag{1.4}$$

where χ_o corresponds to the axial tension stress at infinity and is written as:

$$\chi_o = Tb^2\,\mathrm{Re}\{\bar{\zeta}\varphi_o(\zeta) + \psi_o(\zeta)\}$$

$$\text{with}\quad \varphi_o(\zeta) = \frac{\zeta}{4}\quad \text{and}\quad \psi_o(\zeta) = \frac{\zeta^2}{4} \tag{1.5}$$

χ_1 is a stress function with singularities at the origin. Because stresses are symmetric about the *x* and *y* axes, it is expressed as:

$$\chi_1 = Tb^2\,\mathrm{Re}\{\bar{\zeta}\varphi_1(\zeta) + \psi_1(\zeta)\}$$

$$\varphi_1(\zeta) = \sum_{n=0}^{\infty} E_{2n}\,\zeta^{-(2n+1)} \tag{1.6}$$

$$\psi_1(\zeta) = -D_o \log\zeta + \sum_{n=1}^{\infty} D_{2n}\zeta^{-2n}$$

where the unknown coefficients D_{2n} and E_{2n} are determined from the boundary conditions. The third stress function χ_2 is added to χ_o and χ_1 to satisfy the boundary conditions along the crack surface and the outer edges where the plate meets the stiffeners. Stress function χ_2 is assumed in the integral form:

$$\chi_2 = Tb^2 \int_0^{\infty} [A(m)\,\zeta \sinh m\zeta + B(m)\cosh m\zeta]\cos m\zeta\, dm$$

$$= Tb^2\,\mathrm{Re}\left\{\int_0^{\infty}\left[\frac{A(m)}{2}(\zeta + \bar{\zeta})\sinh m\zeta + B(m)\cosh m\zeta\right] dm\right\} \tag{1.7}$$

Again the unknown functions $A(m)$ and $B(m)$ are determined from the boundary conditions. Inserting these stress functions into Equation 1.2 yields stresses and displacements.

Boundary Conditions

To determine the unknown coefficients and functions, the boundary conditions along the plate-stiffener junction lines $x = \pm b$ (Figure 1.5) and the crack surface ($-a \le x \le a$, $y = 0$) are examined.

From the equilibrium of the stiffener element shown in Figure 1.6, the following relations are obtained:

$$(\tau_{xy})_{\xi=1} t = \frac{\partial \sigma_{ys}}{\partial y} A_s$$
$$(\sigma_x)_{\xi=1} t = -E_s I_s \frac{\partial^4 u_s}{\partial y^4} \tag{1.8}$$

where subscript s denotes the stiffener. The continuity condition along the joint line gives

$$\frac{\sigma_{ys}}{E_s} = \frac{\sigma_y - \nu\sigma_x}{E} \tag{1.9}$$

Therefore, replacing u_s by $(u)_{\xi=1}$, σ_{ys} by $(E_s/E)(\sigma_y - \nu\sigma_x)_{\xi=1}$, and noting that $\sigma_{ys} \approx E_s\epsilon_{ys} \approx E_s(\epsilon_y)_{\xi=1}$, Equations 1.8 are rewritten as:

$$(\tau_{xy})_{\xi=1} = \beta\left[\frac{\partial}{\partial\eta}(\nu\sigma_x - \sigma_y)\right]_{\xi=1}$$
$$(\sigma_x)_{\xi=1} = -\frac{\alpha}{b}\left(\frac{\partial^4 E u}{\partial\eta^4}\right)_{\xi=1} \tag{1.10}$$

where the flexural and axial rigidity ratios are

$$\alpha = \frac{E_s}{E} \cdot \frac{I_s}{b^3 t} \quad \text{and} \quad \beta = \frac{E_s}{E} \cdot \frac{A_s}{bt} \tag{1.11}$$

The stresses and displacements derived from stress functions χ_o, χ_1 and χ_2 must satisfy the boundary condition Equations 1.10. Since χ_o itself satisfies these relations, only stresses and displacements derived from χ_1 and χ_2 are involved in Equations 1.10. By using Equations 1.2, 1.5, 1.6 and 1.10, the unknown functions $A(m)$ and $B(m)$ of the stress function χ_2 can be written in terms of D_{2n} and E_{2n} which are the unknown coefficients of χ_1. Expanding Equation 1.7 into a power series in ζ yields the following form of χ_2 which, together with χ_1, satisfies the boundary conditions along the junction lines:

$$\begin{aligned} \chi_2 &= Tb^2 \, \mathrm{Re}[\bar{\zeta}\varphi_2(\zeta) + \psi_2(\zeta)] \\ \varphi_2(\zeta) &= \sum_{n=0}^{\infty} M_{2n}\zeta^{2n+1} \\ \psi_2(\zeta) &= \sum_{n=0}^{\infty} L_{2n}\zeta^{2n+2} \end{aligned} \tag{1.12}$$

in Equation 1.12, L_{2n} and M_{2n} are expressed in linear forms of D_{2p} and E_{2p}:

$$\begin{aligned} L_{2n} &= \sum_{p=0}^{\infty} (\alpha_{2p}^{2n} D_{2p} + \beta_{2p}^{2n} E_{2p}) \\ M_{2n} &= \sum_{p=0}^{\infty} (\gamma_{2p}^{2n} D_{2p} + \delta_{2p}^{2n} E_{2p}) \end{aligned} \tag{1.13}$$

with coefficients being functions of α and β.

Applying the stress-free boundary condition along the crack surface leads to the following relations:

$$D_{2n} = \frac{1}{2} a_o^{2n} \lambda^{2n+2} + \sum_{p=0}^{\infty} (L_{2p} + M_{2p})\, a_{2p}^{2n} \lambda^{2n-2p+2}$$
$$E_{2n} = -\frac{1}{2} c_o^{2n} \lambda^{2n+2} - \sum_{p-0}^{\infty} (L_{2p} + M_{2p})\, c_{2p}^{2n} \lambda^{2n+2p+2} \qquad (1.14)$$

where the coefficients a_{2p}°, a_{2p}^{2n} and c_{2p}^{2n} are known numerical constants. Assuming all the unknowns may be expanded into power series of λ, and solving Equations 1.13 and 1.14 by the perturbation technique, the unknown coefficients D_{2n}, E_{2n}, L_{2n}, and M_{2n} are determined as functions of α, β and λ.

SIF Results

With the complex potential function determined, the SIF is then obtained from the limit expression:

$$K_I = 2T\sqrt{2\pi b}\ \lim|_{\xi \to \lambda} [\varphi'(\zeta)\sqrt{\zeta - \lambda}] \qquad (1.15)$$

where φ' is calculated by

$$\varphi'(\zeta) = \varphi_o'(\zeta) + \varphi_1'(\zeta) + \varphi_2'(\zeta) \qquad (1.16)$$

Isida numerically calculated SIFs for various combinations of α and β in terms of λ. Poisson's ratio was assumed to be 0.3. Retaining the first 36 terms of the series, gives

$$K_I = T\sqrt{\pi a}\, F(\alpha, \beta, \lambda)$$
$$F(\alpha, \beta, \lambda) = 1 + \sum_{n=1}^{35} c_{2n} \lambda^{2n} \qquad (1.17)$$

where the coefficient c_{2n} is a function of α and β. The function $F(\alpha, \beta, \lambda)$ represents the correction on K_I due to the effects of relative rigidities of plate and stiffeners.

Values of the correction factor $F(\alpha, \beta, \lambda)$, plotted as a function of λ for

different values of α and β (Isida 1973), show that increasing flexural and axial rigidities α and β reduces the value of SIF. This trend becomes more pronounced the longer the crack is. Of the two parameters, the axial rigidity β, which is the cross-sectional area ratio of stiffener-to-plate, has the greater effect on SIF. The flexural rigidity α becomes appreciable only when the crack tip approaches the flanges.

Isida checked the accuracy of his solution by calculating the value of F for several specially chosen cases of α and β and then comparing them with the existing solutions.

- $\alpha = \beta = 0$; the extreme case of a finite width plate with a central crack. Isida's solution yields values of F accurate to less than 0.1% for $\lambda \leq 0.9$.
- $\alpha = \infty$, $\beta = 0$; wide plate with an infinite row of collinear cracks. Isida's solution yields values of F accurate to less than 0.1% for $\lambda \leq 0.9$.
- $\alpha = \beta = \infty$; the other extreme case of a center-cracked plate with clamped edges. Isida's solution yields values varying from $F = 1.0$ at $\lambda \rightarrow 0$ to $F = 0.6$ $\lambda = 0.9$. These results are clearly wrong. Infinitely stiff flanges do not deform and the stress applied at the remote end of the plate cannot be transferred along the plate to the cracked section. Theoretically, the SIF for this case should be zero.

Isida's solution can not be applied to a two-tip cracked I-beam for the following reasons:

- In his analysis, the plate (which is similar to the web of an I-beam) is

under remote axial tension but the stiffeners (flanges) are not, whereas both the web and flanges of an I-beam are stressed.

- Isida's solution is for a central crack, a symmetric problem. Two-tip cracks in the web of an I-beam are always eccentric, making the geometry non-symmetric.

1.3.3 Two-tip Cracked I-Beam

Chen and Albrecht (1994) calculated SIFs for central and eccentric cracks in a finite-width plate using the WFM (Figure 1.7). Weight functions are powerful in the sense that knowing the solution for one loading condition enables one to determine the solutions for the same cracked body under any other loading (Bueckner 1970, Rice 1972, and Wu and Carlsson 1983).

Weight Function for Central Crack

SIFs can be calculated from the weight function *m(a, x)* and the stress distribution σ(x) in the crack-free body along the line of the prospective crack:

$$K = \int_0^a \sigma(x)\, m(a,x)\, dx \tag{1.18}$$

$$m(a,x) = \frac{E}{K_o} \frac{\partial v_o(a,x)}{\partial a} \tag{1.19}$$

where

E = Young's modulus

K_0 = SIF for arbitrary reference loading

v_o = COD for reference loading

To obtain the weight function from Equation 1.19, both the SIF and the corresponding COD are needed for the reference loading.

Reference Loading for Central Crack

For a central crack in a finite-width plate, Chen and Albrecht chose Tada's (1973) solution for axial tension as the reference. This solution is given by:

$$K_o = \sigma_o \sqrt{\pi a}\, f_o\left(\frac{a}{W}\right) \tag{1.20}$$

with

$$f_o\left(\frac{a}{W}\right) = \left[1 - 0.025\left(\frac{a}{W}\right)^2 + 0.06\left(\frac{a}{W}\right)^4\right]\sqrt{\sec\frac{\pi a}{2W}} \tag{1.21}$$

It is accurate to 0.1% for any crack length. With the reference SIF determined, the accuracy of the weight function depends on the accuracy of COD for the reference loading. Wu (1984) assumed an elliptical COD profile of a center-cracked plate under axial tension:

$$v_o(a,x) = v_o(a,0)\sqrt{1 - (x/a)^2} \tag{1.22}$$

where

$$v_o(a,0) = 2\sigma\frac{a}{E} f_o\left(\frac{a}{W}\right) \quad \text{and} \quad f_o\left(\frac{a}{W}\right) = \frac{K_o(a)}{\sigma_o\sqrt{\pi a}} \tag{1.23}$$

Equations 1.22 and 1.23 give good results for $a/W \leq 0.7$. To obtain a more accurate weight function that is valid over a wider range of crack lengths, Chen added a second term to the expression for the COD profile:

$$v_o(a,x) = \frac{\sigma}{E}\left[2f_o\left(\frac{a}{W}\right)\sqrt{a^2 - x^2} + \frac{G(a/W)}{a^2}(a^2 - x^2)^{3/2}\right] \quad (1.24)$$

where G is a function of f_o

$$G\left(\frac{a}{W}\right) = \frac{16}{3}\left[\phi\left(\frac{a}{W}\right) - \frac{f_o(a/W)}{2}\right] \quad (1.25)$$

$$\phi\left(\frac{a}{W}\right) = \frac{1}{a^2}\int_0^a a\, f_o^2\left(\frac{a}{W}\right) da \quad (1.26)$$

Inserting Equations 1.20 and 1.24 through 1.26 into Equation 1.19 yields a closed-form weight function for a finite-width plate with a central crack. Chen and Albrecht applied his weight function to three known cases (single concentrated load, partial uniform pressure acting on arbitrary part of crack, and central crack in a rotating circular disk) and obtained good results.

Weight Functions for Eccentric Crack

For an eccentrically cracked plate, shown in Figure 1.7 (b), the weight functions for each tip are

$$m^A(a_A, a_B, x) = \frac{E}{K_o^A}\frac{\partial v_o(a_A, a_B, x)}{\partial a_A} \quad (1.27)$$

$$m^B(a_A, a_B, x) = \frac{E}{K_o^B}\frac{\partial v_o(a_A, a_B, x)}{\partial a_B} \quad (1.28)$$

where

K_o^A = SIF at crack tip A under reference loading

K_o^B = SIF at crack tip B under reference loading

v_o = COD for reference loading

The SIFs are then given by:

$$K_A = \int_{\text{crack surface}} \sigma(x) m^A(a_A, a_B, x)\, dx \tag{1.29}$$

and

$$K_B = \int_{\text{crack surface}} \sigma(x) m^B(a_A, a_B, x)\, dx \tag{1.30}$$

Self-consistency Conditions

Chen and Albrecht developed self-consistency conditions for determining the accuracy of SIFs and hence weight functions for an eccentric crack. For virtual crack extensions, the energy balance condition requires that

$$\int_{-a_B}^{a_A} \frac{(K_0^A)^2}{E} da_A = \int_{\text{crack surface}} \sigma_o v_o\, dx \tag{1.31}$$

$$\int_{-a_A}^{a_B} \frac{(K_0^B)^2}{E} da_B = \int_{\text{crack surface}} \sigma_o v_o\, dx \tag{1.32}$$

and

$$\int_0^a \left[\frac{(K_o^A)^2}{E} + \frac{(K_o^B)^2}{E} \right] da = \int_{\text{crack surface}} \sigma_o v_o\, dx \tag{1.33}$$

where a_A and a_B are positions of crack tips A and B, and a is the crack length as shown in Figure 1.7 (b). Equation 1.31 was obtained by assuming crack tip A virtually extends by δa_A while crack tip B does not extend. Similarly, Equation

1.32 was obtained by assuming crack tip B virtually extends by δa_B while crack tip A does not extend. Equation 1.33 was obtained by assuming both crack tips A and B extend by equal amounts, $\delta a_A = \delta a_B = \delta a$, without changing the eccentricity $\delta e = 0$. The above three equations are not independent because the right sides of the equations are the same. Let

$$Q_A = \int_{-a_B}^{a_A} \frac{(K_o^A)^2}{E} \Big|_{\delta a_B = 0} da_A = \int_0^a 2 \frac{(K_o^A)}{E} \Big|_{a_B = \text{constant}} da \tag{1.34}$$

$$Q_B = \int_{-a_A}^{a_B} \frac{(K_o^B)^2}{E} \Big|_{\delta a_A = 0} da_B = \int_0^a 2 \frac{(K_o^B)}{E} \Big|_{a_A = \text{constant}} da \tag{1.35}$$

$$Q = \int_0^a \left[\frac{(k_o^A)}{E} + \frac{(K_o^B)^2}{E} \right] \Big|_{\delta e = 0} da \tag{1.36}$$

Two so-called self-consistency conditions were then obtained by equating 1.31 to 1.33 and 1.32 to 1.33:

$$Q_A = Q \quad \text{and} \quad Q_B = Q \tag{1.37}$$

The close the ratios of Q_A/Q and Q_B/Q are to unity, the more accurate is the weight function.

Reference Loading for Eccentric Crack

Chen and Albrecht chose Isida's (1965) solution for an eccentric crack in a finite-width plate under axial tension as the reference, which is given by the following equations:

$$\begin{aligned} K_o^A &= \sigma_o \sqrt{\pi a}\, f_o^A \\ K_o^B &= \sigma_o \sqrt{\pi a}\, f_o^B \end{aligned} \tag{1.38}$$

where

$$f_o^A = 1 + \sum_{i=2}^{19} C_i(\varepsilon)\,\lambda^i$$
$$f_o^B = 1 + \sum_{i=2}^{19} (-1)^i C_i(\varepsilon)\,\lambda^i \qquad (1.39)$$

and $\varepsilon = e/W$ and $\lambda = a/(W-e)$ are the normalized eccentricity and crack length respectively, with e being the eccentricity and W being the half width of the plate. The numerical coefficients $C_i(\varepsilon)$ are given in tabular form for different values of normalized eccentricity. To obtain a closed-form weight function, Chen and Albrecht fitted the tabulated values with a 10th order polynomial:

$$C_i(\varepsilon) = \sum_{j=0}^{10} \gamma_{ij}\,\varepsilon^j \qquad (1.40)$$

The fitting error is less than 1% for C_2 to C_{14}, and less than 2.5% for C_{15} to C_{19}. The self-consistency conditions, Equation 1.37, were checked and the error was found to be less than 2% (Chen and Albrecht 1994).

To obtain the weight functions for the two crack tips, a reasonable COD profile is needed. Chen and Albrecht assumed an expression for the COD of an eccentric crack under axial tension that is similar to Equation 1.24:

$$v_o = \frac{\sigma}{E}\left[\frac{1}{a}\left(f_o^A r_B + f_o^B r_A\right)\sqrt{r_A\, r_B} + \frac{G}{a^2}\left(r_A\, r_B\right)^{\frac{3}{2}}\right] \qquad (1.41)$$

where for crack tips A and B located at a_A and a_B from the origin (Figure 1.7):

$$
\begin{aligned}
a &= \frac{1}{2}(a_A - a_B) \\
e &= \frac{1}{2}(a_A + a_B) \\
r_A &= a_A - x \\
r_B &= x - a_B
\end{aligned}
\tag{1.42}
$$

In Equation 1.41:

$$
f_o^A = \frac{K_o^A}{\sigma_o\sqrt{\pi a}} \quad \text{and} \quad f_o^B = \frac{K_o^B}{\sigma_o\sqrt{\pi a}} \tag{1.43}
$$

and G is obtained by satisfying the energy balance condition of Equation 1.33.

To further check the accuracy of the developed weight functions, Chen and Albrecht (1994) applied them to solve several special problems.

- Central crack in an infinite plate subjected to a pair of symmetric point loads; The result is the same as the theoretical one.
- Central crack in a finite-width plate subjected to bending; The WFM solution is much closer to Benthem's (1972) result than to that of Isida (1956).
- Eccentric crack in a plate under remote tension; this is the reference loading case from which the weight functions were derived. As expected, the results compared well with the error being less than 1% for $a/W \leq 0.9$.

SIFs for Two-tip Cracked I-beam

Chen and Albrecht used the weight function for the finite-width plate to

calculate SIFs for a two-tip cracked I-beam, as shown in Figure 1.8 (if not specifically noted, the two-tip crack is on the web). The underlying idea is to apply on the plate the stress distribution σ(x) that is acting on the web of an I-beam. For example, the stress is uniformly distributed for axial loading:

$$\sigma = \frac{T}{A} = \frac{T}{A_w + 2A_f} \tag{1.44}$$

where T is the axial force and A is the cross-sectional area of the I-beam. For the case of pure bending, the stress is linearly distributed:

$$\sigma = \frac{My}{I} \tag{1.45}$$

where M is the applied moment, y is the distance from the neutral axis, and I is the moment inertia of the I-beam.

Chen and Albrecht calculated the SIFs for a two-tip cracked I-beam by simply multiplying the single plate solution with a correction factor of A_w/A for axial tension, or I_w/I for pure bending. In so doing, the weight function becomes an approximation because the geometries of the plate and I-beam are different. Although the stresses are the same, the web of an I-beam is constrained by the flanges along the junction line while the single plate is not constrained. As crack length increases and the crack tips move closer to the flange, the weight function becomes increasingly inaccurate.

1.3.4 Three-Tip Cracked I-Beam

A solution for a three-tip cracked I-beam (Figure 1.9) was first developed

by Chen (1992). The COD expression and the SIFs were determined with the energy release rate method. The three-tip cracked I-beam was modeled as an edge-cracked web plate combined with a flange plate having a central crack or an eccentric crack, as shown in Figure 1.10.

COD Assumptions for Central Three-tip Crack

Chen made some several assumptions about the COD of the central three-tip crack:

$$v = v(x, y, a_x, a_y) \tag{1.46}$$

where the coordinates x, y and crack lengths a_x, a_y are defined in Figure 1.10 (a).

- The COD vanishes at the flange crack tips:

  $$v(0, \pm a_y, a_x, a_y) = 0 \tag{1.47}$$

  and at the web crack tip:

  $$v(a_x, 0, a_x, a_y) = 0 \tag{1.48}$$

- If any one of the crack lengths is zero, the crack does not open at the junction point where the web and the flange center lines intersect. This is a special case of the three-tip crack. If the web or flange crack length is zero, the COD at the junction point closes as well the entire crack length:

  $$v(x, y, 0, a_y) = 0 \tag{1.49}$$

  $$v(x, y, a_x, 0) = 0 \tag{1.50}$$

- The COD profile of the flange crack is similar to that of a center-cracked plate of the same width and crack length as the flange; the COD profile of the web crack is similar to that of an edge-cracked plate of the same

width and crack length as the web.

- Web and flange cracks interact only through the displacement at the junction point.
- A long web (flange) crack has a small effect on the COD of the flange (web) crack.
- For any point along the web and flange cracks, the COD across the thickness of the element is the same as the COD at mid-thickness.

Based on the assumption cited above, Chen chose the following expression for the COD of a three-tip crack subjected to an opening stress $\sigma(x, y)$ applied on the crack faces:

$$v(x, y, a_x, a_y) \approx v_o \cdot \frac{v_1(x, a_x)}{v_1(0, a_x)} \cdot \frac{v_2(y, a_y)}{v_2(0, a_y)} \cdot \frac{\sigma_o}{E} \qquad (1.51)$$

where

E = Young's modulus

v_1 = COD expression for edge crack in web

v_2 = COD expression for central or eccentric crack in flange

v_o = normalized displacement at the junction

σ_o = reference stress

Reference Stress

The reference stress σ_o is defined differently for the cases of axial load and pure bending. When the I-beam is under axial tension, the value of the uniformly distributed stress across the web and flanges is taken as the

reference stress:

$$\sigma(x,0) = \sigma_o \qquad (o \le x \le d_w)$$
$$\sigma(0,y) = \sigma_o \qquad (-\frac{b_f}{2} \le y \le \frac{b_f}{2}) \tag{1.52}$$

When the I-beam is under pure bending, the stresses over the web and flanges are given by:

$$\sigma(x,0) = \sigma_o (1 - 2\frac{x}{d_w}) \qquad (o \le x \le d_w)$$
$$\sigma(0,y) = \sigma_o \qquad (-\frac{b_f}{2} \le y \le \frac{b_f}{2}) \tag{1.53}$$

and the reference stress σ_o here is taken as the value of the bending stress at the flange-web junction.

CODs of Web and Flange Cracks

As assumed by Chen, the COD profiles of the web and flange cracks are equal to those of the corresponding 2-D edged-cracked and center-cracked plate respectively. If the stress $\sigma(x, y)$ applied on the crack faces is uniformly or linearly distributed, 2-D COD expressions take the following forms for the flange crack ($|y| \le a_y$):

$$v_2(y, a_y) \approx a_y \sum_{i=1}^{m} D_i \left[1 - \left(\frac{y}{a_y} \right)^2 \right]^{i-\frac{1}{2}} \tag{1.54}$$

and the web crack ($0 \le x \le a_x$)

$$v_1(x, a_x) \approx a_x \sum_{i=1}^{n} C_i \left(1 - \frac{x}{a_x} \right)^{i-\frac{1}{2}} \tag{1.55}$$

where the non-dimensional coefficients $C_i(a_x/d_w)$ and $D_i(a_y/b_f)$ can be obtained from two-dimensional analysis.

In Chen's analysis, COD of the flange crack always takes the form of Equation 1.24 which is a special case of the Equation 1.54 with $m = 2$. It makes no difference whether the I-beam is under axial tension or pure bending. The bottom flange in an I-beam is subjected to axial tension.

For the web crack, Chen used Petroski and Achenbach's (1978) edge crack solution:

$$v(a_x, x) = \frac{\sigma_o}{E} v_1 \tag{1.56}$$

where the normalized COD v_1 is given by:

$$v_1(a_x, x) \approx a_x \left[C_1 \left(1 - \frac{x}{a_x} \right)^{\frac{1}{2}} + C_2 \left(1 - \frac{x}{a_x} \right)^{\frac{3}{2}} \right] \tag{1.57}$$

If the I-beam is under axial tension, coefficients C_1 and C_2 become:

$$\begin{aligned} C_1 &= 2\sqrt{2} f_{xo} \\ C_2 &= \frac{G_x}{\sqrt{2}} = \frac{5\pi}{2} \phi_x - \frac{20}{3\sqrt{2}} f_{xo} \end{aligned} \tag{1.58}$$

where f_{xo} and Φ_x are defined as:

$$\begin{aligned} f_{xo}\left(\frac{a_x}{d_w} \right) &= \frac{K_{xo}}{\sigma_o \sqrt{\pi a_x}} \\ &= \frac{0.752 + 2.02\left(\frac{a_x}{d_w} \right) + 0.37 \left[1 - \sin \frac{\pi a_x}{2 d_w} \right]^3}{\cos \frac{\pi a_x}{2 d_w}} \sqrt{\frac{2 d_w}{\pi a_x} \tan \frac{\pi a_x}{2 d_w}} \end{aligned} \tag{1.59}$$

and

$$\Phi_x\left(\frac{a_x}{d_w}\right) = \frac{1}{a_x^2}\int_0^{a_x} a_x f_{xo}^2\, da_x \tag{1.60}$$

If the I-beam is under pure bending, the coefficients C_1 and C_2 are given by:

$$C_1 = 2\sqrt{2} f_{xo}$$

$$C_2 = \frac{G_x}{\sqrt{2}} = \left[\frac{5\pi}{2}\Phi_x - \frac{20}{3\sqrt{2}} f_{xo}\left(1 - \frac{4}{5}\frac{a_x}{d_w}\right)\right] \frac{1}{1 - \frac{4}{7}\frac{a_x}{d_w}} \tag{1.61}$$

where Φ_x is defined as in Equation 1.60, and f_{xo} given by

$$f_{xo} = \frac{K_{xo}}{\sigma_o\sqrt{\pi a_x}}$$

$$= \frac{0.923 + 0.199\left[1 - \sin\frac{\pi a_x}{2d_w}\right]^4}{\cos\frac{\pi a_x}{2d_w}} \sqrt{\frac{2d_w}{\pi a_x}\tan\frac{\pi a_x}{2d_w}} \tag{1.62}$$

Normalized Junction Point COD

The only unknown in Equation 1.51 is the normalized COD at junction point, v_o, which is calculated with the energy release rate method. The crack closure work is given by the potential energy Π:

$$\Pi = \int_{\substack{\text{crack}\\ \text{surface}}} \sigma(x,y)\, v(x,y,a_x,a_y)\, dA \tag{1.63}$$

or, for a three-tip cracked I-beam:

$$\Pi = -\frac{\sigma_o^2}{E} v_o \left[\int_0^{a_x} t_w \frac{\sigma(x,0)}{\sigma_o} \frac{v_1(x,a_x)}{v_1(0,a_x)} dx \right] - \frac{\sigma_o^2}{E} v_o \left[\int_{-a_y}^{a_y} t_f \frac{\sigma(0,y)}{\sigma_o} \frac{v_1(y,a_y)}{v_1(0,a_y)} dy \right] \tag{1.64}$$

Normalizing the integrals by the web and flange areas yields

$$\Pi = -\frac{\sigma_o^2}{E} v_o (H_x + H_y) = -\frac{\sigma_o^2}{E} v_o H \tag{1.65}$$

where

$$H_x = \int_0^{a_x} t_w \frac{\sigma(x,0)}{\sigma_o} \frac{v_1(x,a_x)}{v_1(0,a_x)} dx = A_w \int_0^{a_x} \frac{\sigma(x,0)}{\sigma_o} \frac{v_1(x,a_x)}{v_1(0,a_x)} d\left(\frac{x}{d_W}\right) = A_W R_x \tag{1.66}$$

$$H_y = \int_{-a_y}^{a_y} t_f \frac{\sigma(0,y)}{\sigma_o} \frac{v_1(y,a_y)}{v_1(0,a_y)} dy = A_f \int_0^{a_y} \frac{\sigma(0,y)}{\sigma_o} \frac{v_1(y,a_y)}{v_1(0,a_y)} d\left(\frac{y}{W}\right) = A_f R_y \tag{1.67}$$

Using Irwin's method, the energy release rate is

$$G_x = \frac{K_x^2}{E} = -\frac{\partial \Pi}{\partial A_x}$$
$$2G_y = 2\frac{K_y^2}{E} = -\frac{\partial \Pi}{\partial A_y} \tag{1.68}$$

here $A_x = a_x t_w$ and $A_y = a_y t_f$ are the surface areas of the web and flange cracks respectively. So that the change of the total energy release rate is then obtained by:

$$dG = \frac{K_x^2}{E} dA_x + \frac{K_y^2}{E} 2dA_y = -d\Pi \tag{1.69}$$

Inserting Π from Equation 1.65 into 1.69 leads to:

$$t_w a_x \left(\frac{K_x}{\sigma_o}\right)^2 + 2 t_f a_y \left(\frac{K_y}{\sigma_o}\right)^2 = \frac{\partial (v_o H)}{\partial g} \tag{1.70}$$

where

$$\frac{\partial ( )}{\partial g} = a_x \frac{\partial ( )}{\partial a_x} + a_y \frac{\partial ( )}{\partial a_y} \tag{1.71}$$

Furthermore, from the near-field equation, the COD v is related to K by:

$$v \approx \sqrt{\frac{8}{\pi}} \frac{K}{E} \sqrt{r} \tag{1.72}$$

Equating the two COD expressions, Equations 1.72 and 1.51, near the web crack tip and flange crack tip, the following equations are obtained:

$$\begin{aligned} \frac{K_x}{\sigma_o} &= \sqrt{\frac{\pi}{8}} C_1 \sqrt{a_x} \frac{v_o}{v_{1o}} = \sqrt{\pi a_x} f_{xo} \frac{v_o}{v_{1o}} = \frac{K_{xo}}{\sigma_o} \frac{v_o}{v_{1o}} \\ \frac{K_y}{\sigma_o} &= \sqrt{\frac{\pi}{8}} D_1 \sqrt{2a_y} \frac{v_o}{v_{2o}} = \sqrt{\pi a_y} f_{yo} \frac{v_o}{v_{2o}} = \frac{K_{yo}}{\sigma_o} \frac{v_o}{v_{2o}} \end{aligned} \tag{1.73}$$

where

$$v_{1o} = v_1(0, a_x) \tag{1.74}$$

is the normalized crack mouth COD of single web crack, and

$$v_{2o} = v_2(0, a_y) \tag{1.75}$$

is the normalized crack mouth COD of single flange crack. Equation 1.73 also shows that the v_o scales SIFs also.

Inserting Equation 1.73 into 1.70, and making some necessary

numerical assumptions for the integral calculation yields the normalized COD v_o :

$$v_o \approx \frac{H v_{1o} v_{2o}}{H_x v_{1o} + H_y v_{2o}} \tag{1.76}$$

It is clear from the above equations that the accuracy of determining the normalized COD at the junction point v_o and therefore the SIF depends solely on the accuracy of the assumed three-tip crack opening profile expression.

Eccentric Three-tip Crack

For the eccentric three-tip crack shown in Figure 1.10b, Chen adopted an approach similar to that for the central three-tip crack. In this case, the I-beam was modeled as an edge-cracked web plate combined with an eccentrically cracked flange plate. The two are joined, having the same COD, at the junction point. The COD expressions are given by Equation 1.51 for the three-tip cracked I-beam, Equations 1.56 through 1.62 for the edge crack in the web under tension and bending, and Equation 1.41 for the eccentric crack in the flange under tension.

Shortcomings

The COD expression for a three-tip cracked I-beam, Equation 1.51, is mainly based on the assumptions that the edge crack in the web and central crack in the flange take the same profiles as 2-D cracks, and the cracked web and flange are joined and interact only at the junction point. Those two assumptions are arguable.

In a real I-beam, the cracked web plate and flange plate are not only joined at the junction point but are also stitched along the common junction line. Single cracked webs and flanges deform independently in their own plane. But when they are joined to form an I-beam, the displacements along the junction line should be compatible; that is, the displacement at every point along the centerline of the flange should equal the displacement at the matching point along the edge of the web. If the I-beam is not cracked, the deformations of the flange and web along the junction line under applied loading (axial tension and pure bending) are the same, and no longitudinal shear is transferred between the web and flange. But when the I-beam has a three-tip crack, the flange and web deformations are disturbed along the junction line, inducing longitudinal shear between the web and the flanges in the vicinity of the cracked section. If the displacements along the center line of the flange are larger than those of the corresponding points along the web edge, the web tends to close the flange crack while the flange tends to open the web crack. Conversely, if the displacements along the center line of the flange are smaller than those of the corresponding points along the web edge, the web tends to open the flange crack while the flange tends to close the web crack. The interaction forces between the web and flange will therefore alter the COD and SIFs of the web and flange cracks relative to those of the corresponding single plate solutions.

While web and flange interact along the entire junction line, the interaction is greatest at the junction point and rapidly diminishes with distance

from the junction point, alter the COD profiles of the edge-cracked web plate and center-cracked flange plate under axial tension or pure bending.

An interesting special case is worth noting. With varying crack lengths in web and flange, the interaction may change from the flange pulling open the web crack to the flange restraining the opening of the web crack. This change must be physically continuous as a function of relative crack lengths. So the two behaviors are separated by a pair of matching web and flange crack lengths for which there is no interaction. In this case, called no-interaction, the cracked web and flange can be parted freely, without altering significant the displacement at the junction point. The assumption here is that the junction line displacements mismatching away from the junction point have a much lesser effect and may be neglected.

1.4 Objective

Stress intensity factors are needed in fatigue and fracture analysis of steel bridge girders. But no satisfactory SIF solutions exist for two-tip web cracks and three-tip web and flange cracks. Therefore, to develop SIF solutions for I-beams is the foremost objective of the present study.

SIFs will be determined from finite element analysis of I-beams with different flange-web area ratios, crack eccentricities, web crack lengths, and flange crack lengths.

The numerical results will be fitted with equations suitable for ready use by engineers.

Chapter 2: Finite Element Models of Cracked I-Beam

2.1 Introduction

I-beams with two-tip and three-tip cracks are difficult to model. The interaction forces between the cracked web and flanges invalidate single-plate solutions. Accurate closed-form solutions of the SIF are not available in the literature. After careful evaluation of several options for calculating SIFs, the finite element method was chosen for its powerful ability to treat complex geometric configurations and boundary conditions.

The present chapter discusses the modeling of cracked I-beams. Finite elements and meshes are selected, methods of extracting SIFs are examined, and a simple 2-D method of modeling a cracked I-beam is evaluated. FEAs throughout this study were performed with the ABAQUS program, a general finite element code.

2.2 Modeling of Cracked I-beam

Rolled and welded I-beams are treated in this study as a combination of three plates: one web and two flanges, each represented by its mid-plane, width, and thickness. They are joined along the junction lines defined as the intersection of the web and flange mid-planes shown in Figure 2.1.

The web and flanges are modeled in 3-D with eight-node shell elements — ABAQUS designation S8R5 (ABAQUS/Standard User's Manual 1993). At most nodes, there are five active degrees of freedom: three displacements and two in-surface rotations. But when the node is part of a multi-point constraint (MPC), such as the nodes along the junction lines, the sixth DOF — the out-of-surface rotation — is activated. Figure 2.2 shows typical mesh for a three-tip cracked I-beam.

The fillets at the transition between the web and flanges are neglected. This is compensated by counting twice the area where web and flanges overlap as shown in Figure 2.1. The errors from the two approximations tend to cancel out.

2.3 Crack Tip Elements

A major problem in applying FEM to fracture analysis arises from the square-root singularity of stresses and strains around the crack tip. Several crack tip elements have been developed to overcome this difficulty. Among them, the most common are conventional elements with a special shape function that produces a $1/\sqrt{r}$ singularity, the quarter-point element, and the hybrid approach. All have strong supporters and have been applied with success to a variety of problems. However, no method has been established as optimal for all problems.

The quarter-point element is the most widely used because it describes the desired singularity, is simple to program, and has other advantages such as convergence and continuity. For these reasons it was adopted in the present study.

Quarter-point Singularity Element

Barsoum (1974) and Henshell and Shaw (1975) independently showed that placing two mid-side nodes of an eight-node isoparametric quadrilateral element at the quarter point yields a $1/\sqrt{r}$ singularity (Figure 2.3a). The crack tip is located at node 1. The element exhibits $1/\sqrt{r}$ singularity along the two sides containing the quarter-point nodes but not along other rays emanating from the crack tip.

Barsoum (1974) found that the six-node isoparametric triangular element with quarter-point nodes on two sides also has $1/\sqrt{r}$ singularity (Figure 2.3b). This triangular element better represents the stress field because the $1/\sqrt{r}$ singularity exists along all rays emanating from the crack tip.

It turns out that the six-node triangular element can be obtained by degenerating the eight-node quadrilateral element as shown in Figure 2.4; nodes 1, 8 and 4 are collapsed into one node that is placed at the crack tip; and nodes 5 and 7 are moved from mid-sides to quarter points. According to Freese and Tracy (1976), this degenerated quadrilateral element yields the same stresses and strains as the triangular element (Figure 2.3b). Since this element comes from an isoparametric element, even in its singular form, it still satisfies

the requirements for convergence and passes the patch test. It also possesses rigid body motion, constant strain modes, inter-element compatibility, and continuity of displacements.

From here on, the two elements shown in Figure 2.3 are simply called the quarter-point quadrilateral and triangular elements, while the one in Figure 2.4 is called the degenerated quarter-point element.

ABAQUS' Singularity Element

In this study, the degenerated quarter-point elements come from the ABAQUS library: — CPS8R for plane stress problems and S8R5 for shells. Command *SINGULAR creates the mesh in the region surrounding the crack tip, with quarter-point spacing for the first element and progressive increase in element size with distance from the crack tip. Figure 2.5 shows how element size is increased along any line emanating from the crack tip.

2.4 Mesh Pattern Around Crack Tip

An important problem in modeling a cracked geometry is to choose suitable mesh density, size of crack tip element, and element aspect ratio in a region surrounding the crack tip.

The cracked web or flange was divided into a so-called inner region at the crack tip surrounded by an outer region. Figure 2.6 shows the shaded inner region and nonshaded outer region for crack lengths of $0 < a/W < 0.5$, $a/W =$

0.5, and $0.5 < a/W < 1.0$. The vertical line on the left of each sub-figure represents the centerline of a center-cracked flange, or the edge of an edge-cracked web, or the centerline of an eccentric crack in the web. All three are symmetric about the line of crack extension, meaning that Figure 2.6 shows only the upper half of the cracked web or flange.

Using standard terminology, the width is defined as $W = b_f/2$ for the center-cracked flange, $W = d_j$ for the edge-cracked web, and $W = d_j/2 - e$ for the eccentrically cracked web. The inner region consists of two squares of sides l placed symmetrically about the vertical line through the crack tip, with the left square trailing the crack tip and the right square leading it. The characteristic length l is:

$$l = \begin{cases} a & (0 < a/W \leq 0.5) \\ W - a & (0.5 < a/W < 1) \end{cases} \tag{2.1}$$

Parameter m defines the number of elements around a concentric square in the mesh, and parameter n defines the number of concentric squares (Figure 2.7). The sides of all elements lying on the perimeter of a concentric square have equal lengths. The sides of all elements on a radial line emanating from the crack tip increase in length as specified in the ABAQUS command *SINGULAR. Typical meshes in the outer region are shown in Figure 2.2.

To determine how mesh density affects the accuracy of calculating SIFs, benchmark analyses were performed for three geometries for which reliable solutions are available in the literature:

- Center-cracked finite-width plate under tension
- Edge-cracked finite-width plate under tension
- Edge-cracked finite-width plate under bending

The calculations were repeated for the ten combinations of parameters m and n shown in Figure 2.7. Mesh patterns $m \times n = 2 \times 16$ and $m \times n = 4 \times 2$ were not included because they resulted in large element aspect ratios. The results, presented in Appendix A, lead to the following conclusions:

- Increasing the parameter n improves the accuracy of SIFs more than increasing the parameter m.
- When $n = 8$, the mesh is fine enough to give convergent results.

Since a fine mesh is needed when the crack tip approaches the web-flange junction, it was decided to use the mesh pattern $m \times n = 3 \times 16$ for all analyses of cracked I-beams (center-right in Figure 2.7).

2.5 Extracting SIFs from FEA Output

FEA yields nodal displacements, nodal forces, and stresses and strains at selected positions — but not SIFs. Methods of extracting SIFs are classified as being displacement-based, stress-based, and energy-based.

2.5.1 Displacement-Based Methods

The first method involves examining the crack opening displacements

(COD) of the crack tip elements. The COD around the crack tip is given by:

$$u = 0 + o(r)$$
$$v = K\frac{\kappa + 1}{2G}\sqrt{\frac{r}{2\pi}} + o(r) \tag{2.2}$$

where $\kappa = (3 - \nu)/(1 + \nu)$ for plane stress, $\kappa = 3 - 4\nu$ for plane strain, ν is Poisson's ratio, G is the shear modulus, K_I is the SIF, and r is the distance from the crack tip. The so-called apparent SIF K_I^* can then be calculated from:

$$K^* = v\frac{2G}{\kappa + 1}\sqrt{\frac{2\pi}{r}} \tag{2.3}$$

The three common methods of calculating SIFs from COD are discussed in the following.

Nonlinear Extrapolation

Tracy (1977) proposed to calculate SIFs from the displacements of nodes B and C of the quarter-point element trailing the crack tip, $\alpha = \pi$ in Figure 2.8. According to Barsoum (1976), the COD of the quarter-point element is given by:

$$v = (4v_B - v_C)\sqrt{\frac{r}{L}} + (2v_C - 4v_B)\frac{r}{L} \tag{2.4}$$

where v_B and v_C are the quarter-point and corner node displacements at $r_B = L/4$ and $r_C = L$ respectively, and L is the length of the trailing element along the crack surface shown in Figure 2.8. Inserting Equation 2.4 into 2.3 gives the apparent SIF:

$$K^* = \frac{2G\sqrt{2\pi}}{(\kappa + 1)}\left(\frac{2v_C - 4v_B}{\sqrt{L}}\sqrt{\frac{r}{L}} + \frac{4v_B - v_C}{\sqrt{L}}\right) \tag{2.5}$$

which amounts to nonlinear extrapolation of the apparent SIFs within the crack

tip element:

$$K^{*} = A\sqrt{r} + B \tag{2.6}$$

The SIF at the crack tip is then obtained from Equation 2.5 as $r \to 0$:

$$K = \frac{2G\sqrt{2\pi}}{(\kappa + 1)} \frac{(4v_B - v_C)}{\sqrt{L}} \tag{2.7}$$

Equation 2.7 can also be obtained by equating the coefficients of the $\sqrt{r}$ terms in Equations 2.2 and 2.4.

Linear Extrapolation

The linear extrapolation technique (Chan, et al. 1970) was applied to the quarter-point singularity element by Chen and Kuang (1992). The SIF was extrapolated linearly:

$$K_I^{*} = Ar + B \tag{2.8}$$

Inserting the apparent SIFs at the quarter point B and corner point C yields

$$K^{*} = \frac{2G\sqrt{2\pi}}{\kappa + 1}\left(\frac{4}{3}\frac{v_C - 2v_B}{\sqrt{L}}\frac{r}{L} + \frac{1}{3}\frac{8v_B - v_C}{\sqrt{L}}\right) \tag{2.9}$$

The SIF at the crack tip, which is the intercept of the linear equation, is therefore:

$$K = \frac{2G\sqrt{2\pi}}{\kappa + 1} \frac{(8v_B - v_C)}{3\sqrt{L}} \tag{2.10}$$

Inserting Equation 2.9 into Equation 2.2 gives the corresponding COD:

$$v = \frac{1}{3}(8v_B - v_C)\sqrt{\frac{r}{L}} + \frac{4}{3}(v_C - 2v_B)\left(\frac{r}{L}\right)^{3/2} \tag{2.11}$$

Quarter-point Displacement

In this method, the COD at the quarter point ($r_B = L/4$) trailing the crack

tip is inserted in Equation 2.3, yielding directly the value of the SIF:

$$K = \frac{2G\sqrt{2\pi}}{(\kappa + 1)} \frac{2v_B}{\sqrt{L}} \tag{2.12}$$

Comparison

Equations 2.7, 2.10 and 2.12 are all based on the CODs of the element trailing the crack tip. Shih, et al. 1976, Saouma and Schwemmer 1984, Yehia and Shephard 1985, Lim, et al. 1992, Chen and Kuang 1992, and Pang 1993 studied the relative accuracies of the three equations but reached no consistent conclusions. The three equations yield equal values of SIF only if:

$$v_C = 2v_B \tag{2.13}$$

To satisfy this condition, the crack tip element must be very small. For example, considering the case of an infinite plate with a central crack, the analytical solution for the COD profile is given by:

$$v = \frac{(\kappa + 1)\sigma}{4G}\sqrt{r(2a - r)} \tag{2.14}$$

where a is the half crack length. For a crack tip element of size L, CODs at the quarter point B and corner point C can be calculated as:

$$v_B = \frac{(\kappa + 1)\sigma}{4G}\sqrt{\frac{L}{4}(2a - \frac{L}{4})} \qquad v_C = \frac{(\kappa + 1)\sigma}{4G}\sqrt{L(2a - L)} \tag{2.15}$$

Inserting these values in Equation 2.13 yields

$$\sqrt{L(2a - L)} = 2\sqrt{\frac{L}{4}(2a - \frac{L}{4})} \tag{2.16}$$

Equation 2.16 results in $L = 0$. However, in FEA the size of the crack tip element cannot be zero.

Inserting Equation 2.15 into Equations 2.7, 2.10 and 2.12 yields, for

nonlinear extrapolation:

$$K = \frac{1}{\sqrt{2}}\left(\sqrt{8 - \frac{L}{a}} - \sqrt{2 - \frac{L}{a}}\right)\sigma\sqrt{\pi a} \tag{2.17}$$

linear extrapolation:

$$K = \frac{\sqrt{2}}{6}\left(2\sqrt{8 - \frac{L}{a}} - \sqrt{2 - \frac{L}{a}}\right)\sigma\sqrt{\pi a} \tag{2.18}$$

and quarter-point displacement:

$$K = \frac{\sqrt{2}}{4}\sqrt{\left(8 - \frac{L}{a}\right)}\,\sigma\sqrt{\pi a} \tag{2.19}$$

Equations 2.17, 2.18, and 2.19 are normalized and plotted in Figure 2.9 as a function of the dimensionless element length L/a at the crack tip. The exact solution is $K/\sigma\sqrt{\pi a} = 1$. As can be seen, linear extrapolation (Equation 2.18) gives the most accurate result and is largely insensitive to element length. Its error for $L = 0.5a$ is about 0.2%. As the crack tip element becomes longer, the quarter-point displacement (Equation 2.19) increasingly underestimates SIF. Nonlinear extrapolation (Equation 2.17), the least accurate of the three, increasingly overestimates SIF.

Detailed results of relative accuracy are given in appendix A for finite-width plates under tension and bending.

2.5.2 Stress-Based Methods

SIFs can also be calculated from the normal stress in elements leading the crack tip, $\alpha = 0.0$ in Figure 2.8. From LEFM, this stress in given by:

$$\sigma_y = \frac{K_I}{\sqrt{2\pi r}} \tag{2.20}$$

resulting in the following equation for the SIF:

$$K_I = \text{Lim}\,|_{r \to 0}\, \sigma_y \sqrt{2\pi r} \tag{2.21}$$

Since Equation 2.21 contains only the leading asymptotic term, the result is an apparent SIF at a discrete distance ahead of the crack tip. SIFs are then extrapolated to the crack tip using linear regression.

Since in FEA displacements are more accurate than stresses, K_I should be calculated from displacements of nodes trailing the crack rather than stresses in nodes leading the crack.

2.5.3 Energy-Based Methods

Energy-based computation of SIF is based on the energy release rate, J-integral , and stiffness derivative. These three approaches are discussed next.

Energy Release Rate

Irwin (1957) showed that the SIF is related to the strain energy release rate G for a mode I crack:

$$\begin{aligned} G &= \frac{(1 - \nu^2)}{E} K^2 \quad \textbf{(for plane strain)} \\ G &= \frac{1}{E} K^2 \quad \textbf{(for plane stress)} \end{aligned} \tag{2.22}$$

The strain energy released at the crack tip per unit area of newly formed crack surfaces is:

$$G = \pm\frac{dU}{dA} \approx \frac{\Delta U}{\Delta A} \tag{2.23}$$

where U is the elastic strain energy of the body containing the crack and A is the crack surface. The plus and minus signs refer to constant-load and constant-displacement conditions respectively.

In FEA the strain energy release rate is calculated for two slightly different crack lengths, the difference being of order $\Delta a/a$ = 1/50 of the original crack length. For each cracked body, the stored strain energy is calculated from the sum of the strain energies of all elements. The SIF can then be determined from Equations 2.22 and 2.23. The major weakness of this method is that two FEAs are needed.

J-Integral

Rice (1968) defined the J-integral as:

$$J = \int_{\Gamma}\left[Wn_1 - T_i\frac{\partial u_i}{\partial x}\right]ds \tag{2.24}$$

where Γ is any path beginning at the lower crack surface, encircling the crack tip, and ending at the upper surface. The strain energy density is given by $W = \frac{1}{2}\sigma_{ij}\varepsilon_{ij}$ for linear elasticity. n_1 is the x-component of the outward unit normal to Γ, $T_i = \sigma_{ij}n_j$ is the traction vector, and u_i is the displacement vector. The J-integral, one of seven conservation energy integrals in continuum mechanics, is path independent for any elastic material (Rice 1968) . For a linear elastic material, the J-integral and the energy release rate are equivalent:

$$J = G \tag{2.25}$$

To calculate the J-integral with FEA, stresses, strains and displacements are needed along a path surrounding the crack tip for use in Equation 2.24. But the components comprising the integrand, as determined from FEA, are likely to be inaccurate near the crack tip. Fortunately, path independence allows the contour to be chosen away from the crack tip. With the J-integral value determined, the SIF is then obtained from Equations 2.25 and 2.22:

$$K = \sqrt{EJ} \tag{2.26}$$

By using this method, only one FEA is needed per crack length.

Being an energy approach, the J-integral method has the advantage of not requiring an elaborate representation of the crack tip stress and strain fields. The J value is based on the strain energy of the mesh rather than individual local values of stresses, so that the result is still accurate even when the mesh is coarse.

Stiffness Derivative

A third way of computing SIFs from energy is the stiffness derivative method (Parks 1974), sometimes called the virtual crack extension method; it is a variant of the energy release rate method. The change in strain energy ΔU is associated with elements surrounding the crack tip and is evaluated by displacing the nodal points laying on a contour around the crack tip by an incremental distance, ΔL. This method, as employed widely today, is efficient and accurate.

Parks (1974) and Banks-Sills and Sherman (1992) investigated the equivalency of the J-integral and stiffness derivative methods. The contour J-integral of Equation 2.24 can also be converted into an area integral through Green's divergence theorem. The J-integral (contour or area) and stiffness derivative methods are theoretically equivalent. In reality, the equivalence depends on element type and computation method when the contour and area J-integrals are obtained from FEA.

Parks (1974) showed that the contour J-integral method is the same as the stiffness derivative method if constant-strain triangular elements are used. Banks-Sills and Sherman (1992) pointed out that for triangular and four-node isoparametric elements, stiffness derivative, area J-integral and contour J-integral are equivalent. For eight-node and eight-node quarter-point isoparametric elements, with three-point Gaussian integration, only the area J-integral method is equivalent to the stiffness derivative method. However, if the two-point Gaussian (reduced) integration rule is used, the three results are equivalent. Saouma and Schwemmer (1984) recommended the two-point Gaussian integration rule for fracture mechanics analysis.

The J-integral method is used in all cracked I-beam analyses performed in this study because it yields accurate results and can be obtained directly from the ABAQUS output through its special procedure *J-INTEGRAL.

2.6 Two-dimensional Model

The cracked I-beams were modeled in section 2.2 with shell elements in the actual 3-D configuration of web and flanges. Since the model is three-dimensional and the shell elements have at least five DOFs per node, the FEA is time consuming.

2.6.1 2-D Approach

This section explores the possibility of modeling a cracked I-beam in two dimensions. Figure 2.10 shows the schematic of the 2-D I-beam model, with the mid-planes of the flanges rotated by 90° onto a common plane with the web. The edges of the web mid-planes are joined to the centerlines of the flange mid-planes. This reduces the problem from 3-D to 2-D, making it possible to model the I-beam with eight-node plane-stress elements that have only two DOFs per node and reduced integration — ABAQUS designation CPS8R.

In this method the web and flanges should not be fully joined. Only the *y*-direction displacements of corresponding nodes along the junction line should be equated, thus allowing web and flanges to deform freely in the *x*-direction. If the *x*-direction displacements were also equated, the web and flanges would be over constrained, especially for long cracks.

Theoretically, the flanges could be at any angle. The only requirement is

that corresponding nodes along the junction line of the web and flanges have equal *y*-direction displacements. Practically, the flanges must rotate 90° because the plane-stress element has only two DOFs; therefore, the flanges and web must lie in the same plane.

Because the problem is now planar and the plane-stress element has only two DOFs per node, meshes are easily generated and software runs faster than in the 3-D I-beam model.

2.6.2 Numerical Results and Discussion

Parametric Analyses

Two-tip and three-tip cracked I-beams were analyzed for the following combinations of models, W-shapes, and loading:

- Models: 2-D and 3-D
- W-shapes: W40x149, W40x199, and W18x97; with cross-sectional area ratios of flanges and web $\beta = 2A_f/A_w = 0.83$, 1.37, and 2.05 respectively
- Loading: tension and bending

Besides the variables listed above, the two-tip cracked I-beams were analyzed for the following 27 combinations of:

- Crack eccentricity: $\varepsilon = e/(d_j/2) = 0.0$, 0.3, 0.7
- Web crack length: $\lambda_w = a_w/(d_j/2 - e) = 0.1$ to 0.9, in steps of 0.1

The three-tip cracked I-beams were analyzed for the following 18 combinations

of:

- Web crack length: $\lambda_w = a_w/d_j = 0.1$ and 0.5
- Flange crack length: $\lambda_f = a_f/(b_f/2) = 0.1$ to 0.9, in steps of 0.1

Altogether, 12(27+18) = 540 FEAs were performed to determine whether a simple 2-D model could replace a complex 3-D model without significant loss of accuracy in calculating SIFs.

A two-tip crack in an I-beam web is defined by the non-dimensional eccentricity of the crack midpoint about the major axis of the I-beam, $\varepsilon = e/(d_j/2)$, and the non-dimensional crack length, $\lambda_w = a_w/(d_j/2 - e)$. All dimensions are shown in Figure 1.8. Defining the coordinates as in Figure 2.1, the upper and lower crack tips are located at:

$$x_{upper} = (\varepsilon - \lambda_w + \varepsilon\lambda_w)\frac{d_j}{2}$$
$$x_{lower} = (\varepsilon + \lambda_w - \varepsilon\lambda_w)\frac{d_j}{2} \qquad (2.27)$$

For a three-tip cracked I-beam, the crack lengths are given by the two non-dimensional parameters $\lambda_w = a_w/d_j$ for the web crack and $\lambda_f = a_f/(b_f/2)$ for the flange crack. All dimensions are shown in Figure 1.9. With these definitions, the web and flange crack tips are located at:

$$x_{web} = (1 - 2\lambda_w)\frac{d_j}{2}$$
$$z_{flange} = \pm\lambda_f\frac{b_f}{2} \qquad (2.28)$$

SIFs computed with Equation 2.26 are compared next in terms of their ratio, K_{2D}/K_{3D}, where K_{2D} and K_{3D} are the SIFs from the 2-D and 3-D models.

Two-tip Cracked I-beams

Figures 2.11 and 2.12 compare SIFs for the upper and lower crack tips of an I-beam under tension and Figure 2.13 compares the SIFs for the lower crack tip of an I-beam under bending. Results for the upper crack tip of an I-beam under bending are not presented because the crack tip is near the neutral axes of the section and the SIF values are small. The trends are very similar in all three figures. Specifically:

- Relative to the 3-D model, the 2-D model consistently overestimates the SIFs. The error is always on the safe side. 2-D results exceed 3-D results by less than 1% for $\lambda_w \leq 0.6$ in Figure 2.11 and $\lambda_w \leq 0.5$ in Figures 2.12 and 2.13. The difference is largest at $\lambda_w = 0.9$, with values of 5% for the upper tip and 7% for the lower tip.
- For same eccentricity ε and crack length λ_w, the difference increases with cross-sectional area ratio of flanges to web. In another words, as β increases, the 2-D model underestimates the beneficial constraint provided by a heavier flange.
- For same area ratio β and crack length λ_w, the difference increases with eccentricity ε. That is, the closer a tip of a constant length crack gets to the flange (Equation 2.27), the more 2-D analysis underestimates the beneficial constraint provided by the flange.

Judging by these conclusions, one might expect that SIFs calculated with the 2-D model would approach those calculated with the 3-D model if both

the *x*- and *y*-direction displacements along the junction lines of web and flanges were equated — not just the *y*-direction displacements. To check this hypothesis, the following I-beams were reanalyzed with junction-line displacements equated in both directions:

- W-shapes: W40x149 ($\beta = 0.83$), W18x97 ($\beta = 2.05$)
- Loading: tension and bending
- Eccentricity: $\varepsilon = 0.0$ and 0.7
- Web crack length: $\lambda_w = 0.1$ and 0.9

It was found that a fully joined 2-D model always yields smaller SIF values than the 3-D model. The error is on the unsafe side. The maximum difference is about 20% for the W18X97 shape with $\varepsilon = 0.7$ and $\lambda_w = 0.9$. Clearly, equating also the *x*-direction displacements gives less accurate and unsafe SIF values.

Three-tip Cracked I-beams

SIFs for the web and flange crack tips are compared in Figures 2.14 and 2.15 for I-beams under tension and in Figures 2.16 and 2.17 for I-beams under bending. Good agreement between 2-D and 3-D models was found:

- For the web crack tip, the SIFs calculated with 2-D and 3-D models differ by at most ±1% (Figures 2.14 and 2.16). The only exception is I-beam W18x97 with $\lambda_w = 0.5$ and $\lambda_f = 0.1$ for which the maximum difference is 1.5% (Figure 2.16).
- For the flange crack tip, the difference is at most ±1% for flange cracks λ_f

≥ 0.3 (Figures 2.15 and 2.17). The maximum difference is about 4% for I-beam W18x97 with a web crack (λ_w = 0.5) significantly longer than the flange crack (λ_f = 0.1) (Figure 2.15).

2.6.3 Benefits of 2-D Modeling

Based on the results presented above, cracked I-beams can be conservatively modeled in 2-D, with only small losses in accuracy of determining SIFs.

In a 2-D model, mesh preparation is simplified and FEA software runs faster. For example, it took only 5 minutes to execute a FEA of a three-tip cracked I-beam in 2-D, versus 30 minutes in 3-D.

The small difference between the 2-D and 3-D analysis results strongly suggests that the interaction between the cracked web and flange is controlled mostly by the compatibility of *y*-direction displacements along the junction line.

Chapter 3: Parameters for Cracked I-beams

Most cracks found in I-beams of steel bridges have either two tips or three tips as shown in Figures 1.8 and 1.9. Two-tip web cracks are always eccentrically and, therefore the SIFs have different values for the upper and lower crack tips. Three-tip cracks are usually, but not always symmetric. As a result, two SIFs are needed; one for the web crack tip, and the other for the two flange crack tips.

3.1 Two-tip Cracked I-Beam

The SIF for a two-tip crack in the web of an I-beam, shown in Figure 3.1, is expressed as:

$$K^{A,B} = f^{A,B}\,\sigma\sqrt{\pi a_w} \tag{3.1}$$

where f is the correction factor, a_w is one-half of the web crack length, and the superscripts A and B represent the upper and lower crack tips, respectively. The reference stress σ is defined as the remote uniform stress in an I-beam under tension and the stress at the flange-web junction in an I-beam under bending.

The correction factors for each crack tip:

$$f^A = f^A(\lambda_w, \varepsilon, \beta)$$
$$f^B = f^B(\lambda_w, \varepsilon, \beta) \qquad (3.2)$$

are functions of normalized web crack length:

$$\lambda_w = \frac{a_w}{d_j/2 - e} \qquad (3.3)$$

normalized eccentricity:

$$\varepsilon = \frac{e}{d_j/2} \qquad (3.4)$$

and cross-sectional area ratio of flanges to web:

$$\beta = \frac{2A_f}{A_w} \qquad (3.5)$$

In the above equations, $d_j = d - t_f$ is the web depth between the upper and lower junction points, e is the eccentricity, and A_f and A_w are the cross-sectional areas of the flange and web (Figure 3.1). Parameters λ_w and ε describe the length and eccentricity of the crack.

Parameter β accounts for the constraint imposed by the flanges on the web crack. It is basically an axial rigidity. Isida (1973a) also used the area ratio to account for the interaction between two joined half planes of different thicknesses under tension, and when he analyzed the problem of a series of joined strips under tension, the same parameter was used. Cartwright and Miller (1975) analyzed two uniformly stressed infinite sheets, each containing a central crack. The two sheets bisect each other at a right angle. The cracks lie in the same plane and are centered about a common point on the junction line.

Again the interaction between the two intersecting cracked sheets was expressed in terms of their area ratio. The plates analyzed by Isida (1973a) and Cartwright and Miller (1975) are infinitely wide, and all joined parts are stressed. Therefore, only the axial rigidity needed to be modeled.

Isida (1973) calculated the SIF for a central crack in a plate with edge stiffeners under axial stress applied only on the plate. Both the plate and stiffener widths were finite. He chose two parameters α and β, where α is the ratio of flexural rigidities, EI, and β is the ratio of axial rigidities, EA, of stiffeners and plate. While he accounted for the effect of bending rigidity, Isida pointed out that the axial rigidity affects the SIF most. The flexural rigidity is appreciable only when the crack tip moves close to the stiffeners.

The two-tip cracked I-beam differs from the problems of Isida (1973a) and Cartwright and Miller (1975) in that the web and flange widths are finite. It also differs from Isida's (1973) problem in that both the web and flange plates are stressed.

3.2 Three-tip Cracked I-Beam

The SIF for a symmetric three-tip cracked I-beam, shown in Figure 3.2, is expressed as:

$$K^{w,f} = f^{w,f} \sigma \sqrt{\pi a_{w,f}} \tag{3.6}$$

where f is the correction factor, and a_w and a_f are the web and flange crack

lengths. The subscripts and superscripts *w* and *f* represent the web and flange crack tips, respectively. As for the two-tip crack, the reference stress σ is defined as the remote uniform stress for an I-beam under tension and the stress at the flange-web junction for an I-beam under bending.

Here, the correction factors for the web and flange crack tips:

$$f^w = f^w(\lambda_w, \lambda_f, \beta)$$
$$f^f = f^f(\lambda_w, \lambda_f, \beta) \qquad (3.7)$$

are functions of normalized web crack length:

$$\lambda_w = \frac{a_w}{d_j} \qquad (3.8)$$

normalized flange crack length:

$$\lambda_f = \frac{a_f}{b_f/2} \qquad (3.9)$$

and cross-sectional area ratio of flanges and web:

$$\beta = \frac{2A_f}{A_w} \qquad (3.10)$$

In the above equations, b_f is the flange width. Parameters λ_w and λ_f describe the web and flange crack lengths (Figure 3.2). The web is under uniform or linear stress depending on the loading conditions. The flange is always under uniform stress.

Parameter β, again, is the cross-sectional area ratio of flanges and web. Chen (1992), in his analysis of three-tip cracked I-beams, used the parameter

A_f/A_w. Here the more common ratio of both flange areas divided by the web area is used, $\beta = 2A_f/A_w$.

3.3 Validation of Parameter β

The parameters in the correction factor Equation 3.2 for the two-tip crack and Equation 3.7 for the three-tip crack account for two major effects: (1) the web crack length and eccentricity of the two-tip crack, and the web and flange crack lengths of the three-tip crack; and (2) cross-sectional dimensions of the web and flanges.

The validity of β as an independent parameter is checked numerically by comparing correction factors for W-shapes that have significantly different geometries but equal β values. For example, Table 3.1 lists seven pairs of rolled W-shapes with equal β values. All were taken from the Manual of Steel Construction (Manual 1986). If the correction factors can be shown to be nearly equal for each pair of W-shapes, then β can be used as an independent parameter.

Finite element analyses were performed for the seven pairs of rolled W-shapes identified by the footnote (a) in Table 3.1. These pairs were selected because: (1) their β values of 0.83 to 1.91 cover most of the range of β values for W-shapes listed in the Manual, and (2) the width-thickness ratios of the web and flanges satisfy the minimum requirements for using shell elements. Typical

finite element meshes for two-tip and three-tip cracked I-beams are shown in Figures 2.7 and 2.9.

Parameter β is validated next for both two-tip and three-tip cracked I-beams under tension or bending.

3.3.1 Two-tip Crack under Tension and Bending

Correction factors were calculated for two-tip cracked I-beams under tension, with a central crack in the web varying in length from $\lambda_w = a_w/(d_j/2) =$ 0.1 to 0.9 in steps of 0.2. The material properties for both the web and flanges were Young's modulus, $E = 200$ GPa, and Poisson's ratio, $v = 0.3$. Figure 3.3 compares results for each pair of W-shapes. The ordinate is the ratio of the correction factors for shapes 1 and 2, $f^{(1)}/f^{(2)}$.

As Figure 3.3 shows, the correction factors for two shapes of equal β values differ by less than 1% for crack lengths up to $\lambda_w = 2a_w/d_j \leq 0.7$ and less than 2% for crack lengths up to $\lambda_w < 0.9$. The sole exception is shape 2 with $\beta =$ 1.11 (W36X170 in Table 3.1) whose correction factor is 3.5 % larger than its shape 1 counterpart (W40X192). Differences smaller than 3.5% would be preferable. On the other hand, linear-elastic fracture mechanics would no longer be valid at crack lengths $\lambda_w = 0.9$ since the net ligament would yield. Clearly, β is a valid parameter

Another parameter, besides β, that may affect the SIF is the depth-width

ratio $\gamma = d_j/b_f$, where d_j is the web depth between junction points and b_f is the flange width. In an analogy to the structure of a mammal, the parameter γ is to the skeleton as the parameter β is to the flesh.

Values of γ for all selected W-shapes are listed in Table 3.1. For each pair having equal area ratios, γ is always smaller for shape 1 than shape 2; meaning that, for same area ratio β, shape 2 is relatively deeper and narrower than shape 1. A narrower and thicker flange (shape 2) constrains the web crack more than does a wider and thinner flange (shape 1). This explains why the ratio of correction factors $f^{(1)}/f^{(2)}$ is greater than unity in Figure 3.3.

Ideally, both parameters β and γ should be used to improve the accuracy of calculating SIFs. But γ is about a linear function of β as Figure 3.4 shows for all shapes listed in the Manual. Each data point corresponds to one W-shape. The sections used in validating β are identified with solid symbols. Shapes 1 lie near the bottom of the bandwidth and shapes 2 near the middle. The variation in γ values accounts for the slight differences in correction factors for W-shapes with equal β values — less than 1% for crack lengths up to $\lambda_w = 2a/d_j \leq 0.7$ (Figure 3.3).

Since γ is approximately a linear function of β, and the difference between the correction factors for shapes 1 and 2 is small, the W-shapes are characterized with the parameter β alone in the subsequent finite element calculations.

The exception to the trend shown in Figures 3.3 and 3.4 is the W40X192

(shape 1) section with $\beta = 1.11$ and $\gamma = 2.11$, which has a wider flange relative to the depth than is common in W-shapes used as flexural members for bridges. Because it is an outlier, the W40X192 is omitted in subsequent calculations.

Parameter β was also validated for the two-tip center-cracked I-beam under bending, but on a smaller scale than was done for I-beams in tension. Instead of all seven pairs of W-shapes, only the three pairs with $\beta = 0.83$, 1.37 and 1.91 were analyzed. As Figure 3.5 shows, the maximum difference between the correction factors for two shapes with equal β values is about 1%.

3.3.2 Three-tip Crack under Tension and Bending

Interaction between the web and flanges of a three-tip cracked I-beam differs from that of a two-tip cracked I-beam. In a three-tip cracked I-beam, the cracks bisect the line joining the web and flange, thus complicating the interaction.

Correction factors for both the web and flange cracks were calculated for the following combinations: flange-web area ratio, $\beta = 0.83$ and 1.91 (smallest and largest values); web crack length, $\lambda_w = a_w / d_1 = 0.1$ and 0.5; and flange crack length, $\lambda_f = 2a_f / b_f = 0.1$ to 0.9 in steps of 0.2. The results are shown in Figures 3.6 and 3.7 for tension, and Figures 3.8 and 3.9 for bending. Differences between correction factors were found to be less than 2%,

suggesting that parameter β characterizes cracked W-shapes well.

3.4 Summary and Conclusions

Correction factors for two-tip and three-tip cracked I-beams were found to be functions of crack length, crack position, and area ratio of web and flanges. The validation of β as an independent parameter was checked for both two-tip and three-tip cracked I-beams under tension and bending. The following is concluded:

- Two different W-shapes of equal β values have nearly equal correction factors, the maximum difference being less than 2%. Thus, parameter β accounts for the interaction between the web and flanges.
- The depth-width ratio of a W-shape, $\gamma = d/b_f$, is not a significant parameter in the calculation of SIFs. It becomes noticeable only for long cracks. For all I-beams listed in the Manual, β and γ are related about linearly within a bandwidth.

Since the W-shapes listed in the Manual can be grouped according to parameter β alone, the number of FEAs in Chapter 5 can be reduced. Analyses are needed only for typical W-shapes, and fitted functions for correction factors become simpler.

The Manual lists 297 W-shapes, of which about 170 are typically used as beams. To create a database of correction factors, it is not necessary to

analyze all W-shapes. Instead, in this study, nine W-shapes are retained for finite element analyses in Chapter 5. Besides the seven W-shape 1 sections used for β validation, two more were selected — W33X201 with β = 1.53 and W18X97 with β = 2.05. All nine are identified with a superscript *b* in Table 3.1.

The values of β = 0.83 to 2.05 for the nine W-shapes to be analyzed in Chapter 5 cover the range of β = 0.77 to 2.25 for all W8 to W40 I-beams listed in the Manual (Figure 3.10).

Such selected calculation range also covers part of welded girders. In civil engineering, the size of the top flange and the bottom flange of a welded girder may not be the same. For positive bending girders, A_{tf}/A_w = 0.24 to 0.41 and A_{bf}/A_w = 0.33 to 1.11 (Schilling, private communication), where A_{tf} is the top flange area, A_{bf} is the bottom flange area, and A_w is the web area. For negative bending girders, A_{tf}/A_w = 0.50 to 1.51 and A_{bf}/A_w = 0.61 to 1.71 (Schilling, private communication). Parameter β for a welded girder is defined as β = $2A_{bf}/A_w$, thus β = 0.66 to 2.22 for positive bending girders and β = 1.22 to 3.42 for negative bending girders. Therefore, parameter β selected for finite element analysis covers 77% of positive bending girders and 42% of negative bending girders. However, for welded girders, to use the results of this study, the relationship between skelton ratio γ and cross-sectional area ratio β should lie within the fuzzy band as shown in Figure 3.4.

Chapter 4: Non-interacting Three-tip Cracks

4.1 Introduction

A three-tip cracked I-beam is modeled as a combination of an edge-cracked web and a center-cracked bottom flange, with the top flange remaining uncracked. Starting from the junction point, the cracked web and flange are joined along the full length of the junction line. When separated from each other, the cracked web and flange deform independently in their own planes. However, once joined to form an I-beam, corresponding points on the junction line must displace by equal amounts. In other words, displacements of nodes on the junction line common to both the web and flange must be compatible.

To enforce displacement compatibility, pairs of equal and opposite interaction forces must be applied at each node on the junction line. The values of the interaction forces depend on the relative lengths of web and flange cracks. If the displacements along the flange centerline are larger than those of the corresponding nodes along the web edge, the flange magnifies the opening of the web crack while the web restrains the opening of the flange crack. Conversely, if the displacements along the flange centerline are smaller than those of the corresponding points along the web, the flange restraints the opening of the web crack while the web magnifies the opening of the flange crack. Since the process reverses depending on the relative crack lengths of

web and flange, there should be pairs of matching crack lengths that induce compatible displacements. For each such pair, the interaction forces would be zero at the junction point and small — perhaps even negligible — at points along the junction line away from the junction point. This condition is hereafter referred to as one of non-interacting cracks.

4.2 Joined Infinite Plates

The first problem analyzed in this chapter is that of a center-cracked infinite plate bisected perpendicularly with an edge-cracked semi-infinite plate as shown in Figure 4.1. The plates, joined along the centerline of the infinite plate and the edge of the semi-infinite plate, are under uniform tension.

4.2.1 Centerline Displacements

The exact displacement solutions for a center-cracked infinite plate subject to uniform tension stress σ, shown in Figure 4.2(a), can be found with the Musklishvili stress function method. In two-dimensional elasticity, displacements u in the x direction and v in the y direction can be expressed in terms of a complex function $\phi(z)$:

$$\begin{aligned} 2\mu u &= (\kappa - 1)\mathrm{Re}[\phi(z)] - 2y\,\mathrm{Im}[\phi'(z)] + Ax \\ 2\mu v &= (\kappa + 1)\mathrm{Im}[\phi(z)] - 2y\,\mathrm{Re}[\phi'(z)] - Ay \end{aligned} \qquad (4.1)$$

where $z = x + iy$, $\kappa = 3 - 4\nu$ for plane strain, and $\kappa = (3 - \nu)/(1 + \nu)$ for plane

stress. The material constants are the shear modulus $\mu = E/2(1 + \nu)$, Poisson's ratio ν, and Young's modulus E. The boundary conditions for an infinite-width plate with a central crack:

$$\begin{aligned} \sigma_y &= \tau_{xy} = 0, \qquad (y = 0,\ -a < x < a) \\ \sigma_x &= 0,\ \sigma_y = \sigma,\ \tau_{xy} = 0, \qquad \text{as } |z| \to \infty \end{aligned} \tag{4.2}$$

yield the constant $A = -\sigma/2$ and, in turn, the stress function:

$$\phi(z) = \frac{\sigma}{2}\sqrt{z^2 - a^2} - \frac{\sigma}{4}z \tag{4.3}$$

Inserting the constant A and stress function $\phi(z)$ into Equation 4.1, and assuming plane stress, the displacement along the centerline, on $x = 0$, is obtained as:

$$v = \frac{\sigma}{E}\left[\nu y + \frac{(1 - \nu)y^2 + 2a^2}{\sqrt{y^2 + a^2}}\right] \tag{4.4}$$

At the crack mouth, $x = 0$ and $y = 0$, the displacement is reduced to the simple form:

$$v = 2\frac{\sigma}{E}a \tag{4.5}$$

Therefore, the crack mouth opening displacement (CMOD) is

$$\delta = 2v = 4\frac{\sigma a}{E} \tag{4.6}$$

4.2.2 Edge Displacements

For an edge-cracked semi-infinite plate, the displacement along the edge can be obtained with Paris' (1957) method.

Paris' Method

From Castigliano's theorem, the displacement in the direction of a force

F is

$$\Delta_F = \frac{\partial U_T}{\partial F} \tag{4.7}$$

where the total strain energy U_T is the sum of the strain energy in the noncracked plate and the strain energy generated as the crack is introduced while the load is held constant:

$$U_T = U_{\text{no crack}} + \int_0^A \frac{\partial U_T}{\partial A} dA \tag{4.8}$$

According to Equations 4.7 and 4.8, the displacement is then:

$$\Delta_F = \frac{\partial U_{\text{no crack}}}{\partial F} + \frac{\partial}{\partial F}\int_o^A \frac{\partial U_T}{\partial A} dA \tag{4.9}$$

where the first addend on the right side of Equation 4.9 is the load-point displacement of the noncracked plate:

$$\frac{\partial U_{\text{no crack}}}{\partial F} = \Delta_{F\ \text{no crack}} \tag{4.10}$$

The second term on the right side of Equation 4.9 is calculated as follows. The crack extension force, G, is equal to the rate at which the total strain energy, U_T, increases with crack area, dA, under constant-force loading:

$$G = \frac{\partial U_T}{\partial A}\Big|_{\text{constant force}} \tag{4.11}$$

For a mode I crack, G is related to the SIF by:

$$EG = K_I^2 \tag{4.12}$$

Now in a body loaded by a force, P, and virtual force, F, the SIF is additive:

$$K_I = K_{IP} + K_{IF} \tag{4.13}$$

and Equation 4.12 becomes:

$$EG_I = (K_{IP} + K_{IF})^2 \tag{4.14}$$

Inserting Equations 4.10, 4.11 and 4.14 into Equation 4.9 and letting the

virtual force approach zero ($F \to 0$) yields the displacement of the virtual force:

$$\Delta_F = \Delta_{F \text{ no crack}} + \frac{2}{E}\int_0^A K_{IP} \frac{\partial K_{IF}}{\partial F}\, dA \qquad (4.15)$$

Therefore, Δ_F may be computed from the equations for the displacement with no crack present and the SIFs.

Edge Displacement

According to Equation 4.15, the displacement along the edge of an edge-cracked semi-infinite plate under uniform tension is determined as follows. A pair of virtual forces F is applied at two symmetric points along the edge where the displacement is to be determined, as shown in Figure 4.2(b). The SIF is for uniform tension:

$$K_{IP} = 1.1215\,\sigma\sqrt{\pi a} \qquad (4.16)$$

and for the virtual force pair F (Tada 1973):

$$K_{IF} = \frac{2F}{\sqrt{\pi a}}(1 + \alpha \sin^2\theta)\cos\theta\, F(\theta) \qquad (4.17)$$

where θ is defined in Figure 4.2(b):

$$\theta = \arctan\frac{y}{a} \qquad (4.19)$$

The function $F(\theta)$ is given by:

$$F(\theta) = 1.12 + 0.18\,\mathrm{sech}(\tan\theta) \qquad (4.18)$$

and parameter $\alpha = \frac{1}{2}(1 + \nu)$. Inserting Equations 4.16 through 4.19 into the second term on the right side of Equation 4.15 yields

$$\Delta_{F\ crack} = \frac{2}{E}\int_o^a K_{IP}\frac{\partial K_{IF}}{\partial F}da$$
$$= \frac{2}{E}\cdot 1.1215\sigma\sqrt{\pi a}\cdot\frac{2}{\sqrt{\pi a}}(1+\alpha\sin^2\theta)\cos\theta\, F(\theta)\cdot a \qquad (4.20)$$
$$= \frac{4\sigma a}{E}\cdot 1.1215\,(1+\alpha\sin^2\theta)\cos\theta\, F(\theta)$$

The first term on the right side of Equation 4.15 is calculated as the change in length of a noncracked plate of length, $2a\tan\theta$:

$$\Delta_{F\ no\ crack} = \frac{2\sigma a}{E}\tan\theta \qquad (4.21)$$

The total displacement between the virtual forces F is

$$\Delta_F = \Delta_{F\ crack} + \Delta_{F\ no\ crack} \qquad (4.22)$$

Inserting Equations 4.20 and 4.21 into Equation 4.22 yields

$$\Delta_F = \frac{2\sigma a}{E}\left[\frac{1}{2}\tan\theta + 1.1215\,(1+\alpha\sin^2\theta)\,F(\theta)\cos\theta\right] \qquad (4.23)$$

At the crack mouth, where $\theta = 0$, Δ_F becomes the CMOD:

$$\Delta_F = 2v \qquad (4.24)$$

and the CMOD is

$$\delta = 2v = 4\frac{\sigma^o a}{E}[1.458] \qquad (4.25)$$

4.2.3 Non-interacting Crack Lengths

Non-interacting (matching) crack lengths are obtained by equating the CMOD of the center-cracked infinite plate (Equation 4.6) to that of the edge-cracked semi-infinite plate (Equation 4.25):

$$a_c = 1.458\,a_e \qquad (4.26)$$

where a_c is the central crack length and a_e is the edge crack length.

To check whether the calculated non-interacting crack lengths have

compatible displacements along the junction line, the centerline displacements of an infinite plate and the edge displacements of a semi-infinite plate are compared. Inserting Equation 4.26 into displacement Equations 4.4 yields the non-dimensional displacement of the center-cracked plate:

$$\frac{v_c / a_e}{\sigma / E} = \nu \frac{y}{a_e} + \frac{(1-\nu)(y/a_e)^2 + 2 \cdot 1.458^2}{\sqrt{(y/a_e)^2 + 1.458^2}} \qquad (4.27)$$

while the non-dimensional displacement of the edge-cracked plate is:

$$\frac{v_e / a_e}{\sigma / E} = \frac{y}{a_e} + 2.24 \left[1 + \alpha \left(\frac{y}{a_e} \right)^2 \right] \frac{F\left[\arctan (y/a_e)\right]}{\cos\left[\arctan (y/a_e)\right]} \qquad (4.28)$$

where v_c and v_e are the displacements along the junction line of the center- and edge-cracked plates respectively, and y is the coordinate of the point where the displacement is being calculated. In Figure 4.3, Equations 4.27 and 4.28 are plotted in terms of normalized displacement, $(v/a_e)/(\sigma/E)$, versus normalized distance, y/a_e. Equation 4.28 (for edge crack) is plotted as a solid line, and Equation 4.27 (for central crack) as a dashed line. The CODs are equal at the junction point, but differ somewhat along the junction line for $0 < y < 3a_e$, and are nearly equal for $y > 3a_e$.

The question arises as to how joining the two plates at the junction point only — versus joining them along the entire junction line — affects the SIFs. Unfortunately, an analytical and numerical solutions are difficult to obtain for joined infinite plates. So, in the following section two joined finite plates, one center-cracked and the other edge-cracked, are analyzed with FEA.

4.3 Joined Finite Plates

As was done in section 4.2, when an edge-cracked finite-width plate (called T-web) is joined with a center-cracked finite-width plate (called T-flange) to form a T-section, non-interacting is defined as both cracks having equal CMODs at the junction point. As an example, the T-flange and T-web studied in this section have the same thickness t = 10 mm, width W = 200 mm, and Young's modulus E = 207 GPa. The T-flange is under tension and the T-web is under tension or bending with reference stress of σ = 100 MPa, as shown in figure 4.4.

4.3.1 CMODs

For a center-cracked finite-width plate under tension, the T-flange, the CMOD is given by Tada (1973):

$$\delta = \frac{4\sigma a}{E} V_1\left(\frac{2a}{W}\right) \tag{4.29}$$

where the displacement correction factor is

$$V_1\left(\frac{2a}{W}\right) = -0.071 - 0.535\left(\frac{2a}{W}\right) + 0.169\left(\frac{2a}{W}\right)^2 + 0.020\left(\frac{2a}{W}\right)^3 - 1.071\frac{\ln\left(1-\frac{2a}{W}\right)}{\left(\frac{2a}{W}\right)} \tag{4.30}$$

and a is the half crack length, W is the plate width, and σ is the reference remote stress. This formula has better than 0.6% accuracy for any a/W (Tada

1973).

The CMOD for an edge-cracked finite-width plate under tension, the T-web, is also given by Tada (1973):

$$\delta = \frac{4\sigma a}{E} V_1\left(\frac{a}{W}\right) \tag{4.31}$$

where

$$V_1\left(\frac{a}{W}\right) = \frac{1.46 + 3.42\left(1 - \cos\frac{\pi a}{2W}\right)}{\left(\cos\frac{\pi a}{2W}\right)^2} \tag{4.32}$$

Here, a is the edge crack length.

When the edge-cracked plate is under bending, the CMOD takes the same form as Equation 4.31, but the reference stress σ becomes the remote bending stress at the extreme fiber of the plate, and the displacement correction function is (Tada 1973):

$$V_1\left(\frac{a}{W}\right) = 0.8 - 1.7\left(\frac{a}{W}\right) + 2.4\left(\frac{a}{W}\right)^2 + \frac{0.66}{\left(1 - \frac{a}{W}\right)^2} \tag{4.33}$$

As a/W approaches zero, Equations 4.29 and 4.31 reduce to Equations 4.6 and 4.25 for infinite plates.

4.3.2 Non-interacting Crack Lengths

For T-flange crack lengths of $2a_f/W = 0.1$ to 0.9 in steps 0.05, the corresponding non-interacting T-web crack lengths were calculated by equating 4.29 and 4.31.

The results are listed in Table 4.1, with the first pair of columns listing the T-flange crack length and the second and third pairs of columns listing the corresponding non-interacting T-web crack lengths for tension and bending. As shown in Figure 4.5, the non-interacting T-web crack length a_w is always shorter than the corresponding T-flange crack length a_f.

4.3.3 Comparison with Single Plate Solutions

To validate the calculated non-interacting crack lengths, the SIFs and COD profiles of the non-interacting cracks in the T-section are compared with those of single plate solutions.

This is done first, for SIFs of three non-interacting crack lengths selected from Table 4.1: a_f = 30.0 mm, a_w = 20.55 mm; a_f = 50.0 mm, a_w = 34.79 mm; and a_f = 70.00 mm, a_w = 50.98 mm. SIFs for single plates are given by Tada (1973) while those for the T-section were calculated with FEA. As shown in Figure 4.6, the SIFs of T-section cracks are about equal to those of the single plate cracks. The maximum difference is less than 3.5%.

Compared next, in Figure 4.7, are the COD profiles of the non-interacting flange and web cracks, a_f = 50.0 mm a_w = 34.79 mm. Because there are no analytical solutions for the COD profiles of finite-width plates, the comparison is limited to those calculated with FEA. As can be seen, the COD profiles of the T-section cracks are very similar to the corresponding profiles of

the single plates.

Finally, Figure 4.8 compares the displacements along the junction line of the T-section with those of the corresponding single plates. Again, lacking analytical solutions, the comparison is limited to displacements calculated with FEA. The results agree well, meaning that, for non-interacting crack lengths, displacements along the junction line differ by a small amount, irrespective of whether the plates are joined or separated.

The above examples show that SIFs and CODs for the T-section with non-interacting crack lengths can be calculated with good accuracy from single-plate solutions.

On the other hand, when crack lengths are mismatched, differences between the COD profiles of the T-section and single plates become large. This is shown in Figure 4.9 for a T-section with a_f = 50.0 mm and a_w = 100.0 mm, the latter being about three times the matching crack length of 34.79 mm (table 4.1). When separated, the single edge-cracked plate has a CMOD of 3.29 μm and the single center-cracked plate has 0.39 μm. When the two plates are joined to form a T-section, the interaction forces reduce the CMOD of the edge crack and enlarge the CMOD of the central crack to a common value of 0.56 μm.

Figure 4.10 shows big differences in displacements of the T-section and the single plates along the junction line. Obviously, mismatched crack lengths induce large interaction forces in a T-section, and the SIFs and CODs for the T-

web and T-flange cracks cannot be replaced by single-plate solutions.

4.4 I-beams

Three-tip cracked I-beams are modeled as an edge-cracked web plate joined to a center-cracked bottom flange and a noncracked top flange. The web and flanges are represented by their mid-planes; the web is joined to the flanges along the intersection lines of the mid-planes (Figure 2.2). Non-interacting crack lengths for the eight representative I-beams listed in Table 4.2 were calculated with two methods: one is based on CMODs, the other on a combination of FEA and single plate solutions.

4.4.1 Non-interacting Crack Lengths From CMODs

In this method, an I-beam is replaced by a T-section whose web and flange are equal to the cracked web and bottom flange of the I-beam. The I-beam stress is applied on the T-section. The non-interacting crack lengths are determined by equating the CMODs of the flange and web cracks, Equations 4.29 and 4.31.

In the process, since the T-section has only one flange, the effect of the I-beam's top flange was neglected. The error should be small because the web crack of a non-interacting three-tip cracked I-beam is often short and hence the crack tip does not approach the top flange.

Non-interacting flange crack lengths were calculated for web crack lengths beginning with $\lambda_w = a_w/d_j = 0.05$ and increasing in steps of 0.05. The incrementation was stopped when the corresponding flange crack would have become longer than the flange width, which is not physically possible. The results for the eight I-beams are listed in Table 4.2. Crack lengths, a_w and a_f, net web depth d_j, and flange width b_f are shown in Figure 3.2.

4.4.2 Non-interacting Crack Lengths From FEA

Non-interacting crack lengths were also obtained from FEA of the eight I-beams listed Table 4.2, with the following crack lengths:

- Web crack lengths: $\lambda_w = a_w/d_j = 0.1$ to 0.7, in steps of 0.1
- Flange crack lengths: $\lambda_f = 2a_f/b_f = 0.1$ to 0.9, in steps of 0.1

The web and flange of an I-beam with non-interacting cracks can be separated and the SIFs of the web and flange cracks are equal to those of the corresponding edge-and center-cracked plates. Therefore, the non-interacting crack lengths are determined here as the value at the intersection point of the I-beam and single-plate solutions.

For example, in Figure 4.11, the normalized SIF for the flange crack tip of I-beam W33X201 is plotted with a dashed curve as a function of flange crack length $\lambda_f = 2a_f/b_f$. The web crack length is $\lambda_w = a_w/d_j = 0.1$. In the same figure, the center-cracked plate solution (Tada 1973) is plotted with a solid curve. At

the intersection point of the two curves lies the non-interacting flange crack length with value of $\lambda_f = 2a_f/b_f = 0.50$.

The same non-interacting flange crack length can also be determined by equating the SIF for the web crack to Tada's (1973) solution for an edge-cracked plate. According to Figure 4.12, the non-interacting flange crack length is $\lambda_f = 2a_f/b_f = 0.50$ for a web crack length $\lambda_w = a_w/d_j = 0.1$.

Pairs of non-interacting web and flange crack lengths are listed in Table 4.2 for eight I-beams and two loadings — tension and bending, with the results being determined in the left column by equating K_f values and in the right column by equating K_w values.

4.4.3 Comparison

Figures 4.13 and 4.14 compare non-interacting flange crack lengths determined from CMOD and FEA for I-beams are under tension or bending. The former were determined from matching CMODs from single-plate solutions. The latter were determined from equating SIFs from FEAs and single-plate solutions.

Non-interacting flange crack lengths are plotted as a function of depth-width ratio γ instead of area ratio of flanges to web, β, as was done in Chapter 3. Since the web and flange do not interact, the area ratio is not important in this case.

Figures 4.13 and 4.14 show that the non-interacting crack lengths determined from FEA SIFs for flange or web cracks (dashed lines) agree well. The maximum difference is less than 8%.

The non-interacting crack lengths determined from FEAs (dashed curves) differ from those determined from CMODs (solid curve) by at most 10%. This difference is attributed to matching only CMODs at the junction point in the latter case, which does not account for additional, but limited, interaction forces along the junction line away from the crack mouth.

4.5 Conclusions

Non-interacting crack lengths are useful in understanding the behavior of three-tip cracked I-beams. For example, if the web crack length is shorter than its non-interacting length, the web crack restrains the opening of the flange crack under load while its own opening is being magnified. Conversely, if the web crack is longer than its non-interacting length, it magnifies the opening of the flange crack while its own opening is being restrained.

A clear understanding of interaction between web and flange cracks may assist in developing a rapid, approximate method of calculating SIFs in a three-tip cracked I-beam. Such a method might consist of the following steps:

1. Calculate the SIFs for the web and flange cracks due to the applied load from single-plate solutions.

2. Determine the interaction forces of equal magnitude and opposite signs needed to make the CMODs equal.
3. Calculate the SIFs due to the interaction forces.
4. Add the SIFs due to the applied load (step 1) and interaction forces (step 3) to obtain the SIFs of the three-tip cracked I-beam.

Chapter 5: Stress Intensity Factors for Cracked I-beams

5.1 Introduction

This chapter presents the numerical results of SIFs for two-tip and three-tip cracked I-beams under tension or bending. The SIFs were calculated from the output of finite element analyses. Nine typical I-beams selected from AISC Manual (1986), as listed in Table 3.1, were analyzed with FEA. For each I-beam, crack lengths and eccentricities were varied over wide ranges.

5.2 Two-tip Cracked I-beams

The SIFs for a two-tip crack in the web of an I-beam are expressed as:

$$K^{A,B} = f^{A,B}\sigma\sqrt{\pi a_w} \tag{5.1}$$

where a_w is one-half of the web crack length, and the superscripts A and B represent the upper and lower crack tips, respectively. The reference stress σ is defined as the remote uniform stress in an I-beam under tension and the stress at the flange-web junction in an I-beam under bending. The correction factor f is a function of normalized web crack length λ_w, eccentricity ε, and flanges to web cross-sectional area ratio β.

5.2.1 Variables in Analysis

The variables used in the FEAs of the two-tip cracked I-beams are summarized in the following. These were based on the modeling results of Chapter 2 and the benchmark studies of Appendix A.

- Two-tip crack in web
- Nine normalized web crack lengths: λ_w = 0.1 to 0.9, in steps of 0.1
- Six normalized eccentricities: ε = 0.0 (central crack), and 0.1 to 0.9 in steps of 0.2
- Nine W-shapes listed in Table 3.1
- Two types of loading: tension and bending
- Number of FEAs:

  (9 crack lengths)×(6 eccentricities)×(9 W-shapes)×(2 loadings) = 972
- I-beam modeling method: 3-D model, web and flanges represented by their mid-planes, with all DOFs joined along the junction lines of web and flanges
- Elements: eight-node shell element, reduced integration, five degrees of freedom per node, ABAQUS designation S8R5
- Crack tip elements: degenerated quarter-point elements from S8R5
- Mesh pattern around crack tip: m x n = 3 x 16 (Figure 2.4)
- Mode I SIFs obtained from J-integral of ABAQUS output

The positions of the upper and lower crack tips are described by the crack length λ_w and eccentricity ε. Different combinations of λ_w and ε yield

different upper and lower crack tip positions. In this study, the lowest upper tip position is at $x = 0.89d_j/2$ for $\lambda_w = 0.1$ and $\varepsilon = 0.9$; the highest upper tip is at $x = -0.9d_j/2$ for $\lambda_w = 0.9$ and $\varepsilon = 0.0$. The lowest position of the lower tip is at $x = 0.99d_j/2$ for $\lambda_w = 0.9$ and $\varepsilon = 0.9$; the highest lower tip is at $x = 0.1d_j/2$ for $\lambda_w = 0.1$ and $\varepsilon = 0.0$.

5.2.2 Two-tip Cracked I-beams under Tension

The calculated correction factors for the upper and lower crack tips are listed in Tables 5.1 and 5.2 respectively, as a function of crack length λ_w, eccentricity ε, and flanges to web area ratio β. The same results are plotted in Figures 5.1 through 5.3 as functions of parameters λ_w and β. Each surface corresponds to a constant ε. For a central crack, $\varepsilon = 0$, the correction factors for the upper and lower crack tips are equal (Figure 5.1). For an eccentric crack, the correction factors are plotted in Figure 5.2 for the upper crack tip and in Figure 5.3 for the lower crack tip. Clearly, the surfaces are smooth and well behaved. The effect of parameters λ_w, ε, and β are examined in the following.

Effect of Crack Length λ_w

- For all the β values (I-beams) and eccentricities, the correction factors for both the upper and lower crack tips are $f^A = f^B = 1.0$ in the limit as the web crack length approaches $\lambda_w \to 0$.
- For the upper crack tip and slender sections such as $\beta = 0.83$: as λ_w

increases, the f^A curves become gradually stratified, with the higher curves corresponding to small eccentricities and the lower curves to large eccentricities. The only deviation from this trend is the curve for the central crack ($\varepsilon = 0.0$) which first rises and then falls at large crack length, $\lambda_w = 0.8$. The fall occurs because the upper tip of a long central crack approaches the upper junction point and becomes constrained by the upper flange.

- For the upper tip and stocky sections such as $\beta = 2.05$: when the eccentricity is small, the f^A curves first rise slowly for short cracks and then fall for long cracks; when the eccentricity is large, the crack tip approaches the lower junction point and the f^A curves always fall.
- For the lower crack tip, the trends of the f^B curves are similar to those of the upper crack tip. The major difference occurs in the slender sections with small eccentricities: instead of rising, the f^B curves fall for long cracks. This is because the lower tip of a long crack approaches the lower junction point and becomes constrained.
- For slender sections such as $\beta = 0.83$, when both crack tips are far away from the junction points (small eccentricities and short cracks), the correction factors of the lower tip are larger than those of the upper tip. As the crack tip moves closer to the junction point (large eccentricity and/or long crack), the correction factors of the lower crack tip are smaller than those of the upper tip.
- For stocky sections such as $\beta = 2.05$, the correction factors of the lower tip

are always smaller than those of corresponding upper crack tip.

Effect of Eccentricity ε

- As the eccentricity increases and, as a result, the crack lies farther down the web, the correction factors for both the upper and lower crack tips decrease. The reduction is greater for the lower crack tip because it is much closer to the bottom flange than the upper tip is to the top flange.
- For short cracks, the correction factors of the upper and lower crack tips change little with eccentricity. But as the crack length increases, the correction factors become more sensitive to the eccentricity. For example, when $\lambda_w = 0.9$, the correction factor of the lower crack tip of an I-beam with $\beta = 0.83$ drops from $f^B = 1.056$ for $\varepsilon = 0.0$ to $f^B = 0.815$ for $\varepsilon = 0.9$.

Effect of Flanges-to-Web Ratio β

- As the β value increases, the correction factors for both the upper and lower crack tips decrease. A high β value means the flange is larger and constrains the web crack more.
- For a short crack such as $\lambda_w = 0.1$, the flange constraint is small and both the f^A and f^B curves are flat. For a long crack, $\lambda_w = 0.9$, the flange constraint becomes significant, and the correction factors are more sensitive to parameter β. For example, the correction factor of the lower crack tip drops from 0.94 to 0.82 as β changes from 0.83 to 2.05.

Comparison of I-beam with Single Plates

Figures 5.4 and 5.5 compare the solutions for I-beam W40 x 149 (β =

0.83) with those of single plates of same dimensions and crack lengths as the web and flange of the I-beam. Similar trends can be found for other I-beams. Figure 5.4 is for the upper crack tip while Figure 5.5 is for the lower crack tip. The correction factors are plotted as a function of crack length, with the solid and dashed curves representing the I-beam and single plate solutions respectively. The single plate solutions are given by Tada (1973) for a central crack and Isida (1965) for an eccentric crack. Each curve is for a different eccentricity.

- For any crack length and eccentricity, the correction factors of the I-beam are always smaller than those of corresponding single web plate. Web crack opening in an I-beam is constrained by the flanges, causing stresses to be reduced.
- The difference between the I-beam and single plate solutions increases with web crack length. A long crack deforms more and the crack tip is closer to the junction points. Therefore, the crack tip is constrained more in an I-beam than in a single plate.
- In a single plate, the correction factor of the lower crack tip is always larger than that of the upper tip. In an I-beam, depending on crack tip position (determined by parameters λ_w and ε) and flange size (parameter β), the correction factor of the lower crack tip may be smaller than that of the upper crack tip.
- For a single plate, the correction factor always increases with crack length.

But for an I-beam, the correction factor increases slightly for a short crack but then decreases as the crack becomes longer.

2-D plots

Figures 5.1 to 5.3 were replotted in 2-D as Figures 5.6 through 5.14 to more clearly illustrate the effect of parameters λ_w, ε, and β.

Figures 5.6 through 5.8 show the correction factor as a function of crack length λ_w for values of $\beta = 0.83$, 1.37, and 2.05 respectively. These figures represent three vertical planes normal to the β axis in Figures 5.1 to 5.3. There are two sets of curves in each figure: solid lines for the upper crack tip and dashed lines for the lower crack tip, each line corresponding to a given eccentricity.

Figures 5.9 through 5.12 show the correction factors for the upper and lower crack tips as a function of eccentricity. The first two figures are for the most slender section ($\beta = 0.83$) and the other two figures are for the most stocky section ($\beta = 2.05$). Each curve in the figures corresponds to a web crack length λ_w.

Finally, Figures 5.13 and 5.14 show the correction factor as a function of parameter β for the upper and lower crack tips respectively. These figures represent a vertical cut of the $\varepsilon = 0.5$ surfaces normal to the crack length axis in Figures 5.2 and 5.3. Each curve in the figures corresponds to a given crack length λ_w.

5.2.3 Two-tip Cracked I-beams under Bending

In an I-beam under bending, the web is subjected to a linear stress distribution, with reference stress σ of equal values and opposite signs at the upper and lower junction points. The lower and upper flanges are subjected to equal uniform reference stresses in tension and compression. Compressive stresses act on the portion of the crack length lying above the centroidal axis, causing partial penetration of the crack surfaces and resulting in a negative SIF for the upper crack tip. Such behavior is not physically possible. So the bending solution has meaning only when applied in combination with an axial stress distribution of a magnitude that prevents crack surfaces from penetrating each other. Combining tension and bending shifts the neutral axis from the centroid of the I-beam upward, a condition commonly found in composite steel-concrete beams. In this way, the separate solutions for tension and bending can be used, in combination, to calculate SIFs for composite beams.

Crack closure, without penetration, on the compressive side of a center-cracked single plate increases the SIF at the tip on the tension side by about 10% (Bowie and Freese 1976, Woo et al. 1988).

The correction factors for the upper and lower crack tips of a two-tip cracked I-beam under bending are listed in Tables 5.3 and 5.4. Figures 5.15 and 5.16 show surface plots of the correction factors as functions of parameters λ_w and β. Each surface corresponds to an eccentricity. Figure 5.15 is for the

upper tip while Figure 5.16 is for the lower tip.

The effect of individual parameters λ_w, ε and β are discussed in following.

Effect of Crack Length λ_w

- The correction factors for both the upper and lower crack tips have values of $f^A = f^B = \varepsilon$, in the limit as $\lambda_w \to 0.0$, which is theoretically expected.
- The correction factors for the upper crack tip decreases as the crack length increases. For small eccentricities of $\varepsilon = 0.0$ and 0.1, the correction factors are negative, because the upper crack tip lies in the compressive stress region (except for $\varepsilon = 0.1$ and $\lambda_w = 0.1$).
- For an eccentricity of $\varepsilon = 0.3$ and crack length $\lambda_w \geq 0.5$, the upper crack tip still lies in the compressive stress region, but the correction factors are positive. Since the portion of the crack in the compressive stress region is shorter than that in the tensile stress region, the crack "closing" displacements are overcome by the crack "opening" displacements. As a result, the whole crack is still open and the correction factors are positive.
- For large eccentricities of $\varepsilon \geq 0.5$, the upper crack tip lies in the lower portion of the web and the entire crack is open. Therefore, the correction factors are positive.
- For the lower crack tip which always lies in the tensile stress region, the correction factor curves of f^B first rise with increasing crack length λ_w; then,

as the crack tip approaches the lower junction point, the curves become flat for small eccentricities or fall for larger eccentricities $\varepsilon \geq 0.7$.

- For same crack length and eccentricity, the correction factor of the lower crack tip is always greater than that of the upper crack tip, except for $\varepsilon = 0.9$ and $\lambda_w \geq 0.8$. The correction factor curves for the upper crack tip are more stratified than those for the lower crack tip.

Effect of Eccentricity ε

As the eccentricity increases, so do the correction factors for both the upper and lower crack tips.

Effect of Flanges to Web Ratio β

The correction factors for both the upper and lower crack tips are practically not affected by parameter β for short cracks, but change slightly for long cracks. As an example of the latter, when $\lambda_w = 0.9$ and β increases from 0.83 to 2.05, the correction factor of the upper tip drops from 0.293 to 0.262 and that of the lower tip drops from 0.684 to 0.615.

Comparison of I-beam and Single Plate

The constraining effect that the flange has on the web crack is evident by comparing the I-beam and single plate solutions. The correction factors for cracks in the web of I-beam W40X149 ($\beta = 0.83$) and s single plate of same size as the web are compared in Figures 5.17 and 5.18 as a function of crack length. Similar results can be found for other I-beams. The curves correspond to eccentricities $\varepsilon = 0.0$, 0.1, 0.5 and 0.9. Figures 5.17 and 5.18 are for the

upper and lower crack tips respectively.

The solutions for a single plate with a central or eccentric crack under bending were given by Chen and Albrecht (1994). Their solutions were checked with FEA, and the error was found to be less than 0.5% for all eccentricities and crack lengths $\lambda_w \leq 0.7$ (Appendix A).

The following is observed from the figures:

- The correction factors for the upper and lower crack tips of the I-beam are always smaller than those of the single plate because the flange constrains the web crack opening.
- Differences between correction factors of the I-beam and single plate increase with crack length. A long crack opens more and its tips are closer to the junction points, thus increasing constraint. A short crack, on the other hand, opens much less and its tips are farther from the junction points, remaining largely unaffected by the flange.
- Differences between the I-beam and single plate solutions for the upper crack tip are smaller than those for the lower crack tip, meaning the upper crack tip is constrained less than the lower tip. For example, when $\varepsilon = 0.5$, the crack lies in the lower portion of the web and the upper crack tip is located near the major axis of the I-beam. The upper crack tip is subjected to small stresses and deformations and, therefore, little flange constraint. The lower crack tip is located far from the major axis of the I-beam and the stresses and deformations around the crack tip are large. Also, the lower

crack tip lies near the lower junction point. Therefore, the lower crack tip is highly constrained by the flange.

- The correction factor trends differ greatly for the I-beam and the corresponding single plates. For example, the lower tip correction factor of a single plate increase with crack length; that of an I-beam decreases, especially for long cracks.

Additional 2-D plots of correction factors are presented in Figures 5.19 through 5.27 for other I-beams. The findings are similar to those described above.

5.3 Three-tip Cracked I-beams

The SIFs for a symmetric three-tip crack in an I-beam is expressed as:

$$K^{w,f} = f^{w,f}\sigma\sqrt{\pi a_{w,f}} \tag{5.2}$$

where a_w and a_f are the web and flange crack lengths, and the subscripts and superscripts w and f refer to the web and flange crack tips, respectively. Similar to the two-tip crack, the reference stress σ is defined as the remote uniform stress for an I-beam under tension and the stress at the flange-web junction for an I-beam under bending. The correction factor f is a function of web crack length λ_w, flange crack length λ_f, and flanges to web cross-sectional area ratio β.

5.3.1 Variables in Analysis

The variables used in FEAs of three-tip cracked I-beams are:

- Symmetric three-tip crack, with center-cracked bottom flange
- Seven normalized web crack lengths: λ_w = 0.1 to 0.7, in steps of 0.1
- Nine normalized flange crack lengths: λ_f = 0.1 to 0.9, in steps of 0.1
- Nine W-shapes listed in Table 3.1
- Two types of loading: tension and bending
- Number of FEAs:

  (7 web crack lengths) x (9 flange crack lengths) x (9 W-shapes) x(2 loadings) = 1,134
- I-beam modeling method: 3-D model, web and flanges represented by their mid-planes, with all DOFs joined along the junction lines of web and flanges
- Elements: eight-node shell element, reduced integration, five degrees of freedom per node, ABAQUS designation S8R5
- Crack tip elements: quarter-point element degenerated from element S8R5
- Mesh pattern around crack tip: m x n = 3 x 16 (Figure 2.4)
- Mode I SIFs obtained from J-integral of ABAQUS output.

The maximum web crack length was chosen as λ_w = 0.7 because, in bridge girders, the flange crack has extended across the full flange width when the web crack length exceeds 70% of the depth.

5.3.2 Three-tip Cracked I-beams under Tension

The calculated correction factors for the web and flange crack tips are listed in Tables 5.5 and 5.6, respectively, as a function of λ_w, λ_f, and β. These same values are plotted in Figures 5.28 and Figure 5.29 as functions of parameters λ_f and β. Each surface corresponds to a given web crack length λ_w. Smooth and regular relationships exist between the correction factors and the parameters.

Correction Factor for Flange Crack Tip

From Figure 5.28, the following is observed for the flange crack tip:

- As the flange crack length λ_f increases, the f^f curves first drop slightly and then rise as $\lambda_f \to 0.9$. This trend is uniform for all web crack lengths.
- The correction factor f^f also increases with web crack length λ_w. Clearly, when the web crack is long and the flange crack is short, the interaction forces along the junction line tend to open the flange crack more than would be the case if the flange were separated from the web.
- Finally, as β increases, the correction factor decreases. In a two-tip cracked I-beam, parameter β accounts for the flange constraint on the web crack opening; similarly in a three-tip cracked I-beam, parameter β accounts for interaction between the cracked web and flange. The interaction effect decreases with increasing β value. In other words, the heavier the flange is relative to the web, the less the CMOD of the flange crack is affected by the

web crack.

Correction Factor for Web Crack Tip

Figure 5.29 shows the following effects on the web crack tip,

- As the flange crack length λ_f increases, the correction factor for the web crack tip f^w increases.
- Contrary to the finding for f^f, the correction factor f^w decreases with increasing of web crack length λ_w. The interaction forces acting along the web edge are equal in magnitude and opposite in direction to those acting along the flange. Hence, if the interaction forces tend to open the flange crack, in turn to close the web crack.
- The correction factor for the web crack generally increases with parameter β, the increase being greatest for combination of long flange and short web cracks.

However, by comparing the values of correction factor for the web and flange crack tips, Figures 5.28 and 5.29, it can be seen that the responses of web cracks to the interaction forces are much greater than those of the flange cracks. For example, for I-beam W40 x 149 with web and flange crack lengths of $\lambda_w = 0.7$ and $\lambda_f = 0.9$ (the interaction forces open the flange crack and close the web crack), the correction factor of the flange crack is increased from f^f = 5767 to 4.8346, while the correction factor of the web crack is reduced from f^w .3755 to 1.0387. This is so because, for equal forces and crack lengths, the OD is greater for a single edge crack than for a single center-cracked plate.

Interaction Between Web and Flange

The interaction between the web and flange depends on the relative crack lengths. Figures 5.30 and 5.31 show the correction factor of the flange crack tips as a function of flange crack length. These two figures represent two planes normal to the β axis at 0.83 and 2.05 in Figure 5.28. Each dashed line in the figures corresponds to a web crack length λ_w. To investigate the interaction between the edge-cracked web and the center-cracked flange, a solid curve was added to the figures representing Tada's (1973) solution for a center-cracked plate. It can be seen that:

- Pairs of flange and web crack lengths, λ_f and λ_w, are free of interaction where Tada's solid curve for a single center-cracked plate intersects the dashed curves for the I-beam. SIFs for such pairs may be calculated from single-plate solutions.
- Tada's solution divides the space in Figure 5.30 and 5.31 into two regions of behavior. The opening of the flange crack is restrained by the web crack at points below the solid curve and augmented by the web crack at points above the solid curve. Accordingly, the correction factor for the flange crack f^f is smaller and larger, respectively, than Tada's solution would predict.

.3.2 Three-tip Cracked I-beams under Bending

When a three-tip cracked I-beam is under bending, the stress is constant

in the flanges and linear in the web. The interaction behavior between the cracked web and flange is similar to that for I-beams under tension.

The correction factors are listed in Tables 5.7 and 5.8 for the web and flange crack tips respectively. They are plotted in Figures 5.32 and 5.33 as a function of λ_f and β. Each surface in the figures corresponds to a given web crack length λ_w. Smooth and regular relationships exist between the correction factors and the parameters. Also, the trends in these figures are very similar to those for I-beams under tension (Figures 5.28 and 5.29).

- As the flange crack length λ_f increases, the correction factor for the flange crack tips first drops and then rises; the correction factor for the web crack tip increases gradually.
- As the web crack length λ_w increases, the correction factor increases for the flange crack tips and decreases for the web crack tip.
- As the flanges-to-web area ratio β increases, the correction factor decreases for the flange crack tip and increases for the web crack tip.

5.4 Conclusions

Two-tip and three-tip cracked I-beams under tension or bending were analyzed. The correction factors for the SIFs were obtained from FEAs. The selected I-beams cover most rolled W-sections and welded girders used in highway bridges. For each I-beam, FEAs were performed for a wide range of

eccentricities, web crack lengths and flange crack lengths. Based on the results, the following conclusions were reached:

- The calculated SIFs (correction factors) are smooth and regular functions of eccentricity, crack lengths, and flanges-to-web area ratio.
- Two-tip cracks in I-beam webs are constrained by the flanges on each side. As a result, the SIF for the web crack is smaller than that for a single plate. The flange constraint increases as crack tip, whose position is determined by parameters λ_w and ε, approaches the junction points of web and flanges. As eccentricity, web crack length, and flange area increase, the constraining effect of the flange on the web crack becomes larger.
- SIFs for three-tip cracks are affected by the interaction forces between the web and flange. These forces depend on the web and flange displacements along the junction line. If the displacements of a single flange plate are greater than those of the corresponding points of a single web plate, enforcing displacement compatibility reduces the CMOD of the flange crack and augments the CMOD of the web crack. Conversely, if the displacements of a single flange plate are smaller than those of the corresponding points of a single web plate, the web augments the CMOD of the flange crack and the flange reduces the CMOD of the web crack.

Chapter 6: Equations for Stress Intensity Factors

Correction factors for two-tip and three-tip cracked I-beams under tension or bending were determined with FEAs in Chapter 5. The results were presented in tables and curves. In this chapter, the numerical values were fitted with empirical equations for ready use by engineers.

6.1 Fitting Procedures

The fitting was carried out in two steps. First, the correction factors were fitted as a function of two variables — web crack length λ_w and eccentricity ε for a two-tip crack, and web and flange crack lengths λ_w and λ_f for a three-tip crack. The third parameter, the flanges-to-web area ratio, was kept constant. The purpose of this preliminary step was to explore the functional form of the fitting equation for each I-beam. Software TableCurve3D — a product of Jandel Scientific for surface fitting — was used. TableCurve3D can handle two independent variables and has the advantage of automatically and quickly finding the best fitting functions for complex data from among a large family of possible functions (TableCurve3D User's Manual 1994).

In the second step, the correction factors were fitted with a three-variable equation that included the flanges-to-web area ratio as the third variable. The best fitting equation was determined after several trials with different functional

forms selected based on the results from the first step.

The unknown coefficients were determined with another Jandel Scientific software — SigmaPlot — which can handle as many as 15 dependent variables and 25 coefficients. SigmaPlot uses the Marquardt-Levenberg algorithm (SigmaPlot User's Manual 1994) to find the coefficients of the independent variables that give the best fit between an equation and the data. This algorithm finds the coefficients that minimize the sum of the squared differences between the values of the observed and predicted values of the dependent variable:

$$SS = \sum_{i=1}^{n} (y_i - \hat{y}_i)^2 \qquad (6.1)$$

where y_i is the observed and $\hat{y}_i$ is the predicted value of the dependent variable. The fitting process is iterative. SigmaPLot initially guesses the coefficients, checks to see how well the equation fits, and then continuously improves the guesses until the difference between the residual sum of squares no longer decreases significantly. Curve fitting stops when: (1) all coefficient values stop changing in all significant places; and (2) the absolute value of the difference between the norm of the residuals, $\sqrt{SS}$, from one iteration to the next is less than the tolerance value. The tolerance value used in the present study was 0.0001.

Correction factors predicted with the fitted equation are compared with the FEA results. To exclude meaningless large errors of small values of f, the fitting error is defined as:

$$\Delta = \frac{f_{pred} - f_{FEA}}{\bar{f}_{FEA}} 100 \qquad (6.2)$$

where f_{pred} is the predicted value of the empirical equation, f_{FEA} is the FEA or calculated result, and $\bar{f}_{FEA}$ is the average value of all FEA results.

6.2 Two-tip Cracked I-beam

The SIFs for two-tip cracked I-beams are given by equation 3.1, and the correction factors are defined by equations 3.2. The parameters are the web crack length λ_w, eccentricity ε, and cross-sectional area ratio of flanges-to-web β. Because the web crack is eccentric, the correction factors differ for the upper and lower crack tips.

6.2.1 Parameter Ranges

In Chapter 5, FEAs were performed for eight selected I-beams listed in Table 3.1. Curves were fitted for the following combinations of crack tips and loadings:

- Two crack tips: correction factors f^A and f^B for the upper and lower crack tips
- Two loadings: tension and bending
- Number of curve fittings: (2 crack tips) x (2 loadings) = 4

For each curve fitting, the parameter ranges were:

- Eight cross-sectional area ratios: $\beta = 0.83, 1.00, 1.25, 1.37, 1.53, 1.69, 1.91$, and 2.05. The range of $\beta = 0.83$ to 2.05 covers most I-beams used in civil engineering (Figure 3.10).
- Six eccentricities: $\varepsilon = 0.0$, and 0.1 to 0.9, in steps of 0.2
- Nine web crack lengths: $\lambda_w = 0.0$ to 0.8, in steps of 0.1. FEA data for the longest crack length were not used because $\lambda_w = 0.9$ is rarely found in practice. For example, a central crack ($\varepsilon = 0.0$) of length $\lambda_w = 0.9$, shown in Figure 6.1, extends through most of the web depth, causing significant yielding of the net section that would invalidate linear-elastic calculations of SIFs. In another example, a greatly eccentric crack of length $\lambda_w = 0.9$, shown in Figure 6.2, would extend into the bottom flange whereas, in reality, the analysis should be limited to cracks whose lower tip lies above the upper surface of the bottom flange.
- Total sample points for each curve fitting:

  (8 β values) x (6 eccentricities) x (9 crack lengths) = 432

The limit case of $\lambda_w = 0.0$, which corresponds to no crack, yields additional values of $f^A = f^B = 1$ for an I-beam under tension and $f^A = f^B = \varepsilon$ for an I-beam under bending.

6.2.2 Equations for Two-tip Cracks under Tension

Preliminary fitting results, shown in Figures 6.3 and 6.4 for the upper

crack tip of two I-beams W40x149 ($\beta = 0.83$) and W18x97 ($\beta = 2.05$) under tension, suggested a polynomial functional form. After several trials, the following 15-term equation 6.3 was found to best fit the calculated correction factors for both the upper and lower crack tips:

$$f = a_0 + a_1\varepsilon + a_2\beta\varepsilon + a_3\varepsilon^2 + a_4\lambda_w + a_5\beta\lambda_w + a_6\varepsilon\lambda_w + a_7\lambda_w^2 + a_8\beta\varepsilon\lambda_w + a_9\beta^2\varepsilon + a_{10}\beta\varepsilon^2 + a_{11}\lambda_w\beta^2 + a_{12}\lambda_w\varepsilon^2 + a_{13}\beta\lambda_w^2 + a_{14}\varepsilon\lambda_w^2 \quad (6.3)$$

The constant in the equation is $a_0 = 1$ because $f^{A,B} = 1.0$ for the special case of $\varepsilon = 0.0$ and $\lambda_w = 0.0$. The other 14 coefficients were determined with the SigmaPlot software.

Coefficients for Upper Crack Tip

The coefficients of equation 6.3 for the upper crack tip of a two-tip cracked I-beam under tension are given in Table 6.1.

Figure 6.5 shows the differences between the predicted (fitted) and calculated (FEA) correction factors. The points in the figure are arranged in eight groups, one for each β value of 0.83 to 2.05; within each such group, the eccentricity ε was incremented from 0.0 to 0.9; and for each eccentricity, the crack length λ_w was incremented from 0.0 to 0.8. The average value of the correction factors for all the 432 data points is $\bar{f}_{FEA} = 1.0031$. Good agreement exists between predicted and calculated values. The maximum positive error is 1.4%, and the maximum negative error is -3.0%. Most errors lie within ±1%.

To identify the combinations of parameters that yield the least accurate results, the fitting errors were replotted in Figures 6.6 to 6.8 versus parameters

β, ε, and λ_w respectively. Clearly errors are largest for the long central crack, ε = 0.0 and λ_w = 0.8, a case that rarely occurs in practice and would, in all likelihood, produce net section yielding in violation of LEFM.

Figures 6.9 and 6.10 compare the predicted and calculated correction factors for I-beams W40X149 (β = 0.83) and W18X97 (β = 2.05), further confirming the goodness of fit.

Coefficients for Lower Crack Tip

The coefficients of equation 6.3 for predicting correction factors for the lower crack tip of a two-tip cracked I-beam under tension are given in Table 6.1.

The errors between the predicted and calculated correction factors are shown in Figures 6.11 to 6.14. The average value of all the correction factors is $\bar{f}_{FEA}$ = 0.9933. All errors fall within the range of 1.29% to -1.93%. Figures 6.15 and 6.16 show comparative surface plots for I-beams W40X149 (β = 0.83) and W18X97 (β = 2.05). Again, the fitted equation produces smooth surfaces and good agreement with the calculated values.

6.2.3 Equations for Two-tip Cracks under Bending

The functional form of equation 6.3 was also selected to fit the correction factors for two-tip cracked I-beams under bending. In this case, the constant is a_0 = 0 because, in the limit, when ε = 0.0 and λ_w = 0.0, the correction factors approach $f^{A,B}$ =0.0.

The other 14 coefficients were determined with SigmaPlot software.

Coefficients for Upper Crack Tip

The coefficients of equation 6.3 for predicting the correction factors for the upper crack tip of a two-tip cracked I-beam under bending are given in Table 6.3.

Figures 6.17 to 6.20 show the errors between the predicted and calculated correction factors and their distribution as a function of β, ε, and λ_w. The average of all correction factors is $\bar{f}_{FEA} = 0.2979$. The maximum positive error is 2.25%, and the maximum negative error is -2.73%. The largest fitting errors are those for the central crack, $\varepsilon = 0.0$, and shortest and longest crack lengths $\lambda_w = 0.1$ and 0.9. For most data, the errors fall within ±1%. Good agreement between the predicted and calculated correction factors is further confirmed in Figures 6.21 and 6.22, where the values are compared for I-beams W40x149 ($\beta = 0.83$) and W18x97 ($\beta = 2.05$).

Coefficients for Lower Crack Tip

The coefficients of the fitting equation 6.3 for the lower crack tip are given in Table 6.3. The fitting errors and their distribution are shown in Figures 6.23 to 6.26. The average value of all the correction factors is $\bar{f}_{FEA} = 0.5247$. The maximum positive error between the predicted and calculated correction factors is 1.95%, and the maximum negative error is -2.82%. The largest fitting errors are for $\varepsilon = 0.9$ and $\lambda_w = 0.9$. Surface plots of equation 6.3 for I-beams W40x149 ($\beta = 0.83$) and W18x97 ($\beta = 2.05$) are shown in Figures 6.27 and

6.28. Good agreement between the predicted and calculated correction factors can be observed.

6.2.4 Two-tip Cracks in Engineering Practice

In the above sections, the correction factor for two-tip cracked I-beam under tension or bending were fitted with equation 6.3 for a wide range of parametric crack lengths and eccentricities. In engineering practice, there are some limitations on crack position and crack length.

Minimum Crack Length

In engineering practice, two-tip web cracks found in service are at least 4 times as long as the thickness of the web. That is, the minimum crack length is (Figure 6.29):

$$a_{w,\,min} = 2\,t_w \qquad (6.4)$$

Crack shorter than $a_{w,\,min}$ are virtually not detectable and would typically not have grown yet through the web thickness. Part-through cracks open much less than two-tip through-cracks.

Maximum Crack Length

The maximum web crack length is determined by the lowest position of the lower crack tip. For a given eccentricity e, the lowest possible crack tip position is right above the upper surface of the bottom flange, which is a distance of $t_f/2$ away from the lower junction point. Therefore, the maximum crack length for a given eccentricity is

$$a_{w,\,max} = d_f/2 - e - t_f/2 \qquad (6.5)$$

Maximum Eccentricity

As the eccentricity increases, the crack is located farther down the web, and the difference between the maximum and minimum crack lengths is smaller. When $a_{w,\,max} = a_{w,\,min}$, the eccentricity reaches its maximum value. As shown in Figure 6.30, the maximum eccentricity is

$$e_{max} = d_f/2 - 2t_w - t_f/2 \qquad (6.6)$$

Based on the above analyses, limiting values of eccentricities and crack lengths were calculated for all I-beams.

Figure 6.31 shows the maximum eccentricity for all I-beams of sizes W40 to W8. The circular symbols in each group of nominal size are plotted in the order from heaviest to lightest section. Typically heavy I-beams have smaller maximum eccentricities, and light I-beams have larger maximum eccentricities. For all I-beams combined, the maximum eccentricity falls within the range $\varepsilon = 0.56$ to 0.91.

Figures 6.32 and 6.33 show the maximum and minimum crack lengths for eccentricities $\varepsilon = 0.1$ and 0.7 respectively. For $\varepsilon = 0.1$, practical crack lengths are bound by $\lambda_{w,\,max}$ and $\lambda_{w,\,min}$. The bounds in each group are narrower for heavy sections and wider for light sections. For all I-beams, $\lambda_{w,\,min}$ is about 0.1 and $\lambda_{w,\,max}$ about 0.98. Some heavy sections with large eccentricity $\varepsilon = 0.7$ would have values of $\lambda_{w,\,min}$ greater than $\lambda_{w,\,max}$ as shown in Figure 6.33. This simply means that the geometry of these sections limits the eccentricity to $\varepsilon <$

0.7.

6.3 Three-tip Cracked I-beams

SIFs for the web and flange crack tips of a three-tip cracked I-beam are given by equation 3.6. The correction factors, equation 3.7, are functions of web crack length λ_w, flange crack length λ_f, and flanges-to-web area ratio β.

6.3.1 Parameter Ranges

SIFs calculated with FEAs (Table 3.1) were fitted for the following cracks and loadings:

- Two crack tips: correction factors f^w and f^f for the web and flange crack tips
- Two loadings: tension and bending
- Number of curve fitting: (2 crack tips) x (2 loading) = 4

The parameter for each curve fitting were:

- Eight cross-sectional area ratios: β = 0.83, 1.00, 1.25, 1.37, 1.53, 1.69, 1.91, and 2.05
- Seven web crack lengths: λ_w = 0.1 to 0.7, in steps of 0.1
- Nine flange crack lengths: λ_f = 0.1 to 0.9, in steps of 0.1
- Total sample points for each curve fitting:

($8\ \beta$ values) x (7 web crack lengths) x (9 flange crack lengths) = 504

6.3.2 Equations for Three-tip Cracks under Tension

The preliminary results suggest that a polynomial ratio equation is the best functional form for fitting SIFs of three-tip cracks. Figures 6.34 and 6.35 compare predicted and calculated SIFs for the flange crack tips of I-beams W40x149 ($\beta = 0.83$) and W18x97 ($\beta = 2.05$) under tension.

Based on the preliminary results, different polynomial ratio equations were tried. The following 26-term equation 6.7 yielded the best fit:

$$f = \frac{(a_1 + a_2\beta + a_3\beta^2 + a_4\lambda_W + a_5\lambda_W^2 + a_6\lambda_W^3 + a_7\lambda_F + a_8\lambda_F^2 + a_9\lambda_F^3 + a_{10}\beta\lambda_W\lambda_F + a_{11}\beta\lambda_W^2\lambda_F + a_{12}\beta\lambda_W\lambda_F^2 + a_{13}\beta\lambda_W^2\lambda_F^2)}{(1 + a_{14}\beta + a_{15}\beta^2 + a_{16}\lambda_W + a_{17}\lambda_W^2 + a_{18}\lambda_W^3 + a_{19}\lambda_F + a_{20}\lambda_F^2 + a_{21}\lambda_F^3 + a_{22}\beta\lambda_W\lambda_F + a_{23}\beta\lambda_W^2\lambda_F + a_{24}\beta\lambda_W\lambda_F^2 + a_{25}\beta\lambda_W^2\lambda_F^2)} \qquad (6.7)$$

The unknown coefficients of equation 6.7 were determined with SigmaPlot.

Coefficients for Web Crack Tip

Table 6.2 lists the 25 unknown coefficients of equation 6.7 for predicting correction factors for the web crack of a three-tip cracked I-beam under tension. The average value of all correction factors is $\bar{f}_{FEA} = 0.9517$.

Figure 6.36 shows the errors in fitting equation 6.7 to the calculated correction factors. The points in the figure are again arranged first by β values from 0.83 to 2.05, then by web crack lengths λ_w from 0.1 to 0.7 in steps of 0.1, and finally by flange crack lengths λ_f from 0.1 to 0.9 in steps of 0.1.

In Figures 6.37 to 6.39, the fitting errors are plotted versus β, λ_w, and λ_f respectively. The maximum positive fitting error is 3.34%, and the maximum negative error is -3.58%. But the fitting errors lie within ±2% for most sample

points. Table 6.3 lists the 9 three-tip cracks whose absolute fitting errors are greater than 3%. Evidently, fitting errors are largest when the web and flange crack lengths are greatly mismatched, that is, a short web crack joined with a long flange crack or a long web crack joined with a short flange crack. Figures 6.40 and 6.41 are surface plots for I-beams W40x149 and W18x97 showing that the prediction equation 6.7 yields good agreement with the calculated correction factors.

Coefficients for Flange Crack Tip

The unknown coefficients of equation 6.7 for the flange crack tips of a three-tip cracked I-beam under tension are given in Table 6.2. The average value of all correction factors for the flange crack tips is $\bar{f}_{FEA} = 1.8703$.

The fitting errors and their distributions are shown in Figures 6.42 to 6.45. The maximum positive fitting error is 4.42%, and the maximum negative error is -4.76%. For most data, the fitting errors are within ±2%. Table 6.4 lists the 16 three-tip cracks whose absolute fitting errors are greater than 3%. These errors occur in three-tip cracks with short web crack and long flange crack or vice versa. Figures 6.41 and 6.42, which are surface plots of equation 6.7 for I-beams W40x149 and W18x97, indicate that the prediction equation fits well the calculated correction factors.

6.3.3 Equations for Three-tip Cracks under Bending

The same 26-term polynomial ratio of equation 6.7 was also used to predict the correction factors for the web and flange crack tips of three-tip cracked I-beam under bending.

Coefficients for Web Crack Tip

The coefficients of equation 6.7 for the web crack are given in Table 6.2. In this case, the maximum positive fitting error is 6.31%, and the maximum negative error is -6.50%, with most falling within ±2% (Figures 6.48). Figures 6.49 to 6.51 show the fitting error versus β, λ_w and λ_f respectively. Table 6.5 lists the 37 three-tip cracks whose absolute fitting errors exceed 3%. These large errors, in most cases, occur when the web crack is short and the flange crack is long. The surface plots in Figures 6.52 and 6.53 for I-beams W40X149 and W18X97 illustrate the good prediction accuracy.

Coefficients for Flange Crack Tip

The coefficients of equation 6.7 for the flange crack tips are given in Table 6.2. The maximum positive fitting error is 4.14%, and the maximum negative error is -3.66 %. The average of all the correction factors is $\bar{f}_{FEA}$ = 1.6789. For most sample points, the fitting error lies within ±2%. The errors between the predicted and calculated correction factors and their distributions are shown in Figures 6.54 to 6.57. As listed in Table 6.6, there are only 6 three-tip cracks whose absolute fitting errors exceed 3%. Surface plots of equation

6.7 for I-beams W40X149 and W18X97 are shown in Figures 6.58 and 6.59. As expected, the obtained empirical equation produces good fitting results.

6.4 Fatigue and Fracture Analysis

6.4.1 Input for Analysis

Before a cracked bridge girder is analyzed for fatigue and fracture, the following information must be obtained:

Material Properties

- Measure the fracture toughness, K_{Ic}, at the lowest service temperature, or estimate the fracture toughness from the Charpy V-notch energy (CVN) tests.

If fatigue analysis is needed, then:

- Estimate the threshold value of the SIF range, ΔK_{th}.
- Obtain the parameters C and n of the crack growth rate equation (Paris' Law).

Crack Geometry and Dimension

- Two-tip web crack: measure the crack length and the eccentricity, that is, the distance from mid-length of the crack to the centroid of the girder section.
- Three-tip crack: measure the web and flange crack lengths. The web crack length is the distance from the crack tip to the junction

point between web and flange.

Loading

- Obtain the dead load and live load moments at the cracked section from the bending moment diagram.

If fatigue analysis is needed, then:

- Count the number of trucks that cross the bridge every day (ADTT or average daily truck traffic)

Stress Intensity Factor

- Calculate the SIF, K, by choosing Equation 6.3 or 6.7 according to crack type and loading condition, or using the software FACI — a windows application software for Fracture Analysis of Cracked I-beams written by the author.

6.4.2 Analysis Methods

With the above information as input, perform fracture and fatigue analyses as follows:

Fracture Analysis

- Calculate the maximum SIF, K_{max}, under combined dead load and live load stresses.
- Compare K_{max} with the fracture toughness, K_{Ic}, reduced by a safety factor (S. F.): if $K_{max} \geq K_{Ic} / (S.F.)$, recommend to the

bridge engineer the closing of the traffic lane above the girder, or the closing of the entire bridge if the member is fracture critical; if $K_{max} < K_{Ic} / (S.F.)$, perform fatigue crack propagation analysis to determine the remaining safe life and recommend a crack arrest treatment.

Fatigue Analysis

- Calculate SIF range, ΔK, corresponding to stress ranges induced by the fatigue truck as defined in the Specifications for Highway Bridges (1994).
- Compare the ΔK value with the crack growth threshold, ΔK_{th}: if $\Delta K > \Delta K_{th}$ for one of the crack tips, perform fatigue analysis; if $\Delta K \leq \Delta K_{th}$ for all crack tips, then the cracks will not propagate and no fatigue analysis is needed.

Fatigue analysis for both two-tip (on the web) and three-tip (symmetric) cracked I-beams involves two propagation equations.

- Two-tip crack:

$$\frac{da_{upper}}{dN} = C(\Delta K_{upper})^n$$

$$\frac{da_{lower}}{dN} = C(\Delta K_{lower})^n$$

- Three-tip crack:

$$\frac{da_w}{dN} = C(\Delta K_w)^n$$

$$\frac{da_f}{dN} = C(\Delta K_f)^n$$

- Substitute ΔK into the crack growth rate equation and calculate the number of cycles, ΔN, needed for the crack to grow from its current length to the critical length where $K_{max} = K_{Ic} / (S.F.)$.
- Convert the calculated number of truck crossings, N, into a number of days: **days** $= N / ADTT$.
- Advise the bridge engineer how much time he has to repair the cracked bridge girders.

6.5 Composite and Singly Symmetric Beams

The above equations 6.3 and 6.7 were developed for rolled W-shapes. However, in engineering practice, composite and singly symmetric beams may be used. As shown in Figure 6.60, such sections consist of:

- Composite rolled beam
- Composite plate girder with doubly symmetric steel section
- Noncompsite plate girder with singly symmetric steel section
- Composite plate girder with singly symmetric steel section

In bridge girders, these sections are always subjected to bending.

The equations for calculating correction factors for cracks in doubly symmetric beams are not directly applicable to the four section types listed

above. In the following, procedures are outlined for obtaining approximate correction factors.

6.5.1 Composite Rolled Beam

The following procedure is recommended for calculating SIFs for a cracked composite rolled beam (Figure 6.60a):

- Calculate the position of the elastic neutral axis and the stress distribution through the depth of the composite rolled beam.
- Separate the stress distribution through the depth of the steel section into an axial tensile stress component:

$$\sigma_a = \frac{\sigma_{bf} + \sigma_{tf}}{2}$$

and a bending stress component

$$\sigma_b = \frac{\sigma_{bf} - \sigma_{tf}}{2}$$

Where

σ_{br} - Stress at mid-thickness of bottom flange

σ_{tr} = stress at mid-thickness of top flange

- Determine the values of λ_w, ε and β for the steel section with a two-tip crack and λ_w, λ_f and β for the three-tip crack as defined for rolled beams without a composite concrete deck (equations 3.3 to 3.5 and 3.8 to 3.10).
- For two-tip and three-tip cracked I-beams, calculate the correction

factors with equations 6.3 and 6.7 respectively.

- Calculate the SIFs with equations 3.1 and 3.6, using σ_a as the reference stress for the axial component and σ_b for the bending component. The final SIF values are obtained by superposing the SIF values for axial tension and bending.

6.5.2 Composite Plate Girder with Doubly Symmetric Section

The procedure for calculating SIFs for a composite plate girder with doubly symmetric steel section is the same as that for a composite rolled beam. Since equations 6.3 and 6.7 were developed for rolled W-shapes, the correction factors are strictly valid only for sections whose flanges-to-web area ratio β and skeleton ratio γ lie within the band shown in Figure 3.4.

If the steel section falls inside the β-γ band of Figure 3.4, equations 6.3 and 6.7 yield accurate SIFs for doubly symmetric welded girder.

But, the calculated SIFs are overestimated (conservative) if the section falls above the β-γ band and underestimated (non-conservative) if the section falls below the β-γ band. In this latter case, SIFs should be determined from FEAs of the specific steel section.

6.5.3 Noncompsite Plate Girder with Singly Symmetric Section

For a noncomposite plate girder with a singly symmetric steel section

(top flange smaller than bottom flange) as shown in Figure 6.60c, the following procedure of calculating SIFs is recommended:

- Calculate the position of the elastic neutral axis.
- Calculate the stress distribution through the depth of singly symmetric steel section.
- Retain the stress at mid-thickness of the bottom flange, σ_{bf}, Figure 6.61, as the reference stress in calculating SIFs.
- Choose the elastic neutral axis as a second axis of symmetric as in Figure 6.61c.
- Determine the values of λ_w, ε and β (equations 3.3 to 3.5) for a section with a two-tip crack and λ_w, λ_f and β (equations 3.8 to 3.10) for a section with a three-tip crack from the equivalent doubly symmetric section that is created by mirroring the lower portion about the elastic neutral axis.
- Calculate the correction factors with equations 6.3 and 6.7 for two-tip and three-tip cracked I-beams respectively.
- Calculate the SIFs with equations 3.1 and 3.6.

Because equations 6.3 and 6.7 are for doubly symmetric rolled I-beam or plate girder, the recommended procedure of calculating SIFs for singly symmetric section is an approximation. FEA calculations are needed to determine the accuracy of such an approximation. Unfortunately, no solution exist for this case. For more accurate results, FEA is recommended.

6.5.4 Composite Plate Girder with Singly Symmetric Section

For this case, SIFs should be calculated using a combination of the procedures described in section 6.5.1 and 6.5.3.

6.6 40-Ft Simple-span Composite Beam

SIFs are calculated for a three-tip cracked I-beam as an example.

Problem

Given is a simple-span composite girder bridge with 2 lanes of traffic. It has a deck width of 33'-4" and a span length of 40 ft. The girders consist of a W27 x 84 section with a cover plate welded to the bottom flange along the 25-ft center portion of the span. The 7-in. thick concrete slab is compositely connected to the girders with shear studs. The girder elevation is shown in Figure 6. 62 and the composite section in Figure 6.63. A three-tip crack is found at the welded end of the cover plate, 7'-6" from the end bearing.

W-shape Geometry Properties

The W27 x 84 section has a web depth $d = 26.71$ in., web thickness $_w = 0.46$ in., flange width $b_f = 9.96$ in., and flange thickness $t_f = 0.64$ in. herefore, the web depth between the upper and lower junction points is $= d - t_f = 26.07$ in. and the cross-sectional areas of the web and flange are: $= d_j t_w = 11.99$ in.^{2} and $A_f = t_f b_f = 26.71$ in.^{2}. Parameters β and γ are ulated as: $\beta = 2A_f / A_w = 1.06$ and $\gamma = d_j / b_f = 2.62$. The section lies

near the lower bound of Figure 3.4, meaning that the SIF can be calculated with equation 6.7.

Crack Lengths

The flange crack length is assumed to be $2a_f = 5$ in. and the web crack length $a_w = 3$ in. Such cracks are typical of those found in the I-95 bridge over the Yellow Mill Pond in Connecticut.

Therefore, $\lambda_f = \frac{2a_f}{b_f} = \frac{5}{9.96} = 0.502$ and $\lambda_w = \frac{a_w}{d_j} = \frac{3}{26.07} = 0.115$

Properties of Composite Section

As shown in Figure 6.63, section properties are computed for the steel beam compositely connected to the concrete deck, with n = 8 and 3n = 24.

Composite Section, n = 8, for maximum positive moment

Materials	A	d	Ad	Ad^2	I_0	I
Steel Section	24.8	0	0	0	300	2825
Conc. 84x7/8	73.5	17.85	1312	23419		23719
Σ	98.3		1312			26543

$d_s = \frac{1312}{98.3} = 13.35$ in. $\quad I_{NA} = 26543 - 13.35 \times 1312 = 9028$ in.^{4}

$d_{\text{Top of steel}} = 13.35 - 13.35 = 0$ in.

$d_{\text{Bot. of steel}} = 13.35 + 13.35 = 26.70$ in.

$S_{\text{Bot. of steel}} = \frac{9028}{26.7} = 338$ in.^{3}.

Composite Section, 3n = 24, for maximum positive moment

Materials	A	d	Ad	Ad^2	I_0	I

Steel Section	24.8	0	0	0		2825
Conc. 84x7/24	24.5	17.85	437.3	7806	100	7906
Σ	49.3		437.3			10731

$$d_{24} = \frac{437.3}{49.3} = 8.87 \text{ in.} \qquad I_{NA} = 10731 - 8.87 \times 437.3 = 6852 \text{ in.}^4$$

$$d_{\text{Top of steel}} = 13.35 - 8.87 = 4.48 \text{ in.} \qquad d_{\text{Bot. of steel}} = 13.35 + 8.87 = 22.22 \text{ in.}$$

$$S_{\text{Top of steel}} = \frac{6852}{4.48} = 1529 \text{ in.}^3 \qquad S_{\text{Bot. of steel}} = \frac{6852}{22.22} = 308 \text{ in.}^3$$

Loads and Moments

The moment diagram is shown in Figure 6.64 from which the applied moments at the weld end of the cover plate are determined as:

Dead load moment: $M_{DL_1} = 102.27$ kip-ft

Dead load moment: $M_{DL_2} = 18.18$ kip-ft

Live load + impact: $M_{LL+I} = 295.45$ kip-ft

Stresses in Steel Beam

The stresses at the top and bottom of the steel beam are calculated for M_{DL_1}, M_{DL_2}, and M_{LL+I}.

The dead load moment M_DL_1 is supported by the steel beam alone. Therefore, the stresses at the top and bottom of the beam are calculated for the

op flange:

$$_{DL_1} = -\frac{M_{DL_1} d/2}{I} = -\frac{102.27 \times 12 \times 13.35}{2825} = -5.80 \text{ ksi}$$

d bottom flange:

$$\sigma_{DL_1} = 5.80 \text{ ksi}$$

The dead load moment M_{DL_2} is supported by the composite section with $3n = 24$. The stresses at the top and bottom of the beam are calculated for the top flange:

$$\sigma_{DL_2} = -\frac{M_{DL_2}}{S_{\text{Top of steel}}} = -\frac{18.18 \times 12}{1529} = -0.14 \text{ ksi}$$

and bottom flange:

$$\sigma_{DL_2} = \frac{M_{DL_2}}{S_{\text{Bot. of steel}}} = \frac{18.18 \times 12}{308} = 0.71 \text{ ksi}$$

The live load + impact load moment M_{LL+I} is supported by the composite section with $n = 8$. The stresses at the top and bottom of beam are for the top flange:

$$\sigma_{LL+I} = 0.0 \text{ ksi}$$

and bottom flange:

$$\sigma_{LL+I} = \frac{LL+I}{S_{\text{Bot. of steel}}} = \frac{295.45 \times 12}{338} = 10.49 \text{ ksi}$$

Therefore, the stresses acting on the top and bottom flanges of the steel beam are:

$$\sigma_{\text{Top}} = -(5.80 + 0.14 + 0) = -5.94 \text{ ksi}$$

$$\sigma_{\text{Bottom}} = (5.80 + 0.71 + 10.49) = 17.0 \text{ ksi}$$

As shown in Figure 6.65, such linearly distributed stresses are decomposed into axial tension and pure bending components of:

$$\sigma'_t = \frac{\sigma_{\text{Top}} + \sigma_{\text{Bottom}}}{2} = 5.53 \text{ ksi} \quad \text{and} \quad \sigma'_b = \frac{\sigma_{\text{Top}} - \sigma_{\text{Bottom}}}{2} = 11.47 \text{ ksi}$$

Then, the corresponding reference stresses are:

$$\sigma_t = \sigma'_t = 5.53 \text{ ksi and } \sigma_b = \sigma'_b \frac{d_f}{d} = 11.47 \times \frac{26.07}{26.71} = 11.20 \text{ ksi}$$

SIFs for Web and Flange Crack Tips

The SIFs for the web and flange crack tips are obtained by superposition:

$$K_w = (f_{w,t}\,\sigma_t + f_{w,b}\,\sigma_b)\sqrt{\pi a_w}$$

$$K_f = (f_{f,t}\,\sigma_t + f_{f,b}\,\sigma_b)\sqrt{\pi a_f}$$

With parameter $\beta = 1.06, \lambda_f = 0.502$ and $\lambda_w = 0.112$, the correction factors are determined from equation 6.7: $f_{w,t} = 1.0196$, $f_{w,b} = 0.8838$, $f_{f,t} = 1.240$ and $f_{f,b} = 1.2363$. Therefore, the SIFs are given by:

$$K_w = (1.0196 \times 5.53 + 0.9938 \times 11.47)\sqrt{3.1416 \times 3} = 52.30 \text{ ksi}\sqrt{\text{in.}}$$

$$K_f = (1.2406 \times 5.53 + 1.2363 \times 11.47)\sqrt{3.1416 \times 2.5} = 58.97 \text{ ksi}\sqrt{\text{in.}}$$

6.7 Conclusions

SIF equations for the two-tip and three-tip cracked I-beams under tension or bending were obtained. For a two-tip cracked I-beam, the best fitting equation is a 15-term polynomial equation of web crack length, eccentricity, anc flanges-to-web area ratio. For a three-tip cracked I-beam, the best fitting equation is a 26-term polynomial ratio equation of web crack length, flange crack length and flanges-to-web area ratio. The maximum positive and negative fitting errors are summarized in Table 6.7. For the interpolation values of the empirical equations between the sample points, no solutions are available for direct comparison, however the equation appears reasonable based on

engineering judgement.

The obtained SIF equations can be applied to I-beams used in civil engineering from W8 to W40 with a wide range of crack geometries. Howe to use these empirical equations to calculate SIFs for welded girders, the relationship between the skeleton ratio γ and cross-sectional area ratio β should fall into the fuzzy band of Figure 3.4 as discussed in Chapter 3.

If the applied loading is simple uniform tension or pure bending, the abov obtained empirical equations can be applied directly. If the applied loading ca be decomposed into the components of uniform tension and pure bending, the equations can be used based on the principle of superposition. Otherwise, the obtained equations cannot be used directly. In this case other numerical methods, e.g., weight function methods, should be used. The SIF equations presented in this chapter provide the necessary reference solutions.

Chapter 7: Summary and Conclusions

Based on the results of this study, the following conclusions are dra

Parameters

- The SIF or correction factor for a two-tip crack in the web of an I-beam a function of eccentricity $\varepsilon = e/(d_j/2)$, web crack length $\lambda_w = a_w/(d_j/2 - e)$, an flanges-to-web cross-sectional area ratio $\beta = 2A_f/A_w$. The SIF for a three-t crack in the web and flange of an I-beam are a function of web crack lengt $\lambda_w = a_w/d_j$, flange crack length $\lambda_f = a_f/(b_j/2)$, and flanges-to-web cross-sectional area ratio β.
- The depth-width ratio $\gamma = d_j/b_f$ of a cracked I-beam is not a significant parameter in the calculation of SIFs. Its effect becomes noticeable only for very long cracks. For all I-beams listed in the LRFD Manual, the flanges-to-web area ratio and the depth-width ratio are linearly related, within a bandwidth. Therefore, the I-beams can be characterized in terms of parameter β alone.

Two-tip Cracked I-beam

- The calculated (FEA) SIFs have smooth and flat relationships with parameters λ_w, ε, and β. The 15-term polynomial equation 6.3 (a cubic equation of the three parameters) best fits the calculated SIFs for the upper or lower crack tips under tension or bending. The prediction errors are withir ±1% for most of the data.

- The web crack is constrained by the two flanges. As a result, the SIF for the web crack is smaller than that for a single plate. The flange constraint increases as the crack tip approaches the junction point of web and flange. Increasing the flanges-to-web area ratio also increases the constraining effect.

Three-tip Cracked I-beam

- The calculated SIFs have smooth and flat relationships with parameters λ_w, λ_f and β. The 26-term polynomial-ratio equation 6.7 (a fourth power equation of the three parameters) best fits the calculated SIFs for the web and flange crack tips under tension or bending. The prediction errors are again within ±2% for most data.

- The SIFs are affected by the interaction forces between the web and flange. These forces depend on the compatibility of the web and flange displacements along the junction line. If the displacements along the centerline of the flange are larger than those of the corresponding points along the web edge, the web tends to close the flange crack while the flange tends to open the web crack. Conversely, if the displacements along the centerline of the flange are smaller than those of the corresponding points along the web edge, the web tends to open the flange crack while the flange tends to close the web crack.

- The interaction forces are negligible when the web and flange cracks — in separated plates — have equal CMODs. Such a pair of crack lengths is

called non-interacting, and in this case the SIFs of I-beams can be calculated from those of corresponding single plates. Non-interacting crack lengths help in understanding the behavior of three-tip cracked I-beams and assist in developing a rapid, approximate method of calculating SIFs.

Applications

- The SIF equations 6.3 and 6.7 can be applied to I-beams of sizes W8 to W40 and welded girders with $0.83 \leq \beta \leq 2.05$. However, these equations were developed for rolled W-shapes, they should be applied with caution to plate girders because the SIFs may be affected by the depth-width ratio. Section 6.4 outlines approximation procedures for calculating SIFs for composite and singly symmetric sections.

2-D Simplified Modeling

- The 3-D problem of a cracked I-beam can be simplified to a 2-D problem by joining the web and flanges only in the direction of the junction lines. For a two-tip crack, 2-D analysis is accurate to 1% for crack lengths $\lambda_w \leq 0.5$ and 5% for $\lambda_w \leq 0.9$; for a three-tip crack, 2-D analysis is accurate to 1% except in I-beams with long web and short flange cracks. The agreement between 2-D and 3-D analyses strongly suggests that the interaction between the cracked web and flange is controlled mostly by the compatibility of displacements in the direction of the junction line.

SIF Calculation from FEA

- The J-integral method yields more accurate SIFs than the displacement-

based methods as long as the integral contours are chosen away from the crack tip.

- In the inner region around the crack tip, increasing parameter *n*, which defines the number of elements around a concentric square, improves the accuracy of SIFs more than increasing parameter *m*, which defines the number of concentric squares. When $n = 8$, the mesh is fine enough to give converging results.
- The three displacement-based methods yield nearly equal results. For a coarse mesh of $n = 2$ or 4, the quarter-point displacement method (equation 2.12) is more accurate than the nonlinear and linear extrapolation methods (equation 2.7 and 2.10).

Appendix A: Benchmark Studies

A.1 Objective

The objectives of the work described in this appendix are to:

- Choose a suitable mesh pattern — element density and aspect ratio — in the inner region around the crack tip.
- Examine methods of extracting SIFs from FEA results, including COD (equations 2.7, 2.10, and 2.12) and J-integral methods.

A.2 Benchmark Problems

The following three geometries/loadings, for which accurate SIF solutions exist, were analyzed:

- Center-cracked finite-width plate under 100-MPa tension (Tada 1973). The plate shown in Figure A.1a was $2W = 200$ mm wide, $2h = 600$ mm long, and $t = 10$ mm thick.
- Edge-cracked finite-width plate under ±100-MPa bending (Brown 1966, Tada 1973). The plate was $W = 100$ mm wide, $2h = 300$ mm long, and $t = 10$ mm thick Figure A.1b.
- Edge-cracked finite-width plate under 100-MPa tension (Tada 1973). The plate dimensions are shown in Figure A.1b.

For each geometry/loading, the parameters were varied as follows:

- Crack lengths: $a/W = 0.1$, 0.5 and 0.9
- Mesh patterns: up to 10 combinations of number of elements around a concentric square m = 2, 3, and 4; and number of concentric squares n = 2, 4, 8 and 16 (Figure 2.7).
- Methods of calculating SIFs: nonlinear extrapolation (equation 2.7), linear extrapolation (equation 2.10), quarter-point displacement (equation 2.12), and J-integral (equation 2.26).

All three geometries were modeled with eight-node, plane stress elements — ABAQUS designation CPS8R — throughout the inner and outer regions of the plates (Figure 2.6). Elements sharing a node with the crack tip were generated with ABAQUS' *SINGULAR command (Figure 2.4).

SIFs calculated with FEA were compared with those from existing solutions in terms of the ratio K_{FEA} / K_{exist}.

A.3 Results and Discussions

The results are summarized in Tables A.1, A.2 and A.3 for the center-cracked plate under tension, edge-cracked plate under bending, and edge-cracked plate under tension respectively.

A.3.1 Mesh Pattern in Inner Region

Effect of Parameter *m*

Presented in the upper halves of Tables A.1 and A.2 are the effect of parameter *m* on the SIFs for the center-cracked plate under tension and edge-cracked plate under bending respectively. This is done for one crack length, $a/W = 0.5$, and each of the four values of parameter $n = 2, 4, 8$ and 16. Clearly parameter *m* has practically no effect on the SIFs for any of the *n* values and four calculation methods.

Effect of Parameter *n*

The lower halves of Tables A.1, A.2 and A.3 show the effect of parameter *n* on the SIFs for all three geometries/loadings. This is done for a constant parameter $m = 3$ and three crack lengths $a/W = 0.1$, 0.5 and 0.9. The following is concluded from the results:

- For the displacement-based methods, increasing parameter *n* from 2 to 4 and 8 improves the accuracy of the SIF; but increasing it further to 16 yields no additional gain in accuracy.
- For the J-integral method, parameter *n* has practically no effect on the accuracy of calculating SIFs.

A.3.2 Accuracy

J-integral Method

SIFs calculated from J values are more accurate than those calculated All J-based SIFs agree with the existing solutions within ±0.5%, even for the coarsest mesh, $m \times n = 2 \times 2$.

While in theory the J-integral is path-independent, in FEA it is only approximately path-independent. Figure A.2 shows the J-integral values as a function of distance from the crack tip to the intersection point of concentric contours with the crack extension line. The first contour — zero distance — is the crack tip. J-integral values were determined for a center-cracked plate under tension, with crack length $a = 50$ mm and half plate width $W = 100$ mm. Parameter n was varied from $n = 2$ to 16 while parameter m was kept constant at $m = 3$. As can be seen, the accuracy increases with mesh refinement. When the mesh is coarse ($m \times n = 3 \times 2$ and 3×4), J-integral values should be calculated along the outermost contour. When the mesh is fine ($m \times n = 3 \times 8$ and 3×16), J-integral values rapidly converge to the exact solution.

COD Methods

Among the COD methods whose results are given in Tables A.1, A.2 and A.3, the quarter-point displacement method (equation 2.12) is the most accurate followed closely by linear extrapolation (equation 2.10). Nonlinear extrapolation (equation 2.7) is the least accurate, but only so for the smaller

values of parameter n = 2 and 4. For finer meshes, the differences between equations 2.7, 2.10 and 2.12 are smaller.

Figure A.3 compares COD profiles calculated with equations 2.4 and 2.11 for a center-cracked plate under tension, with a/W = 0.5 and mesh pattern m x n = 3 x 8. The COD profiles are nearly equal, the maximum difference being about ± 0.2%. Therefore, the corresponding SIFs (equations 2.7 and 2.10) are also nearly equal. Similar trends can be found for other crack lengths.

Apparent SIF

As stated in section 2.5.1, equations 2.7, 2.10 and 2.12 give equal SIFs only when the condition $2v_B = v_C$ (equation 2.13) is satisfied. This strict condition requires the size of the crack-tip element to be zero, which cannot be met in FEA.

According to the FEA calculations, $(2v_B - v_C) > 0.0$ (Table A.4) for the central and edge cracks with a/W = 0.1 and the central crack with a/W = 0.5. In these cases, the first derivatives of the apparent SIF equations 2.5 and 2.9 with respect to r, which are the slopes of the curves, become negative. So equations 2.5 and 2.9 approach the crack tip from below as shown in Figures A.4 and A.5. The figures also show that the convex curve equation 2.5 (negative curvature) and straight line equation 2.9 intersect at both the quarter point B and corner point C; at the quarter point, equations 2.5, 2.9 and 2.12 have equal SIF values. Therefore, equation 2.12 always predicts the smallest SIF value, and equation 2.5 predicts the largest. The result of equation 2.10 falls inbetween.

For longer crack lengths of $a/W = 0.5$ and 0.9, the FEA results yield $2v_B - v_C < 0$ (Table A.4) and, therefore, the first derivatives of equations 2.5 and 2.9 with respect to r become positive. As shown in Figure A.6, the concave equation 2.5 (positive curvature) and straight line equation 2.9 approach the crack tip from above. In this case, equation 2.5 produces the smallest SIF value and equation 2.12 produces the largest. Again, the result of equation 2.10 falls inbetween.

A.3.3 Additional Cases

Having determined the effects of mesh pattern and method of calculating K from FEA results, the focus of the benchmark studies shifted to further ascertaining accuracy for the following cases:

- Center-cracked plate under tension or bending; with crack lengths $a/W =$ 0.1 to 0.9 in steps of 0.1 for tension, and $a/W = 0.1$ to 0.9 in steps of 0.2 for bending (Figure A.1a).
- Edge-cracked plate under tension or bending; with crack lengths $a/W =$ 0.1 to 0.9 in steps of 0.1 (Figure A.1b).
- Eccentrically cracked plate under tension or bending; with crack lengths $a/(W - e) = 0.1$ to 0.9 in steps of 0.2; and eccentricities $e/W =$ 0.1 to 0.9 in steps of 0.2 (Figure A.7).

In all subsequent FEAs, the mesh pattern was $m \times n = 3 \times 8$ and SIFs

were determined from J-integral values.

FEA SIFs for the center-cracked plate with $0.1 \leq a/W \leq 0.9$ agree very well with those reported by Tada (1973) for tension and Chen and Albrecht (1992) for bending as shown in Figure A.8. Maximum absolute differences are 0.2% at $a/W = 0.1$ in the former and 0.5% at $a/W = 0.7$ in the latter. FEA clearly yields accurate SIF values. Isida's (1956) and Benthem and Koiter's (1972) solutions for bending are very accurate only for $0.1 \leq a/W \leq 0.3$, but the solutions become more inaccurate as the crack length increases.

In the second evaluation of accuracy, FEA SIFs for the edge-cracked plate are seen in Figure A.9 to agree very well with those from Tada (1973) for tension and Brown (1966) for bending, with maximum differences of 0.7% at $a/W = 0.1$ and 0.2% at $a/W = 0.3$ respectively. The FEA solution for bending agrees very well with Tada's (1973) solution for a short crack, $a/W = 0.1$, and long cracks, $0.6 \leq a/W \leq 0.9$; but the differences are larger for intermediate length cracks, $0.2 \leq a/W \leq 0.5$, with a maximum of 2.2% at $a/W = 0.3$.

Finally, Figures A.10 and A.11 compare the FEA SIFs for an eccentrically cracked plate with those reported by Isida (1965) for tension and Chen and Albrecht (1992) for bending respectively. Again, the agreement is very good for combinations of crack lengths, $0.1 \leq a/(W - e) \leq 0.7$, and eccentricities, $0.1 \leq e/W \leq 0.7$; within these ranges, maximum differences are ± 0.5%. Larger differences are found for the largest crack length, $a/(W - e) = 0.9$, and/or eccentricity, $e/W = 0.9$, at which differences are ± 3%.

In summary, FEA with $m \times n = 3 \times 8$ mesh pattern at the crack tip yields very accurate J-based SIFs. This was shown consistently for all combinations of three geometries and two loading conditions.

FEA SIFs were compared with those from existing solutions in terms of the ratio K_{FEA} / K_{exist}. Existing solutions were used as the yardstick simply because they preceded the FEA solutions of this study, not because existing solutions are necessarily more accurate. Since no exact analytical solutions exist for any of the three geometries, it is not known whether FEA or existing solutions are more accurate.

A.4 Conclusions

Based on the results of the benchmark studies, the following conclusions can be drawn:

- The J-integral method yields the most accurate SIF values, even for a coarse mesh.
- Increasing parameter n improves the accuracy of SIFs more than increasing parameter m.
- When $n = 8$, the mesh is fine enough the results converge.
- The displacement-based methods produce close results. For coarse meshes of $n = 2$ and 4, the quarter-point displacement method (equation 2.12) is the most accurate.

Appendix B: Tables and Figures

Table 1.1. Methods of determining stress intensity factors.

Category 1	Category 2	Category 3
Handbooks	Superposition	Collocation (Mapping)
	Stress Concentration	Integral Transform/continuous Dislocation
	Stress Distribution	Body Force Method
	Green's Function	Edge Function Method
	Weight Function	Method of Lines
	Compounding	Finite Elements Method
		Boundary Element Method
		Alternating Technique

Table 3.1. W-shapes used in calculations of SIFs.

β	W-Shape	d_j (mm)	t_w (mm)	b_f (mm)	t_f (mm)	γ	Shape
0.83	W40X149[a, b, d]	949.2	16.0	300.0	21.1	3.16	1
0.83	W24X62[a]	588.0	10.9	178.8	15.0	3.29	2
1.00	W30X108[a, b]	738.4	13.8	266.1	19.3	2.77	1
1.00	W40X167[a]	954.2	16.5	300.0	26.0	3.18	2
1.11	W40X192[a, b, c]	949.2	18.0	449.8	21.1	2.11	1
1.11	W36X170[a, c]	890.8	17.3	305.6	27.9	2.91	2
1.25	W21X62[a, b]	517.5	10.2	209.3	15.6	2.47	1
1.25	W27X114[a]	669.5	14.5	255.8	23.6	2.62	2
1.37	W40X199[a, b, d]	955.2	16.5	400.1	27.1	2.39	1
1.37	W24X103[a]	598.2	14.0	228.6	24.9	2.62	2
1.69	W30X191[a, b]	749.2	18.0	382.0	30.1	1.96	1
1.69	W36X280[a]	887.7	22.5	421.5	39.9	2.11	2
1.91	W21X101[a, b]	522.2	12.7	312.2	20.3	1.67	1
1.91	W21X147[a]	531.1	18.3	317.8	29.2	1.67	2
1.53	W33X201[b]	826.26	18.2	399.9	29.2	2.07	...
2.05	W18X97[b, d]	450.09	13.6	283.1	22.1	1.59	...

[a] W-shapes used in validation of β (chapter 3)
[b] W-shapes for which SIFs were calculated (chapter 5)
[c] W-shapes deleted from subsequent analyses (chapters 3 and 5)
[d] W-shapes used in comparison of 2-D and 3-D modelings(chapter 2)

Table 4.1. Non-interacting crack lengths for T-section.

Non-interacting crack lengths					
T-flange (tension)		T-web (tension)		T-web (bending)	
$2a_f/W$	a_f (mm)	a_w/W	a_w (mm)	a_w/W	a_w (mm)
0.0	0.0	0.0	0.0	0.0	0.0
0.05	5.0	0.0171	3.42	0.0172	3.44
0.10	10.0	0.0342	6.84	0.0346	6.92
0.15	15.0	0.0513	10.26	0.0524	10.47
0.20	20.0	0.0684	13.68	0.0704	14.07
0.25	25.0	0.0855	17.10	0.0888	17.75
0.30	30.0[a]	0.1028	20.55[a]	0.1077	21.53
0.35	35.0	0.1201	24.01	0.1271	25.42
0.40	40.0	0.1377	27.54	0.1473	29.45
0.45	45.0	0.1556	31.12	0.1681	33.61
0.50	50.0[a, b]	0.1740	34.79[a, b]	0.1898	37.95
0.55	55.0	0.1929	38.58	0.2124	42.47
0.60	60.0	0.2126	42.51	0.2361	47.21
0.65	65.0	0.2332	46.63	0.2610	52.20
0.70	70.0[a]	0.2549	50.98[a]	0.2875	57.49
0.75	75.0	0.2783	55.66	0.3159	63.17
0.80	80.0	0.3039	60.78	0.3468	69.36
0.85	85.0	0.3328	66.56	0.3816	76.32
0.90	90.0	0.3673	73.45	0.4227	84.53

[a] Crack pairs for comparing SIFs for T-section and single plates.
[b] Crack pairs for comparing CODs and displacements along junction line.

Table 4.2. Non-interacting crack lengths for three-tip cracked I-beams.

W-shapes	Web depth d_j (mm)	Flange width b_f (mm)	Depth-width ratio d_j/b_f	Web crack length a_w/d_j	Non-interacting flange crack length, $2a_f/b_f$					
					Tension			Bending		
					From CMOD	From K_f (FEA)	From K_w (FEA)	From CMOD	From K_f (FEA)	From K_w (FEA)
W40 X149	949.2	300.0	3.16	0.05	0.42	...	...	0.41	...	...
				0.10	0.67	0.60	0.65	0.66	0.60	0.62
W30 X108	738.4	266.1	2.77	0.05	0.37	...	...	0.37	...	...
				0.10	0.63	0.57	0.60	0.61	0.55	0.57
W21 X 62	517.5	209.3	2.47	0.05	0.34	...	...	0.34	...	...
				0.10	0.58	0.52	0.56	0.57	0.50	0.52
W40 X199	955.2	400.1	2.39	0.05	0.33	...	...	0.32	...	...
				0.10	0.57	0.51	0.54	0.56	0.50	0.51
W33 X201	826.3	399.9	2.07	0.05	0.29	...	...	0.29	...	...
				0.10	0.52	0.50	0.50	0.51	0.46	0.46
				0.15	0.68	...	...	0.66	...	...
W30 X191	749.2	382.0	1.96	0.05	0.28	...	...	0.27	...	...
				0.10	0.50	0.47	0.47	0.49	0.45	0.45
				0.15	0.67	...	...	0.65	...	...
W21 X101	522.2	312.2	1.67	0.05	0.24	...	...	0.24	...	...
				0.10	0.45	0.41	0.42	0.43	0.40	0.40
				0.15	0.61	...	...	0.59	...	...
W18 X 97	450.0	283.1	1.59	0.05	0.23	...	...	0.22	...	...
				0.10	0.43	0.40	0.40	0.42	0.39	0.38
				0.15	0.59	...	...	0.57	...	...
				0.20				0.69		

Table 5.1. Correction factors f^A for two-tip cracked I-beam under tension; upper tip.

β =	ε =	$\lambda_w = 2a_w/(d_1 - 2e)$								
$2A_f/A_w$	$2e/d_1$	0.1	0.2	0.3	0.4	0.5	0.6	0.7	0.8	0.9
	0.0	1.0019	1.0076	1.0169	1.0307	1.0475	1.0678	1.0866	1.0979	1.0562
	0.1	1.0015	1.0062	1.0139	1.0243	1.0375	1.0531	1.0705	1.0875	1.0995
	0.3	1.0011	1.0043	1.0098	1.0170	1.0257	1.0357	1.0465	1.0571	1.0653
0.83	0.5	1.0007	1.0031	1.0067	1.0114	1.0172	1.0235	1.0302	1.0358	1.0386
	0.7	1.0002	1.0010	1.0024	1.0040	1.0058	1.0078	1.0085	1.0082	1.0052
	0.9	0.9995	0.9983	0.9963	0.9936	0.9893	0.9884	0.9783	0.9706	0.9621
	0.0	1.0015	1.0060	1.0138	1.0244	1.0371	1.0512	1.0624	1.0595	1.0048
	0.1	1.0012	1.0052	1.0111	1.0194	1.0297	1.0413	1.0534	1.0637	1.0671
	0.3	1.0009	1.0035	1.0077	1.0132	1.0199	1.0275	1.0352	1.0421	1.0463
1.00	0.5	1.0005	1.0022	1.0049	1.0086	1.0124	1.0166	1.0209	1.0237	1.0235
	0.7	1.0001	1.0004	1.0009	1.0015	1.0020	1.0022	1.0014	0.9992	0.9939
	0.9	0.9994	0.9979	0.9954	0.9919	0.9870	0.9812	0.9743	0.9658	0.9565
	0.0	1.0014	1.0055	1.0122	1.0223	1.0326	1.0464	1.0523	1.0546	0.9895
	0.1	1.0012	1.0047	1.0103	1.0178	1.0271	1.0376	1.0483	1.0572	1.0595
	0.3	1.0008	1.0033	1.0072	1.0124	1.0184	1.0253	1.0322	1.0383	1.0417
1.11	0.5	1.0006	1.0021	1.0049	1.0080	1.0117	1.0158	1.0195	1.0221	1.0220
	0.7	1.0002	1.0006	1.0013	1.0021	1.0030	1.0035	1.0033	1.0013	0.9967
	0.9	0.9995	0.9983	0.9965	0.9941	0.9903	0.9855	0.9798	0.9724	0.9642
	0.0	1.0011	1.0044	1.0099	1.0170	1.0254	1.0319	1.0352	1.0180	0.9507
	0.1	1.0009	1.0038	1.0083	1.0143	1.0213	1.0289	1.0356	1.0393	1.0341
	0.3	1.0006	1.0025	1.0055	1.0096	1.0141	1.0189	1.0236	1.0268	1.0268
1.25	0.5	1.0004	1.0014	1.0030	1.0051	1.0074	1.0096	1.0113	1.0109	1.0082
	0.7	0.9999	0.9997	0.9994	0.9989	0.9979	0.9964	0.9939	0.9895	0.9822
	0.9	0.9992	0.9973	0.9943	0.9903	0.9842	0.9774	0.9694	0.9600	0.9500

Table 5.1. Correction factors f^A for two-tip cracked I-beam under tension; upper tip.

β =	ε =	$\lambda_w = 2a_w/(d_1 - 2e)$								
$2A_f/A_w$	$2e/d_1$	0.1	0.2	0.3	0.4	0.5	0.6	0.7	0.8	0.9
	0.0	1.0009	1.0038	1.0083	1.0142	1.0205	1.0255	1.0246	1.0069	0.9334
	0.1	1.0008	1.0031	1.0069	1.0116	1.0172	1.0229	1.0271	1.0276	1.0191
1.37	0.3	1.0005	1.0021	1.0044	1.0075	1.0111	1.0148	1.0180	1.0196	1.0177
	0.5	1.0002	1.0009	1.0022	1.0034	1.0050	1.0063	1.0068	1.0057	1.0014
	0.7	0.9999	0.9994	0.9987	0.9977	0.9962	0.9943	0.9909	0.9858	0.9778
	0.9	0.9992	0.9972	0.9939	0.9894	0.9832	0.9760	0.9677	0.9577	0.9472
	0.0	1.0007	1.0031	1.0064	1.0106	1.0147	1.0165	1.0115	0.9882	0.9095
	0.1	1.0006	1.0023	1.0051	1.0089	1.0128	1.0164	1.0179	1.0151	1.0025
1.53	0.3	1.0003	1.0015	1.0034	1.0056	1.0080	1.0104	1.0119	1.0118	1.0081
	0.5	1.0002	1.0005	1.0012	1.0019	1.0025	1.0027	1.0021	0.9997	0.9941
	0.7	0.9998	0.9990	0.9980	0.9965	0.9944	0.9912	0.9874	0.9815	0.9729
	0.9	0.9992	0.9971	0.9934	0.9889	0.9825	0.9749	0.9664	0.9561	0.9455
	0.0	1.0005	1.0024	1.0048	1.0075	1.0097	1.0081	0.9997	0.9692	0.8856
	0.1	1.0004	1.0018	1.0041	1.0067	1.0092	1.0110	1.0104	1.0049	0.9890
	0.3	1.0002	1.0011	1.0025	1.0040	1.0056	1.0067	1.0069	1.0054	1.0001
1.69	0.5	1.0000	1.0001	1.0003	1.0004	1.0001	0.9997	0.9978	0.9944	0.9879
	0.7	0.9997	0.9986	0.9972	0.9952	0.9924	0.9886	0.9840	0.9771	0.9681
	0.9	0.9991	0.9969	0.9929	0.9880	0.9813	0.9734	0.9644	0.9539	0.9428
	0.0	1.0004	1.0017	1.0033	1.0051	1.0051	1.0034	0.9905	0.9632	0.8741
	0.1	1.0003	1.0013	1.0028	1.0045	1.0061	1.0065	1.0042	0.9968	0.9794
	0.3	1.0002	1.0007	1.0016	1.0024	1.0035	1.0039	1.0032	1.0004	0.9942
1.91	0.5	0.9999	0.9999	0.9998	0.9996	0.9990	0.9979	0.9956	0.9916	0.9842
	0.7	0.9996	0.9987	0.9971	0.9949	0.9921	0.9880	0.9827	0.9755	0.9660
	0.9	0.9992	0.9968	0.9933	0.9884	0.9816	0.9738	0.9651	0.9545	0.9438

Table 5.1. Correction factors f^A for two-tip cracked I-beam under tension; upper tip.

β =	ε =	$\lambda_w = 2a_w/(d_1 - 2e)$								
$2A_f/A_w$	$2e/d_1$	0.1	0.2	0.3	0.4	0.5	0.6	0.7	0.8	0.9
2.05	0.0	1.0003	1.0011	1.0021	1.0031	1.0022	0.9975	0.9840	0.9507	0.8629
	0.1	1.0002	1.0009	1.0020	1.0029	1.0034	1.0024	0.9984	0.9889	0.9686
	0.3	1.0000	1.0004	1.0008	1.0012	1.0014	1.0014	0.9996	0.9959	0.9886
	0.5	0.9999	0.9996	0.9991	0.9984	0.9971	0.9953	0.9918	0.9869	0.9788
	0.7	0.9997	0.9982	0.9964	0.9937	0.9903	0.9859	0.9801	0.9726	0.9626
	0.9	0.9990	0.9967	0.9928	0.9877	0.9807	0.9725	0.9634	0.9526	0.9418

Table 5.2. Correction factors f^B for two-tip cracked I-beam under tension; lower tip.

β =	ε =	$\lambda_w = 2a_w/(d_1 - 2e)$								
$2A_f/A_w$	$2e/d_1$	0.1	0.2	0.3	0.4	0.5	0.6	0.7	0.8	0.9
	0.0	1.0019	1.0076	1.0169	1.0307	1.0475	1.0678	1.0866	1.0979	1.0562
	0.1	1.0015	1.0066	1.0149	1.0267	1.0419	1.0598	1.0773	1.0857	1.0476
	0.3	1.0012	1.0084	1.0111	1.0202	1.0313	1.0438	1.0540	1.0524	1.0024
0.83	0.5	1.0008	1.0032	1.0071	1.0124	1.0183	1.0233	1.0232	1.0087	0.9427
	0.7	1.0002	1.0008	1.0016	1.0020	1.0007	0.9958	0.9833	0.9531	0.8752
	0.9	0.9994	0.9976	0.9942	0.9883	0.9780	0.9623	0.9377	0.8960	0.8149
	0.0	1.0015	1.0060	1.0138	1.0244	1.0371	1.0512	1.0624	1.0595	1.0048
	0.1	1.0012	1.0052	1.0117	1.0211	1.0324	1.0446	1.0544	1.0515	0.9987
	0.3	1.0009	1.0038	1.0085	1.0150	1.0229	1.0304	1.0336	1.0225	0.9605
1.00	0.5	1.0005	1.0023	1.0049	1.0081	1.0109	1.0117	1.0061	0.9833	0.9096
	0.7	1.0001	1.0001	0.9998	0.9985	0.9951	0.9873	0.9708	0.9355	0.8531
	0.9	0.9993	0.9970	0.9930	0.9860	0.9747	0.9573	0.9309	0.8869	0.8031
	0.0	1.0014	1.0055	1.0122	1.0223	1.0326	1.0464	1.0523	1.0546	0.9895
	0.1	1.0012	1.0047	1.0108	1.0194	1.0297	1.0409	1.0496	1.0472	0.9998
	0.3	1.0008	1.0038	1.0079	1.0141	1.0215	1.0285	1.0321	1.0231	0.9680
1.11	0.5	1.0006	1.0022	1.0049	1.0080	1.0112	1.0126	1.0088	0.9899	0.9240
	0.7	1.0000	1.0004	1.0005	1.0001	0.9979	0.9924	0.9793	0.9492	0.8740
	0.9	0.9995	0.9979	0.9947	0.9896	0.9803	0.9659	0.9433	0.9042	0.8264
	0.0	1.0011	1.0044	1.0099	1.0170	1.0254	1.0319	1.0352	1.0180	0.9507
	0.1	1.0010	1.0038	1.0087	1.0150	1.0221	1.0289	1.0307	1.0169	0.9502
	0.3	1.0006	1.0026	1.0058	1.0101	1.0141	1.0165	1.0128	0.9924	0.9189
1.25	0.5	1.0004	1.0013	1.0025	1.0036	1.0034	0.9999	0.9880	0.9580	0.8759
	0.7	0.9999	0.9992	0.9979	0.9948	0.9889	0.9778	0.9570	0.9191	0.8294
	0.9	0.9991	0.9966	0.9918	0.9835	0.9704	0.9512	0.9222	0.8754	0.7880

Table 5.2. Correction factors f^B for two-tip cracked I-beam under tension; lower tip.

β =	ε =	$\lambda_w = 2a_w/(d_1 - 2e)$								
$2A_f/A_w$	$2e/d_1$	0.1	0.2	0.3	0.4	0.5	0.6	0.7	0.8	0.9
1.37	0.0	1.0009	1.0038	1.0083	1.0142	1.0205	1.0255	1.0246	1.0069	0.9334
	0.1	1.0008	1.0031	1.0071	1.0120	1.0173	1.0212	1.0196	1.0015	0.9291
	0.3	1.0005	1.0021	1.0044	1.0075	1.0099	1.0101	1.0035	0.9791	0.9002
	0.5	1.0002	1.0007	1.0012	1.0014	1.0001	0.9946	0.9806	0.9474	0.8611
	0.7	0.9996	0.9990	0.9970	0.9933	0.9865	0.9740	0.9514	0.9088	0.8175
	0.9	0.9991	0.9962	0.9911	0.9824	0.9687	0.9485	0.9180	0.8690	0.7783
1.53	0.0	1.0007	1.0031	1.0064	1.0106	1.0147	1.0165	1.0115	0.9882	0.9095
	0.1	1.0006	1.0023	1.0054	1.0089	1.0121	1.0132	1.0076	0.9844	0.9071
	0.3	1.0003	1.0015	1.0030	1.0047	1.0055	1.0030	0.9931	0.9647	0.8830
	0.5	1.0000	1.0002	1.0002	0.9991	0.9962	0.9888	0.9724	0.9363	0.8491
	0.7	0.9995	0.9985	0.9961	0.9916	0.9836	0.9700	0.9458	0.9022	0.8123
	0.9	0.9990	0.9963	0.9907	0.9818	0.9679	0.9474	0.9170	0.8683	0.7787
1.69	0.0	1.0005	1.0024	1.0048	1.0075	1.0097	1.0081	0.9997	0.9692	0.8856
	0.1	1.0004	1.0018	1.0041	1.0062	1.0078	1.0063	0.9975	0.9699	0.8877
	0.3	1.0002	1.0010	1.0021	1.0024	1.0016	0.9971	0.9842	0.9518	0.8664
	0.5	1.0000	0.9998	0.9991	0.9973	0.9927	0.9834	0.9643	0.9253	0.8356
	0.7	0.9997	0.9981	0.9951	0.9897	0.9806	0.9654	0.9396	0.8942	0.8026
	0.9	0.9990	0.9960	0.9899	0.9807	0.9662	0.9448	0.9135	0.8636	0.7725
1.91	0.0	1.0004	1.0017	1.0033	1.0051	1.0051	1.0034	0.9905	0.9632	0.8741
	0.1	1.0003	1.0013	1.0028	1.0042	1.0042	1.0014	0.9908	0.9616	0.8793
	0.3	1.0001	1.0006	1.0010	1.0011	0.9992	0.9937	0.9796	0.9465	0.8613
	0.5	0.9999	0.9995	0.9986	0.9963	0.9914	0.9818	0.9624	0.9234	0.8341
	0.7	0.9996	0.9981	0.9951	0.9897	0.9807	0.9654	0.9399	0.8949	0.8045
	0.9	0.9990	0.9961	0.9903	0.9813	0.9671	0.9460	0.9153	0.8662	0.7762

Table 5.2. Correction factors f^B for two-tip cracked I-beam under tension; lower tip.

β =	ε =	$\lambda_w = 2a_w/(d_1 - 2e)$								
$2A_f/A_w$	$2e/d_1$	0.1	0.2	0.3	0.4	0.5	0.6	0.7	0.8	0.9
2.05	0.0	1.0003	1.0011	1.0021	1.0031	1.0022	0.9975	0.9840	0.9507	0.8629
	0.1	1.0002	1.0009	1.0017	1.0021	1.0008	0.9959	0.9825	0.9499	0.8642
	0.3	1.0000	1.0002	1.0000	0.9990	0.9960	0.9888	0.9727	0.9365	0.8491
	0.5	0.9999	0.9992	0.9975	0.9944	0.9882	0.9767	0.9553	0.9138	0.8246
	0.7	0.9997	0.9977	0.9942	0.9879	0.9778	0.9615	0.9347	0.8888	0.7985
	0.9	0.9990	0.9959	0.9899	0.9806	0.9657	0.9443	0.9130	0.8632	0.7729

Table 5.3. Correction factors f^A for two-tip cracked I-beam under bending; upper tip.

β =	ε =	$\lambda_w = 2a_w/(d_1 - 2e)$								
$2A_f/A_w$	$2e/d_1$	0.1	0.2	0.3	0.4	0.5	0.6	0.7	0.8	0.9
0.83	0.0	-0.0500	-0.1000	-0.1501	-0.2004	-0.2512	-0.3029	-0.3559	-0.4096	-0.4553
	0.1	0.0551	0.0106	-0.0336	-0.0777	-0.1217	-0.1659	-0.2107	-0.2570	-0.3062
	0.3	0.2653	0.2313	0.1980	0.1651	0.1328	0.1007	0.0688	0.0363	0.0020
	0.5	0.4754	0.4515	0.4283	0.4058	0.3836	0.3618	0.3399	0.3174	0.2930
	0.7	0.6850	0.6707	0.6567	0.6427	0.6290	0.6151	0.6007	0.5851	0.5672
	0.9	0.8947	0.8884	0.8816	0.8740	0.8653	0.8556	0.8452	0.8332	0.8205
1.00	0.0	-0.0500	-0.1000	-0.1500	-0.2003	-0.2509	-0.3021	-0.3541	-0.4056	-0.4467
	0.1	0.0551	0.0105	-0.0339	-0.0781	-0.1224	-0.1668	-0.2119	-0.2583	-0.3071
	0.3	0.2652	0.2310	0.1973	0.1640	0.1310	0.0982	0.0652	0.0315	-0.0041
	0.5	0.4752	0.4510	0.4274	0.4041	0.3812	0.3582	0.3351	0.3111	0.2849
	0.7	0.6850	0.6701	0.6555	0.6410	0.6262	0.6113	0.5956	0.5786	0.5592
	0.9	0.8945	0.8879	0.8807	0.8725	0.8631	0.8529	0.8416	0.8288	0.8153
1.11	0.0	-0.0500	-0.1000	-0.1501	-0.2003	-0.2508	-0.3021	-0.3542	-0.4063	-0.4500
	0.1	0.0551	0.0105	-0.0340	-0.0783	-0.1226	-0.1672	-0.2124	-0.2589	-0.3077
	0.3	0.2652	0.2310	0.1971	0.1637	0.1305	0.0975	0.0643	0.0304	-0.0053
	0.5	0.4752	0.4511	0.4273	0.4040	0.3808	0.3578	0.3345	0.3104	0.2844
	0.7	0.6850	0.6704	0.6558	0.6415	0.6270	0.6122	0.5968	0.5802	0.5613
	0.9	0.8947	0.8884	0.8818	0.8746	0.8661	0.8567	0.8466	0.8348	0.8222
1.25	0.0	-0.0500	-0.1000	-0.1500	-0.2002	-0.2506	-0.3014	-0.3523	-0.4016	-0.4379
	0.1	0.0551	0.0104	-0.0342	-0.0786	-0.1231	-0.1679	-0.2132	-0.2596	-0.3079
	0.3	0.2651	0.2307	0.1966	0.1628	0.1292	0.0955	0.0615	0.0266	-0.0102
	0.5	0.4751	0.4506	0.4264	0.4024	0.3785	0.3545	0.3301	0.3045	0.2769
	0.7	0.6848	0.6698	0.6544	0.6391	0.6233	0.6071	0.5901	0.5716	0.5510
	0.9	0.8945	0.8875	0.8797	0.8710	0.8607	0.8492	0.8373	0.8236	0.8094

Table 5.3. Correction factors f^A for two-tip cracked I-beam under bending; upper tip.

β =	ε =	$\lambda_w = 2a_w/(d_j - 2e)$								
$2A_f/A_w$	$2e/d_j$	0.1	0.2	0.3	0.4	0.5	0.6	0.7	0.8	0.9
	0.0	-0.0500	-0.1000	-0.1500	-0.2001	-0.2504	-0.3010	-0.3515	-0.3999	-0.4342
	0.1	0.0551	0.0103	-0.0343	-0.0789	-0.1235	-0.1684	-0.2138	-0.2602	-0.3083
1.37	0.3	0.2651	0.2306	0.1963	0.1622	0.1283	0.0942	0.0597	0.0244	-0.0131
	0.5	0.4750	0.4504	0.4260	0.4017	0.3774	0.3529	0.3278	0.3017	0.2733
	0.7	0.6849	0.6695	0.6540	0.6383	0.6222	0.6055	0.5880	0.5690	0.5476
	0.9	0.8943	0.8871	0.8793	0.8703	0.8597	0.8482	0.8356	0.8215	0.8068
	0.0	-0.0500	-0.1000	-0.1500	-0.2001	-0.2503	-0.3006	-0.3506	-0.3980	-0.4305
	0.1	0.0550	0.0102	-0.0345	-0.0792	-0.1239	-0.1689	-0.2145	-0.2609	-0.3087
	0.3	0.2650	0.2304	0.1959	0.1616	0.1273	0.0928	0.0578	0.0219	-0.0161
1.53	0.5	0.4749	0.4502	0.4254	0.4008	0.3760	0.3510	0.3253	0.2984	0.2694
	0.7	0.6846	0.6691	0.6533	0.6373	0.6207	0.6035	0.5854	0.5658	0.5440
	0.9	0.8942	0.8871	0.8788	0.8697	0.8589	0.8471	0.8343	0.8200	0.8053
	0.0	-0.0500	-0.1000	-0.1500	-0.2000	-0.2501	-0.3003	-0.3498	-0.3962	-0.4268
	0.1	0.0550	0.0102	-0.0346	-0.0794	-0.1242	-0.1694	-0.2150	-0.2615	-0.3090
	0.3	0.2650	0.2302	0.1956	0.1611	0.1265	0.0916	0.0563	0.0198	-0.0187
1.69	0.5	0.4748	0.4499	0.4250	0.4000	0.3749	0.3493	0.3231	0.2957	0.2661
	0.7	0.6845	0.6688	0.6530	0.6363	0.6193	0.6016	0.5829	0.5627	0.5405
	0.9	0.8940	0.8867	0.8783	0.8688	0.8577	0.8455	0.8324	0.8179	0.8026
	0.0	-0.0500	-0.1000	-0.1500	-0.2000	-0.2500	-0.3001	-0.3496	-0.3959	-0.4266
	0.1	0.0550	0.0101	-0.0347	-0.0796	-0.1245	-0.1698	-0.2155	-0.2620	-0.3095
	0.3	0.2649	0.2301	0.1954	0.1607	0.1258	0.0907	0.0550	0.0184	-0.0204
1.91	0.5	0.4748	0.4498	0.4247	0.3996	0.3743	0.3485	0.3219	0.2942	0.2643
	0.7	0.6845	0.6689	0.6527	0.6361	0.6190	0.6011	0.5821	0.5617	0.5394
	0.9	0.8941	0.8869	0.8786	0.8693	0.8580	0.8459	0.8331	0.8185	0.8037

Table 5.3. Correction factors f^A for two-tip cracked I-beam under bending; upper tip.

β =	ε =	$\lambda_w = 2a_w/(d_1 - 2e)$								
$2A_f/A_w$	$2e/d_1$	0.1	0.2	0.3	0.4	0.5	0.6	0.7	0.8	0.9
2.05	0.0	-0.0500	-0.0999	-0.1499	-0.1999	-0.2500	-0.2997	-0.3488	-0.3942	-0.4234
	0.1	0.0550	0.0101	-0.0348	-0.0797	-0.1248	-0.1701	-0.2159	-0.2623	-0.3096
	0.3	0.2649	0.2300	0.1951	0.1602	0.1252	0.0899	0.0539	0.0168	-0.0224
	0.5	0.4746	0.4495	0.4242	0.3989	0.3731	0.3470	0.3200	0.2918	0.2616
	0.7	0.6843	0.6684	0.6520	0.6351	0.6176	0.5994	0.5801	0.5593	0.5366
	0.9	0.8938	0.8865	0.8780	0.8683	0.8568	0.8445	0.8314	0.8166	0.8016

Table 5.4. Correction factors f^B for two-tip cracked I-beam under bending; lower tip.

β =	ε =	$\lambda_w = 2a/(d_1 - 2e)$								
$2A_f/A_w$	$2e/d_1$	0.1	0.2	0.3	0.4	0.5	0.6	0.7	0.8	0.9
0.83	0.0	0.0500	0.1000	0.1501	0.2004	0.2512	0.3029	0.3559	0.4096	0.4553
	0.1	0.1448	0.1906	0.2365	0.2829	0.3301	0.3782	0.4269	0.4743	0.5076
	0.3	0.3353	0.3715	0.4084	0.4462	0.4848	0.5240	0.5625	0.5960	0.6058
	0.5	0.5253	0.5515	0.5786	0.6062	0.6342	0.6615	0.6861	0.7012	0.6840
	0.7	0.7148	0.7306	0.7461	0.7613	0.7753	0.7867	0.7922	0.7838	0.7376
	0.9	0.9041	0.9077	0.9095	0.9092	0.9049	0.8956	0.8782	0.8446	0.7741
1.00	0.0	0.0500	0.1000	0.1500	0.2003	0.2509	0.3021	0.3541	0.4056	0.4467
	0.1	0.1451	0.1905	0.2362	0.2823	0.3289	0.3759	0.4230	0.4674	0.4954
	0.3	0.3352	0.3710	0.4075	0.4446	0.4821	0.5194	0.5553	0.5848	0.5886
	0.5	0.5252	0.5510	0.5773	0.6040	0.6303	0.6555	0.6768	0.6874	0.6650
	0.7	0.7149	0.7299	0.7447	0.7588	0.7712	0.7804	0.7830	0.7710	0.7209
	0.9	0.9040	0.9072	0.9086	0.9071	0.9019	0.8911	0.8718	0.8363	0.7632
1.11	0.0	0.0500	0.1000	0.1501	0.2003	0.2508	0.3021	0.3542	0.4063	0.4500
	0.1	0.1451	0.1905	0.2361	0.2821	0.3286	0.3756	0.4227	0.4678	0.4993
	0.3	0.3352	0.3711	0.4074	0.4443	0.4816	0.5190	0.5552	0.5861	0.5946
	0.5	0.5252	0.5510	0.5774	0.6040	0.6306	0.6562	0.6789	0.6922	0.6754
	0.7	0.7151	0.7301	0.7453	0.7600	0.7733	0.7842	0.7894	0.7816	0.7376
	0.9	0.9042	0.9081	0.9102	0.9103	0.9071	0.8990	0.8832	0.8522	0.7848
1.25	0.0	0.0500	0.1000	0.1500	0.2002	0.2506	0.3014	0.3523	0.4016	0.4379
	0.1	0.1451	0.1904	0.2359	0.2816	0.3276	0.3736	0.4189	0.4603	0.4832
	0.3	0.3351	0.3707	0.4066	0.4429	0.4792	0.5147	0.5478	0.5732	0.5712
	0.5	0.5250	0.5504	0.5761	0.6016	0.6263	0.6490	0.6671	0.6733	0.6451
	0.7	0.7146	0.7292	0.7434	0.7561	0.7668	0.7735	0.7729	0.7570	0.7029
	0.9	0.9036	0.9066	0.9072	0.9051	0.8980	0.8854	0.8640	0.8257	0.7492

Table 5.4. Correction factors f^B for two-tip cracked I-beam under bending; lower tip.

β =	ε =	$\lambda_w = 2a/(d_1 - 2e)$								
$2A_f/A_w$	$2e/d_1$	0.1	0.2	0.3	0.4	0.5	0.6	0.7	0.8	0.9
1.37	0.0	0.0500	0.1000	0.1500	0.2001	0.2504	0.3010	0.3515	0.3999	0.4342
	0.1	0.1451	0.1903	0.2357	0.2812	0.3270	0.3726	0.4171	0.4574	0.4780
	0.3	0.3351	0.3706	0.4063	0.4421	0.4778	0.5126	0.5445	0.5683	0.5636
	0.5	0.5250	0.5503	0.5755	0.6006	0.6246	0.6464	0.6632	0.6675	0.6366
	0.7	0.7148	0.7291	0.7427	0.7551	0.7651	0.7709	0.7690	0.7512	0.6940
	0.9	0.9038	0.9064	0.9066	0.9039	0.8966	0.8830	0.8601	0.8198	0.7402
1.53	0.0	0.0500	0.1000	0.1500	0.2001	0.2503	0.3006	0.3506	0.3980	0.4305
	0.1	0.1450	0.1902	0.2355	0.2808	0.3262	0.3714	0.4151	0.4540	0.4729
	0.3	0.3350	0.3703	0.4058	0.4412	0.4763	0.5102	0.5409	0.5627	0.5566
	0.5	0.5248	0.5499	0.5749	0.5993	0.6226	0.6433	0.6586	0.6613	0.6297
	0.7	0.7145	0.7288	0.7420	0.7537	0.7630	0.7678	0.7649	0.7464	0.6900
	0.9	0.9036	0.9063	0.9062	0.9032	0.8956	0.8819	0.8590	0.8191	0.7405
1.69	0.0	0.0500	0.1000	0.1500	0.2000	0.2501	0.3003	0.3498	0.3962	0.4268
	0.1	0.1449	0.1901	0.2353	0.2805	0.3257	0.3703	0.4133	0.4509	0.4676
	0.3	0.3349	0.3701	0.4054	0.4404	0.4750	0.5081	0.5376	0.5578	0.5494
	0.5	0.5248	0.5496	0.5743	0.5982	0.6206	0.6403	0.6542	0.6552	0.6218
	0.7	0.7143	0.7283	0.7413	0.7523	0.7608	0.7645	0.7603	0.7403	0.6827
	0.9	0.9035	0.9058	0.9056	0.9023	0.8940	0.8797	0.8557	0.8148	0.7346
1.91	0.0	0.0500	0.1000	0.1500	0.2000	0.2500	0.3001	0.3496	0.3959	0.4266
	0.1	0.1450	0.1901	0.2352	0.2803	0.3253	0.3697	0.4125	0.4499	0.4670
	0.3	0.3349	0.3700	0.4051	0.4400	0.4743	0.5070	0.5362	0.5563	0.5485
	0.5	0.5247	0.5496	0.5741	0.5978	0.6201	0.6395	0.6533	0.6545	0.6216
	0.7	0.7143	0.7282	0.7412	0.7523	0.7608	0.7645	0.7604	0.7409	0.6842
	0.9	0.9034	0.9059	0.9059	0.9027	0.8948	0.8807	0.8576	0.8172	0.7381

Table 5.4. Correction factors f^B for two-tip cracked I-beam under bending; lower tip.

β =	ε =	$\lambda_w = 2a/(d_j - 2e)$								
$2A_f/A_w$	$2e/d_j$	0.1	0.2	0.3	0.4	0.5	0.6	0.7	0.8	0.9
2.05	0.0	0.0500	0.0999	0.1499	0.1999	0.2500	0.2997	0.3488	0.3942	0.4234
	0.1	0.1449	0.1899	0.2350	0.2800	0.3247	0.3688	0.4109	0.4472	0.4627
	0.3	0.3348	0.3698	0.4047	0.4393	0.4731	0.5055	0.5337	0.5523	0.5431
	0.5	0.5245	0.5492	0.5734	0.5954	0.6183	0.6366	0.6492	0.6488	0.6154
	0.7	0.7141	0.7280	0.7402	0.7509	0.7586	0.7616	0.7566	0.7363	0.6796
	0.9	0.9032	0.9055	0.9052	0.9018	0.8933	0.8788	0.8551	0.8142	0.7350

Table 5.5. Correction factors f^w for three-tip cracked I-beam under tension; web crack tip.

$\beta =$	$\lambda_w =$	$\lambda_f = 2a_f/b_f$								
$2A_f/A_w$	a_w/d_1	0.1	0.2	0.3	0.4	0.5	0.6	0.7	0.8	0.9
0.83	0.1	0.7019	0.7558	0.8252	0.9092	1.0093	1.1296	1.2782	1.4724	1.7585
	0.2	0.7017	0.7260	0.7596	0.8024	0.8568	0.9258	1.0163	1.1426	1.3438
	0.3	0.7091	0.7389	0.7532	0.7839	0.8234	0.8750	0.9449	1.0575	1.2151
	0.4	0.7255	0.7387	0.7571	0.7816	0.8138	0.8565	0.9153	1.0024	1.1538
	0.5	0.7363	0.7473	0.7627	0.7833	0.8107	0.8472	0.8983	0.9752	1.1127
	0.6	0.7461	0.7553	0.7684	0.7859	0.8093	0.8407	0.8850	0.9526	1.0762
	0.7	0.7518	0.7640	0.7750	0.7897	0.8093	0.8359	0.8734	0.9483	1.0387
1.00	0.1	0.7031	0.7664	0.8475	0.9451	1.0603	1.1984	1.3686	1.5915	1.9207
	0.2	0.6967	0.7249	0.7633	0.8122	0.8741	0.9524	1.0550	1.1982	1.4269
	0.3	0.7055	0.7242	0.7500	0.7843	0.8283	0.8861	0.9638	1.0765	1.2662
	0.4	0.7155	0.7298	0.7500	0.7769	0.8122	0.8590	0.9235	1.0193	1.1864
	0.5	0.7244	0.7362	0.7529	0.7752	0.8046	0.8443	0.8995	0.9830	1.1326
	0.6	0.7325	0.7423	0.7562	0.7750	0.8000	0.8336	0.8810	0.9536	1.0865
	0.7	0.7405	0.7486	0.7601	0.7757	0.7965	0.8246	0.8646	0.9261	1.0408
1.11	0.1	0.7263	0.8147	0.9236	1.0494	1.1938	1.3615	1.5631	1.8201	2.1889
	0.2	0.7078	0.7479	0.7996	0.8650	0.9455	1.0451	1.1727	1.3460	1.6155
	0.3	0.7117	0.7374	0.7726	0.8179	0.8758	0.9497	1.0480	1.1875	1.4168
	0.4	0.7188	0.7382	0.7653	0.8008	0.8468	0.9071	0.9890	1.1088	1.3142
	0.5	0.7257	0.7414	0.7635	0.7927	0.8311	0.8820	0.9523	1.0574	1.2436
	0.6	0.7321	0.7451	0.7635	0.7879	0.8202	0.8634	0.9239	1.0156	1.1821
	0.7	0.7386	0.7492	0.7643	0.7846	0.8113	0.8474	0.8983	0.9763	1.1208

Table 5.5. Correction factors f^w for three-tip cracked I-beam under tension; web crack tip.

$\beta =$	$\lambda_w =$	$\lambda_f = 2a_f/b_f$								
$2A_f/A_w$	a_w/d_1	0.1	0.2	0.3	0.4	0.5	0.6	0.7	0.8	0.9
1.25	0.1	0.7035	0.7765	0.8699	0.9814	1.1132	1.2705	1.4653	1.7204	2.1006
	0.2	0.6916	0.7232	0.7664	0.8218	0.8912	0.9793	1.0949	1.2561	1.5154
	0.3	0.6974	0.7177	0.7464	0.7841	0.8328	0.8963	0.9823	1.1071	1.3180
	0.4	0.7052	0.7206	0.7423	0.7715	0.8097	0.8606	0.9307	1.0349	1.2173
	0.5	0.7124	0.7248	0.7425	0.7662	0.7978	0.8402	0.8993	0.9887	1.1497
	0.6	0.7188	0.7290	0.7436	0.7634	0.7896	0.8252	0.8754	0.9523	1.0933
	0.7	0.7243	0.7328	0.7448	0.7610	0.7828	0.8122	0.8540	0.9186	1.0391
1.37	0.1	0.7022	0.7781	0.8754	0.9924	1.1307	1.2962	1.5016	1.7729	2.1802
	0.2	0.6886	0.7209	0.7654	0.8227	0.8947	0.9863	1.1068	1.2759	1.5495
	0.3	0.6932	0.7140	0.7431	0.7816	0.8315	0.8969	0.9858	1.1149	1.3347
	0.4	0.7002	0.7156	0.7376	0.7671	0.8059	0.8578	0.9294	1.0363	1.2244
	0.5	0.7076	0.7190	0.7366	0.7606	0.7924	0.8352	0.8952	0.9862	1.1506
	0.6	0.7122	0.7223	0.7368	0.7565	0.7829	0.8187	0.8693	0.9469	1.0898
	0.7	0.7167	0.7249	0.7369	0.7530	0.7746	0.8041	0.8461	0.9110	1.0326
1.53	0.1	0.7113	0.8030	0.9185	1.0546	1.2134	1.4138	1.6342	1.9383	2.3924
	0.2	0.6899	0.7290	0.7845	0.8489	0.9327	1.0382	1.1797	1.3673	1.6754
	0.3	0.6918	0.7163	0.7505	0.7953	0.8530	0.9282	1.0294	1.1758	1.4236
	0.4	0.6970	0.7150	0.7405	0.7745	0.8191	0.8782	0.9595	1.0802	1.2920
	0.5	0.7021	0.7164	0.7367	0.7641	0.8002	0.8487	0.9164	1.0189	1.2034
	0.6	0.7065	0.7180	0.7347	0.7570	0.7869	0.8272	0.8840	0.9710	1.1311
	0.7	0.7095	0.7190	0.7324	0.7506	0.7749	0.8080	0.8549	0.9274	1.0629

Table 5.5. Correction factors f^w for three-tip cracked I-beam under tension; web crack tip.

β =	λ_w =	$\lambda_f = 2a_f/b_f$								
$2A_f/A_w$	a_w/d_j	0.1	0.2	0.3	0.4	0.5	0.6	0.7	0.8	0.9
	0.1	0.7130	0.8112	0.9344	1.0879	1.2481	1.4485	1.6951	2.0194	2.5051
	0.2	0.6882	0.7297	0.7859	0.8571	0.9458	1.0574	1.2030	1.4059	1.7330
	0.3	0.6888	0.7147	0.7507	0.7978	0.8586	0.9375	1.0438	1.1979	1.4590
1.69	0.4	0.6930	0.7119	0.7387	0.7741	0.8207	0.8823	0.9672	1.0934	1.3150
	0.5	0.6974	0.7123	0.7334	0.7618	0.7992	0.8497	0.9200	1.0263	1.2183
	0.6	0.7011	0.7132	0.7302	0.7534	0.7842	0.8258	0.8845	0.9744	1.1400
	0.7	0.7032	0.7129	0.7267	0.7454	0.7705	0.8045	0.8527	0.9273	1.0667
	0.1	0.7278	0.8473	0.9937	1.1630	1.3571	1.5854	1.8642	2.2274	2.7675
	0.2	0.6935	0.7440	0.8116	0.8961	1.0001	1.1297	1.2972	1.5285	1.8979
	0.3	0.6906	0.7218	0.7648	0.8207	0.8918	0.9839	1.1065	1.2832	1.5799
1.91	0.4	0.6930	0.7154	0.7471	0.7887	0.8430	0.9147	1.0125	1.1571	1.4092
	0.5	0.6959	0.7134	0.7381	0.7712	0.8147	0.8730	0.9539	1.0756	1.2940
	0.6	0.6984	0.7123	0.7322	0.7590	0.7945	0.8425	0.9098	1.0125	1.2011
	0.7	0.6992	0.7103	0.7264	0.7479	0.7767	0.8156	0.8708	0.9558	1.1144
	0.1	0.7319	0.8599	1.0157	1.1944	1.3994	1.6400	1.9331	2.3155	2.8845
	0.2	0.6934	0.7475	0.8195	0.9094	1.0194	1.1559	1.3322	1.5756	1.9642
	0.3	0.6890	0.7222	0.7680	0.8270	0.9023	0.9990	1.1280	1.3133	1.6243
2.05	0.4	0.6910	0.7142	0.7477	0.7916	0.8489	0.9240	1.0263	1.1776	1.4415
	0.5	0.6928	0.7114	0.7374	0.7721	0.8177	0.8786	0.9629	1.0898	1.3177
	0.6	0.6954	0.7095	0.7303	0.7583	0.7955	0.8452	0.9153	1.0221	1.2195
	0.7	0.6946	0.7063	0.7232	0.7456	0.7756	0.8160	0.8731	0.9612	1.1253

Table 5.6. Correction factors f^f for three-tip cracked I-beam under tension; flange crack tip.

β =	λ_w =	$\lambda_f = 2a_f/b_f$								
$2A_f/A_w$	a_w/d_1	0.1	0.2	0.3	0.4	0.5	0.6	0.7	0.8	0.9
0.83	0.1	1.4339	1.2977	1.2487	1.2384	1.2580	1.3108	1.4055	1.5739	1.9403
	0.2	1.6683	1.5114	1.4589	1.4544	1.4881	1.5630	1.6971	1.9394	2.4698
	0.3	1.8640	1.7077	1.6388	1.6405	1.6881	1.7851	1.9584	2.2910	2.9667
	0.4	2.0483	1.8637	1.8098	1.8305	1.8793	1.9982	2.2092	2.5923	3.4563
	0.5	2.2269	2.0300	1.9755	1.9901	2.0645	2.2046	2.4527	2.9065	3.9405
	0.6	2.3986	2.1891	2.1339	2.1545	2.2414	2.4016	2.6851	3.2054	4.4053
	0.7	2.5571	2.3374	2.2817	2.3148	2.4055	2.5923	2.9000	3.5651	4.8346
1.00	0.1	1.3773	1.2544	1.2111	1.2045	1.2268	1.2816	1.3773	1.5472	1.9151
	0.2	1.5886	1.4445	1.3979	1.3966	1.4312	1.5067	1.6399	1.8775	2.3991
	0.3	1.7576	1.6009	1.5533	1.5578	1.6049	1.7000	1.8678	2.1700	2.8330
	0.4	1.9141	1.7458	1.6983	1.7085	1.7677	1.8819	2.0834	2.4482	3.2724
	0.5	2.0634	1.8848	1.8364	1.8527	1.9232	2.0561	2.2897	2.7162	3.6901
	0.6	2.2056	2.0166	1.9682	1.9892	2.0709	2.2210	2.4851	2.9697	4.0873
	0.7	2.3382	2.1393	2.0905	2.1157	2.2069	2.3728	2.6639	3.2002	4.4504
1.11	0.1	1.3647	1.2260	1.1733	1.1597	1.1739	1.2198	1.3028	1.4514	1.7755
	0.2	1.5854	1.4255	1.3665	1.3558	1.3810	1.4456	1.5629	1.7743	2.2386
	0.3	1.7581	1.5833	1.5235	1.5175	1.5543	1.6378	1.7890	2.0628	2.6718
	0.4	1.9143	1.7278	1.6663	1.6655	1.7137	1.8164	2.0006	2.3364	3.0942
	0.5	2.0601	1.8628	1.8011	1.8051	1.8642	1.9850	2.2014	2.5981	3.5061
	0.6	2.1983	1.9900	1.9272	1.9360	2.0054	2.1432	2.3899	2.8448	3.8975
	0.7	2.3245	2.1075	2.0435	2.0562	2.1346	2.2879	2.5613	3.0688	4.2550

Table 5.6. Correction factors f^f for three-tip cracked I-beam under tension; flange crack tip.

β =	λ_w =	$\lambda_f = 2a_f/b_f$								
$2A_f/A_w$	a_w/d_j	0.1	0.2	0.3	0.4	0.5	0.6	0.7	0.8	0.9
1.25	0.1	1.3247	1.2133	1.1770	1.1756	1.2012	1.2590	1.3582	1.5323	1.9079
	0.2	1.5111	1.3808	1.3408	1.3436	1.3815	1.4581	1.5916	1.8287	2.3483
	0.3	1.6570	1.5146	1.4738	1.4822	1.5301	1.6244	1.7891	2.0839	2.7423
	0.4	1.7892	1.6366	1.5954	1.6084	1.6667	1.7782	1.9719	2.3221	3.1135
	0.5	1.9133	1.7518	1.7102	1.7276	1.7960	1.9232	2.1447	2.5475	3.4692
	0.6	2.0304	1.8600	1.8184	1.8400	1.9176	2.0593	2.3064	2.7581	3.8018
	0.7	2.1386	1.9604	1.9177	1.9435	2.0289	2.1836	2.4537	2.9503	4.1050
1.37	0.1	1.2925	1.1982	1.1686	1.1707	1.1989	1.2607	1.3644	1.5448	1.9349
	0.2	1.4473	1.3441	1.3143	1.3231	1.3637	1.4440	1.5808	1.8225	2.3527
	0.3	1.5670	1.4585	1.4310	1.4458	1.4980	1.5945	1.7607	2.0573	2.7176
	0.4	1.6769	1.5631	1.5374	1.5578	1.6194	1.7323	1.9257	2.2738	3.0600
	0.5	1.7768	1.6610	1.6373	1.6630	1.7352	1.8619	2.0808	2.4773	3.3845
	0.6	1.8729	1.7531	1.7311	1.7618	1.8428	1.9827	2.2248	2.6668	3.6864
	0.7	1.9604	1.8379	1.8173	1.8521	1.9409	2.0928	2.3562	2.8371	3.9581
1.53	0.1	1.2714	1.1778	1.1485	1.1497	1.1767	1.2488	1.3391	1.5151	1.8950
	0.2	1.4206	1.3178	1.2924	1.2958	1.3351	1.4101	1.5516	1.7816	2.2959
	0.3	1.5321	1.4252	1.3972	1.4110	1.4610	1.5550	1.7164	2.0038	2.6439
	0.4	1.6305	1.5202	1.4944	1.5140	1.5739	1.6825	1.8697	2.2064	2.9666
	0.5	1.7217	1.6086	1.5846	1.6094	1.6785	1.8008	2.0119	2.3943	3.2693
	0.6	1.8069	1.6909	1.6689	1.6980	1.7755	1.9100	2.1434	2.5676	3.5494
	0.7	1.8847	1.7662	1.7454	1.7787	1.8635	2.0090	2.2621	2.7239	3.7997

Table 5.6. Correction factors f^f for three-tip cracked I-beam under tension; flange crack tip.

β =	λ_w =	$\lambda_f = 2a_f/b_f$								
$2A_f/A_w$	a_w/d_1	0.1	0.2	0.3	0.4	0.5	0.6	0.7	0.8	0.9
1.69	0.1	1.2524	1.1646	1.1378	1.1384	1.1700	1.2331	1.3363	1.5150	1.9009
	0.2	1.3923	1.2959	1.2700	1.2795	1.3198	1.3995	1.5338	1.7698	2.2871
	0.3	1.4950	1.3948	1.3705	1.3864	1.4373	1.5320	1.6929	1.9794	2.6174
	0.4	1.5844	1.4817	1.4598	1.4811	1.5416	1.6499	1.8354	2.1690	2.9209
	0.5	1.6668	1.5621	1.5421	1.5681	1.6375	1.7584	1.9666	2.3427	3.2035
	0.6	1.7431	1.6359	1.6181	1.6490	1.7260	1.8585	2.0870	2.5028	3.4626
	0.7	1.8126	1.7035	1.6872	1.7219	1.8058	1.9484	2.1950	2.6450	3.6938
1.91	0.1	1.2326	1.1402	1.1117	1.1149	1.1419	1.2015	1.2999	1.4714	1.8414
	0.2	1.3808	1.2742	1.2435	1.2500	1.2877	1.3637	1.4920	1.7179	2.2128
	0.3	1.4889	1.3746	1.3440	1.3552	1.4018	1.4922	1.6463	1.9210	2.5327
	0.4	1.5815	1.4579	1.4306	1.4466	1.5020	1.6056	1.7831	2.1027	2.8248
	0.5	1.6654	1.5408	1.5109	1.5302	1.5933	1.7089	1.9080	2.2689	3.0955
	0.6	1.7422	1.6130	1.5840	1.6068	1.6766	1.8029	2.0216	2.4200	3.3422
	0.7	1.8118	1.6784	1.6496	1.6755	1.7514	1.8871	2.1226	2.5535	3.5601
2.05	0.1	1.2205	1.1313	1.1044	1.1080	1.1362	1.1968	1.2962	1.4687	1.8411
	0.2	1.3639	1.2608	1.2318	1.2397	1.2776	1.3545	1.4831	1.7093	2.2045
	0.3	1.4672	1.3565	1.3276	1.3398	1.3875	1.4781	1.6320	1.9056	2.5149
	0.4	1.5551	1.4385	1.4108	1.4268	1.4825	1.5859	1.7627	2.0798	2.7960
	0.5	1.6327	1.5124	1.4852	1.5057	1.5688	1.6836	1.8810	2.2381	3.0556
	0.6	1.7066	1.5803	1.5536	1.5773	1.6471	1.7722	1.9882	2.3811	3.2956
	0.7	1.7683	1.6409	1.6142	1.6416	1.7171	1.8511	2.0831	2.5068	3.4972

Table 5.7. Correction factors f^w for three-tip cracked I-beam under bending; web crack tip.

β =	λ_w =	$\lambda_f = 2a_f/b_f$								
$2A_f/A_w$	a_w/d_1	0.1	0.2	0.3	0.4	0.5	0.6	0.7	0.8	0.9
	0.1	0.5977	0.6504	0.7186	0.8014	0.9004	1.0189	1.1662	1.3587	1.6423
	0.2	0.4909	0.5139	0.5458	0.5869	0.6388	0.7054	0.7929	0.9147	1.1095
	0.3	0.3913	0.4080	0.4292	0.4592	0.4938	0.5440	0.6068	0.7009	0.8589
0.83	0.4	0.2931	0.3044	0.3205	0.3421	0.3705	0.4084	0.4607	0.5381	0.6732
	0.5	0.1903	0.1992	0.2119	0.2291	0.2526	0.2827	0.3257	0.3906	0.5070
	0.6	0.0845	0.0916	0.1017	0.1155	0.1339	0.1588	0.1940	0.2478	0.3464
	0.7	-0.0253	-0.0187	-0.0107	-0.0020	0.0146	0.0321	0.0623	0.1056	0.1861
	0.1	0.5992	0.6611	0.7409	0.8371	0.9512	1.0881	1.2565	1.4776	1.8044
	0.2	0.4873	0.5138	0.5504	0.5975	0.6571	0.7329	0.8323	0.9712	1.1936
	0.3	0.3875	0.4044	0.4283	0.4600	0.5011	0.5551	0.6280	0.7340	0.9123
1.00	0.4	0.2870	0.2995	0.3173	0.3412	0.3728	0.4148	0.4728	0.5592	0.7102
	0.5	0.1845	0.1938	0.2078	0.2267	0.2518	0.2857	0.3331	0.4048	0.5338
	0.6	0.0788	0.0865	0.0975	0.1125	0.1326	0.1599	0.1985	0.2577	0.3663
	0.7	-0.0290	-0.0230	-0.0144	-0.0027	0.0132	0.0347	0.0654	0.1128	0.2014
	0.1	0.6213	0.7081	0.8154	0.9396	1.0826	1.2489	1.4489	1.7042	2.0704
	0.2	0.4971	0.5344	0.5846	0.6477	0.7255	0.8221	0.9458	1.1145	1.3770
	0.3	0.3929	0.4162	0.4488	0.4910	0.5450	0.6146	0.7071	0.8387	1.0555
1.11	0.4	0.2900	0.3070	0.3310	0.3628	0.4041	0.4586	0.5326	0.6414	0.8283
	0.5	0.1858	0.1988	0.2175	0.2424	0.2753	0.3192	0.3800	0.4711	0.6330
	0.6	0.0796	0.0899	0.1046	0.1244	0.1506	0.1861	0.2357	0.3114	0.4492
	0.7	-0.0286	-0.0206	-0.0092	0.0062	0.0269	0.0549	0.0945	0.1555	0.2688

Table 5.7. Correction factors f^w for three-tip cracked I-beam under bending; web crack tip.

β =	λ_w =	$\lambda_f = 2a_f/b_f$								
$2A_f/A_w$	a_w/d_1	0.1	0.2	0.3	0.4	0.5	0.6	0.7	0.8	0.9
1.25	0.1	0.6000	0.6714	0.7635	0.8737	1.0042	1.1600	1.3534	1.6069	1.9847
	0.2	0.4832	0.5132	0.5547	0.6080	0.6753	0.7609	0.8732	1.0306	1.2834
	0.3	0.3818	0.4005	0.4271	0.4623	0.5080	0.5680	0.6493	0.7674	0.9675
	0.4	0.2808	0.2943	0.3138	0.3399	0.3746	0.4207	0.4846	0.5797	0.7468
	0.5	0.1780	0.1883	0.2034	0.2238	0.2511	0.2880	0.3397	0.4181	0.5594
	0.6	0.0731	0.0812	0.0931	0.1092	0.1309	0.1605	0.2023	0.2665	0.3847
	0.7	-0.0338	-0.0275	-0.0183	-0.0057	0.0113	0.0346	0.0677	0.1191	0.2150
1.37	0.1	0.5989	0.6733	0.7695	0.8848	1.0218	1.1863	1.3904	1.6599	2.0649
	0.2	0.4809	0.5116	0.5544	0.6098	0.6798	0.7690	0.8864	1.0514	1.3190
	0.3	0.3790	0.3980	0.4251	0.4612	0.5084	0.5703	0.6545	0.7774	0.9868
	0.4	0.2777	0.2913	0.3111	0.3378	0.3732	0.4206	0.4864	0.5847	0.7580
	0.5	0.1749	0.1853	0.2005	0.2213	0.2491	0.2867	0.3396	0.4200	0.5658
	0.6	0.0703	0.0784	0.0903	0.1067	0.1288	0.1588	0.2015	0.2672	0.3885
	0.7	-0.0362	-0.0299	-0.0206	-0.0079	0.0094	0.0330	0.0667	0.1191	0.2173
1.53	0.1	0.6077	0.6977	0.8117	0.9463	1.1040	1.2913	1.5221	1.8246	2.2763
	0.2	0.4824	0.5196	0.5705	0.6355	0.7171	0.8198	0.9543	1.1417	1.4436
	0.3	0.3783	0.4009	0.4329	0.4751	0.5298	0.6012	0.6975	0.8375	1.0744
	0.4	0.2760	0.2921	0.3151	0.3460	0.3836	0.4412	0.5162	0.6281	0.8246
	0.5	0.1729	0.1850	0.2026	0.2265	0.2584	0.3014	0.3617	0.4530	0.6183
	0.6	0.0682	0.0776	0.0914	0.1101	0.1353	0.1696	0.2181	0.2927	0.4302
	0.7	-0.0380	-0.0307	-0.0201	-0.0056	0.0141	0.0410	0.0793	0.1388	0.2502

Table 5.7. Correction factors f^w for three-tip cracked I-beam under bending; web crack tip.

β =	λ_w =	$\lambda_f = 2a_f/b_f$								
$2A_f/A_w$	a_w/d_1	0.1	0.2	0.3	0.4	0.5	0.6	0.7	0.8	0.9
1.69	0.1	0.6094	0.7059	0.8276	0.9701	1.1384	1.3375	1.5830	1.9056	2.3895
	0.2	0.4812	0.5208	0.5750	0.6440	0.7303	0.8395	0.9818	1.1807	1.5015
	0.3	0.3762	0.4001	0.4339	0.4784	0.5361	0.6113	0.7129	0.8605	1.1111
	0.4	0.2737	0.2905	0.3147	0.3472	0.3900	0.4470	0.5257	0.6431	0.8497
	0.5	0.1705	0.1832	0.2016	0.2266	0.2599	0.3048	0.3678	0.4634	0.6363
	0.6	0.0661	0.0758	0.0901	0.1097	0.1359	0.1717	0.2223	0.3000	0.4436
	0.7	-0.0398	-0.0323	-0.0213	-0.0061	0.0143	0.0423	0.0822	0.1441	0.2602
1.91	0.1	0.6239	0.7414	0.8862	1.0538	1.2467	1.4742	1.7512	2.1130	2.6507
	0.2	0.4863	0.5340	0.5999	0.6821	0.7837	0.9107	1.0748	1.3009	1.6649
	0.3	0.3783	0.4071	0.4476	0.5006	0.5685	0.6566	0.7743	0.9440	1.2299
	0.4	0.2743	0.2943	0.3231	0.3615	0.4118	0.4784	0.5697	0.7052	0.9419
	0.5	0.1703	0.1853	0.2070	0.2364	0.2754	0.3278	0.4008	0.5113	0.7099
	0.6	0.0655	0.0770	0.0938	0.1167	0.1473	0.1889	0.2475	0.3374	0.5027
	0.7	-0.0404	-0.0317	-0.0188	-0.0011	0.0228	0.0553	0.1015	0.1731	0.3070
2.05	0.1	0.6278	0.7538	0.9078	1.0850	1.2884	1.5278	1.8197	2.2005	2.7675
	0.2	0.4863	0.5381	0.6078	0.6951	0.8026	0.9364	1.1094	1.3486	1.7309
	0.3	0.3772	0.4080	0.4511	0.5073	0.5790	0.6717	0.7955	0.9740	1.2743
	0.4	0.2729	0.2942	0.3247	0.3652	0.4182	0.4882	0.5842	0.7261	0.9743
	0.5	0.1689	0.1847	0.2076	0.2386	0.2795	0.3344	0.4110	0.5265	0.7346
	0.6	0.0641	0.0762	0.0939	0.1179	0.1501	0.1936	0.2549	0.3488	0.5218
	0.7	-0.0416	-0.0324	-0.0188	0.0002	0.0246	0.0586	0.1069	0.1816	0.3213

Table 5.8. Correction factors f' for three-tip cracked I-beam under bending; flange crack tip.

$\beta =$	$\lambda_w =$	$\lambda_f = 2a_f/b_f$								
$2A_f/A_w$	a_w/d_1	0.1	0.2	0.3	0.4	0.5	0.6	0.7	0.8	0.9
0.83	0.1	1.4090	1.2792	1.2334	1.2255	1.2460	1.2993	1.3936	1.5613	1.9254
	0.2	1.5914	1.4475	1.4011	1.4002	1.4352	1.5099	1.6419	1.8775	2.3926
	0.3	1.7110	1.5620	1.5174	1.5262	1.5699	1.6674	1.8275	2.1214	2.7739
	0.4	1.8013	1.6455	1.6023	1.6135	1.6709	1.7802	1.9712	2.3157	3.0899
	0.5	1.8604	1.7019	1.6601	1.6762	1.7406	1.8641	2.0768	2.4631	3.3416
	0.6	1.8923	1.7325	1.6928	1.7125	1.7842	1.9156	2.1447	2.5625	3.5227
	0.7	1.8985	1.7401	1.7019	1.7173	1.7994	1.9297	2.1763	2.6144	3.6318
1.00	0.1	1.3574	1.2389	1.1986	1.1942	1.2175	1.2723	1.3681	1.5370	1.9030
	0.2	1.5205	1.3889	1.3487	1.3502	1.3866	1.4620	1.5929	1.8256	2.3343
	0.3	1.6259	1.4879	1.4489	1.4569	1.5047	1.5970	1.7575	2.0439	2.6794
	0.4	1.7001	1.5582	1.5211	1.5346	1.5913	1.6981	1.8829	2.2154	2.9639
	0.5	1.7490	1.6047	1.5697	1.5873	1.6514	1.7697	1.9741	2.3441	3.1873
	0.6	1.7747	1.6300	1.5962	1.6174	1.6870	1.8136	2.0325	2.4308	3.3488
	0.7	1.7794	1.6360	1.6029	1.6266	1.6995	1.8315	2.0598	2.4765	3.4459
1.11	0.1	1.3421	1.2103	1.1620	1.1502	1.1656	1.2120	1.2949	1.4431	1.7658
	0.2	1.5148	1.3697	1.3186	1.3122	1.3399	1.4052	1.5214	1.7290	2.1835
	0.3	1.6233	1.4707	1.4215	1.4216	1.4605	1.5434	1.6891	1.9506	2.5292
	0.4	1.6977	1.5412	1.4941	1.4995	1.5483	1.6463	1.8177	2.1274	2.8210
	0.5	1.7455	1.5875	1.5423	1.5528	1.6093	1.7196	1.9120	2.2616	3.0556
	0.6	1.7713	1.6122	1.5692	1.5831	1.6458	1.7654	1.9739	2.3543	3.2300
	0.7	1.7755	1.6181	1.5764	1.5932	1.6601	1.7860	2.0052	2.4066	3.3418

Table 5.8. Correction factors f^f for three-tip cracked I-beam under bending; flange crack tip.

$\beta =$	$\lambda_w =$	$\lambda_f = 2a_f/b_f$								
$2A_f/A_w$	a_w/d_1	0.1	0.2	0.3	0.4	0.5	0.6	0.7	0.8	0.9
1.25	0.1	1.3056	1.2001	1.1667	1.1670	1.1939	1.2519	1.3506	1.5240	1.8981
	0.2	1.4508	1.3326	1.2985	1.3050	1.3436	1.4206	1.5524	1.7851	2.2941
	0.3	1.5418	1.4175	1.3848	1.3964	1.4455	1.5382	1.6968	1.9788	2.6047
	0.4	1.6040	1.4764	1.4453	1.4619	1.5190	1.6247	1.8051	2.1283	2.8559
	0.5	1.6442	1.5149	1.4859	1.5059	1.5695	1.6849	1.8828	2.2394	3.0523
	0.6	1.6648	1.5350	1.5069	1.5302	1.5988	1.7218	1.9320	2.3136	3.1922
	0.7	1.6680	1.5388	1.5125	1.5374	1.6090	1.7367	1.9554	2.3532	3.2775
1.37	0.1	1.2786	1.1885	1.1610	1.1643	1.1934	1.2552	1.3587	1.5385	1.9264
	0.2	1.3992	1.3037	1.2788	1.2897	1.3315	1.4115	1.5465	1.7840	2.3041
	0.3	1.4737	1.3767	1.3546	1.3716	1.4237	1.5184	1.6786	1.9630	2.5951
	0.4	1.5246	1.4272	1.4074	1.4295	1.4894	1.5961	1.7768	2.1008	2.8277
	0.5	1.5573	1.4597	1.4421	1.4681	1.5343	1.6501	1.8470	2.2012	3.0081
	0.6	1.5739	1.4765	1.4606	1.4895	1.5600	1.6827	1.8912	2.2684	3.1367
	0.7	1.5761	1.4798	1.4647	1.4956	1.5691	1.6958	1.9118	2.3044	3.2144
1.53	0.1	1.2603	1.1710	1.1437	1.1461	1.1739	1.2348	1.3356	1.5110	1.8895
	0.2	1.3771	1.2822	1.2575	1.2675	1.3084	1.3860	1.5176	1.7487	2.2549
	0.3	1.4465	1.3511	1.3288	1.3450	1.3953	1.4879	1.6442	1.9211	2.5359
	0.4	1.4929	1.3966	1.3775	1.3990	1.4488	1.5612	1.7376	2.0528	2.7610
	0.5	1.5222	1.4264	1.4090	1.4344	1.4989	1.6120	1.8042	2.1497	2.9363
	0.6	1.5368	1.4413	1.4260	1.4541	1.5230	1.6429	1.8464	2.2148	3.0619
	0.7	1.5385	1.4442	1.4298	1.4597	1.5314	1.6558	1.8668	2.2498	3.1398

Table 5.8. Correction factors f^f for three-tip cracked I-beam under bending; flange crack tip.

$\beta =$	$\lambda_w =$	$\lambda_f = 2a_f/b_f$								
$2A_f/A_w$	a_w/d_1	0.1	0.2	0.3	0.4	0.5	0.6	0.7	0.8	0.9
1.69	0.1	1.2440	1.1599	1.1353	1.1368	1.1688	1.2314	1.3341	1.5122	1.8969
	0.2	1.3534	1.2646	1.2426	1.2543	1.2958	1.3751	1.5079	1.7406	2.2500
	0.3	1.4175	1.3277	1.3088	1.3271	1.3780	1.4712	1.6275	1.9043	2.5197
	0.4	1.4595	1.3699	1.3536	1.3768	1.4356	1.5397	1.7152	2.0280	2.7333
	0.5	1.4859	1.3967	1.3826	1.4093	1.4740	1.5867	1.7772	2.1197	2.8992
	0.6	1.4988	1.4102	1.3979	1.4272	1.4960	1.6152	1.8166	2.1798	3.0176
	0.7	1.5002	1.4126	1.4012	1.4320	1.5041	1.6271	1.8356	2.2132	3.0910
1.91	0.1	1.2211	1.1334	1.1073	1.1111	1.1393	1.1986	1.2969	1.4679	1.8370
	0.2	1.3372	1.2400	1.2155	1.2248	1.2642	1.3403	1.4677	1.6898	2.1797
	0.3	1.4047	1.3055	1.2824	1.2971	1.3456	1.4353	1.5859	1.8526	2.4442
	0.4	1.4484	1.3865	1.3266	1.3462	1.4021	1.5030	1.6726	1.9750	2.6564
	0.5	1.4751	1.3744	1.3554	1.3783	1.4401	1.5495	1.7342	2.0654	2.8215
	0.6	1.4882	1.3878	1.3699	1.3962	1.4619	1.5778	1.7737	2.1268	2.9410
	0.7	1.4896	1.3900	1.3735	1.4014	1.4702	1.5904	1.7936	2.1616	3.0173
2.05	0.1	1.2120	1.1272	1.1023	1.1070	1.1337	1.1958	1.2949	1.4668	1.8381
	0.2	1.3244	1.2312	1.2072	1.2180	1.2574	1.3340	1.4615	1.6850	2.1739
	0.3	1.3889	1.2928	1.2715	1.2871	1.3360	1.4258	1.5765	1.8423	2.4334
	0.4	1.4301	1.3329	1.3135	1.3341	1.3902	1.4907	1.6598	1.9609	2.6392
	0.5	1.4551	1.3578	1.3404	1.3647	1.4262	1.5352	1.7190	2.0482	2.7997
	0.6	1.4670	1.3702	1.3542	1.3812	1.4473	1.5625	1.7570	2.1075	2.9155
	0.7	1.4681	1.3721	1.3576	1.3863	1.4549	1.5746	1.7762	2.1413	2.9898

Table 6.1. Fitting coefficients for two-tip cracked I-beam.

Coef.	Tension		Bending	
	Upper Crack Tip	Lower Crack Tip	Upper Crack Tip	Lower Crack Tip
a_0	1.0	1.0	0.0	0.0
a_1	-0.07184	-0.03591	1.02395	1.02052
a_2	0.05916	0.03257	-0.02824	-0.03142
a_3	0.07266	0.01609	-0.02660	-0.02841
a_4	0.16801	0.17113	-0.51095	0.48403
a_5	-0.15810	-0.17469	-0.00309	-0.02169
a_6	-0.09645	0.00540	0.66587	-0.19538
a_7	0.13248	0.19882	0.02106	0.10116
a_8	0.11124	0.10355	-0.03243	-0.02670
a_9	-0.01464	-0.01573	0.00337	0.00206
a_{10}	-0.03299	0.00399	0.02660	0.03282
a_{11}	0.04288	0.05901	0.00483	0.01704
a_{12}	-0.14373	-0.13149	-0.14302	-0.20652
a_{13}	-0.09648	-0.16125	-0.01281	-0.06069
a_{14}	-0.03380	-0.27916	-0.04610	-0.28079

Table 6.2. Fitting coefficients for three-tip cracked I-beam.

Coef.	Tension		Bending	
	Web Crack Tip	Flange Crack Tip	Web Crack Tip	Flange Crack Tip
a_1	0.82991	1.48266	0.82922	1.39283
a_2	-0.67499	0.29636	-0.58851	0.06970
a_3	0.21031	0.07549	0.16098	0.04610
a_4	5.48154	4.44880	3.18865	3.37633
a_5	-7.24174	2.74806	-1.92470	-2.78526
a_6	6.51764	-8.92438	-5.45652	-1.04763
a_7	-1.22688	-9.01819	-0.87320	-7.16218
a_8	2.27070	10.67798	1.30689	9.95421
a_9	-0.04335	-2.79219	0.75006	-3.94745
a_{10}	-3.53419	39.40912	1.92329	24.63804
a_{11}	5.23305	-33.56530	-1.28348	-20.37830
a_{12}	1.11541	-32.7345	-2.84890	-19.76580
a_{13}	-2.53266	30.52621	3.09458	18.05231
a_{14}	-0.67489	0.31779	-0.67725	0.14847
a_{15}	0.19608	0.08256	0.17624	0.04106
a_{16}	9.15477	2.56783	7.93375	1.27056
a_{17}	-13.48190	-6.28871	-0.68127	-3.72795
a_{18}	10.74853	3.32973	1.25324	2.41420
a_{19}	-2.99836	-6.42741	-2.47185	-5.07106
a_{20}	5.46394	8.44963	4.36222	7.53843
a_{21}	-2.86079	-2.83403	-2.15147	-3.33554
a_{22}	-6.27909	38.11440	-3.59192	23.75073
a_{23}	10.41571	-35.78230	11.11301	-20.20160
a_{24}	3.65483	-38.73570	1.49894	-23.70230
a_{25}	-7.95641	36.97307	-11.80580	20.59509

Table 6.3. Three-tip cracks under tension with fitting error for web crack tip $|\Delta| \geq 3\%$.

β	λ_w	λ_f	f_{FEM}	f_{pred}	Diff.	Δ %
1.69	0.1	0.9	2.5051	2.5391	-0.0340	-3.58
0.83	0.1	0.3	0.8252	0.8590	-0.0338	-3.55
2.05	0.7	0.1	0.6946	0.7273	-0.0328	-3.44
1.53	0.2	0.9	1.6754	1.6436	0.0318	3.34
1.00	0.1	0.9	1.9207	1.8893	0.0313	3.29
1.53	0.1	0.6	1.4138	1.3830	0.0309	3.24
0.83	0.1	0.4	0.9092	0.9389	-0.0297	-3.12
0.83	0.1	0.2	0.7558	0.7852	-0.0294	-3.09
1.37	0.2	0.8	1.2759	1.3046	-0.0287	-3.02

Table 6.4. Three-tip cracks under tension with fitting error for flange crack tip $|\Delta| \geq 3\%$.

β	λ_w	λ_f	f_{FEM}	f_{pred}	Diff.	Δ %
1.37	0.6	0.1	1.8729	1.9620	-0.0891	-4.76
1.69	0.1	0.9	1.9009	1.8169	0.0840	4.49
1.37	0.5	0.1	1.7768	1.8548	-0.0781	-4.17
1.37	0.1	0.9	1.9349	1.8612	0.0737	3.94
1.53	0.6	0.1	1.8069	1.8802	-0.0733	-3.92
0.83	0.2	0.1	1.6683	1.5957	0.0726	3.88
0.83	0.7	0.1	2.5571	2.4889	0.0682	3.65
1.69	0.6	0.1	1.7431	1.8110	-0.0679	-3.63
2.05	0.1	0.9	1.8411	1.7735	0.0676	3.61
0.83	0.3	0.1	1.8640	1.7973	0.0666	3.56
1.53	0.5	0.1	1.7217	1.7844	-0.0627	-3.35
0.83	0.1	0.8	1.5739	1.6361	-0.0621	-3.32
0.83	0.2	0.8	1.9394	2.0003	-0.0608	-3.25
1.69	0.5	0.1	1.6668	1.7242	-0.0574	-3.07
1.53	0.1	0.9	1.8950	1.8382	0.0568	3.03
1.00	0.2	0.8	1.8775	1.9339	-0.0564	-3.02

Table 6.5. Three-tip cracks under bending with fitting error for web crack tip $|\Delta| \geq 3\%$.

β	λ_w	λ_f	f_{FEM}	f_{pred}	Diff.	Δ %
1.37	0.2	0.8	1.0514	1.0846	-0.0332	-6.50
1.53	0.1	0.9	2.2763	2.2441	0.0323	6.31
1.00	0.1	0.9	1.8044	1.7733	0.0311	6.08
1.37	0.1	0.8	1.6599	1.6908	-0.0309	-6.04
1.53	0.2	0.9	1.4436	1.4136	0.0300	5.87
1.37	0.3	0.8	0.7774	0.8036	-0.0262	-5.12
0.83	0.2	0.8	0.9147	0.9406	-0.0259	-5.07
1.69	0.1	0.8	1.9056	1.9311	-0.0255	-4.98
1.00	0.1	0.6	1.0881	1.0631	0.0250	4.89
1.53	0.3	0.9	1.0744	1.0495	0.0249	4.88
1.91	0.2	0.9	1.6649	1.6405	0.0244	4.77
1.00	0.1	0.7	1.2565	1.2324	0.0241	4.71
1.37	0.2	0.7	0.8864	0.9094	-0.0230	-4.50
1.37	0.4	0.8	0.5847	0.6064	-0.0217	-4.24
1.37	0.1	0.9	2.0649	2.0866	-0.0217	-4.24
1.53	0.1	0.7	1.5221	1.5011	0.0210	4.11
1.00	0.3	0.9	0.9123	0.8914	0.0209	4.10
1.69	0.1	0.9	2.3895	2.4104	-0.0209	-4.10
0.83	0.1	0.2	0.6504	0.6710	-0.0207	-4.04
1.00	0.4	0.9	0.7102	0.6895	0.0207	4.04
1.69	0.2	0.8	1.1807	1.2004	-0.0197	-3.86
1.37	0.1	0.7	1.3904	1.4100	-0.0197	-3.85
1.53	0.1	0.6	1.2913	1.2718	0.0195	3.82
1.37	0.5	0.8	0.4200	0.4385	-0.0185	-3.61
1.00	0.1	0.8	1.4776	1.4592	0.0183	3.59
1.00	0.1	0.5	0.9512	0.9333	0.0179	3.51
1.91	0.3	0.9	1.2299	1.2121	0.0178	3.48
1.53	0.4	0.9	0.8246	0.8068	0.0178	3.48
1.37	0.3	0.7	0.6545	0.6721	-0.0176	-3.43
1.53	0.1	0.8	1.8246	1.8076	0.0171	3.33
1.00	0.5	0.9	0.5338	0.5168	0.0170	3.32
1.25	0.2	0.8	1.0306	1.0472	-0.0166	-3.25
1.69	0.3	0.8	0.8605	0.8771	-0.0166	-3.25
0.83	0.1	0.3	0.7186	0.7352	-0.0166	-3.24
1.91	0.1	0.7	1.7512	1.7348	0.0165	3.22
2.05	0.5	0.9	0.7346	0.7501	-0.0154	-3.02
0.83	0.3	0.8	0.7009	0.7162	-0.0154	-3.00

Table 6.6. Three-tip cracks under bending with fitting error for flange crack tip $|\Delta| \geq 3\%$.

β	λ_w	λ_f	f_{FEM}	f_{pred}	Diff.	Δ %
1.69	0.1	0.9	1.8969	1.8273	0.0695	4.14
0.83	0.2	0.1	1.5914	1.5253	0.0661	3.94
1.37	0.1	0.9	1.9264	1.8615	0.0649	3.86
1.37	0.6	0.1	1.5739	1.6353	-0.0614	-3.66
0.83	0.3	0.1	1.7110	1.6513	0.0597	3.56
1.37	0.5	0.1	1.5573	1.6128	-0.0555	-3.31

Table 6.7. Fitting errors for two-tip and three-tip cracked I-beams.

Crack	Loading	Crack tip	Maximum fitting error Δ %	
			Positive	Negative
2-tip	Tension	Upper	1.45	-2.98
2-tip	Tension	Lower	1.29	-1.93
2-tip	Bending	Upper	2.25	-2.73
2-tip	Bending	Lower	1.95	-2.82
3-tip	Tension	Flange	4.49	-4.76
3-tip	Tension	Web	3.34	-3.58
3-tip	Bending	Flange	4.14	-3.66
3-tip	Bending	Web	6.31	-6.50

Table A.1. Comparison of SIFs for center-cracked plate under tension.

Mesh Pattern	Crack Length	SIF Ratio, K_{FEA}/K_{Tada}			
m x n	a/W	Nonlinear Extrapolation Eq. 2.7	Linear Extrapolation Eq. 2.10	Quarter-point Displacement Eq. 2.12	J Integral
Effect of Parameter *m*					
2 x 2	0.5	1.0468	1.0116	0.9941	0.9974
3 x 2	0.5	1.0472	1.0118	0.9941	0.9974
2 x 4	0.5	1.0192	1.0104	1.0061	1.0000
3 x 4	0.5	1.0193	1.0106	1.0062	1.0001
4 x 4	0.5	1.0192	1.0105	1.0062	1.0001
2 x 8	0.5	1.0122	1.0099	1.0088	1.0002
3 x 8	0.5	1.0122	1.0010	1.0089	1.0004
4 x 8	0.5	1.0121	1.0099	1.0088	1.0003
3 x 16	0.5	1.0110	1.0104	1.0101	1.0004
4 x 16	0.5	1.0109	1.0104	1.0101	1.0004
Effect of Parameter *n*					
3 x 2	0.1	1.0475	1.0125	0.9950	0.9974
3 x 4	0.1	1.0188	1.0103	1.0060	0.9997
3 x 8	0.1	1.0125	1.0103	1.0092	1.0000
3 x 16	0.1	1.0107	1.0101	1.0098	1.0000
3 x 2	0.5	1.0472	1.0118	0.9941	0.9974
3 x 4	0.5	1.0193	1.0106	1.0062	1.0001
3 x 8	0.5	1.0122	1.0100	1.0089	1.0004
3 x 16	0.5	1.0110	1.0104	1.0101	1.0004
3 x 2	0.9	1.0143	1.0101	1.0079	0.9982
3 x 4	0.9	1.0112	1.0103	1.0099	1.0008
3 x 8	0.9	1.0114	1.0111	1.0110	1.0010
3 x 16	0.9	1.0113	1.0111	1.0111	1.0010

Table A.2. Comparison of SIFs for edge-cracked plate under bending.

Mesh Pattern	Crack Length	SIF Ratio, K_{FEA}/K_{exist} [a]			
m x n	a/W	Nonlinear Extrapolation Eq. 2.7	Linear Extrapolation Eq. 2.10	Quarter-point Displacement Eq. 2.12	J Integral
Effect of Parameter *m*					
2 x 2	0.5	0.9205	1.0014	1.0418	0.9956
3 x 2	0.5	0.9248	1.0044	1.0442	0.9968
2 x 4	0.5	0.9869	1.0084	1.0191	1.0011
3 x 4	0.5	0.9869	1.0086	1.0195	1.0014
4 x 4	0.5	0.9872	1.0088	1.0196	1.0014
2 x 8	0.5	1.0049	1.0103	1.0130	1.0015
3 x 8	0.5	1.0051	1.0105	1.0132	1.0017
4 x 8	0.5	1.0051	1.0105	1.0132	1.0017
3 x 16	0.5	1.0103	1.0116	1.0123	1.0017
4 x 16	0.5	1.0102	1.0116	1.0123	1.0017
Effect of Parameter *n*					
3 x 2	0.1	1.0194	1.0137	1.0109	1.0006
3 x 4	0.1	1.0143	1.0126	1.0118	1.0031
3 x 8	0.1	1.0140	1.0135	1.0132	1.0033
3 x 16	0.1	1.0136	1.0135	1.0134	1.0034
3 x 2	0.5	0.9248	1.0044	1.0442	0.9968
3 x 4	0.5	0.9869	1.0086	1.0195	1.0014
3 x 8	0.5	1.0051	1.0105	1.0132	1.0017
3 x 16	0.5	1.0103	1.0116	1.0123	1.0017
3 x 2	0.9	0.9166	0.9999	1.0416	0.9943
3 x 4	0.9	0.9839	1.0060	1.0170	0.9988
3 x 8	0.9	1.0034	1.0088	1.0116	0.9992
3 x 16	0.9	1.0080	1.0092	1.0098	0.9992

[a] Brown (1966) solution for $a/W = 0.1$ and 0.5; Tada (1973) for $a/W = 0.9$

Table A.3. Comparison of SIFs for edge-cracked plate under tension.

Mesh Pattern	Crack Length	SIF Ratio, K_{FEA}/K_{Tada}			
m x n	a/W	Nonlinear Extrapolation Eq. 2.7	Linear Extrapolation Eq. 2.10	Quarter-point Displacement Eq. 2.12	J Integral
Effect of Parameter *m*					
3 x 2	0.1	1.0212	1.0057	0.9976	1.0080
3 x 4	0.1	1.0085	1.0042	1.0019	0.9943
3 x 8	0.1	1.0057	1.0047	1.0042	0.9948
3 x 16	0.1	1.0047	1.0047	1.0042	0.9948
3 x 2	0.5	0.9703	1.0049	1.0222	0.9949
3 x 4	0.5	0.9987	1.0078	1.0123	0.9988
3 x 8	0.5	1.0056	1.0082	1.0095	0.9992
3 x 16	0.5	1.0087	1.0092	1.0095	0.9992
3 x 2	0.9	0.9218	0.9984	1.0367	0.9925
3 x 4	0.9	0.9838	1.0042	1.0144	0.9951
3 x 8	0.9	1.0014	1.0066	1.0092	0.9973
3 x 16	0.9	1.0056	1.0069	1.0076	0.9973

Table A.4. CODs at quarter point B and corner point C calculated with FEA (m x n = 3 x 8).

Crack Length a/W	Crack Tip Element Size L (μm)	Crack Type	Loading	Crack Opening Displacement		
				v_B (μm)	v_C (μm)	$2v_B - v_C$ (μm)
0.1	156	Central	Tension	0.8672	1.7286	0.0058
		Edge	Tension	1.0254	2.0472	0.0036
		Edge	Bending	0.9032	1.8050	0.0014
0.5	781	Central	Tension	5.1142	10.1946	0.0338
		Edge	Tension	12.1938	24.4800	-0.0924
		Edge	Bending	6.4712	13.0468	-0.1044
0.9	156	Central	Tension	6.6752	13.3452	-0.0052
		Edge	Tension	89.7800	180.9400	-1.3800
		Edge	Bending	32.3200	65.1600	-0.5200

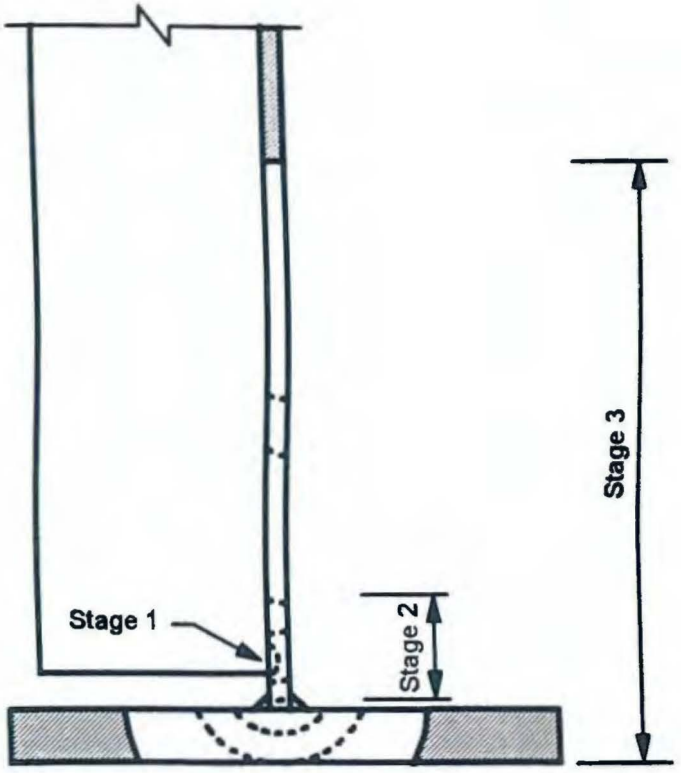

Figure 1.1. Stages of crack growth for stiffener welded to web only.

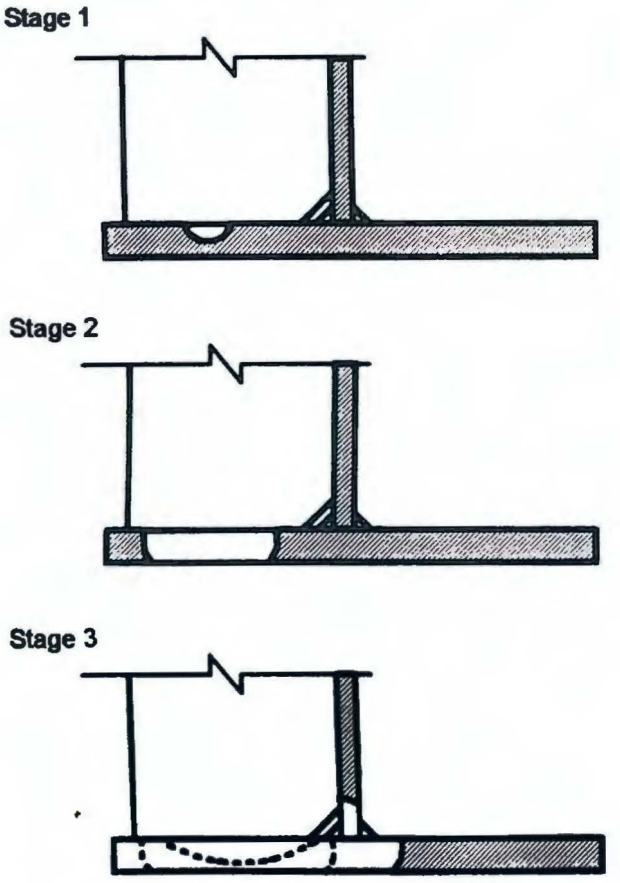

Figure 1.2. Stages of crack growth for stiffener welded to web and flange.

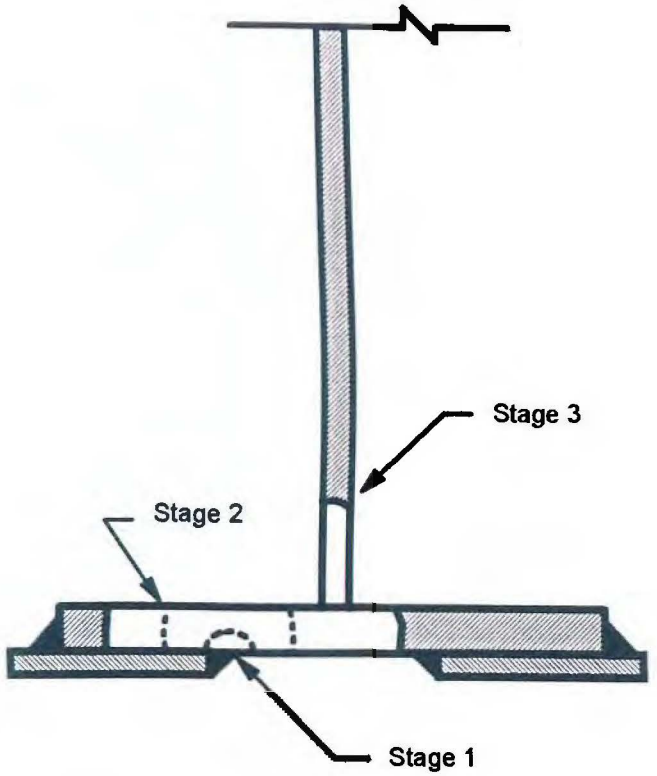

Figure 1.3. Stages of crack growth for attachment welded to flange.

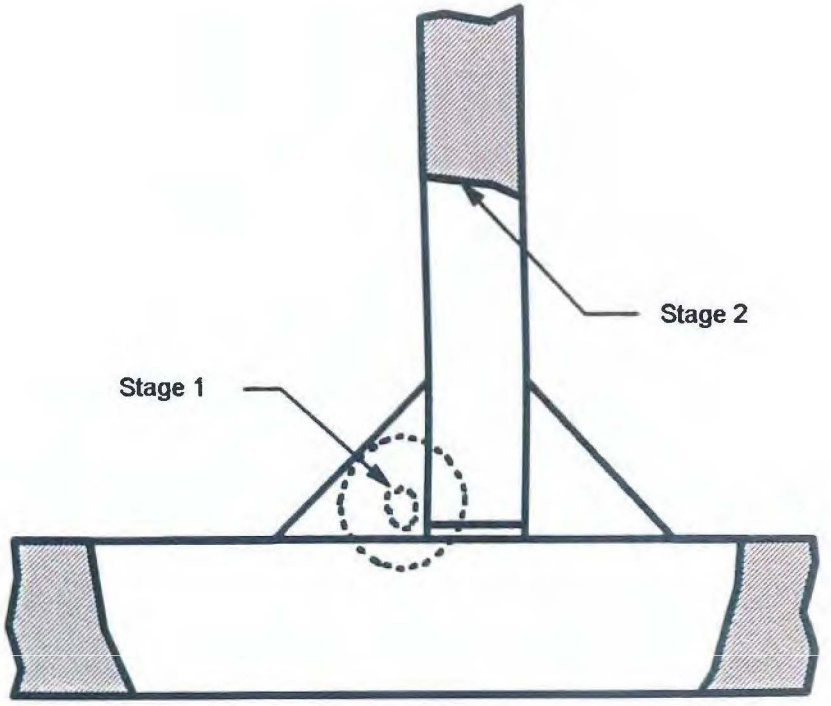

Figure 1.4. Stages of crack growth for welded I-beam.

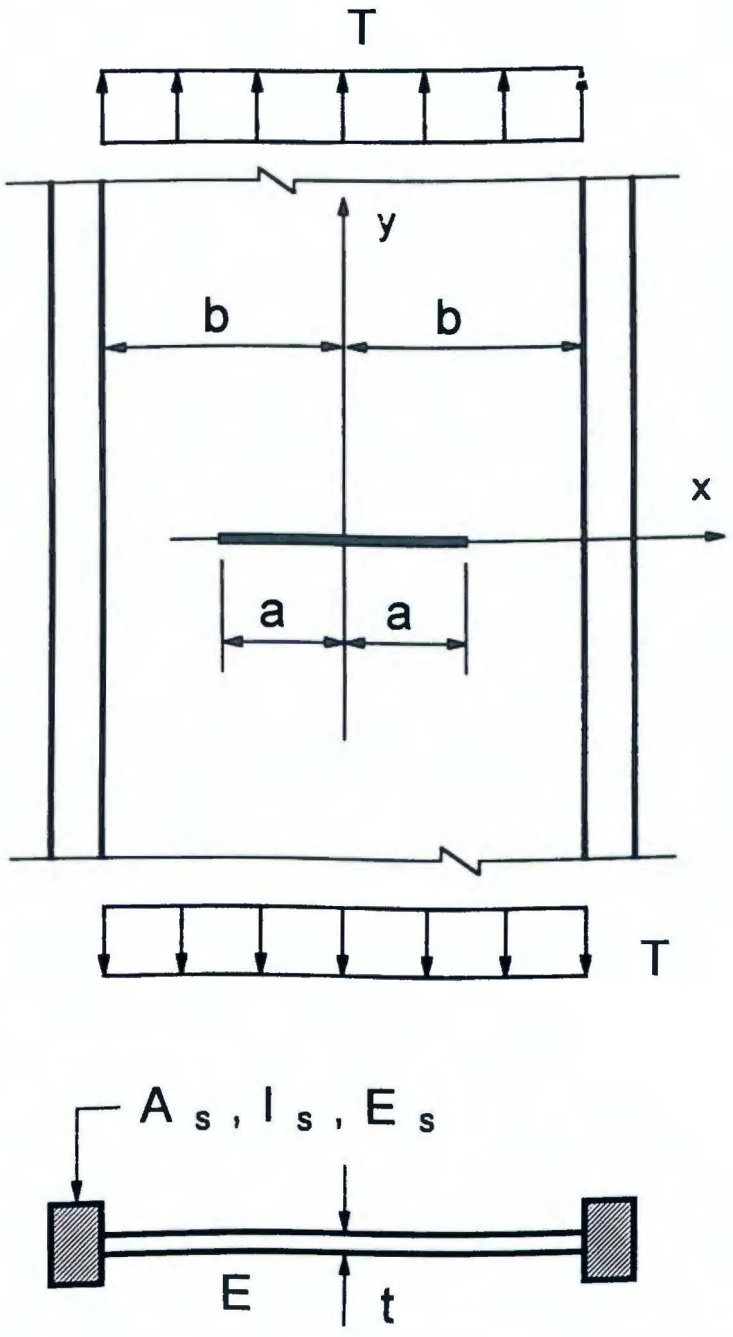

Figure 1.5. Center-cracked plate with stiffened edges.

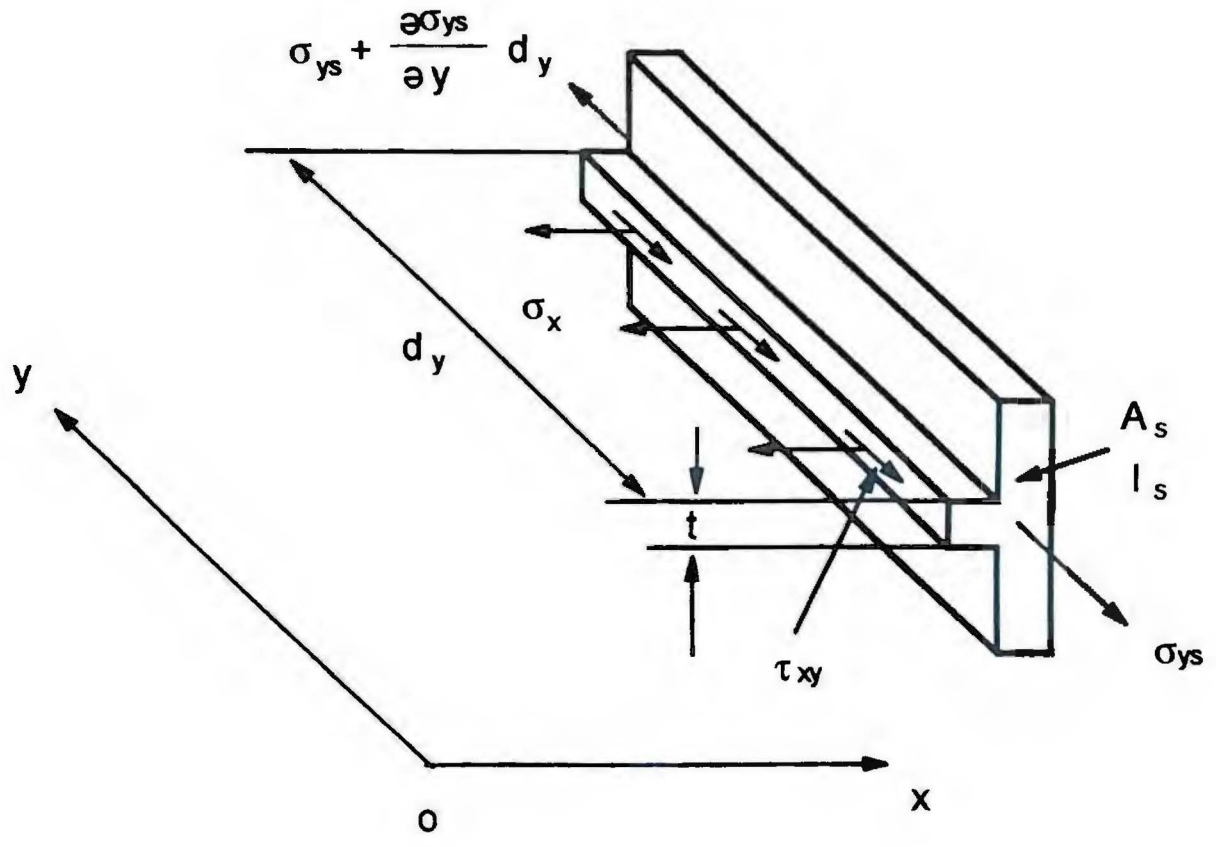

Figure 1.6. Equilibrium of stiffener element.

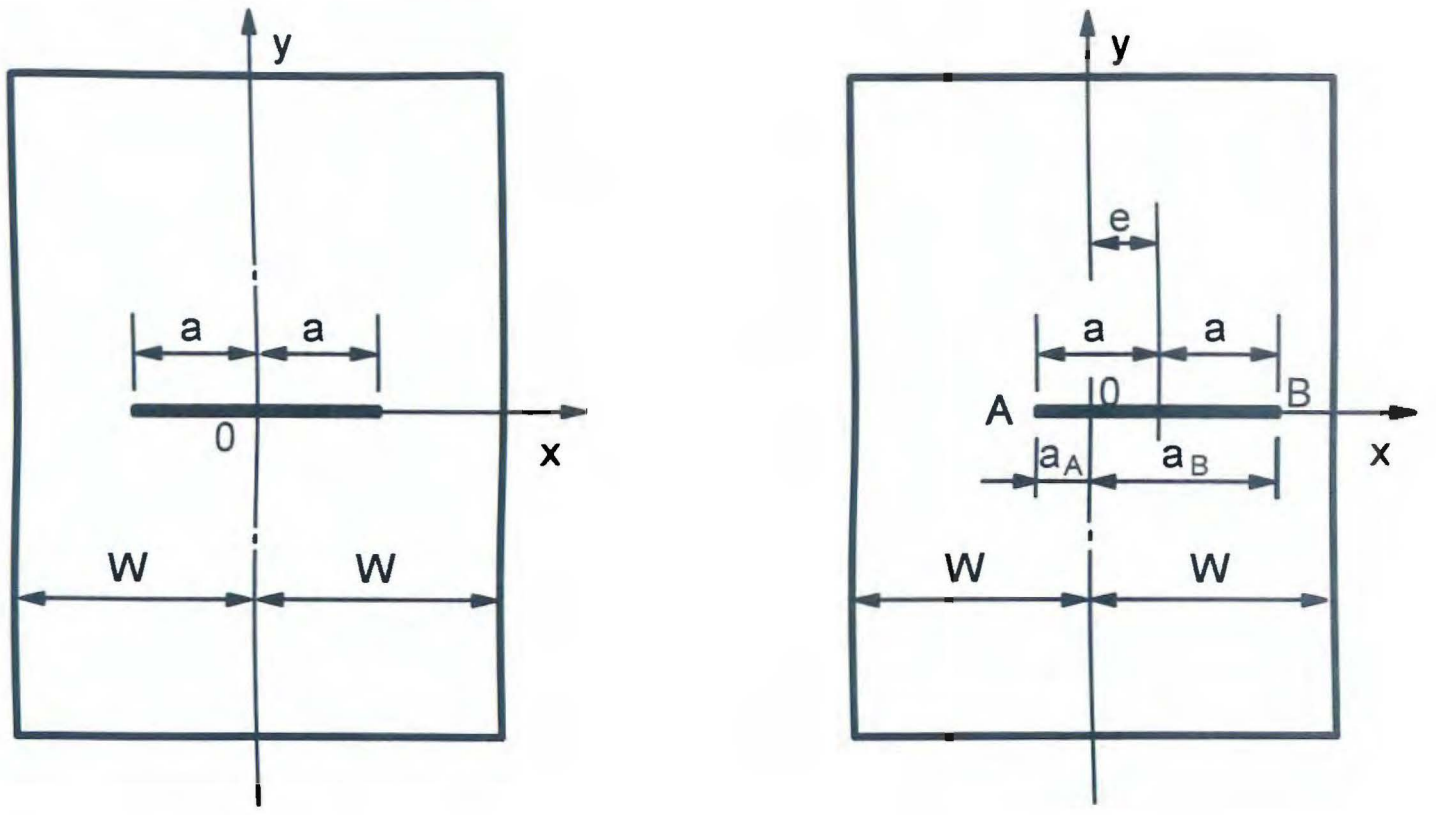

(a) Central crack

(b) Eccentric crack

Figure 1.7. Plate with central and eccentric cracks.

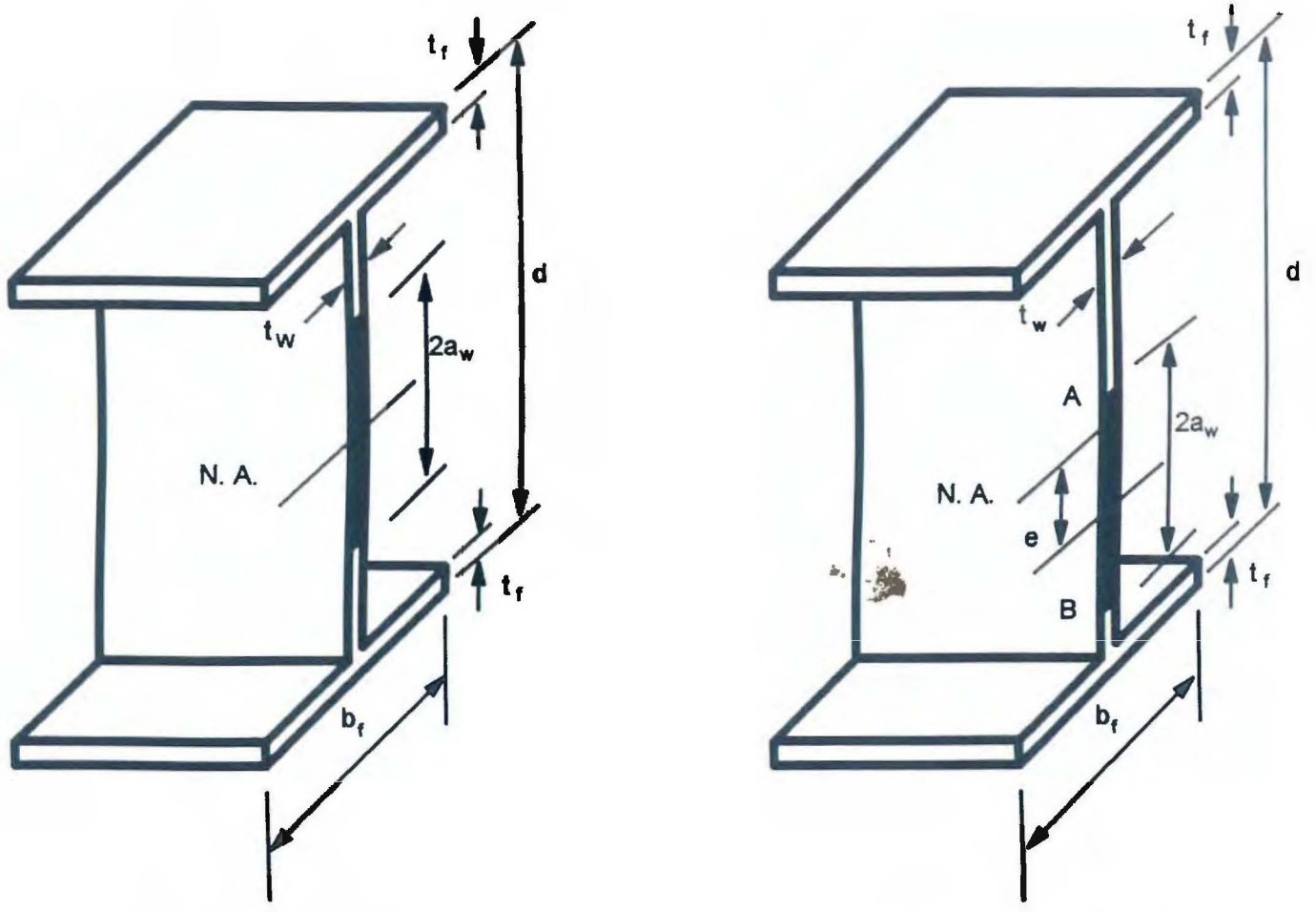

(a) Central crack

(b) Eccentric crack

Figure 1.8. Two-tip cracked I-beam.

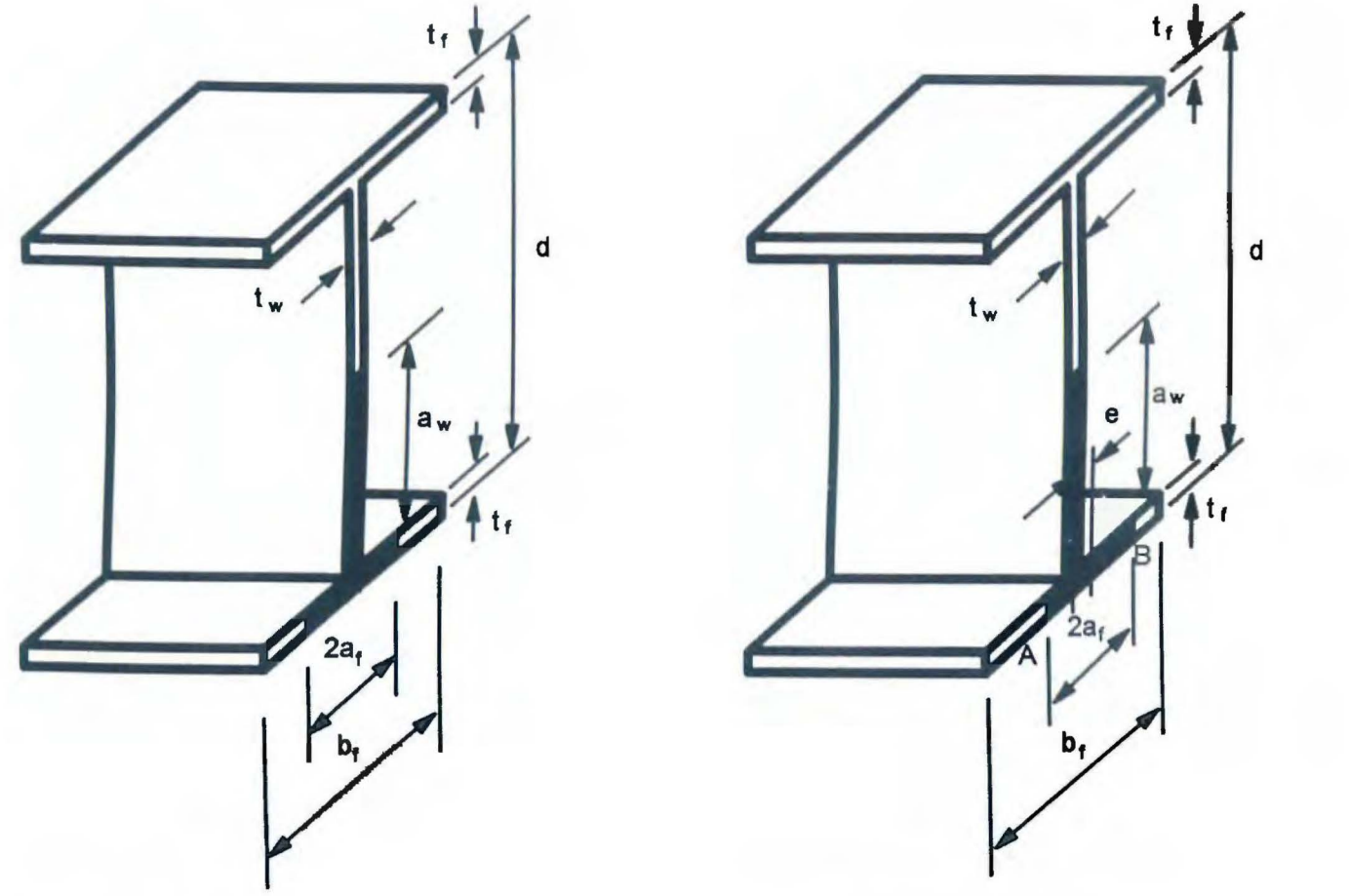

(a) Central crack

(b) Eccentric crack

Figure 1.9. Three-tip cracked I-beam.

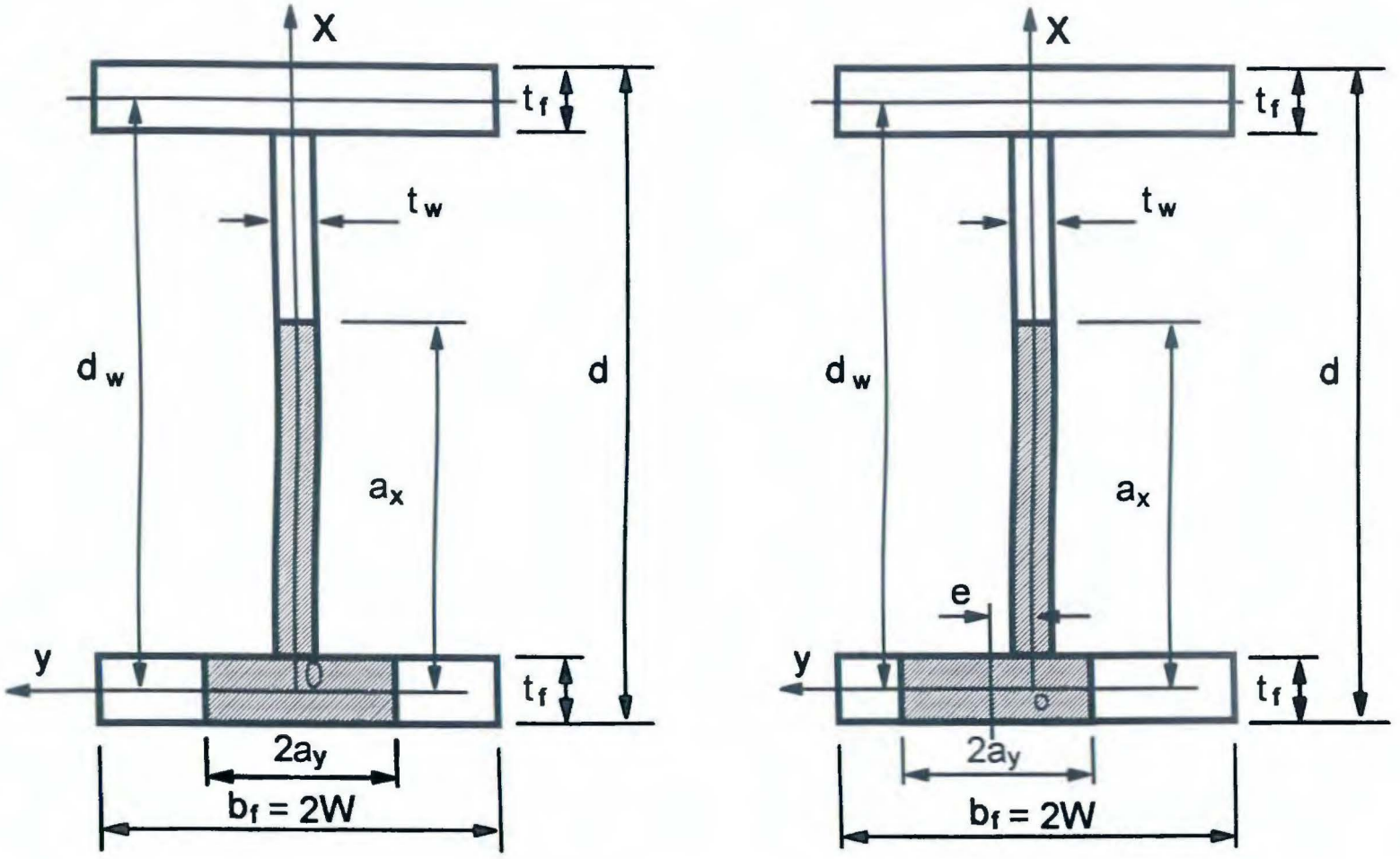

(a) Central three-tip cracked I-beam

(b) Eccentric three-tip cracked I-beam

Figure 1.10. Coordinate and symbols used in previous analyses of three-tip crack (Chen and Albrecht 1994).

Figure 2.1. Dimensions used for modeling of I-beam.

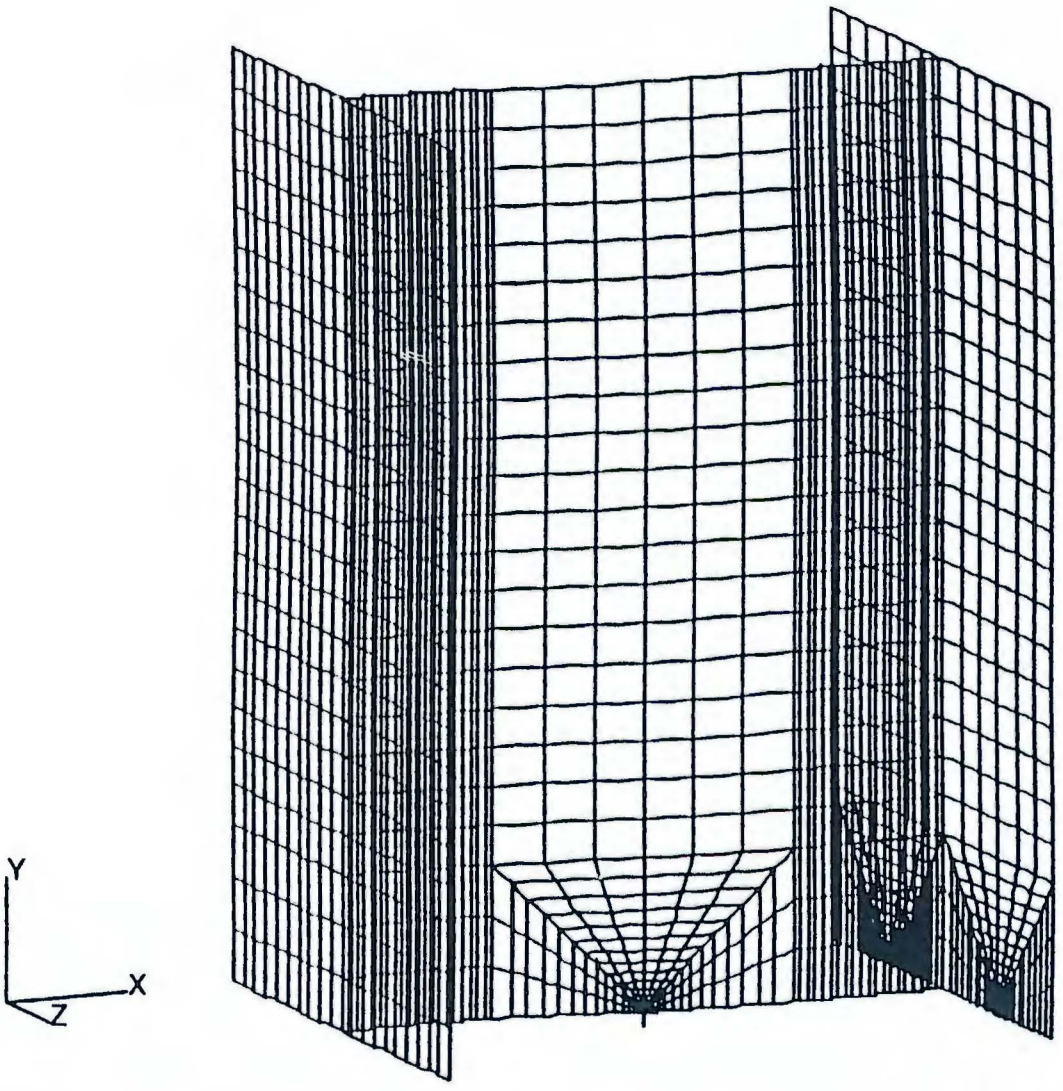

(a) Before deformation

Figure 2.2 (a). Typical three-dimensional I-beam mesh for three-tip crack.

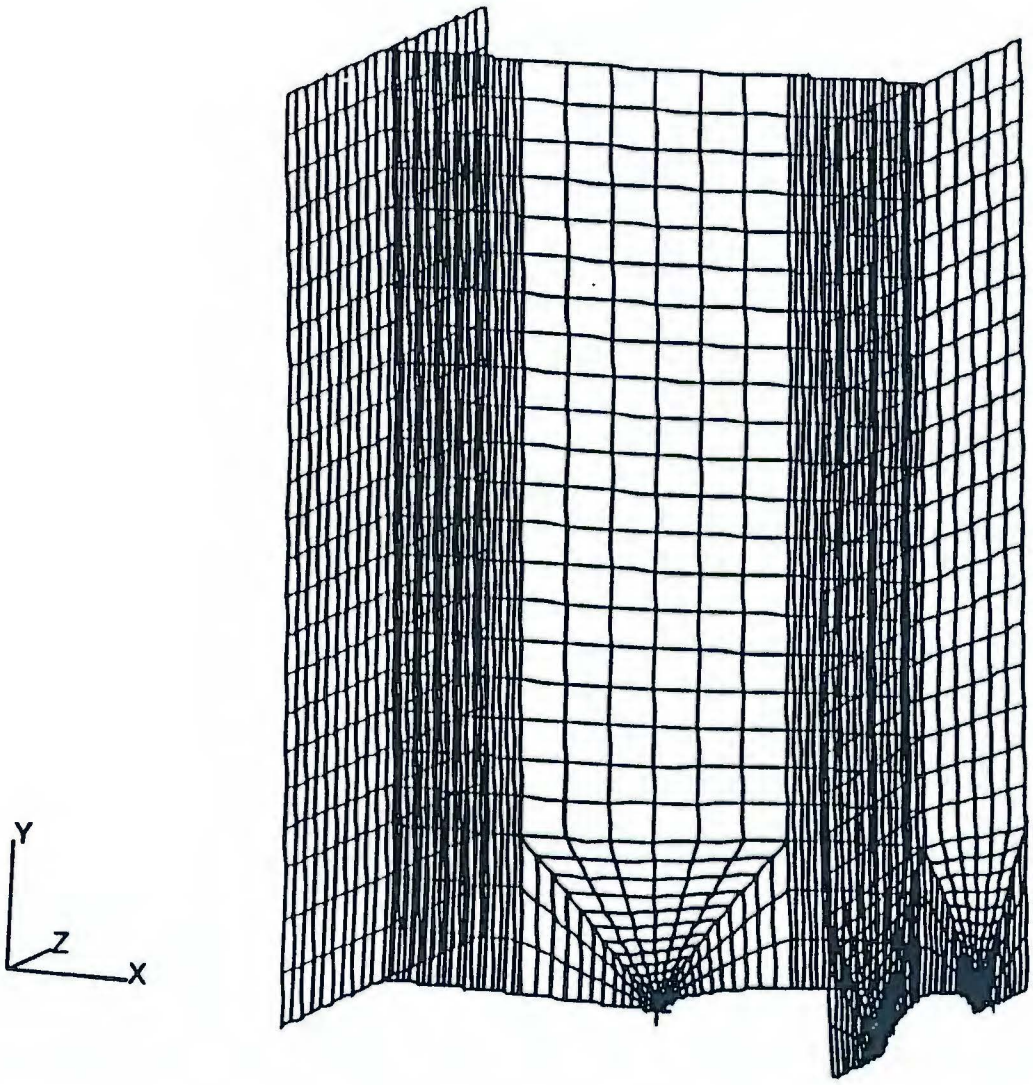

(b) After deformation

Figure 2.2 (b). Typical three-dimensional I-beam mesh for three-tip crack.

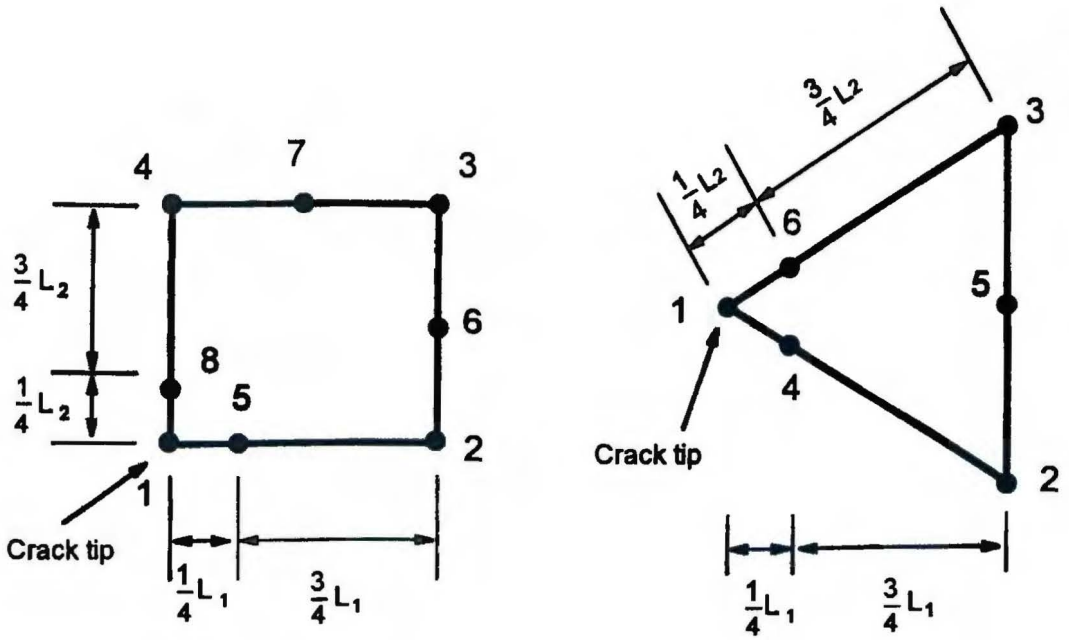

Figure 2.3. Quarter-point elements with $1/\sqrt{r}$ singularity.

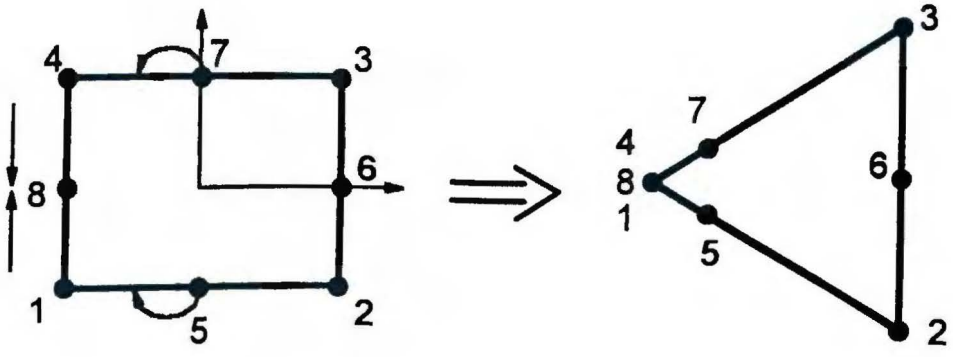

Figure 2.4. Degenerated quarter-point element with $1/\sqrt{r}$ singularity.

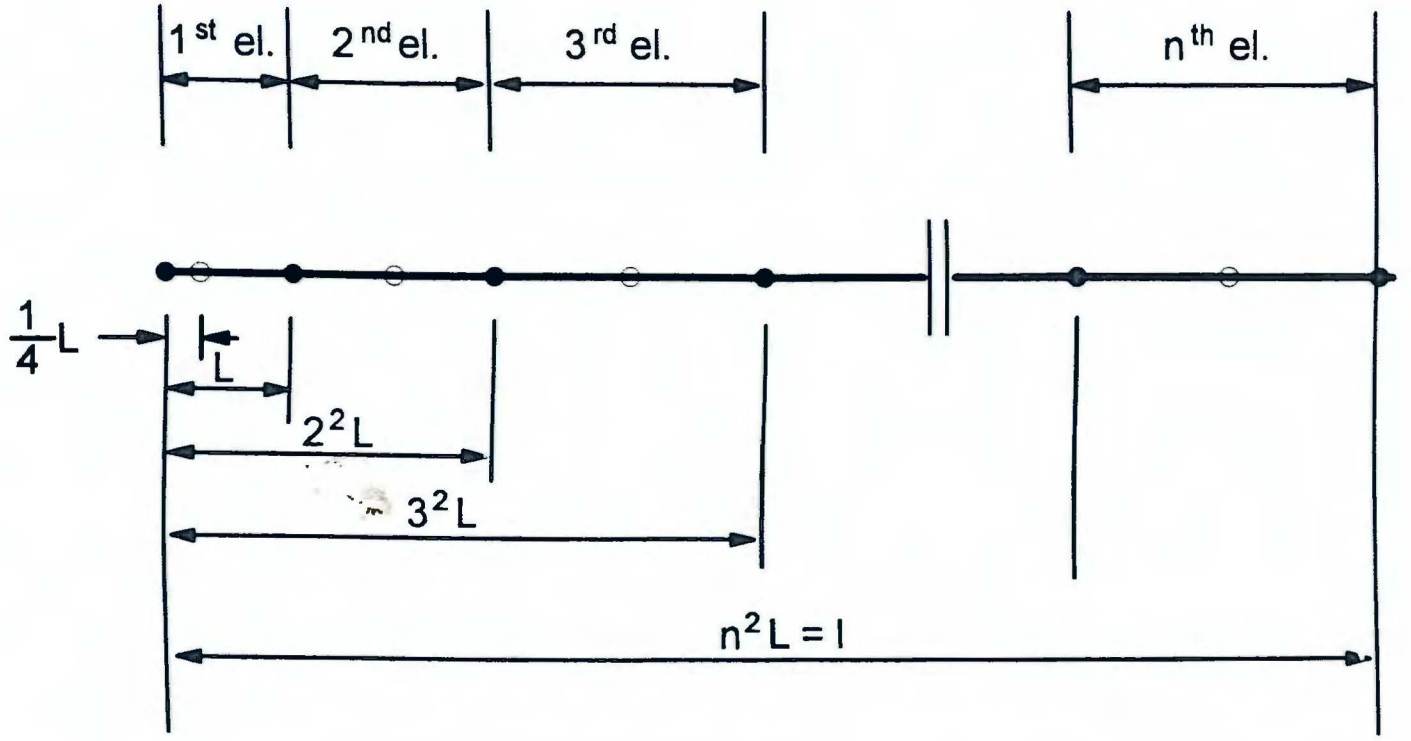

Figure 2.5. Element sizes in inner region generated by ABAQUS' * SINGULAR command.

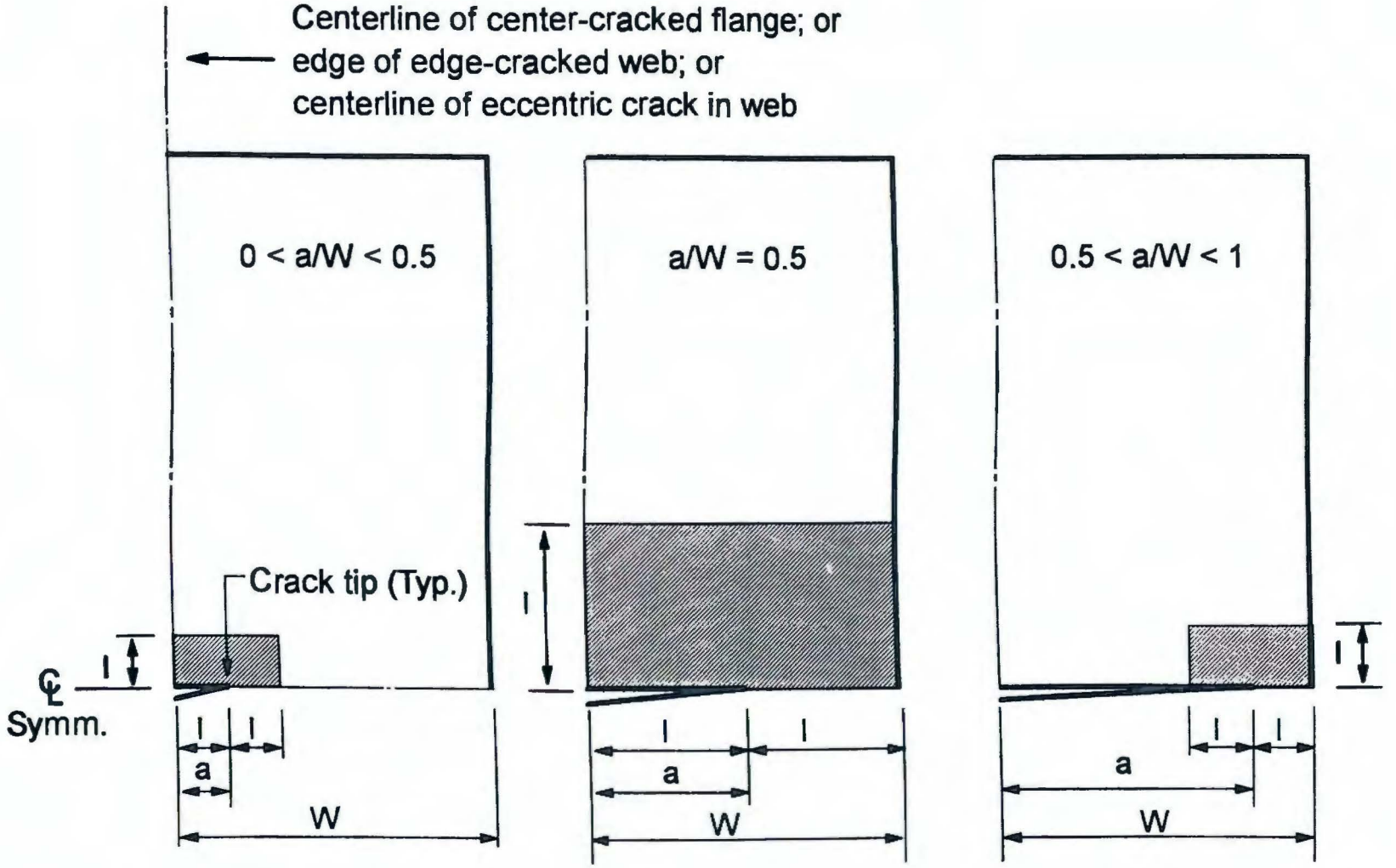

Figure 2.6. Mesh scheme for different crack lengths.

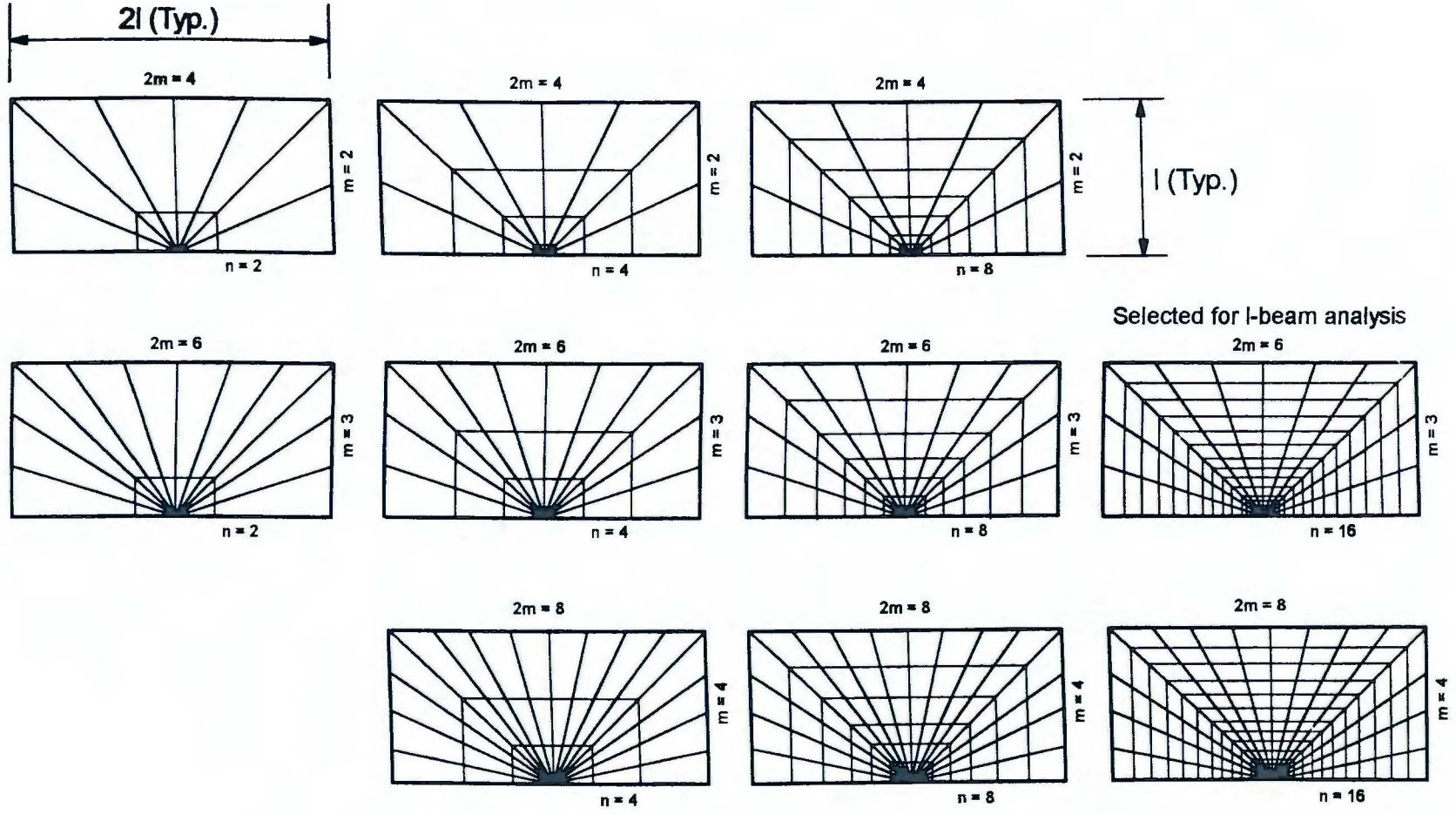

Figure 2.7. Mesh patterns in inner region around crack tip.

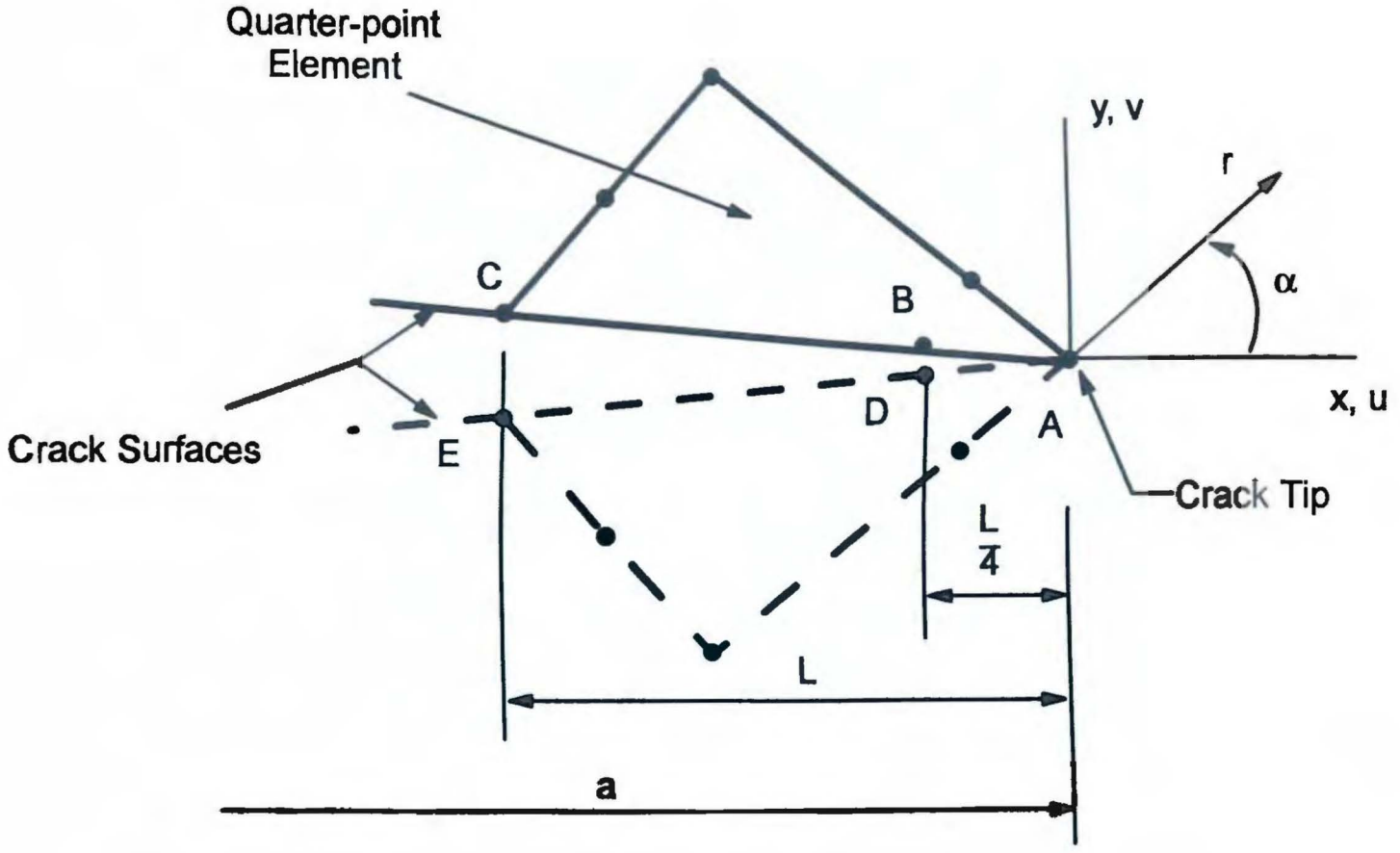

Figure 2.8. Nodes used for calculating SIFs.

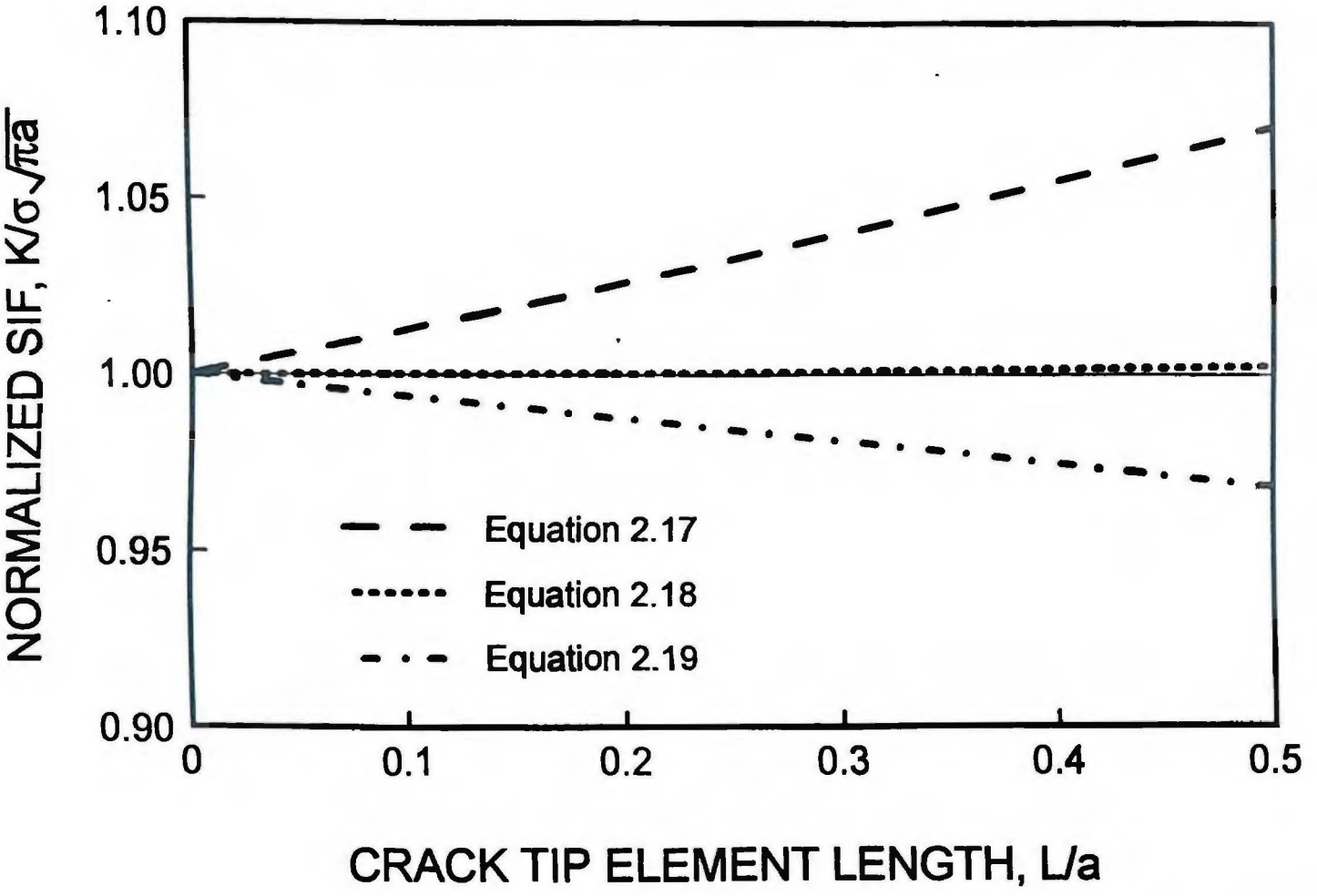

Figure 2.9. SIFs calculated from displacement-based methods.

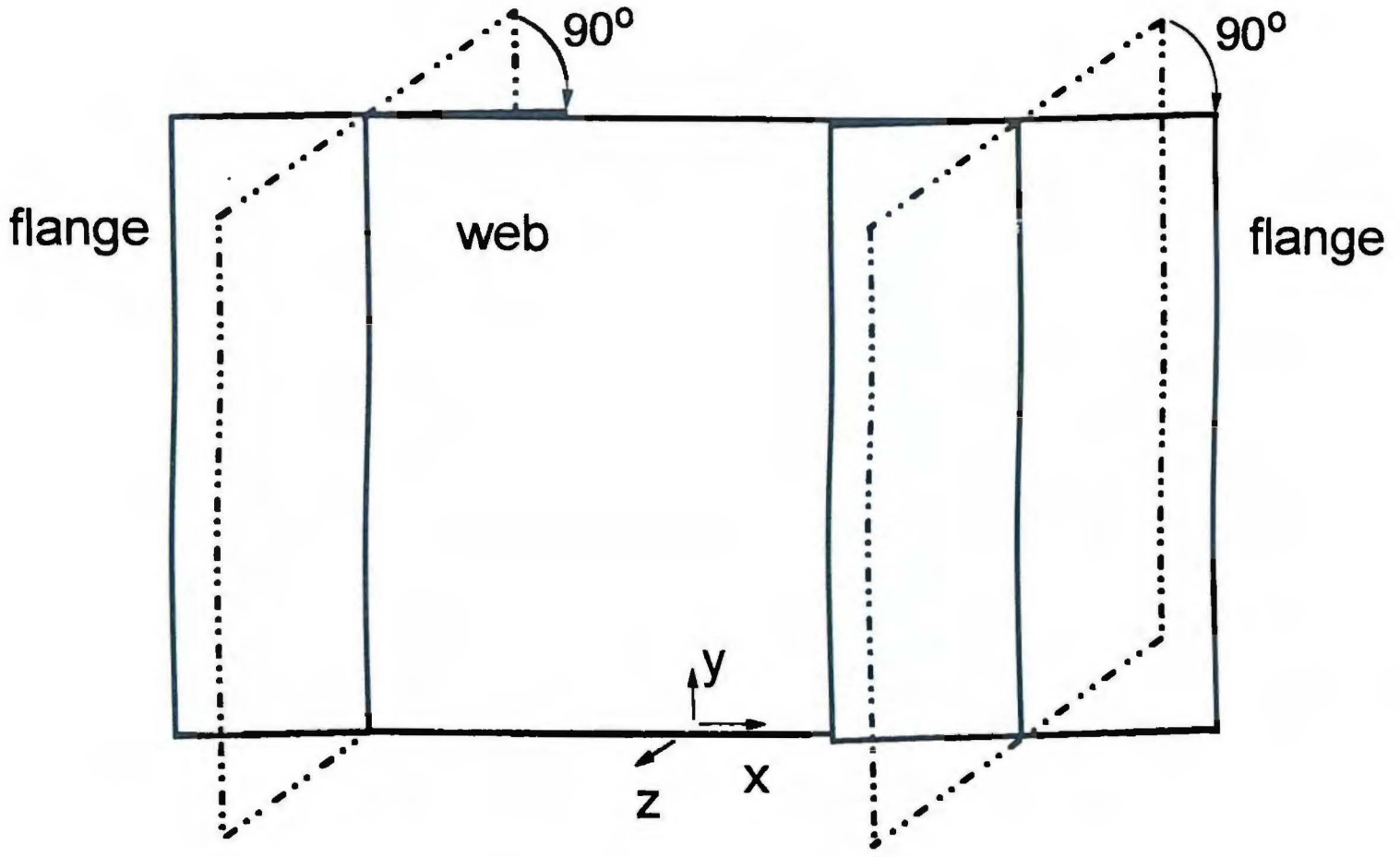

Figure 2.10. Schematic of two-dimensional I-beam model.

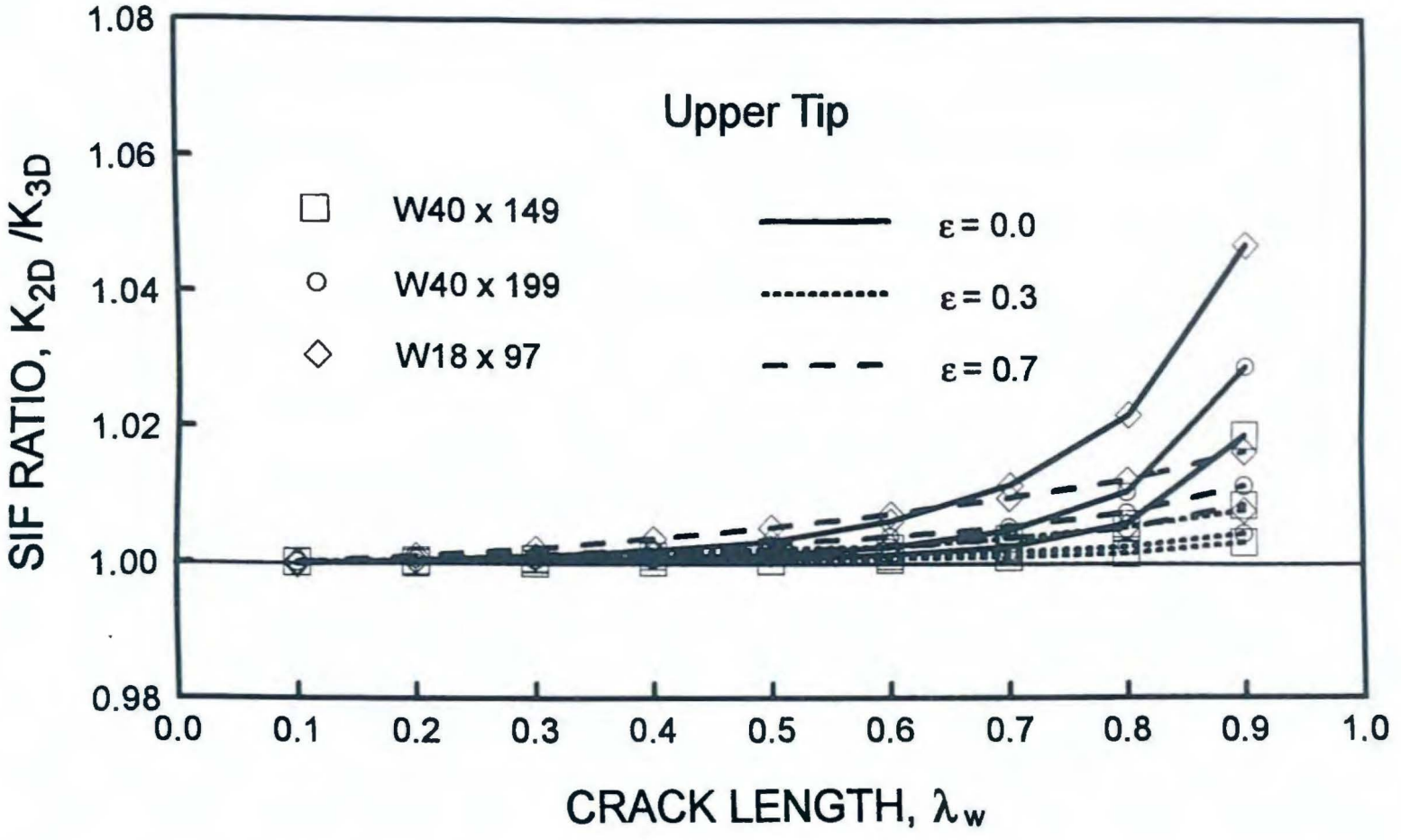

Figure 2.11. Comparison of 2-D and 3-D model results for SIFs of two-tip cracked I-beam under tension; upper tip.

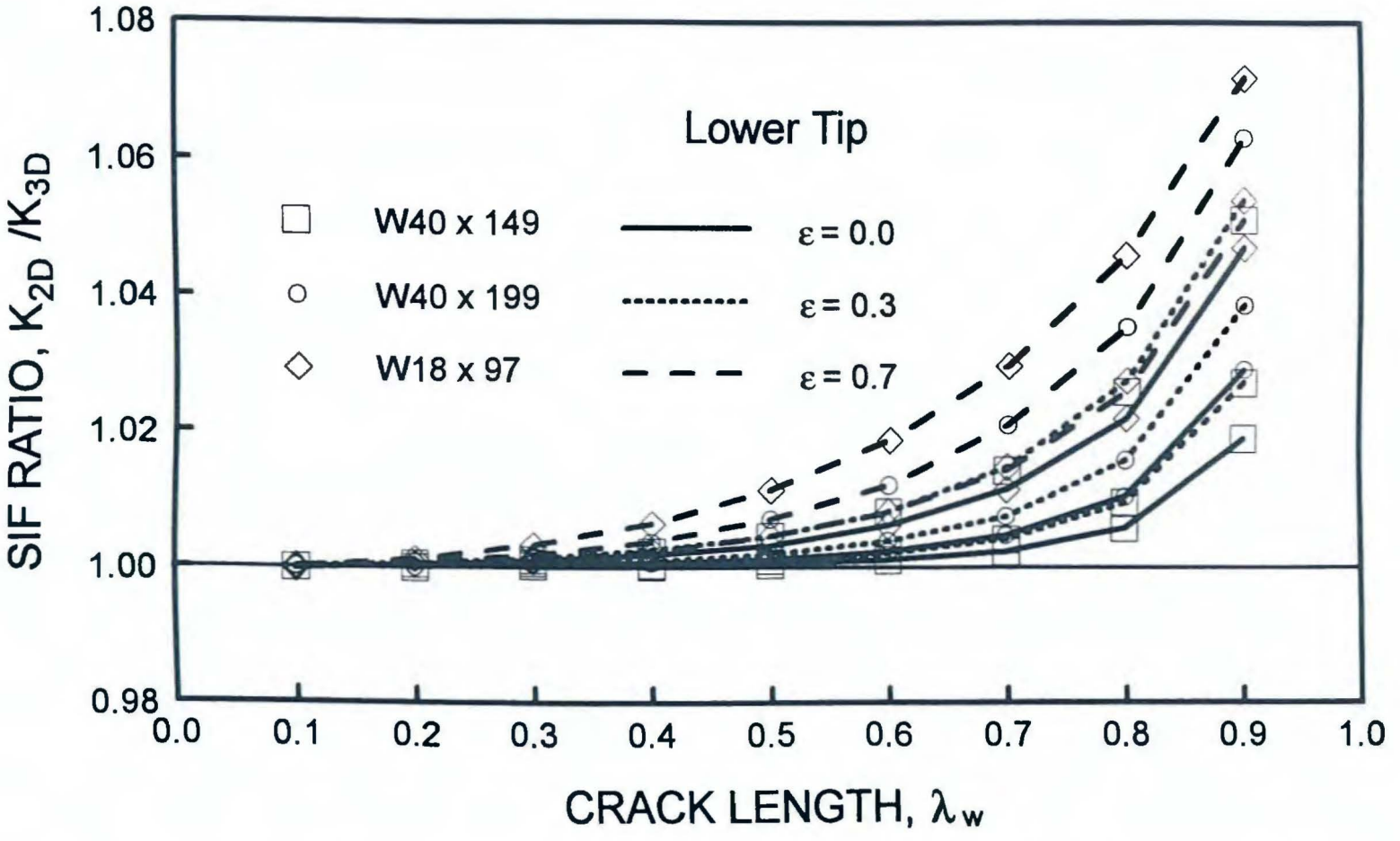

Figure 2.12. Comparison of 2-D and 3-D model results for SIFs of two-tip cracked I-beam under tension; lower tip.

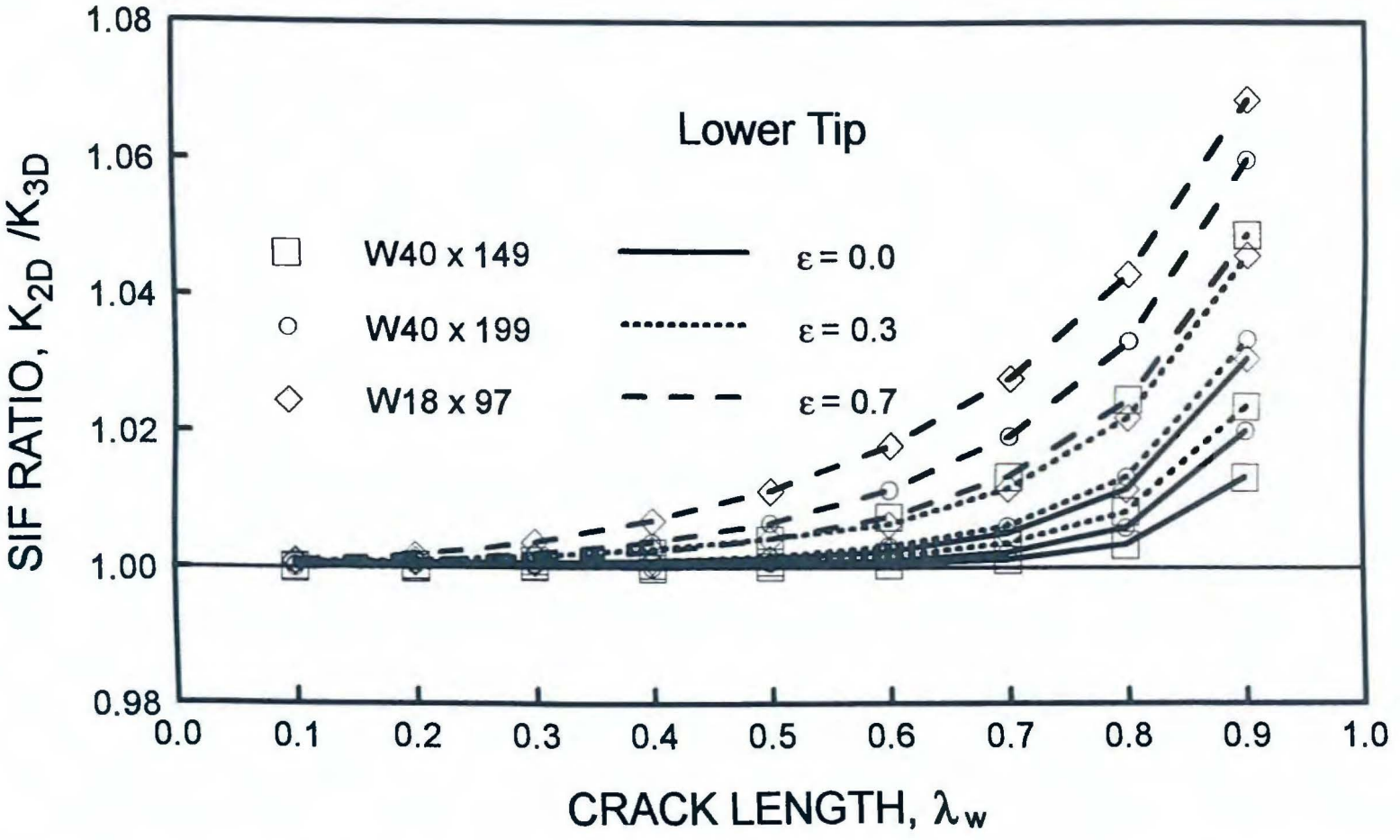

Figure 2.13. Comparison of 2-D and 3-D model results for SIFs of two-tip cracked I-beam under bending; lower tip.

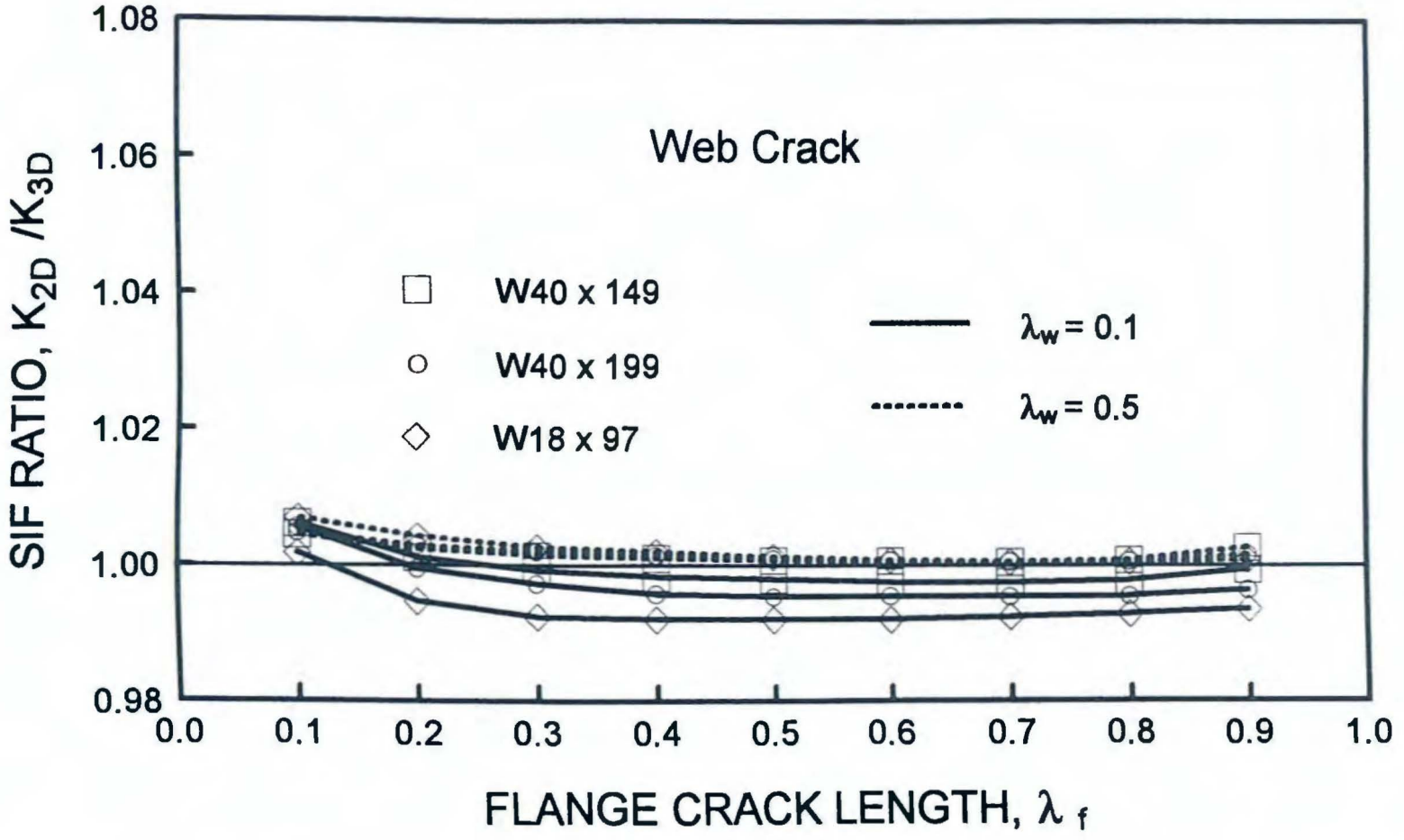

Figure 2.14. Comparison of 2-D and 3-D model results for SIFs of three-tip cracked I-beam under tension; web crack tip.

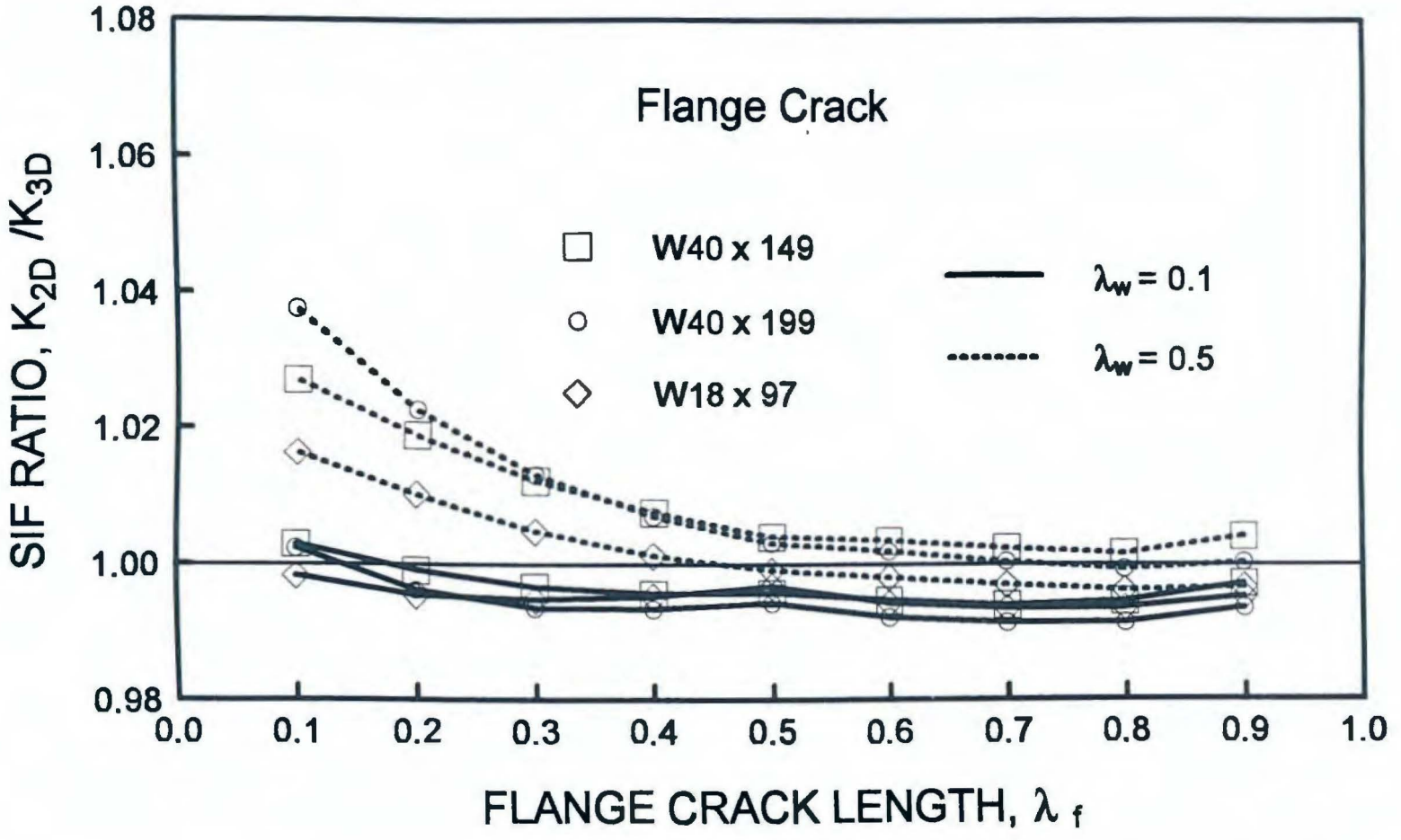

Figure 2.15. Comparison of 2-D and 3-D model results for SIFs of three-tip cracked I-beam under tension; flange crack tip.

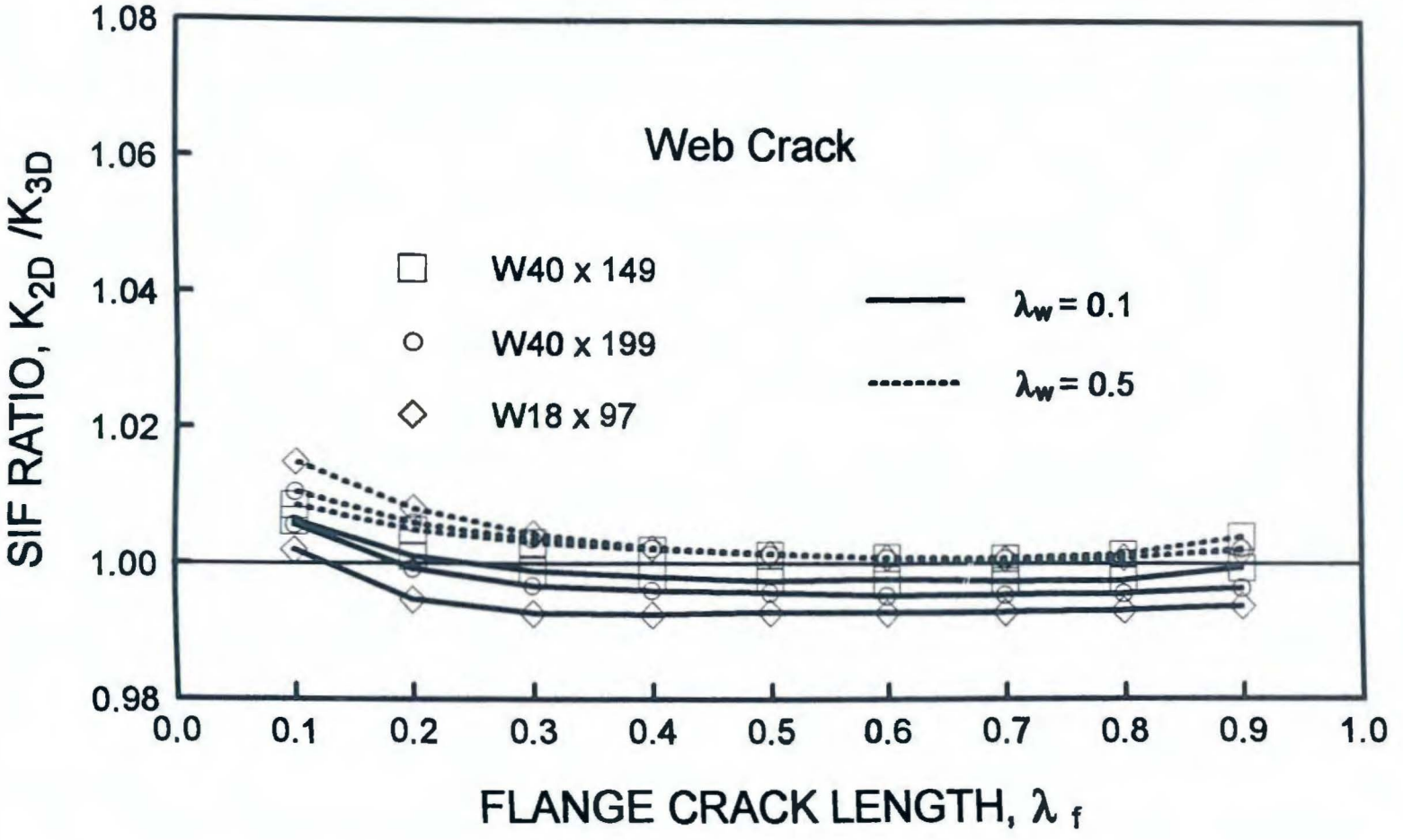

Figure 2.16. Comparison of 2-D and 3-D model results for SIFs of three-tip cracked I-beam under bending; web crack tip.

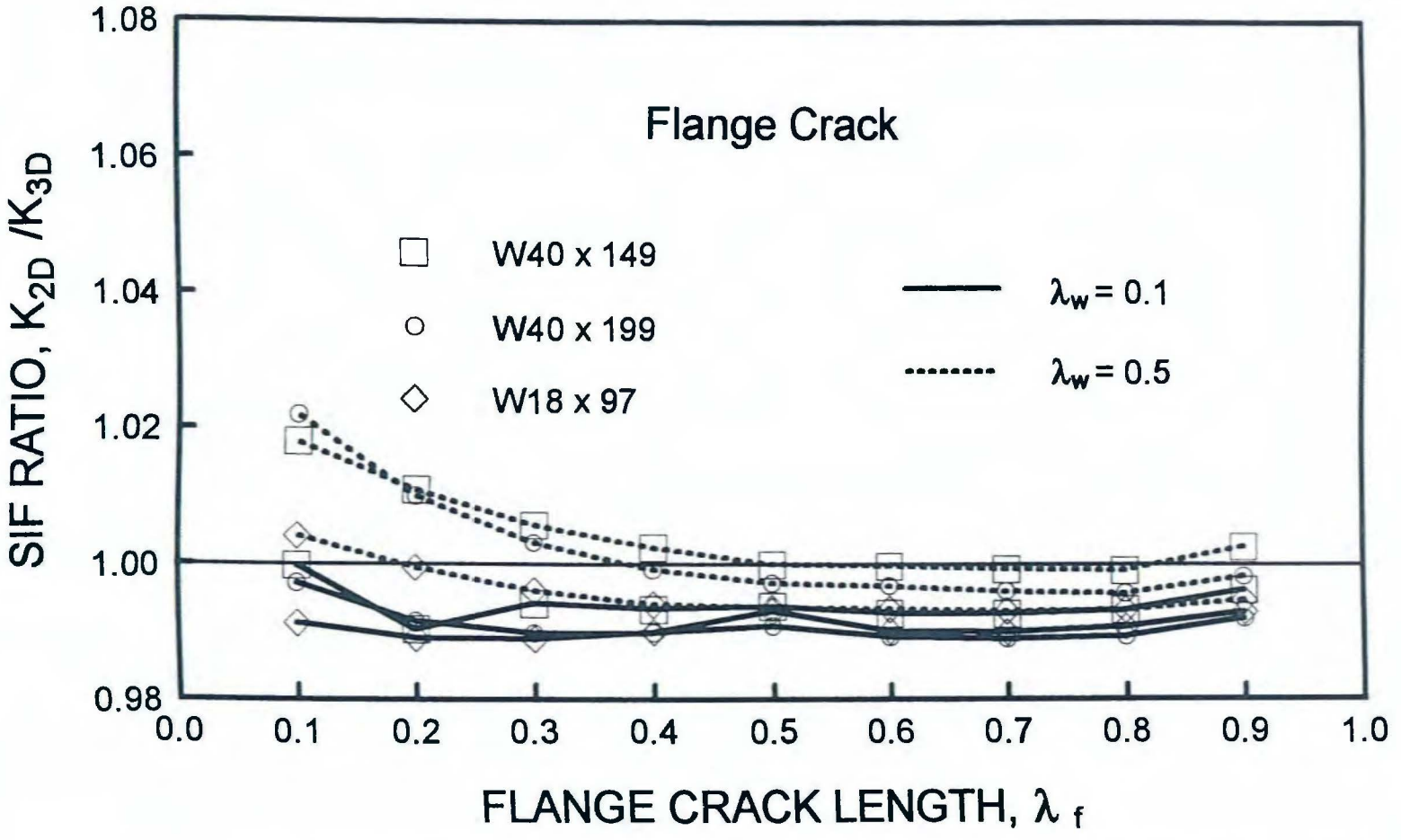

Figure 2.17. Comparison of 2-D and 3-D model results for SIFs of three-tip cracked I-beam under bending; flange crack tip.

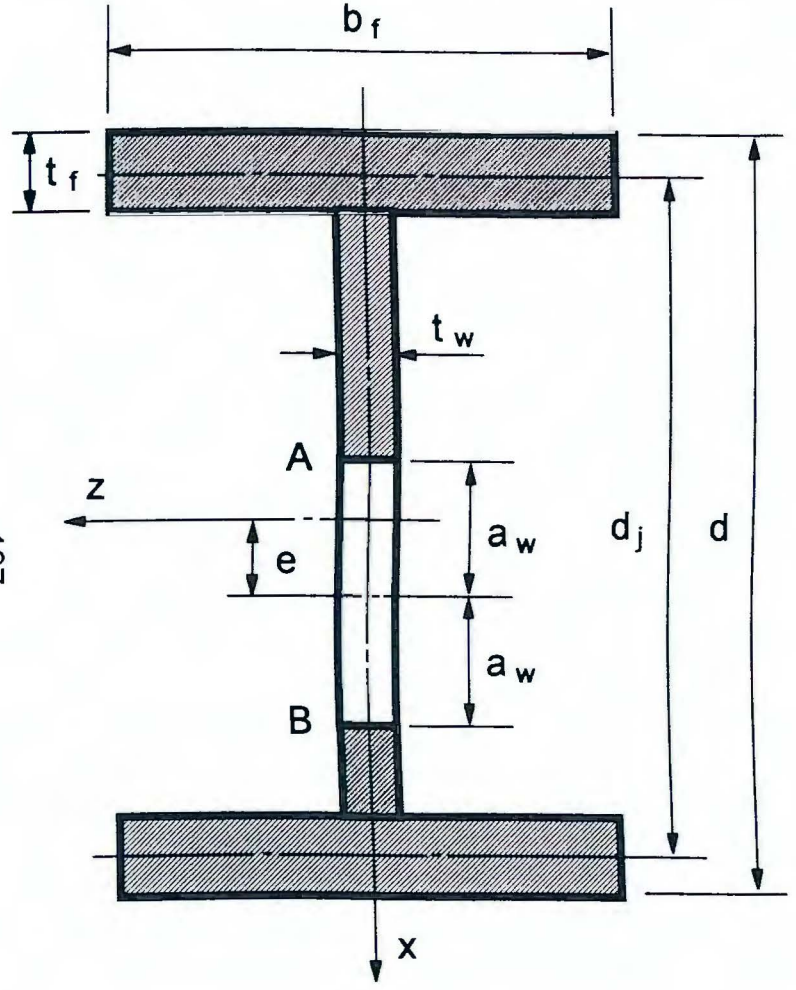

Figure 3.1. Dimensions of two-tip web crack.

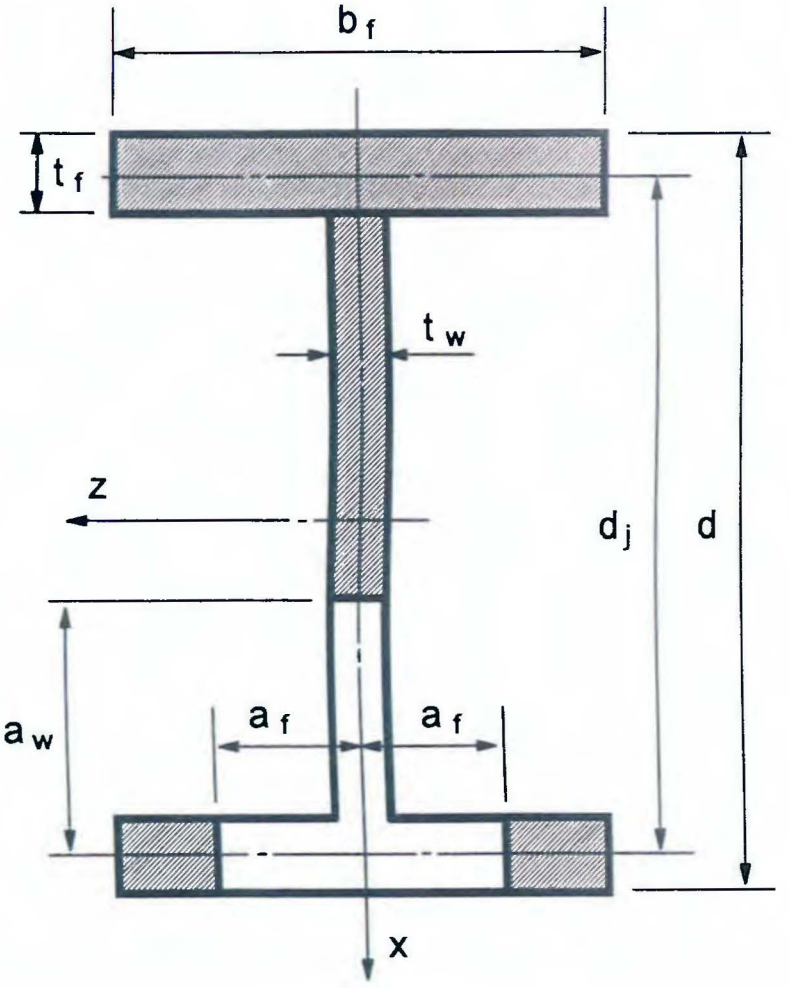

Figure 3.2. Dimensions of symmetric three-tip crack.

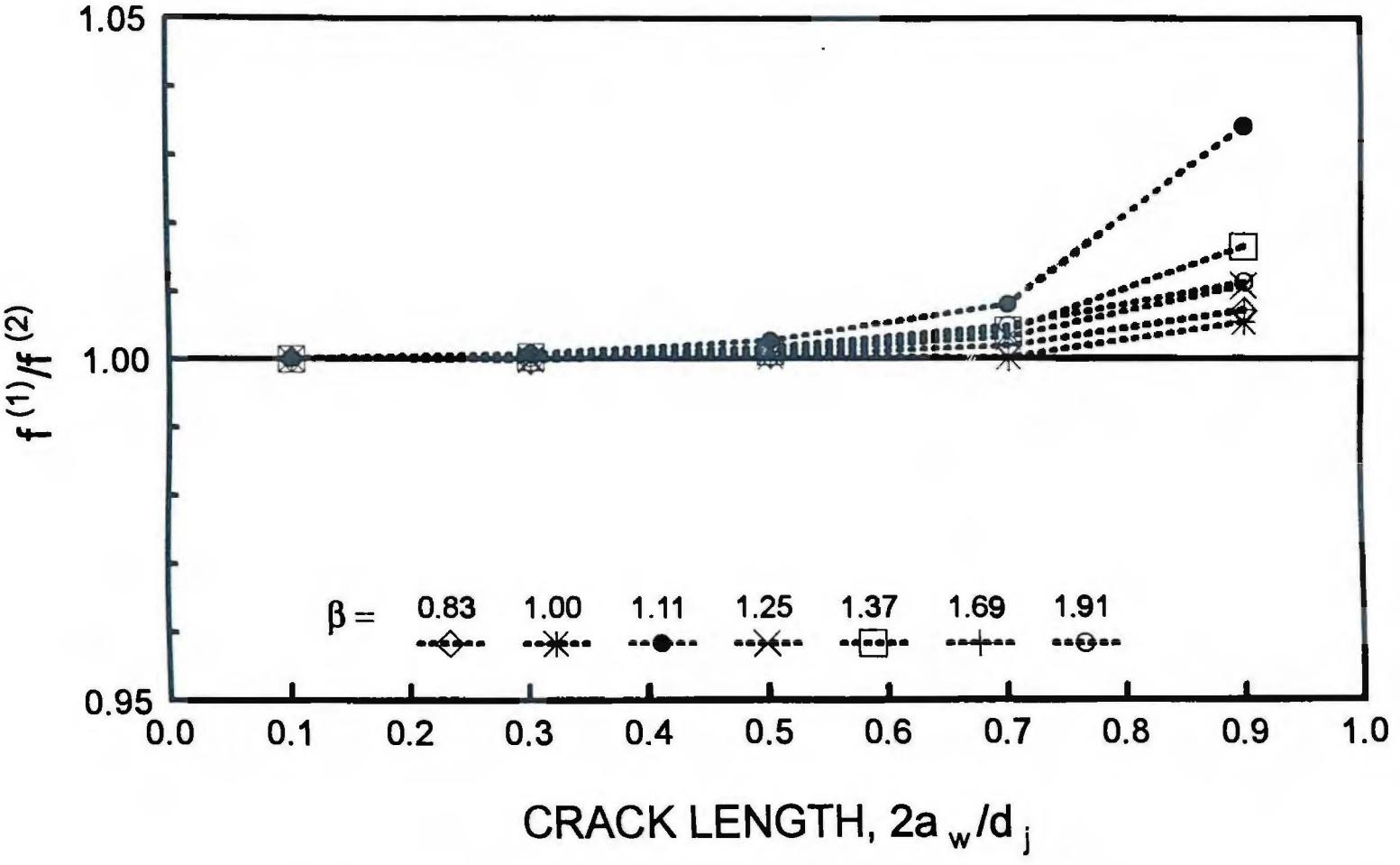

Figure 3.3. Effect of parameter β on correction factor for two-tip center-cracked I-beams under tension.

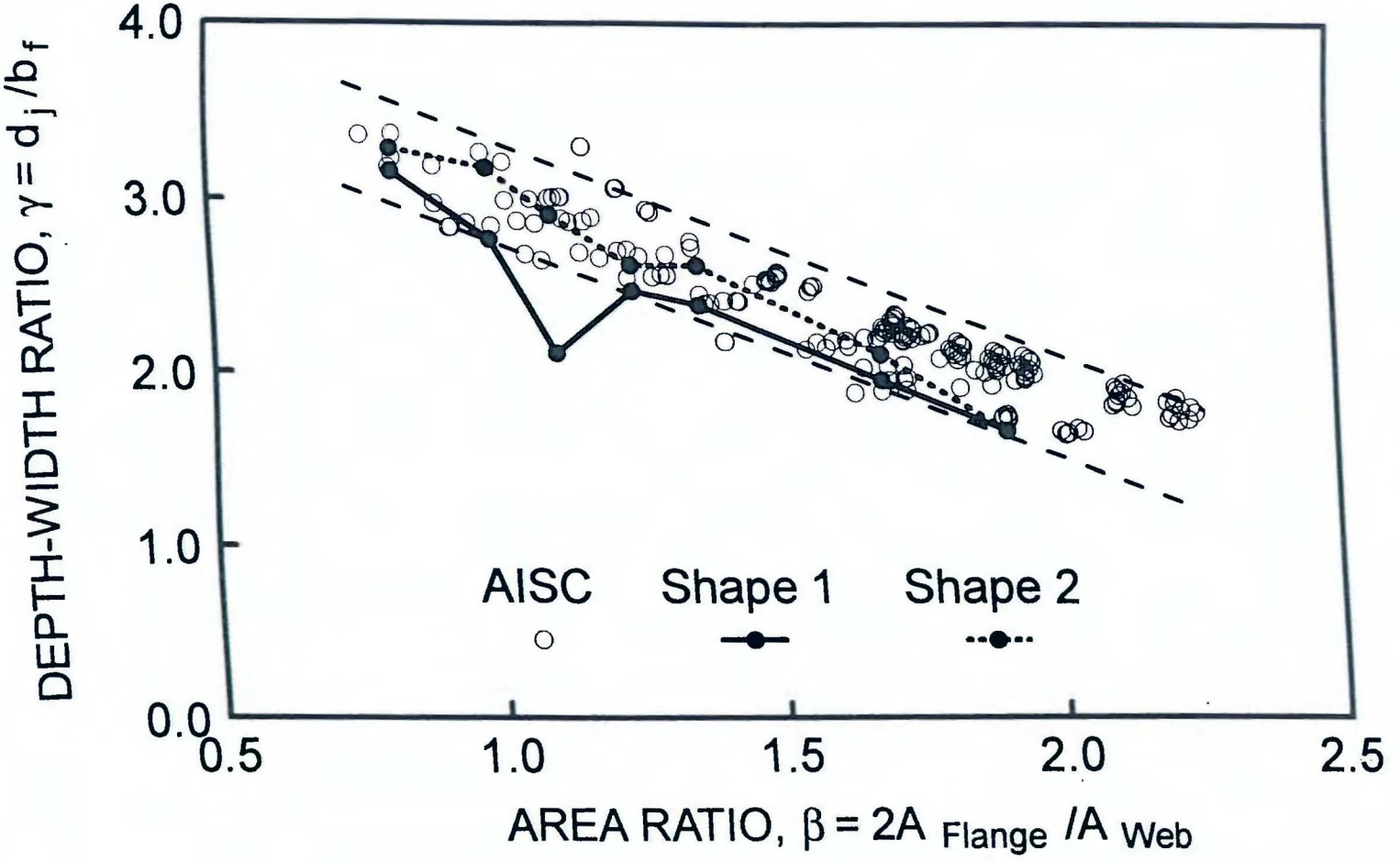

Figure 3.4. Selected W-shapes for validation of β parameter.

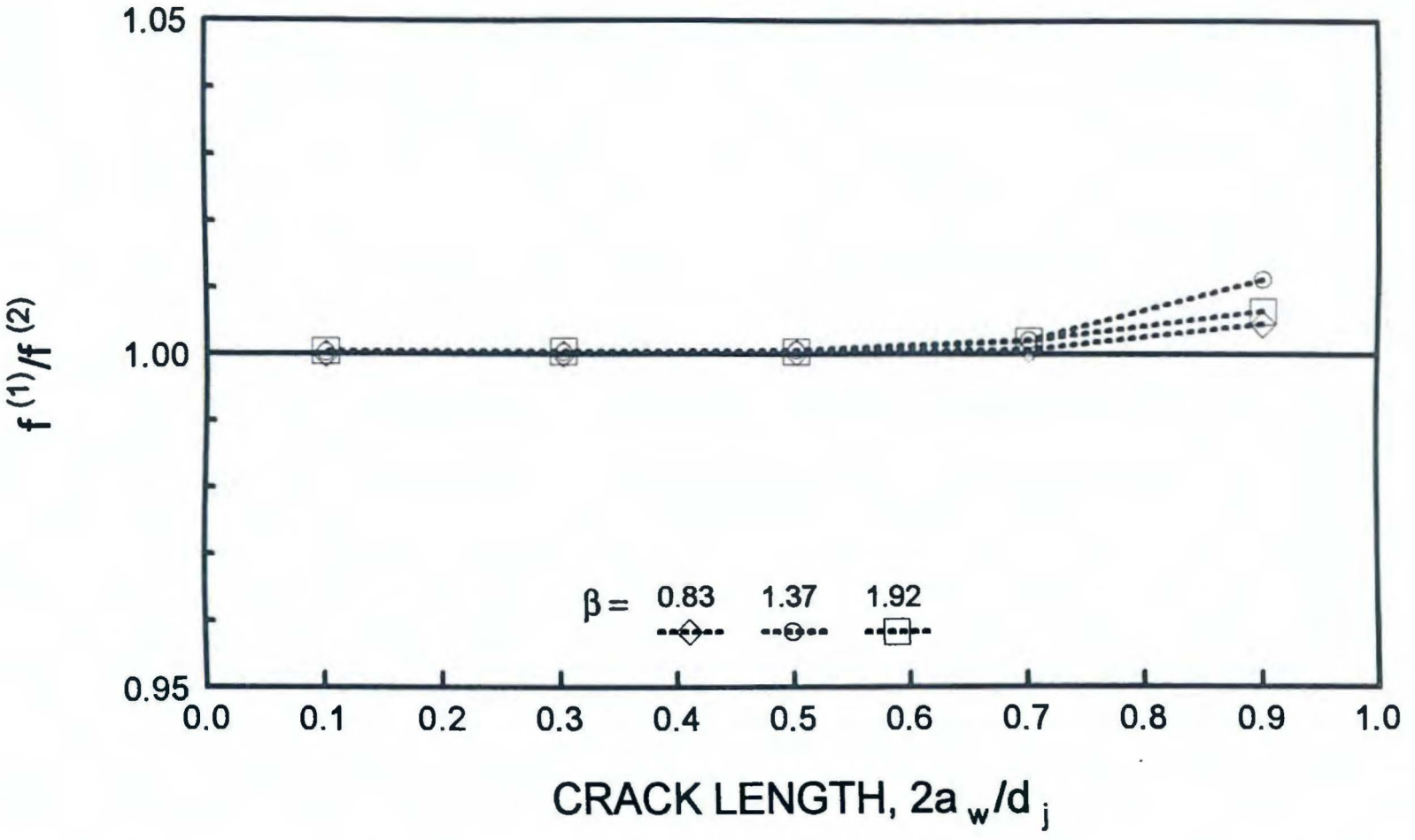

Figure 3.5. Effect of parameter β on correction factor for two-tip center-cracked I-beams under bending.

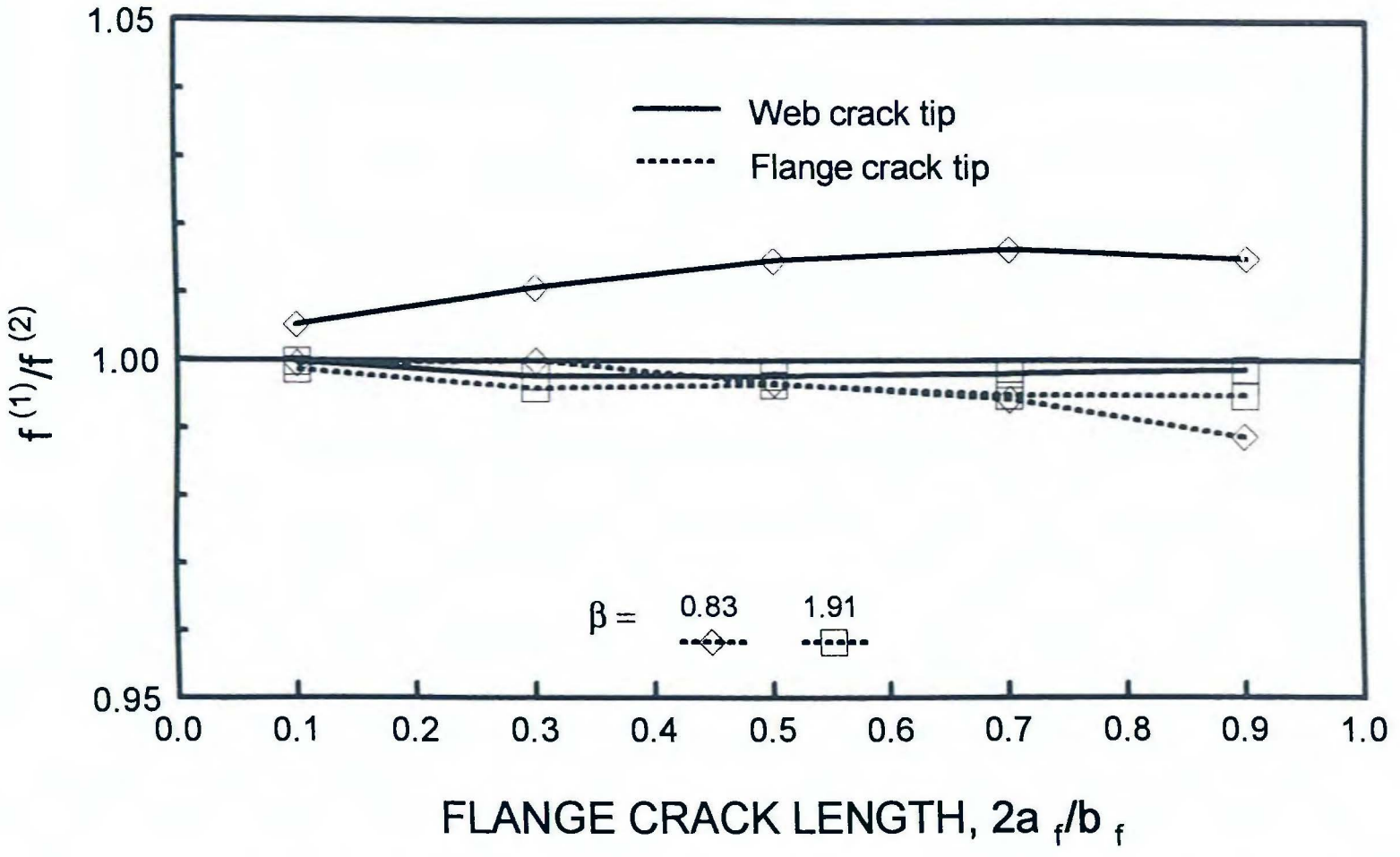

Figure 3.6. Effect of parameter β on correction factor for three-tip cracked I-beams under tension; $\lambda_w = 0.1$.

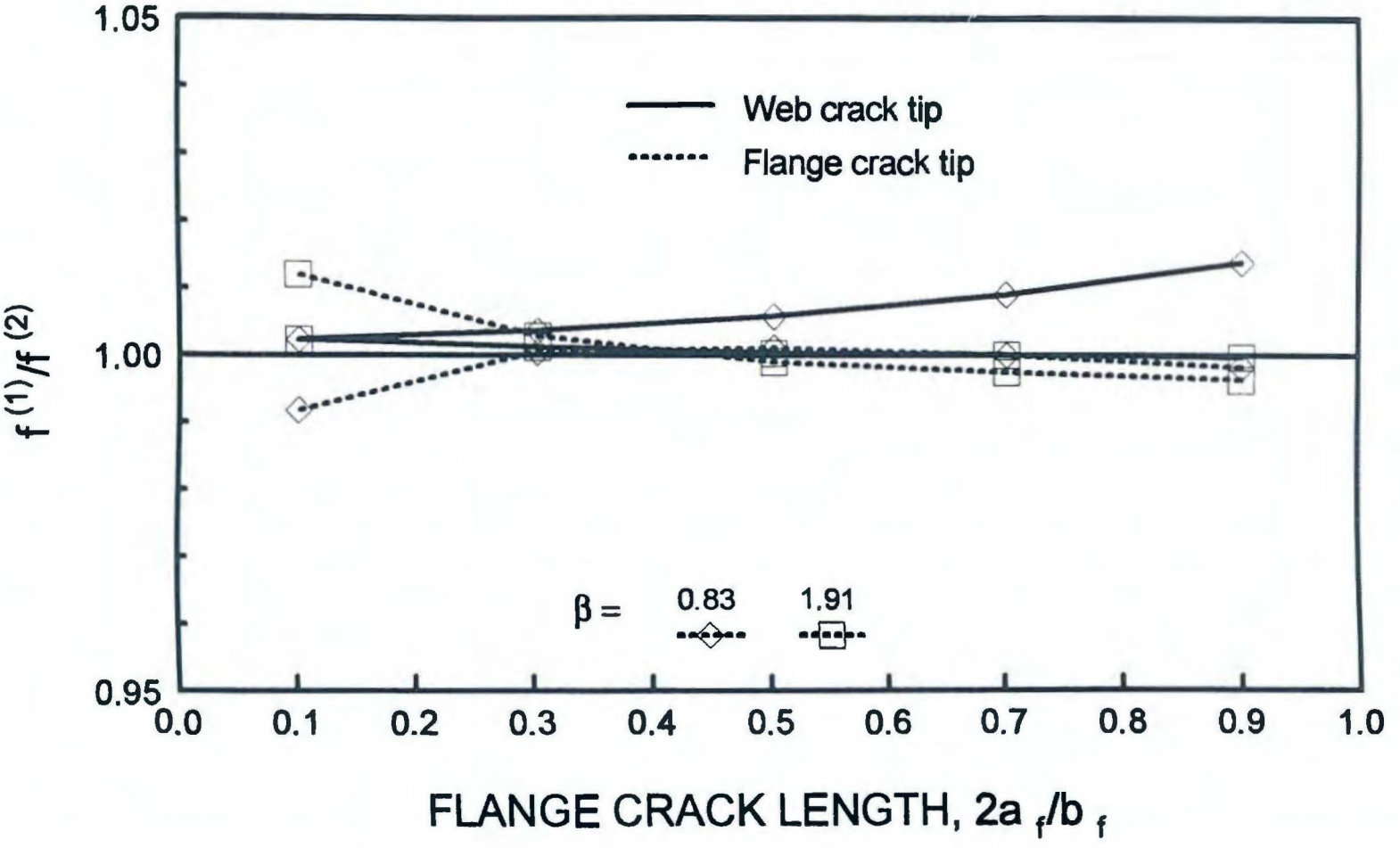

Figure 3.7. Effect of parameter β on correction factor for three-tip cracked I-beams under tension; $\lambda_w = 0.5$.

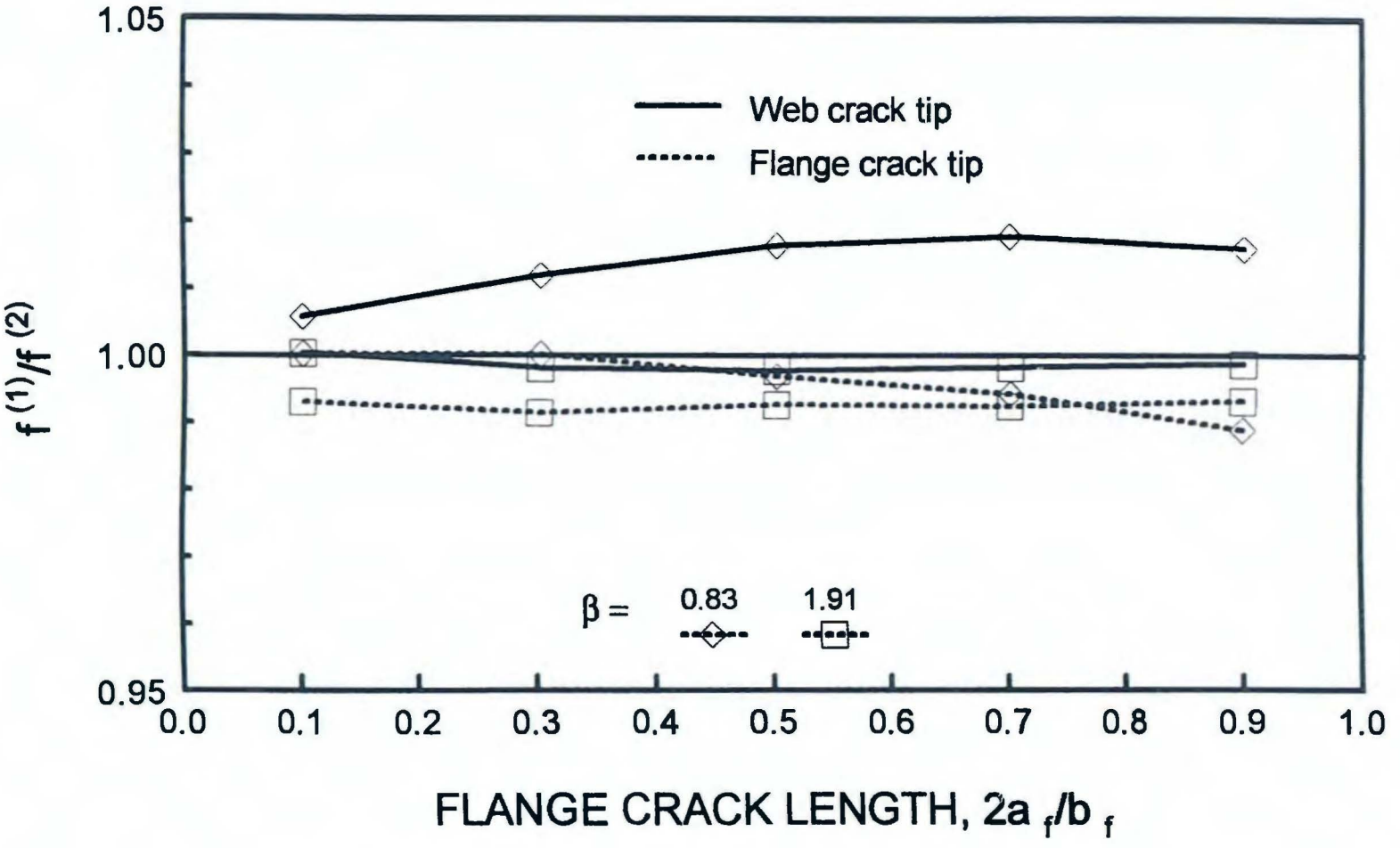

Figure 3.8. Effect of parameter β on correction factor for three-tip cracked I-beams under bending; $\lambda_w = 0.1$.

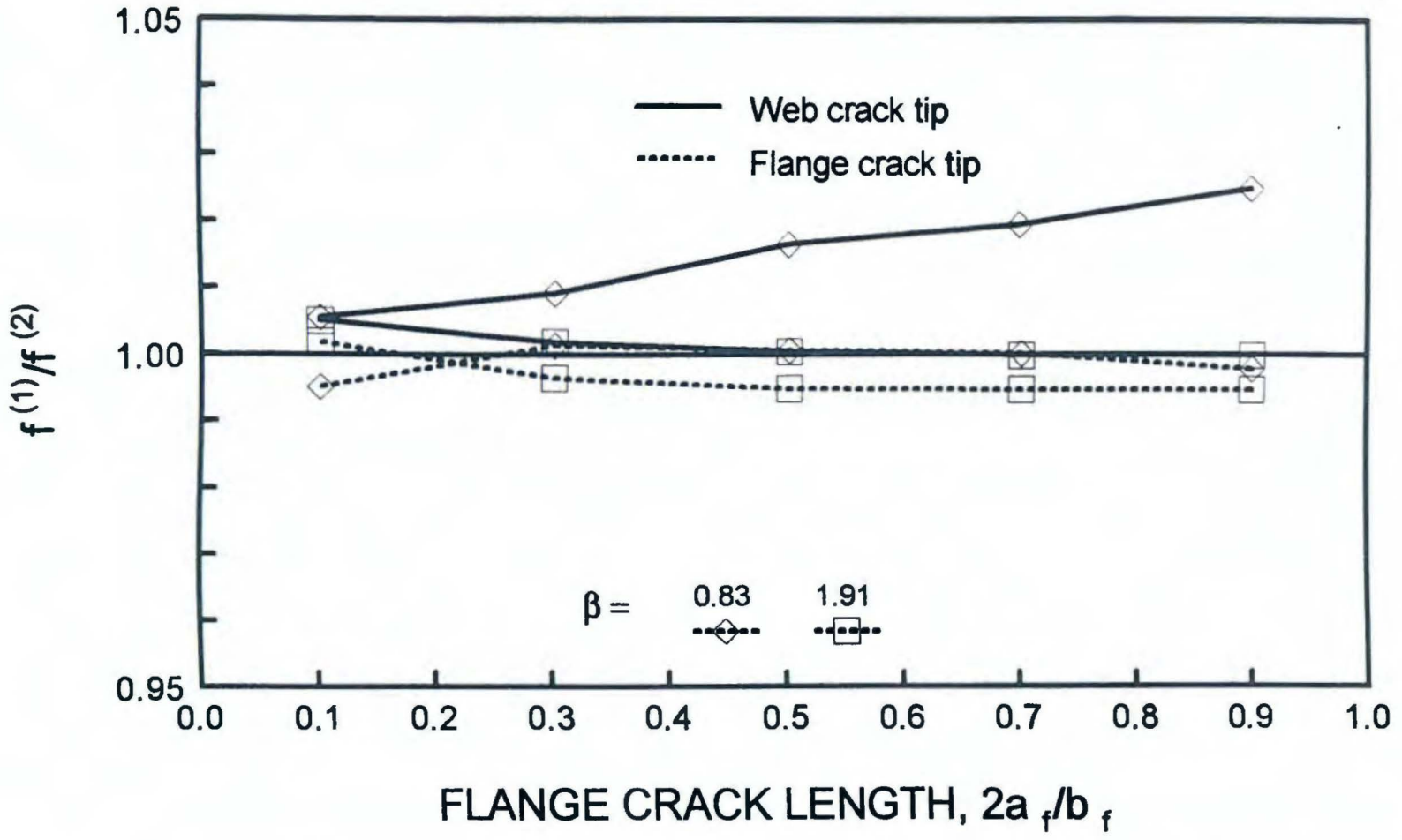

Figure 3.9. Effect of parameter β on correction factor for three-tip cracked I-beams under bending; $\lambda_w = 0.5$.

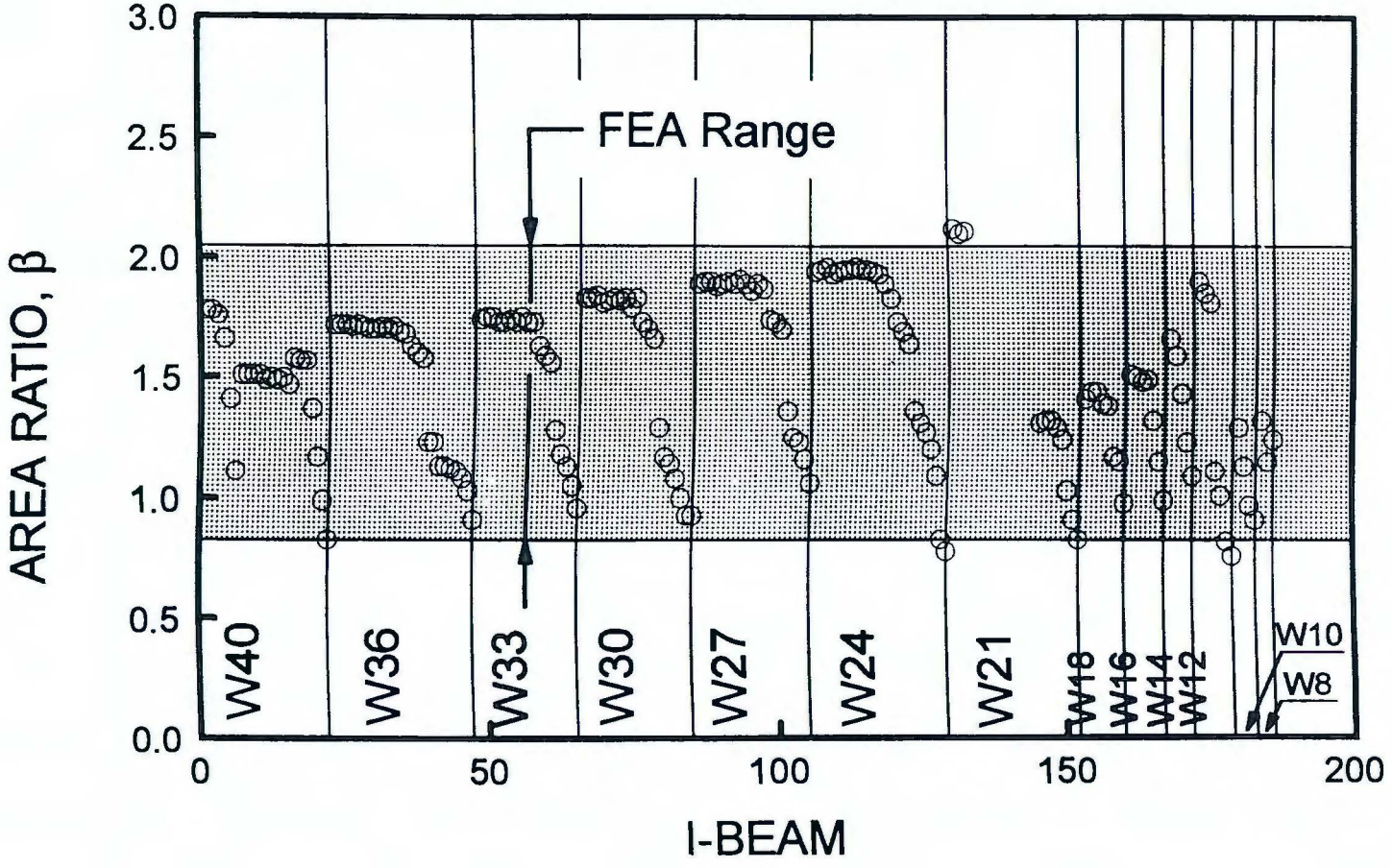

Figure 3.10. Range of parameter β in finite element analysis.

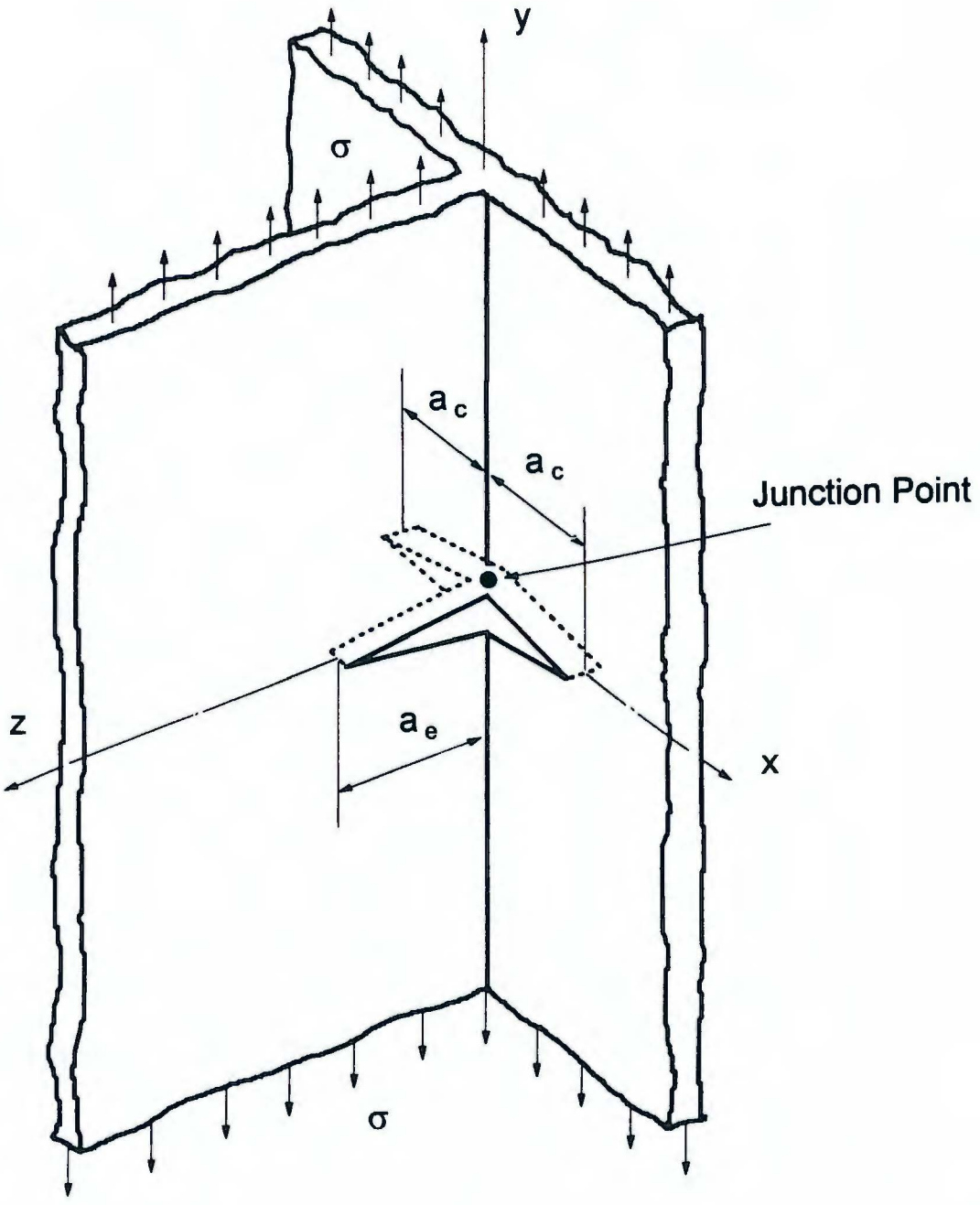

Figure 4.1. Center-cracked infinite plate joined with edge-cracked semi-infinite plate.

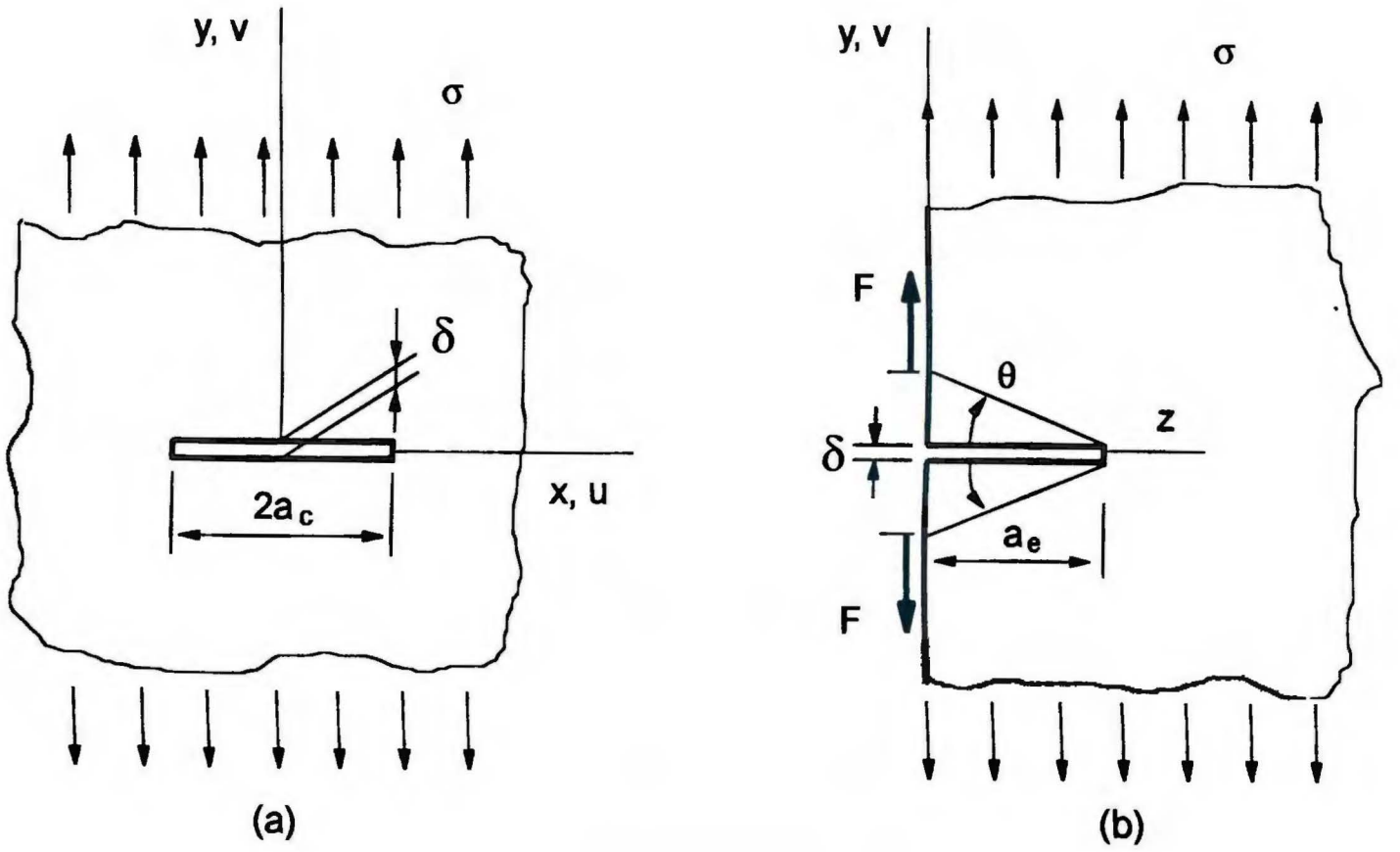

Figure 4.2. (a) Infinite plate with central crack under tension; (b) Semi-infinite plate with edge crack under tension.

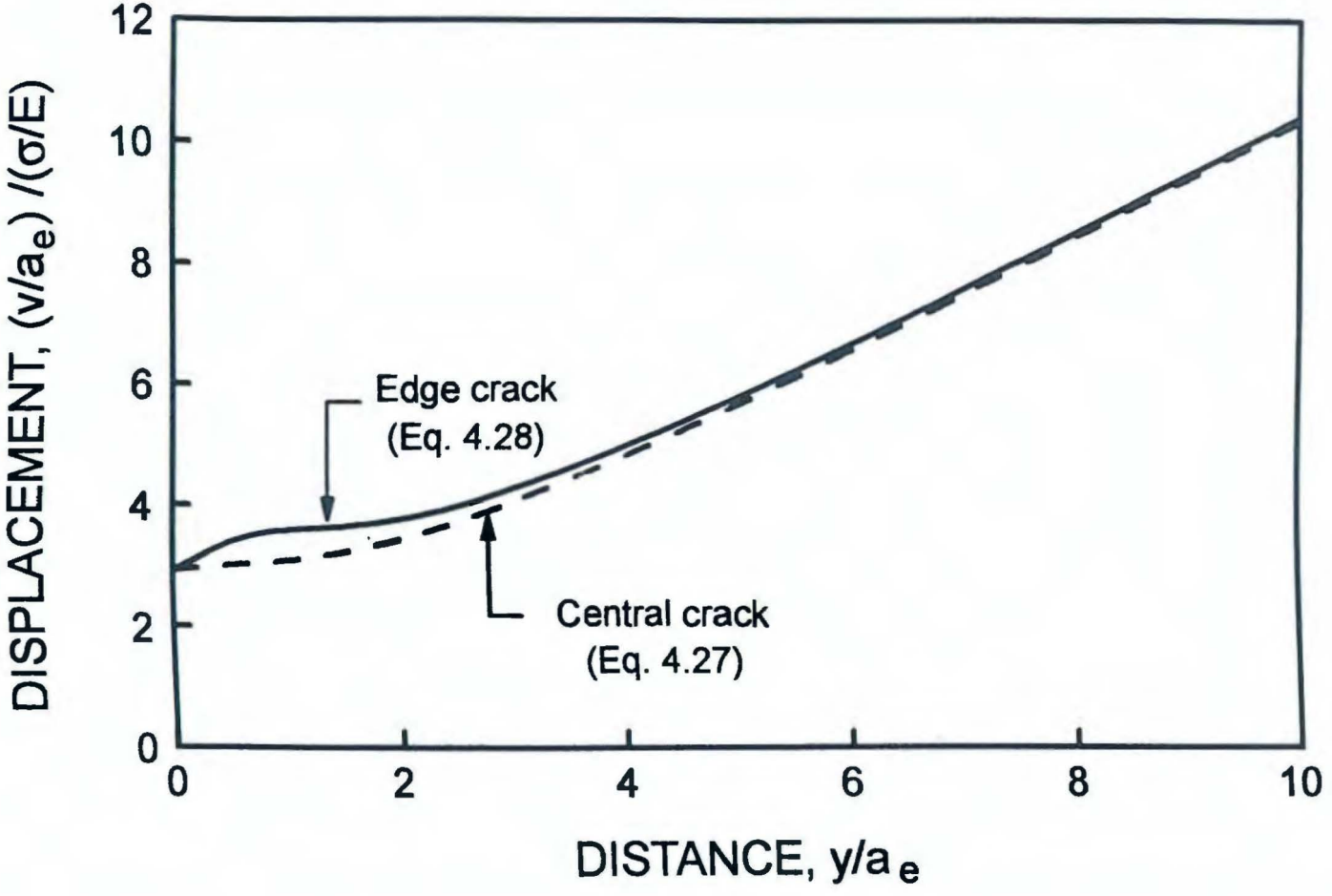

Figure 4.3. Displacements along junction line of center-cracked infinite plate and edge-cracked semi-infinite plate under tension.

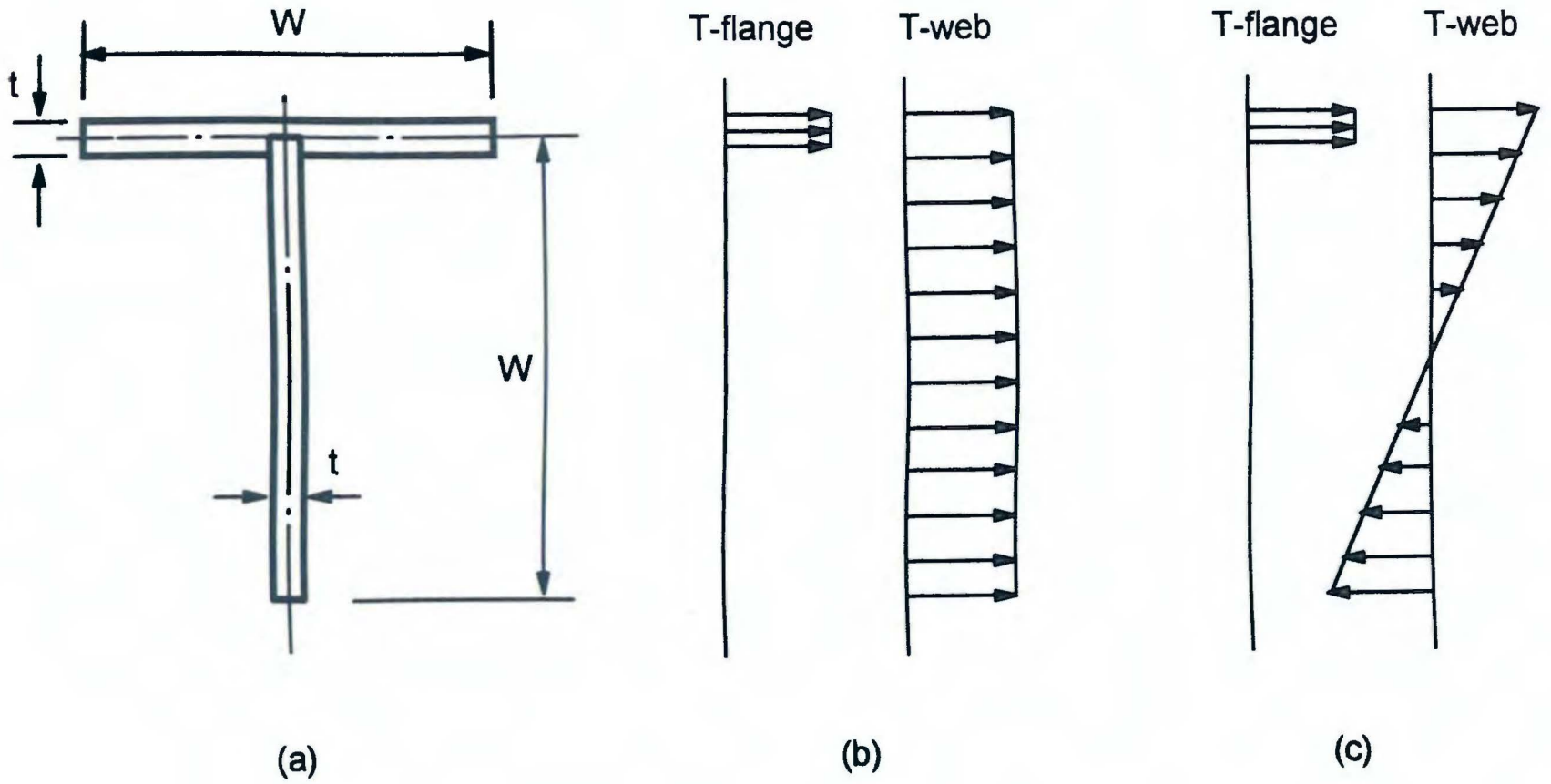

Figure 4.4. (a) Joined two finite plates; (b) T-flange and T-web under tension; (c) T-flange under tension and T-web under bending.

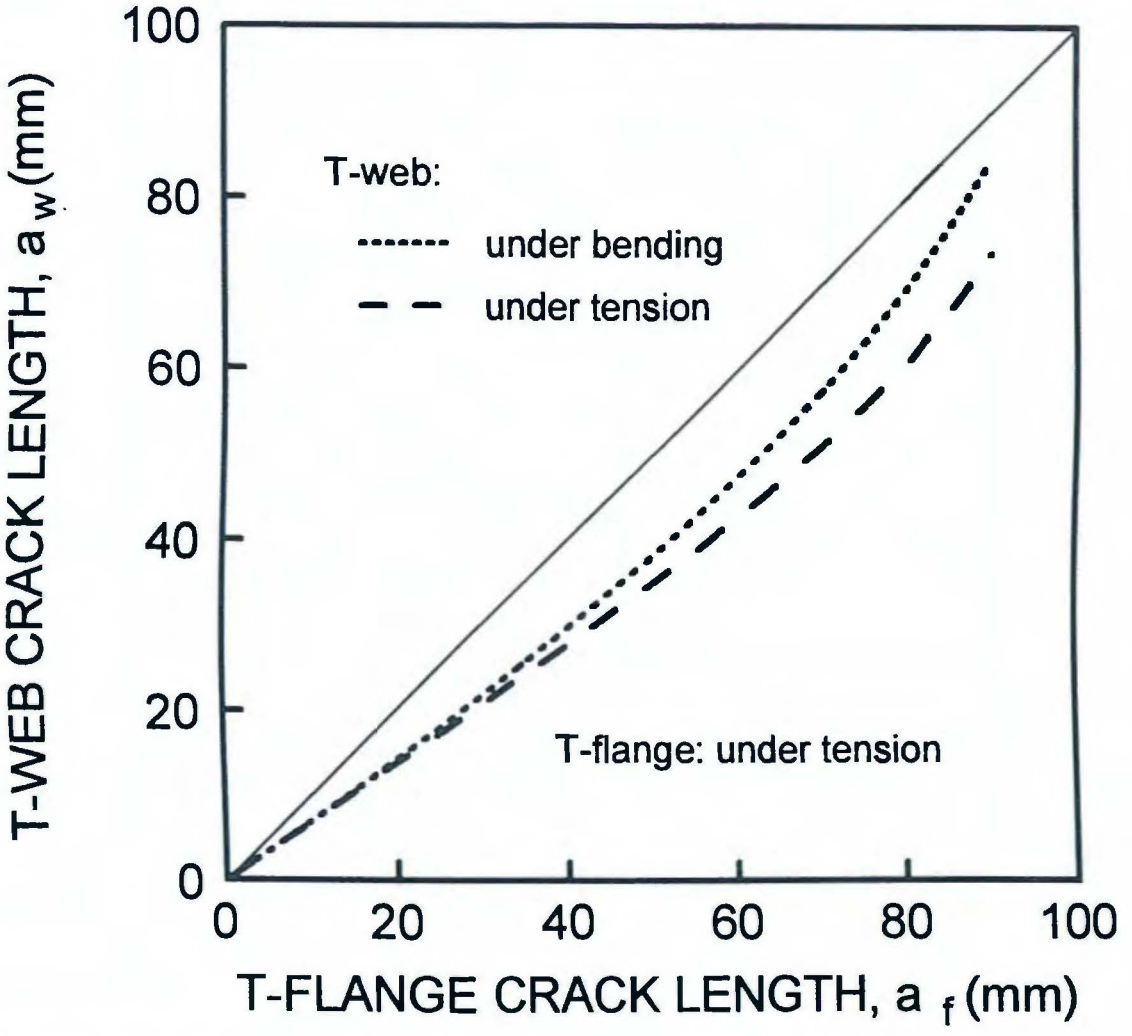

Figure 4.5. Relationship between non-interacting T-flange and T-web crack lengths.

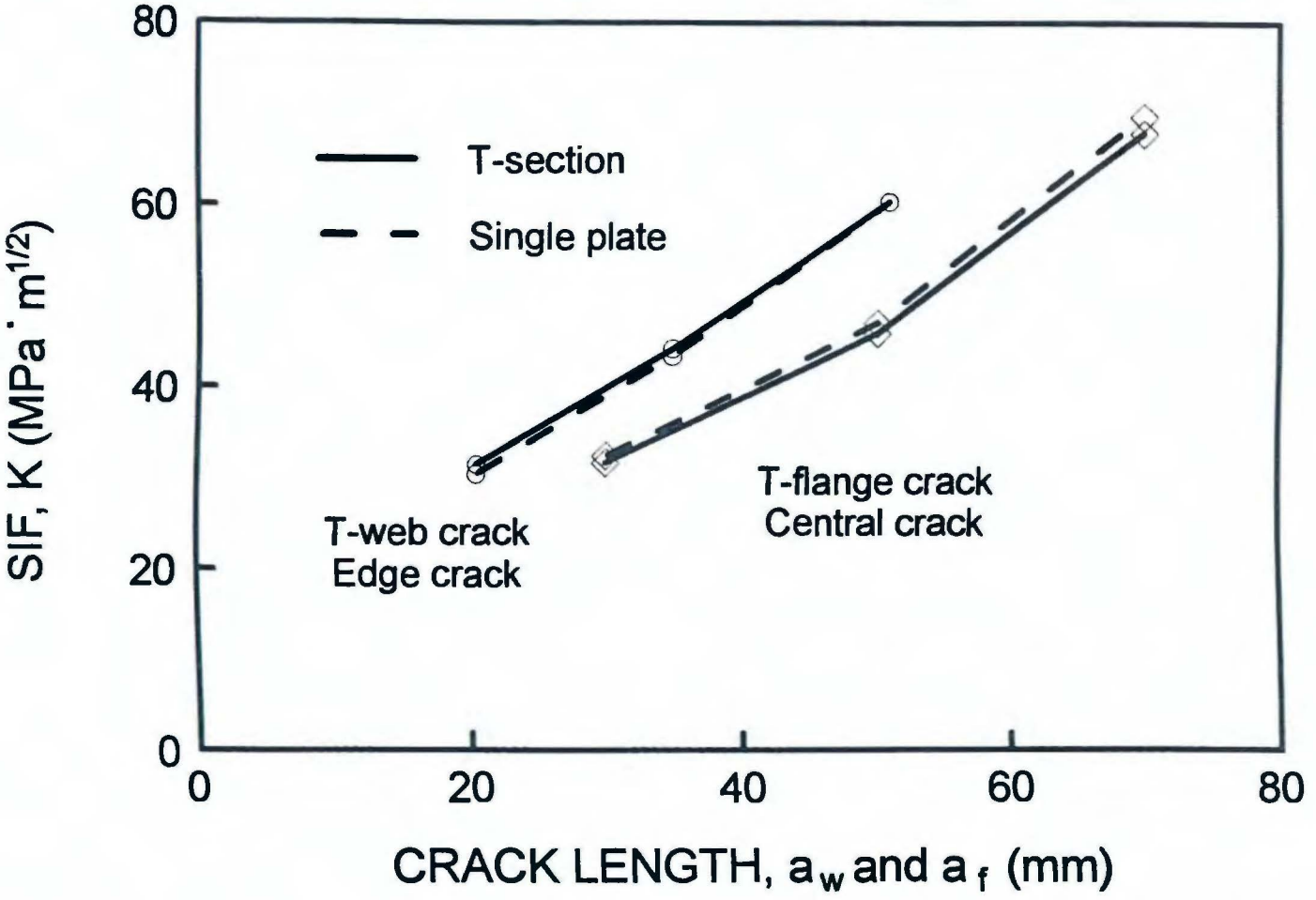

Figure 4.6. Comparison of SIFs for non-interacting T-section and single plates under tension.

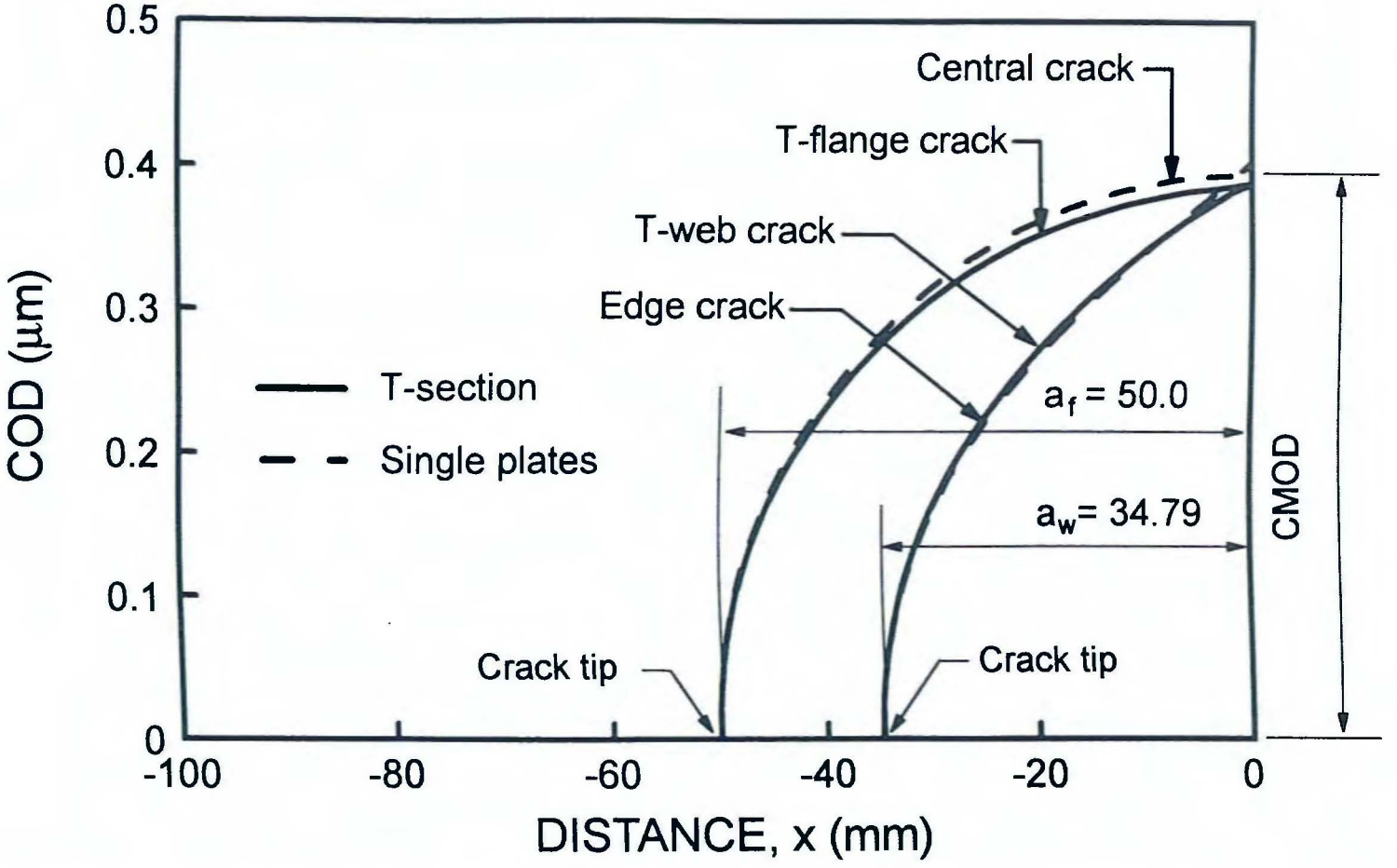

Figure 4.7. Comparison of CODs for non-interacting T-section and single plates under tension.

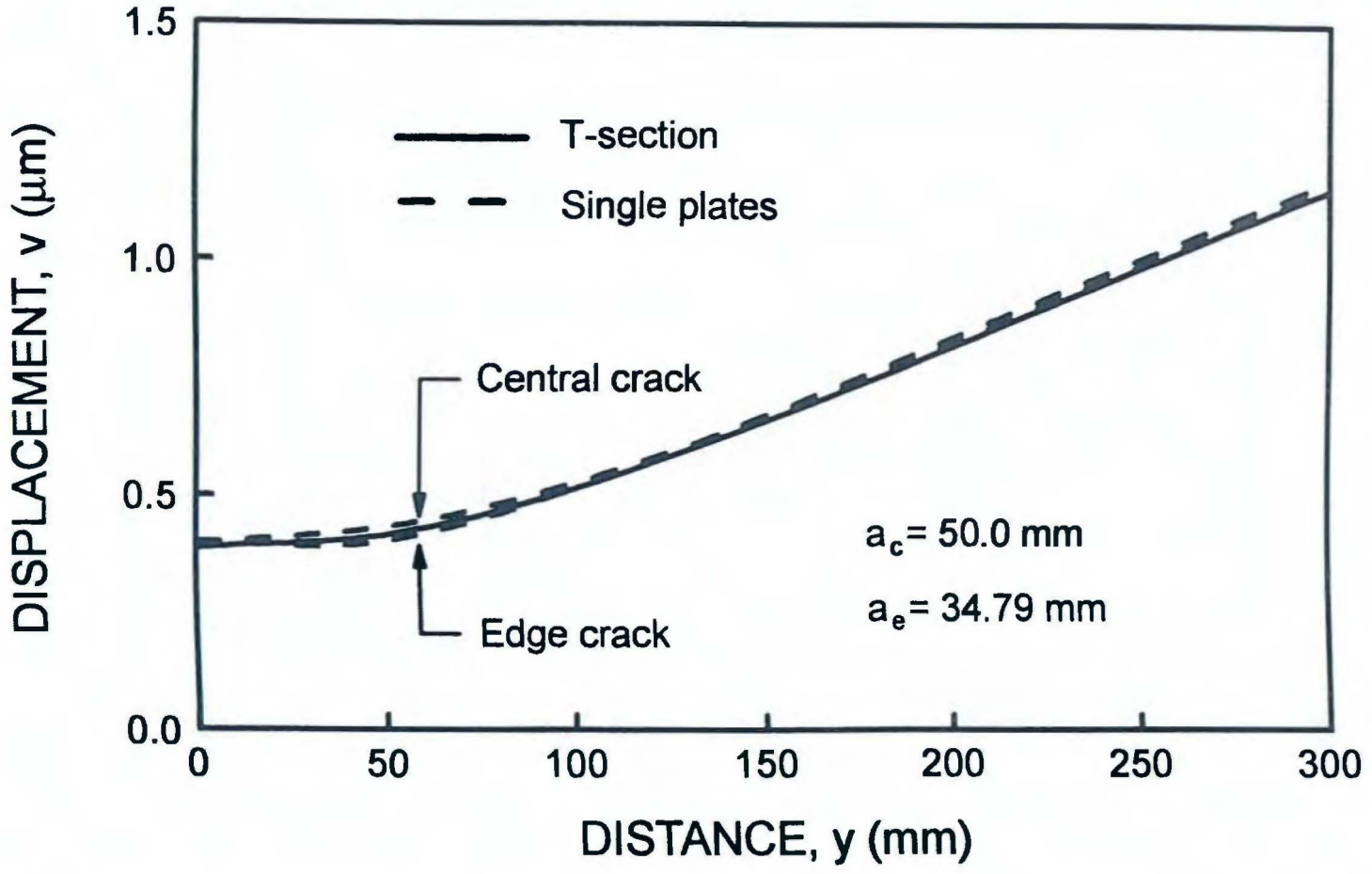

Figure 4.8. Comparison of displacements along junction line of non-interacting T-section and single plates under tension.

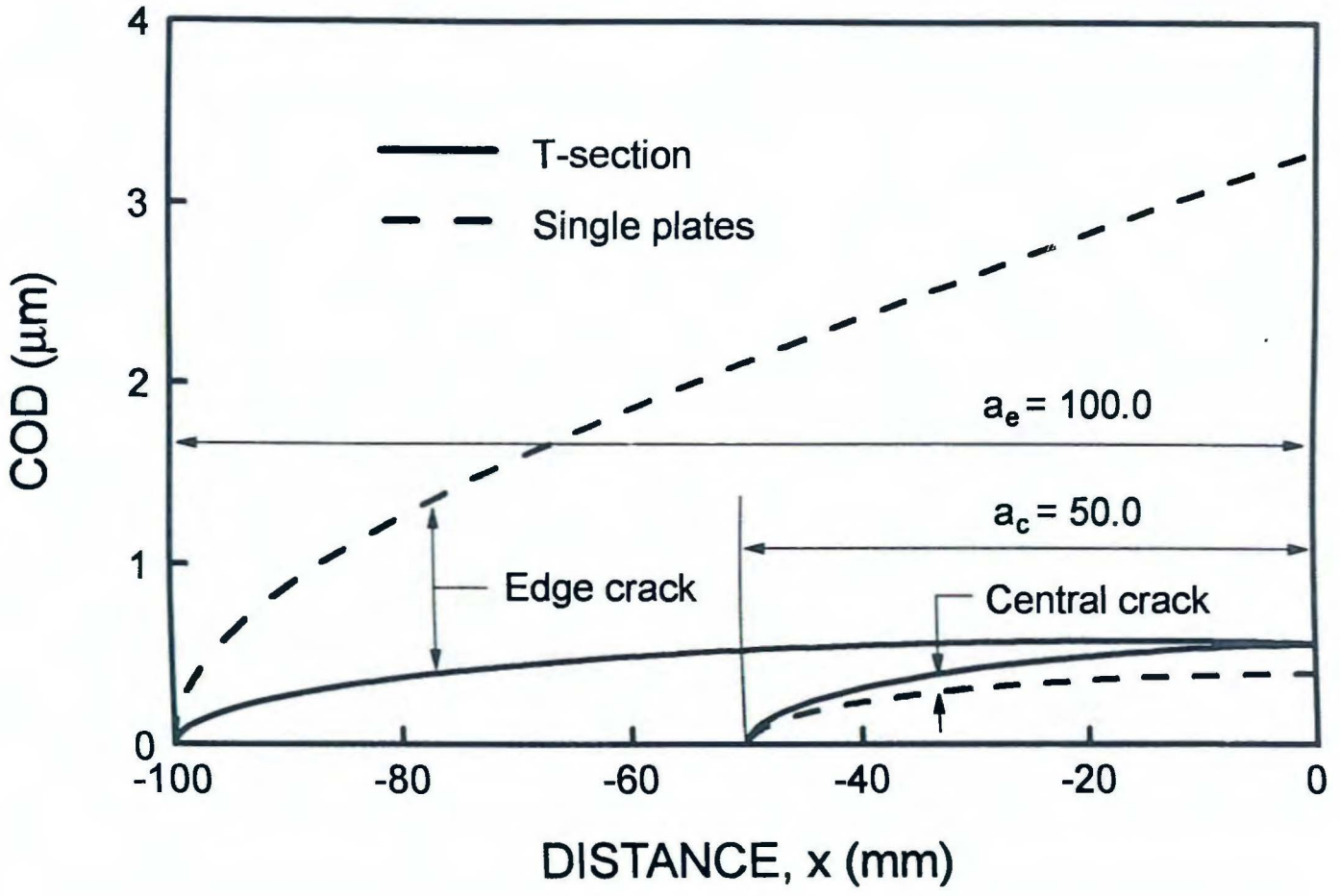

Figure 4.9. Comparison of CODs for T-section and single plates under tension.

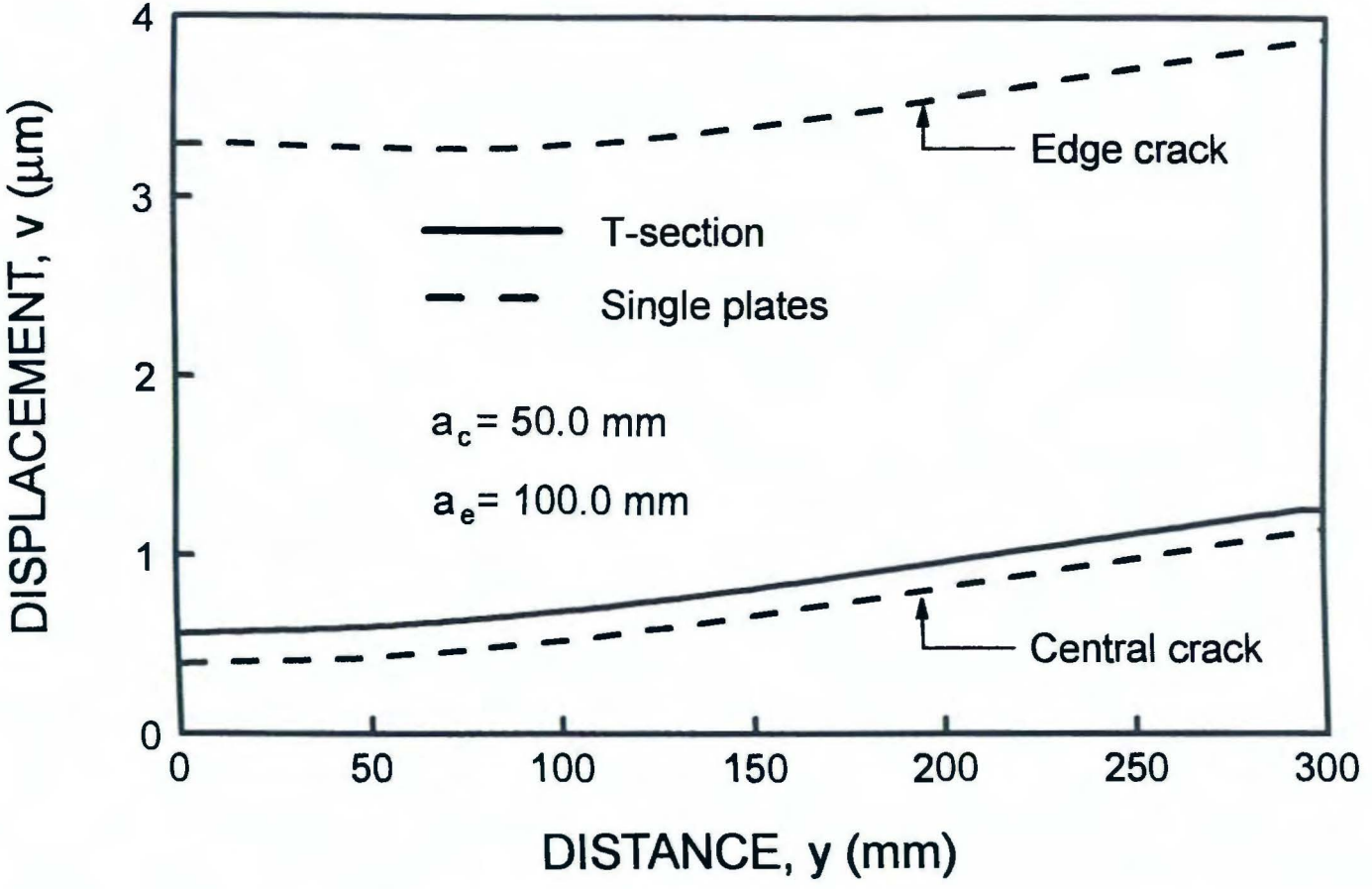

Figure 4.10. Comparison of displacements along junction line of T-section and single plates under tension.

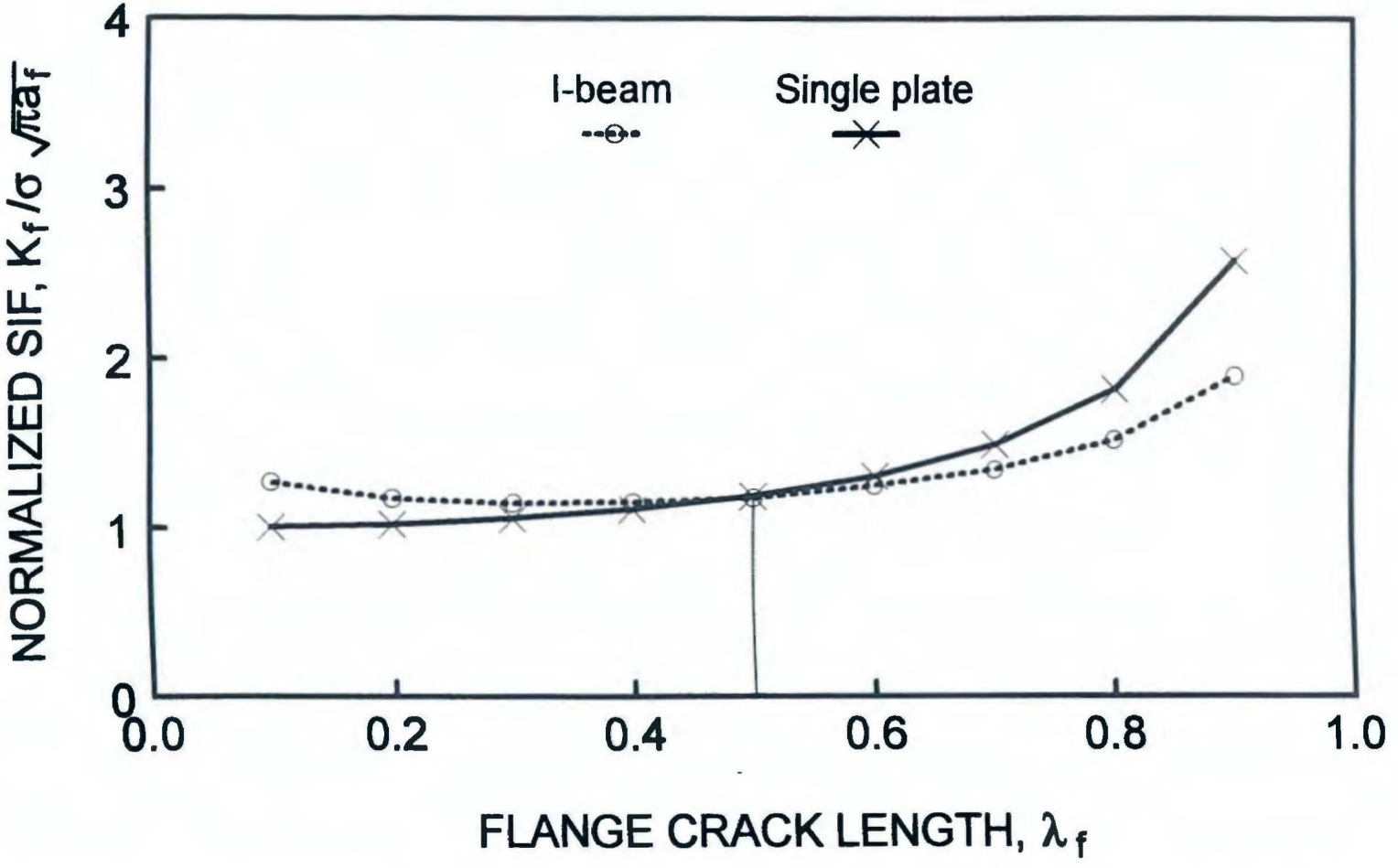

Figure 4.11. Non-interacting flange crack length determined by equating K_f; W33 x 201, $\lambda_w = 0.1$, under tension.

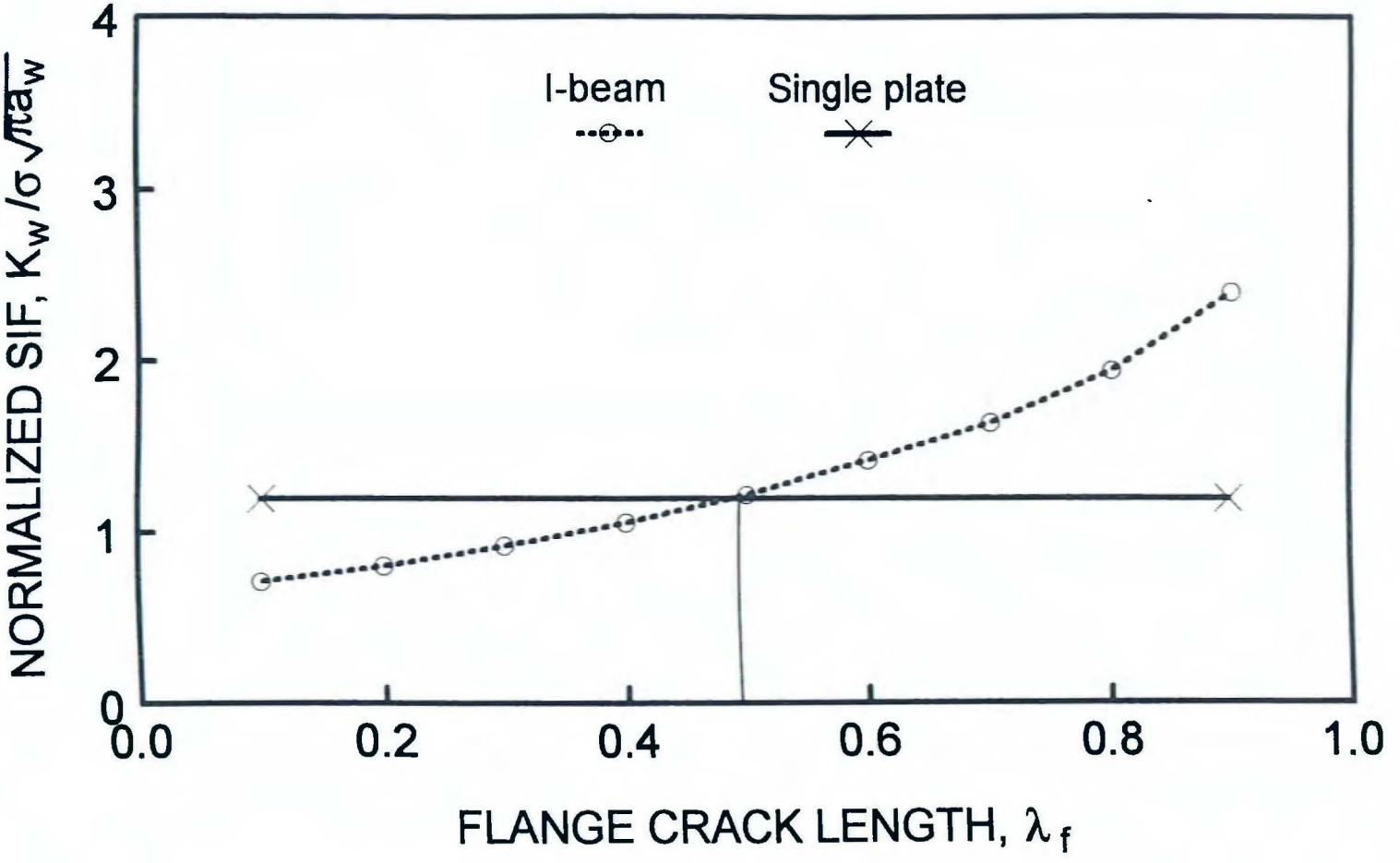

Figure 4.12. No-interacting flange crack length determined by equating K_w; W33 x 201, λ_w= 0.1, under tension.

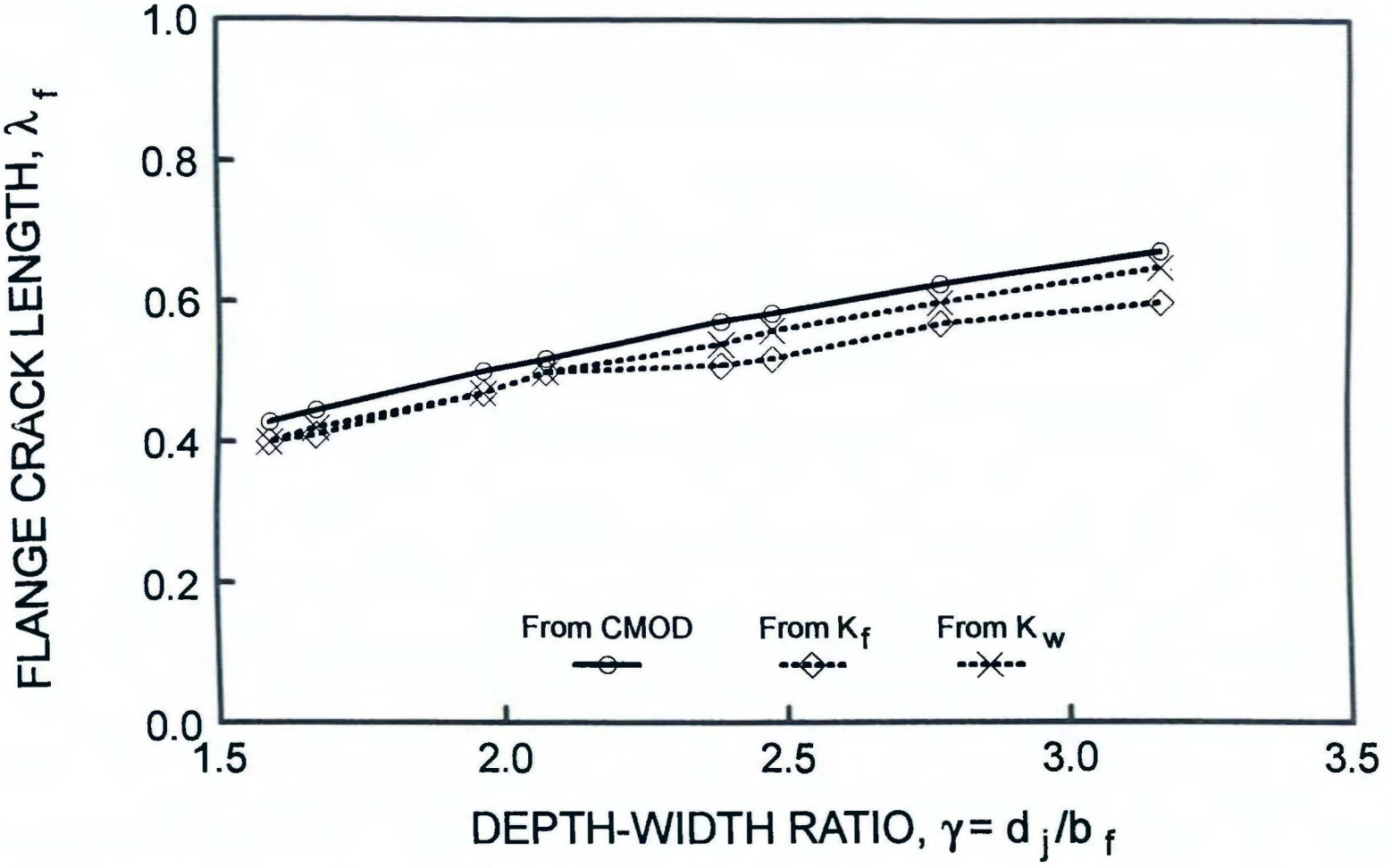

Figure 4.13. Comparison of non-interacting flange crack lengths determined from CMOD and SIFs; $\lambda_w = 0.1$, under tension.

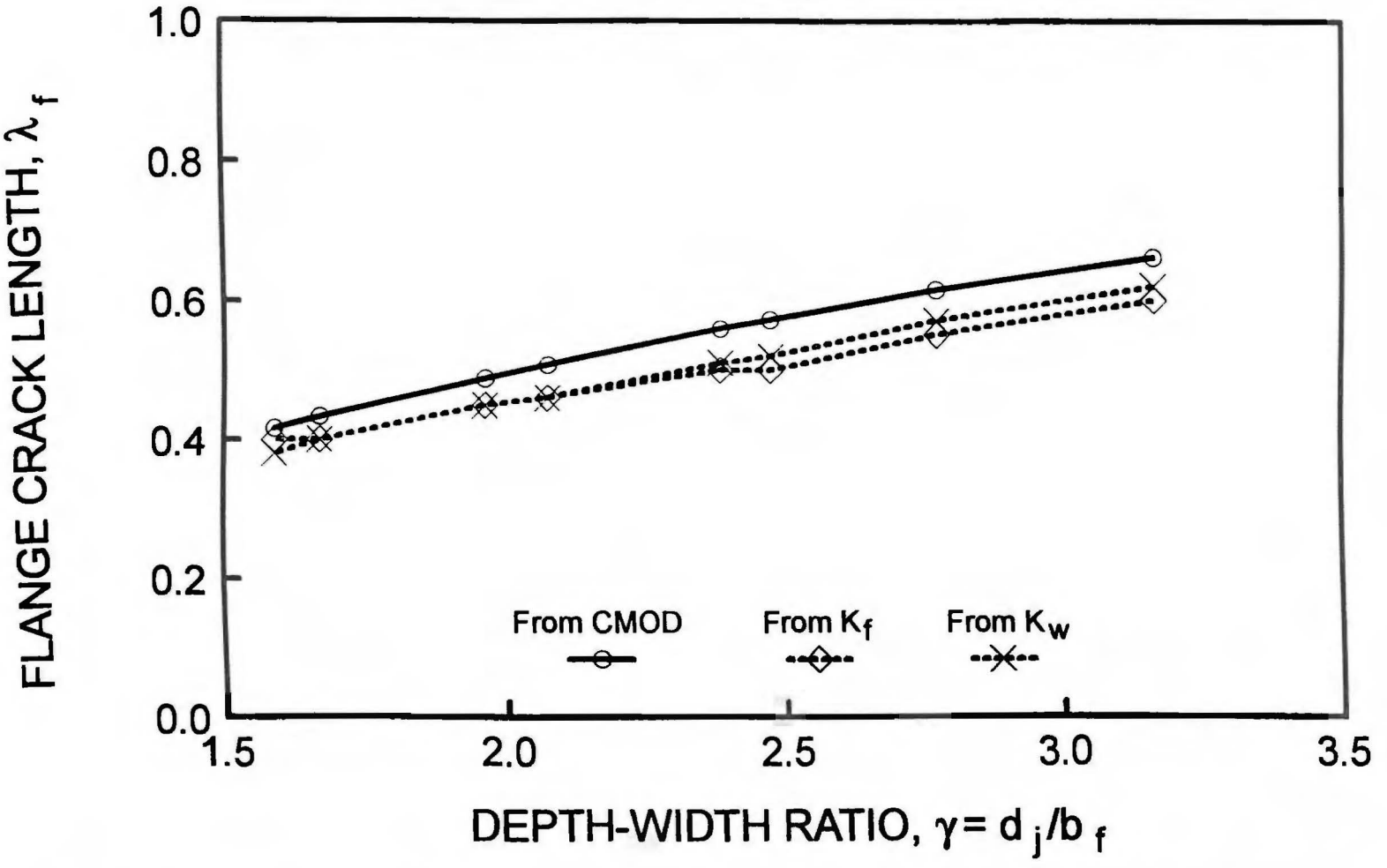

Figure 4.14. Comparison of non-interacting flange crack lengths determined from CMOD and SIFs; $\lambda_w = 0.1$, under bending.

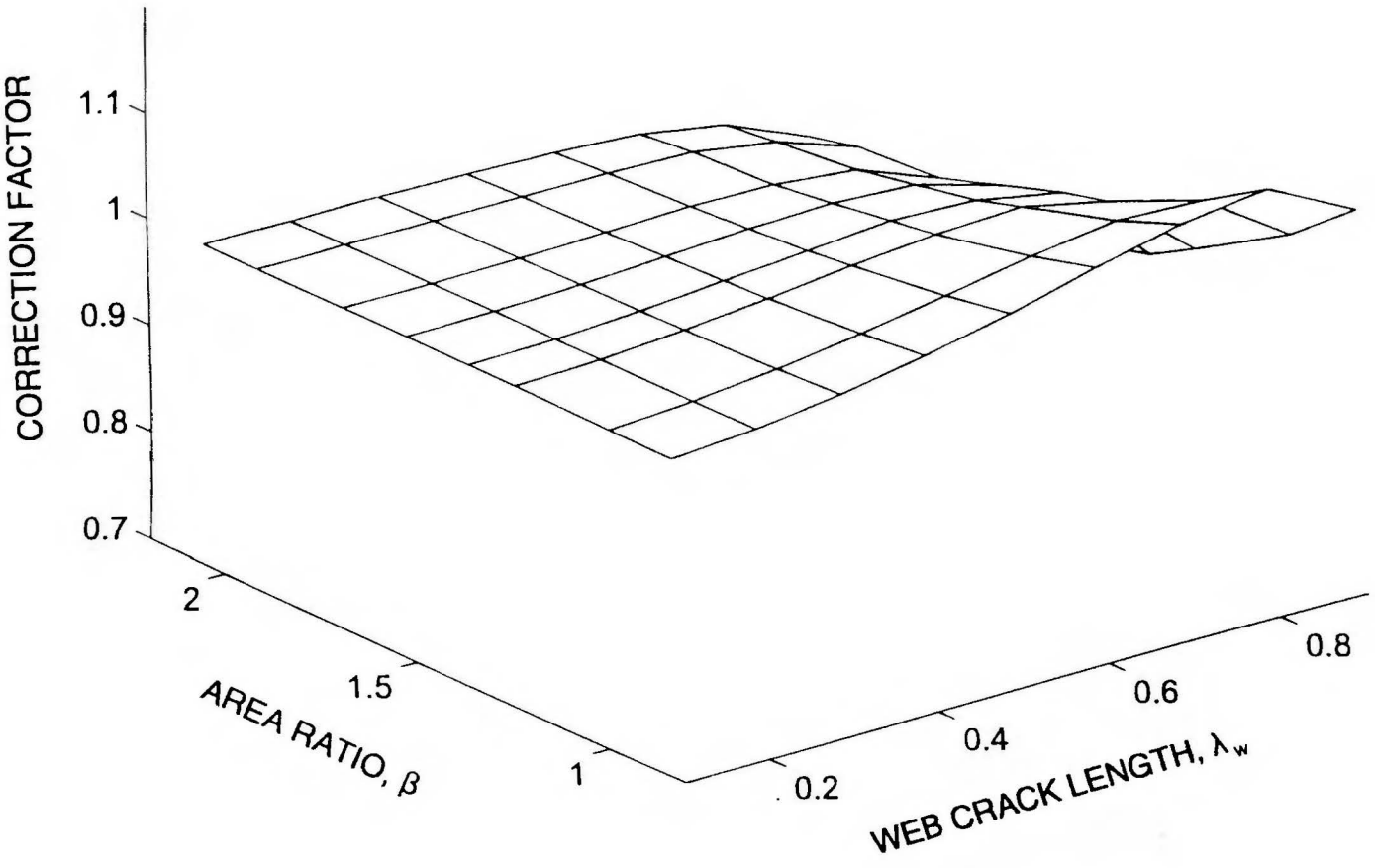

Figure 5.1. Correction factor for two-tip cracked I-beam under tension; central crack.

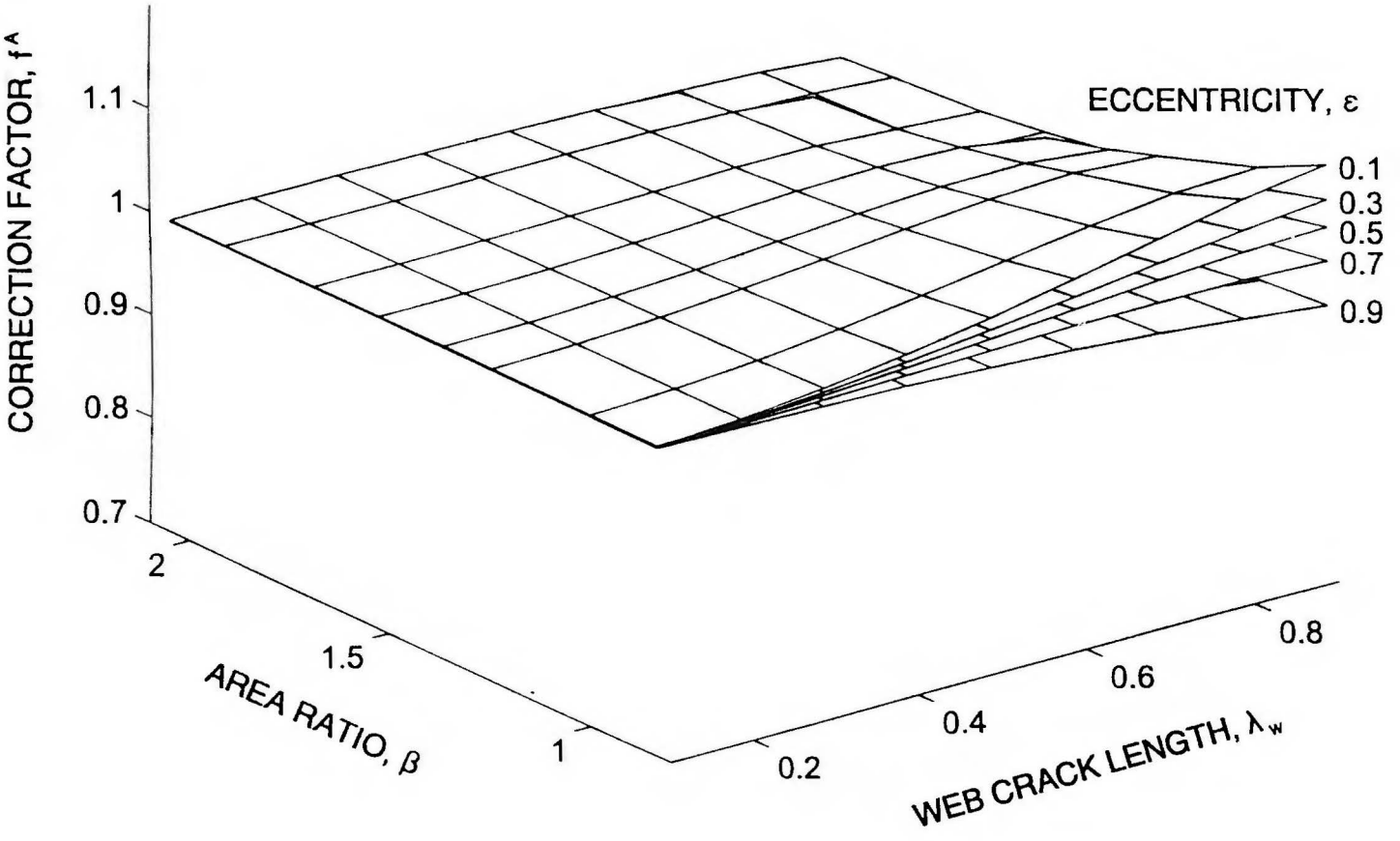

Figure 5.2. Correction factor for two-tip cracked I-beam under tension; eccentric crack, upper tip.

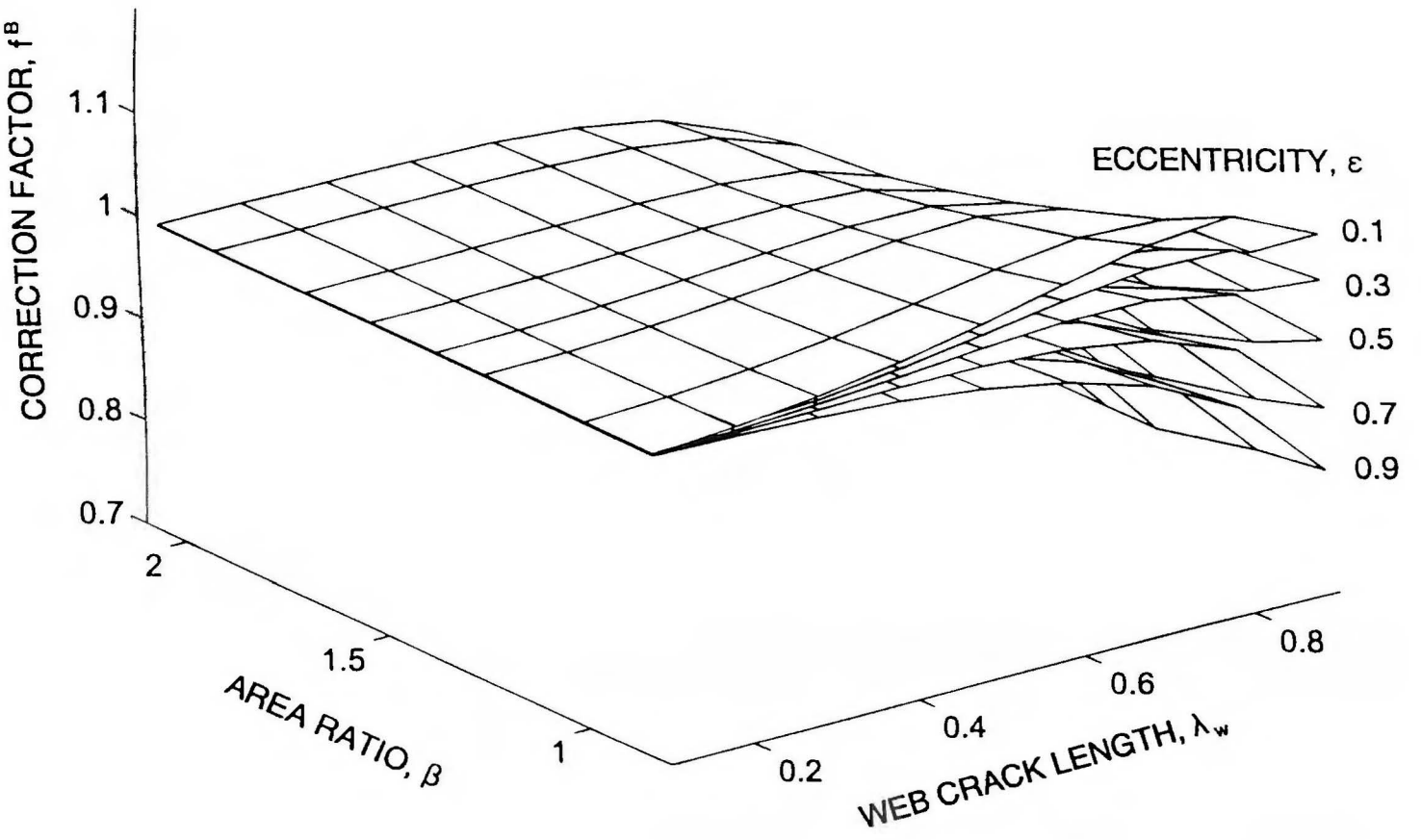

Figure 5.3. Correction factor for two-tip cracked I-beam under tension; eccentric crack, lower tip.

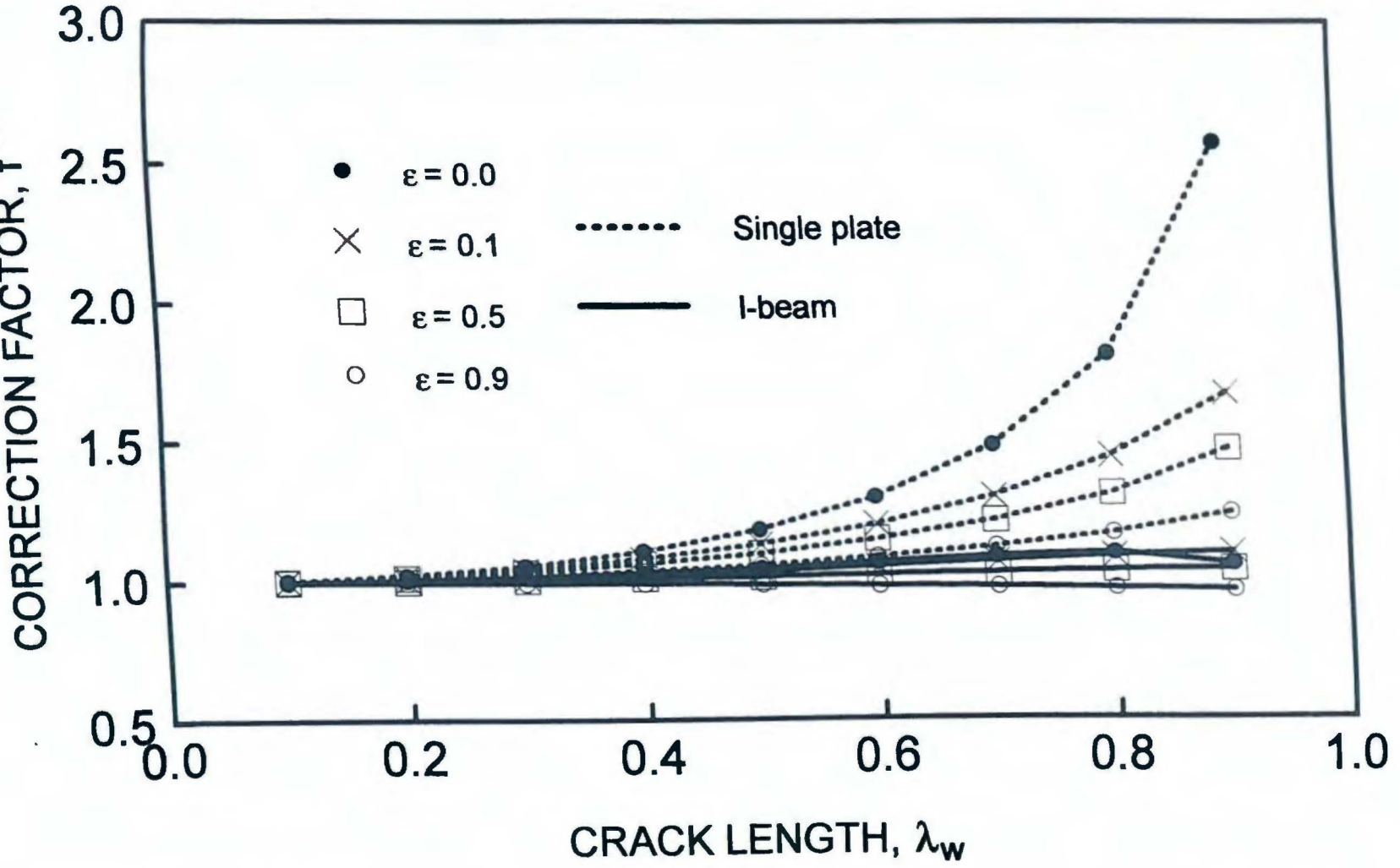

Figure 5.4. Comparison of I-beam and single plate under tension; upper tip, $\beta = 0.83$.

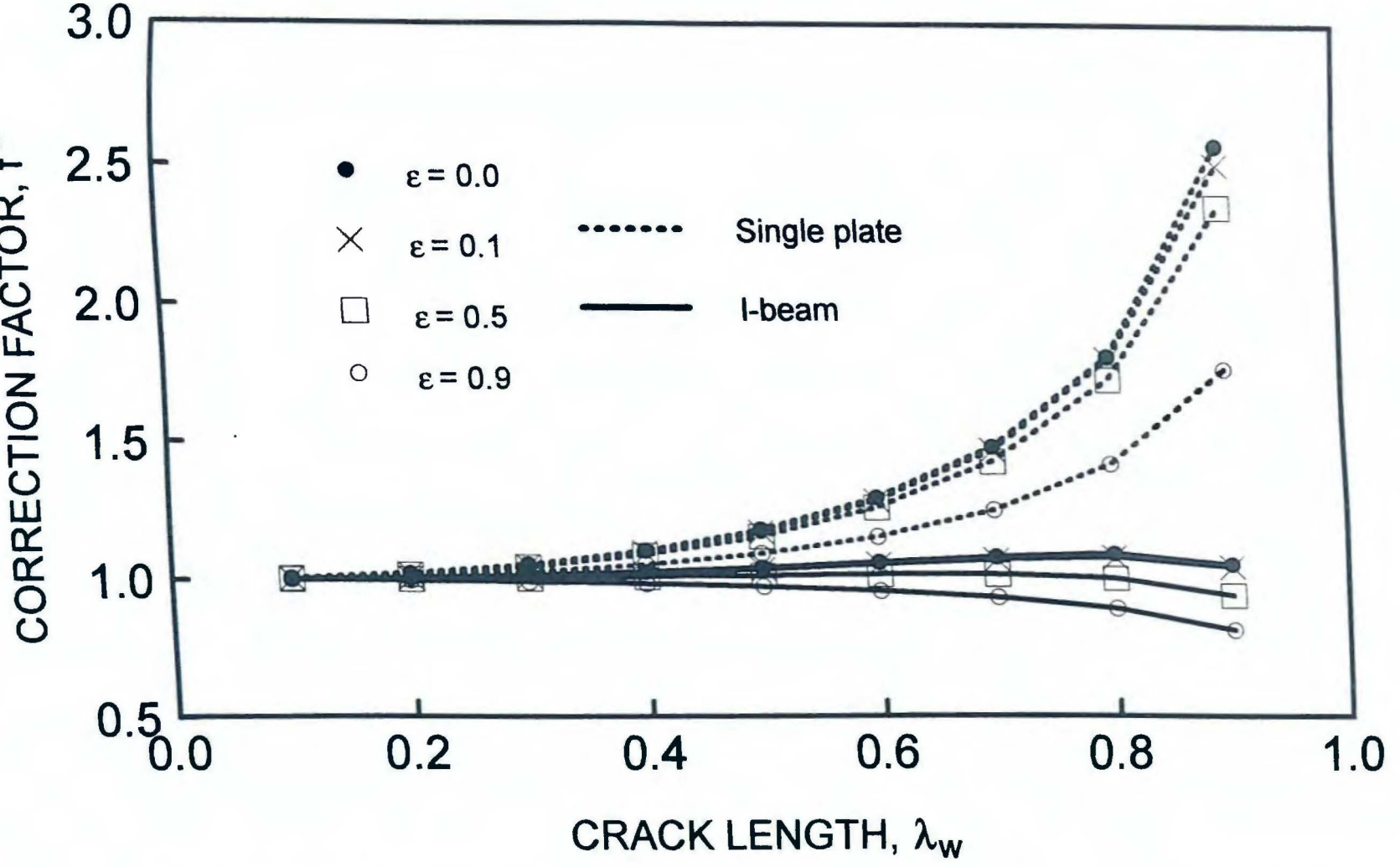

Figure 5.5. Comparison of I-beam and single plate under tension; lower tip, $\beta = 0.83$.

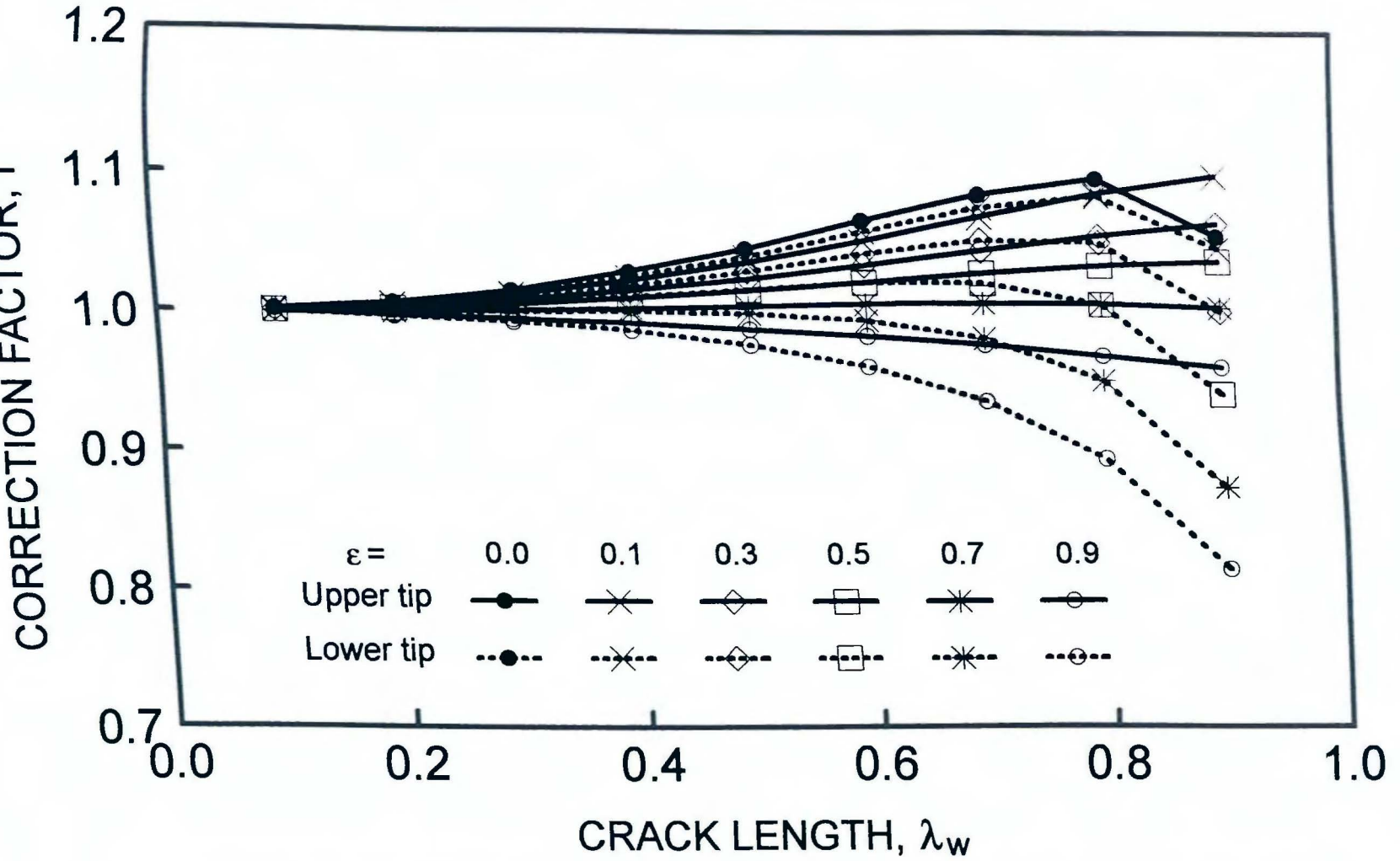

Figure 5.6. Correction factors for two-tip cracked I-beam under tension; $\beta = 0.83$.

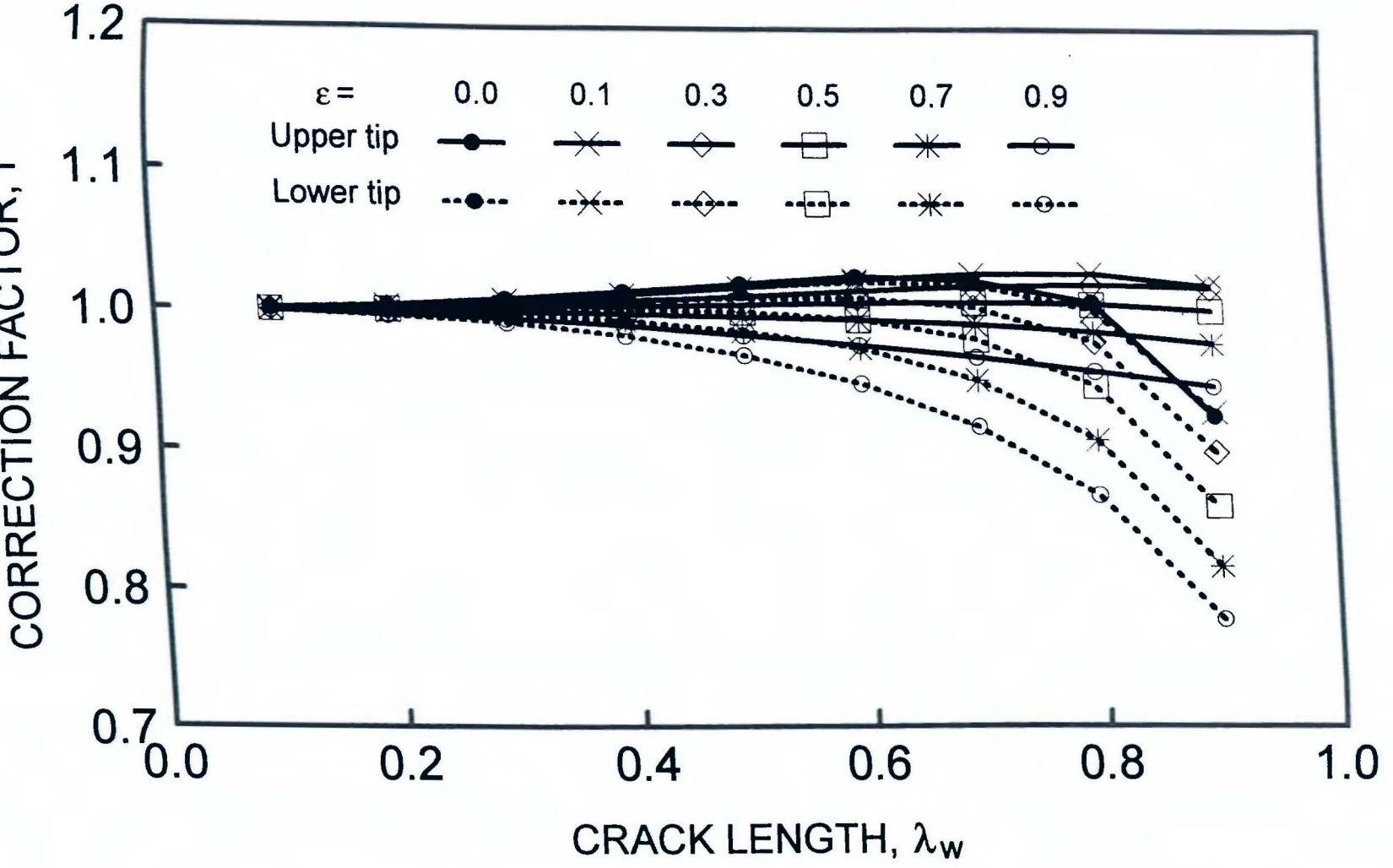

Figure 5.7. Correction factors for two-tip cracked I-beam under tension; $\beta = 1.37$.

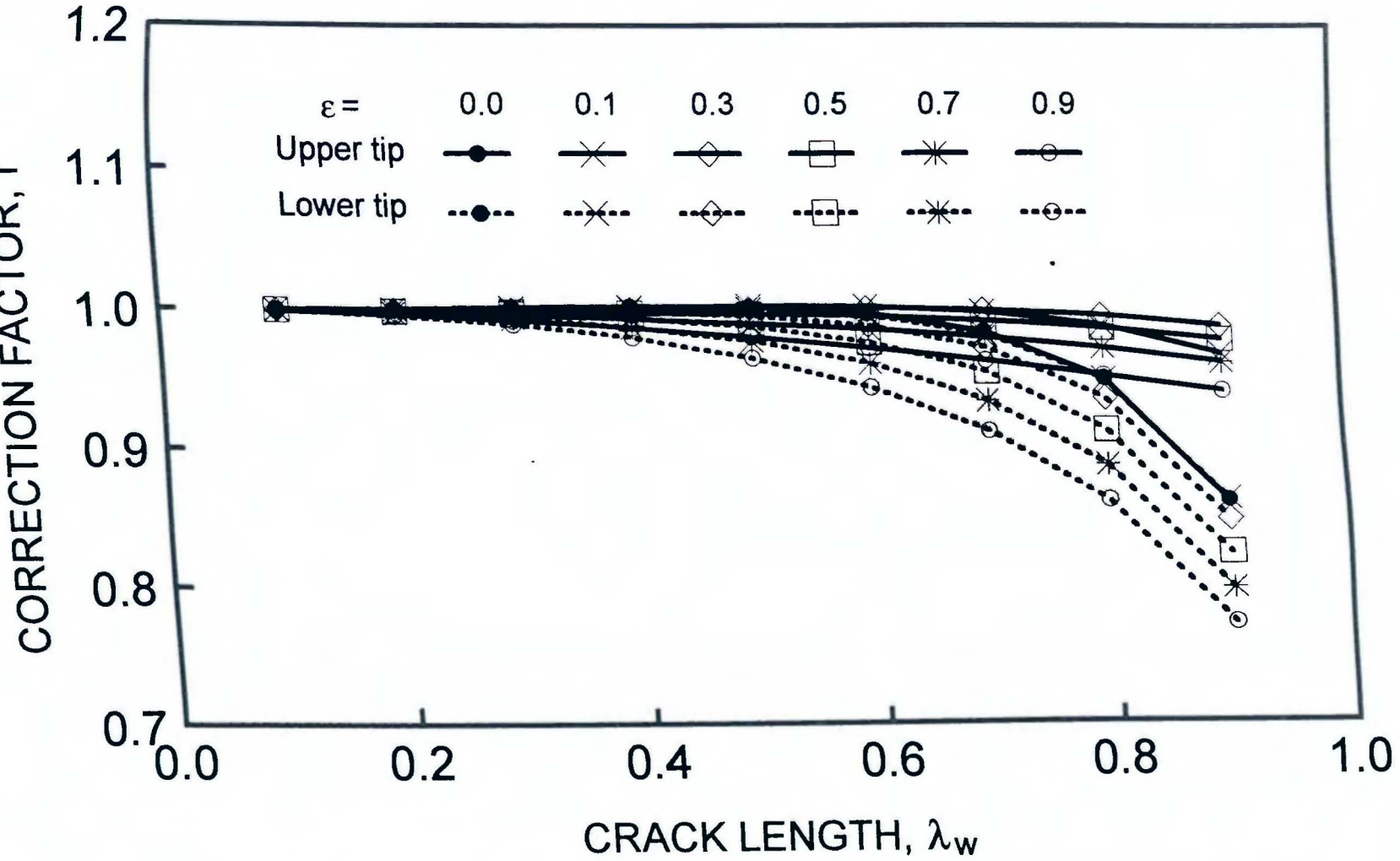

Figure 5.8. Correction factors for two-tip cracked I-beam under tension; $\beta = 2.05$.

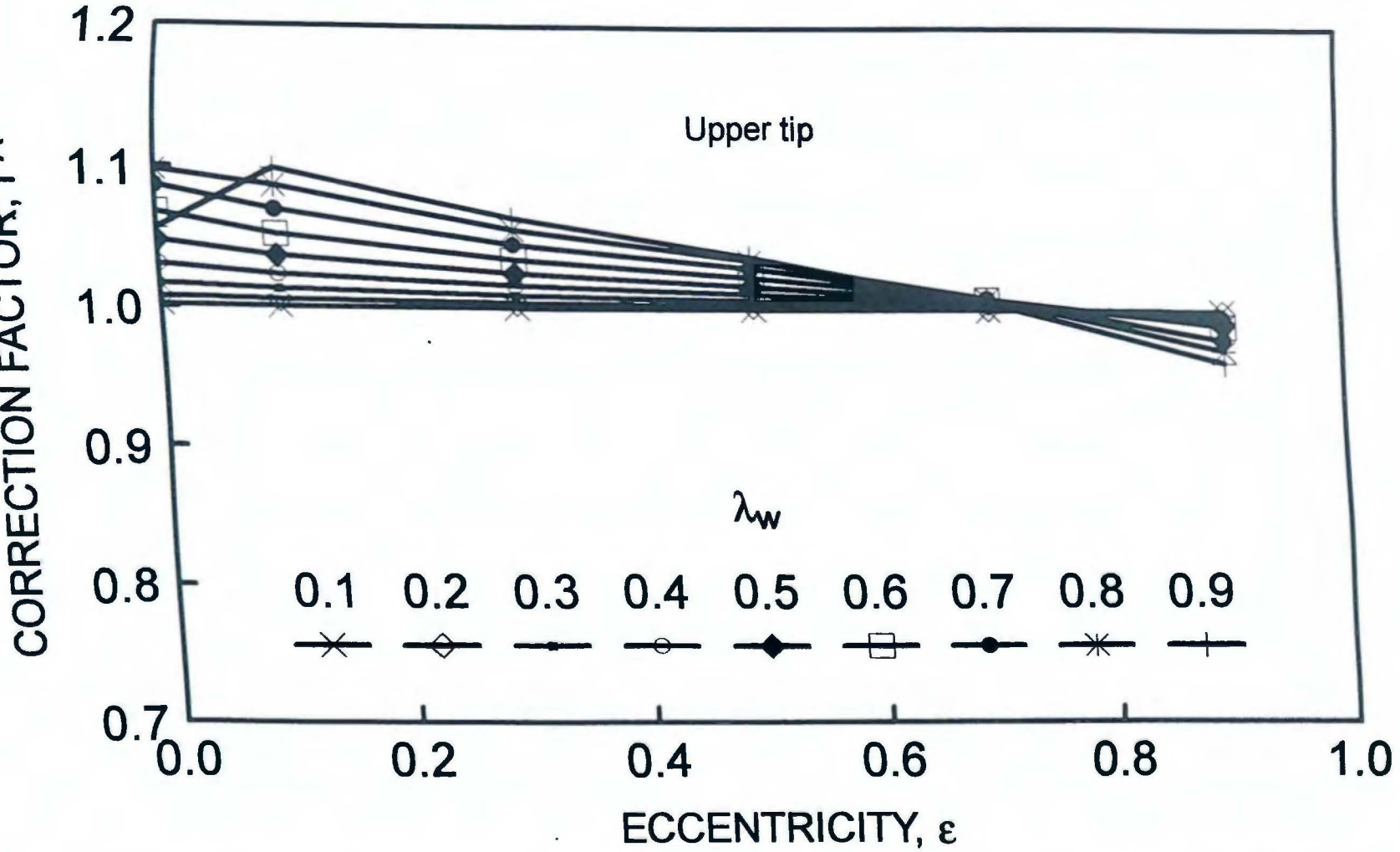

Figure 5.9. Correction factors for two-tip cracked I-beam under tension; upper tip, $\beta = 0.83$.

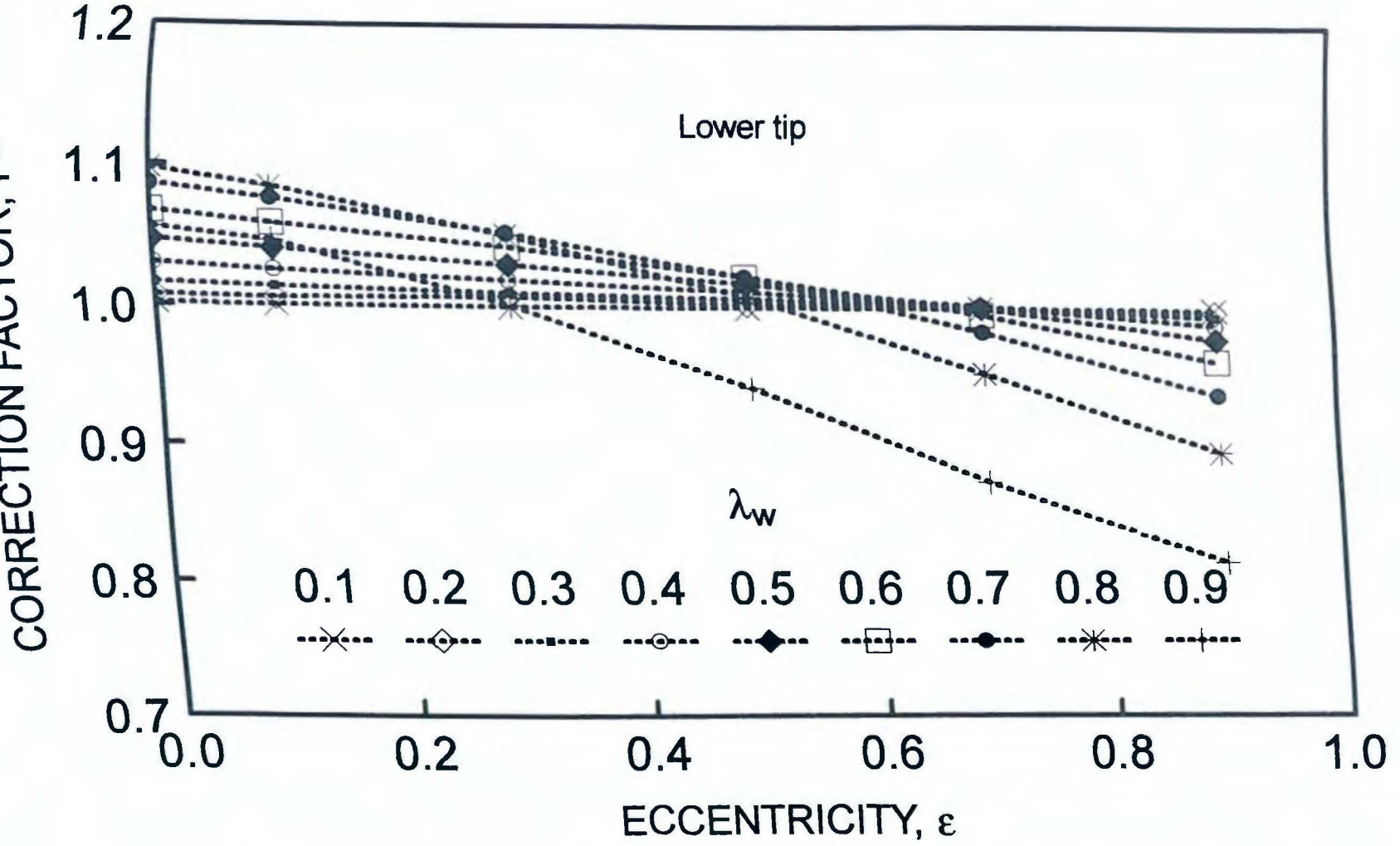

Figure 5.10. Correction factors for two-tip cracked I-beam under tension; lower tip, $\beta = 0.83$.

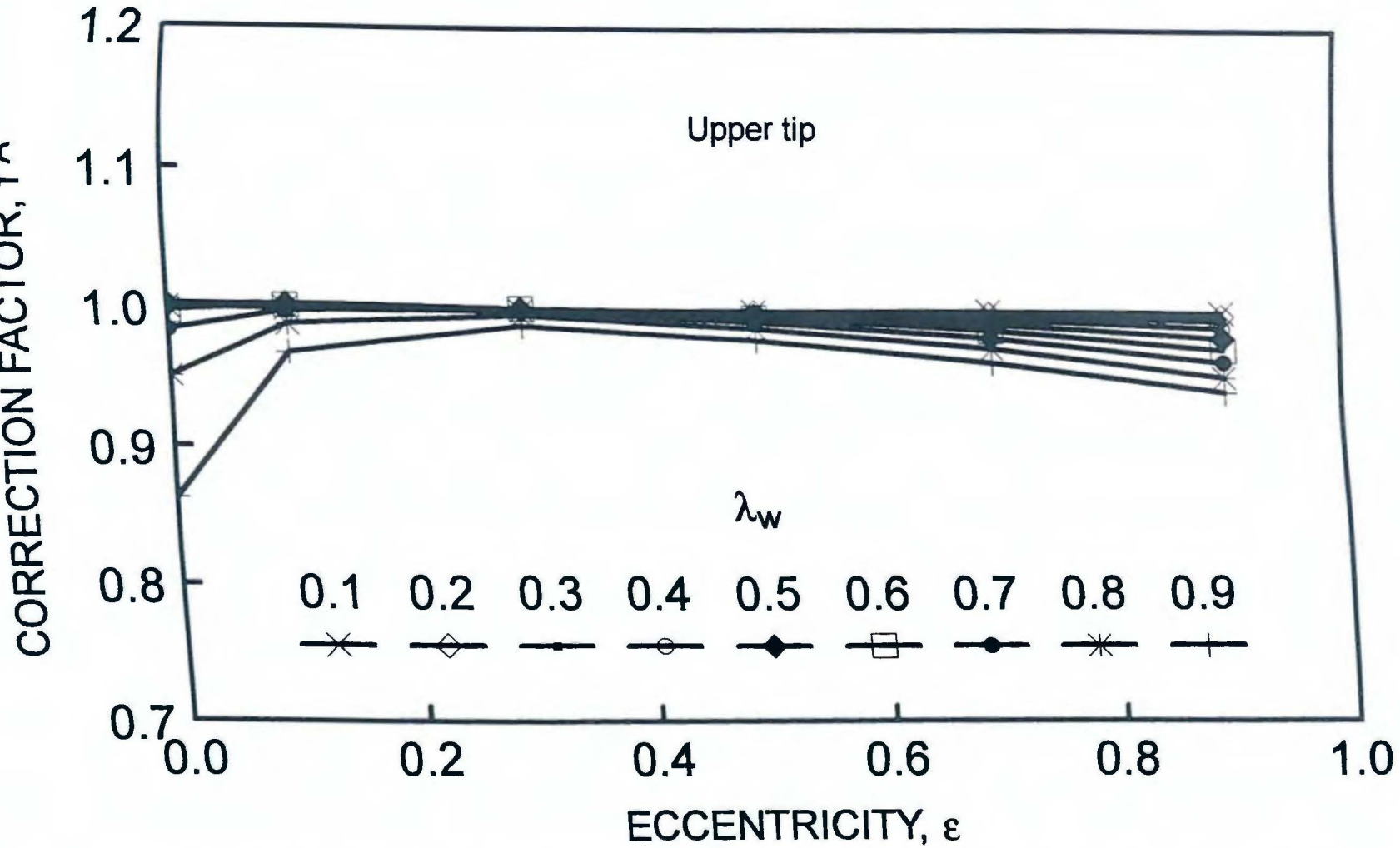

Figure 5.11. Correction factors for two-tip cracked I-beam under tension; upper tip, $\beta = 2.05$.

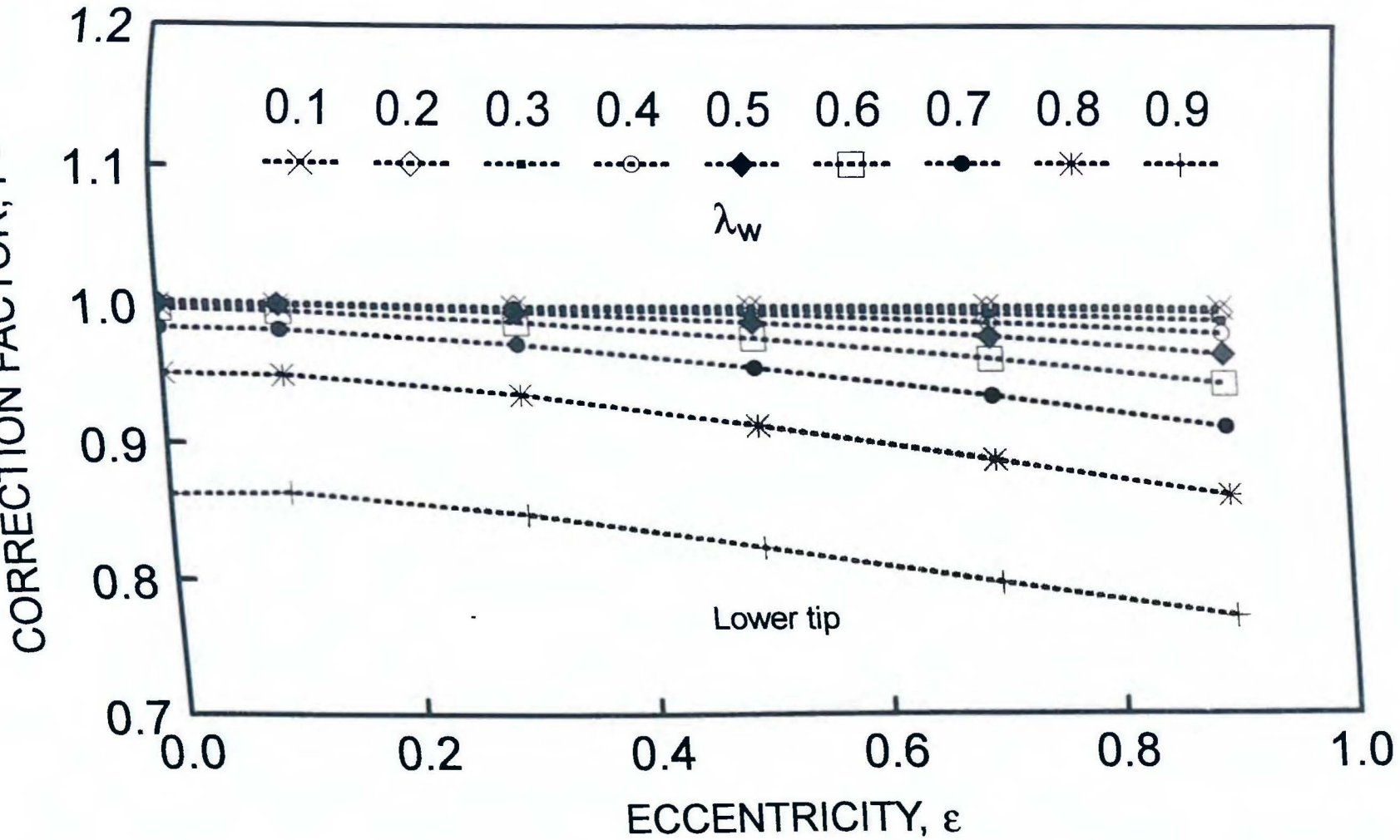

Figure 5.12. Correction factors for two-tip cracked I-beam under tension; lower tip, $\beta = 2.05$.

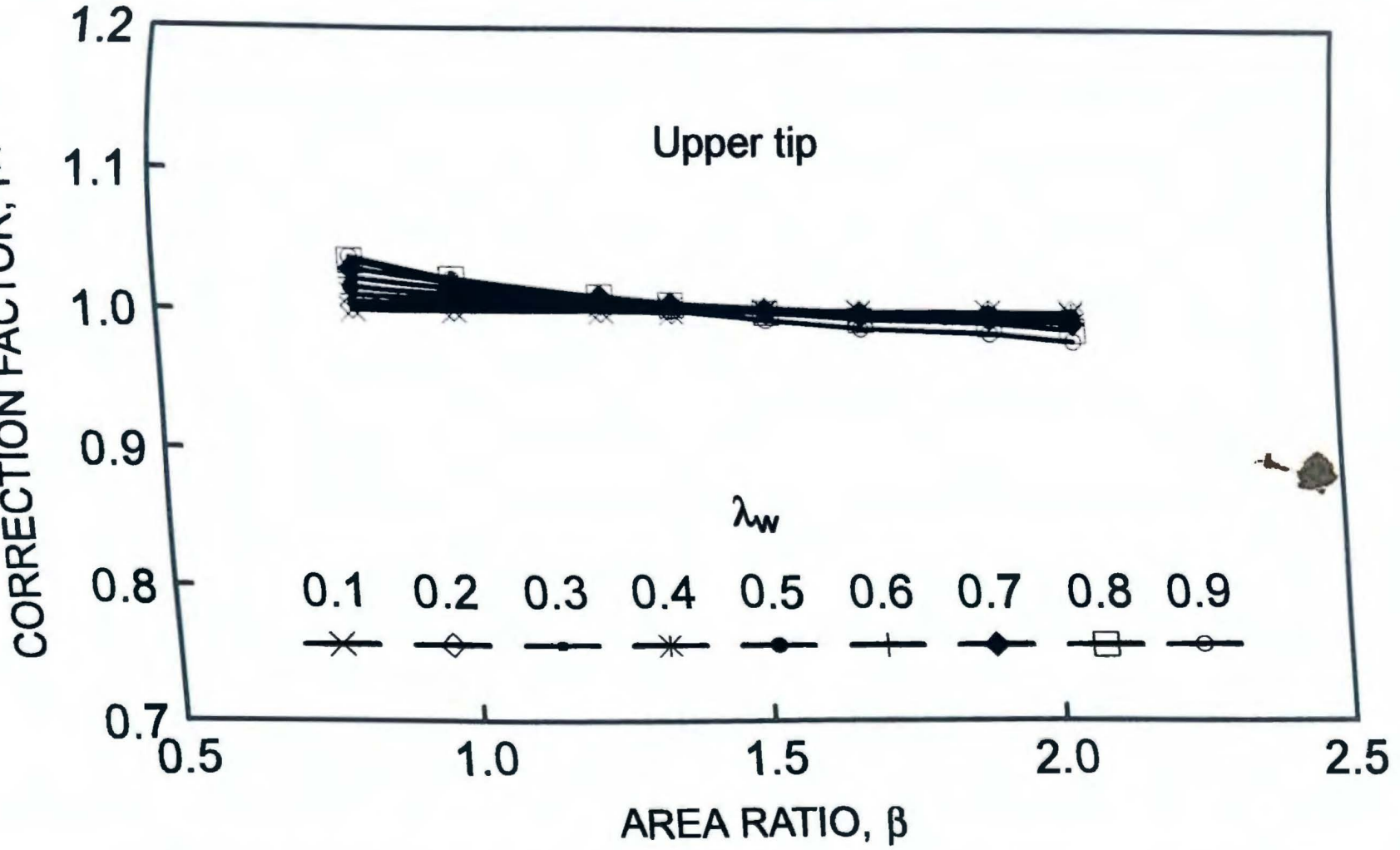

Figure 5.13. Correction factors for two-tip cracked I-beam under tension; upper tip, $\varepsilon = 0.5$.

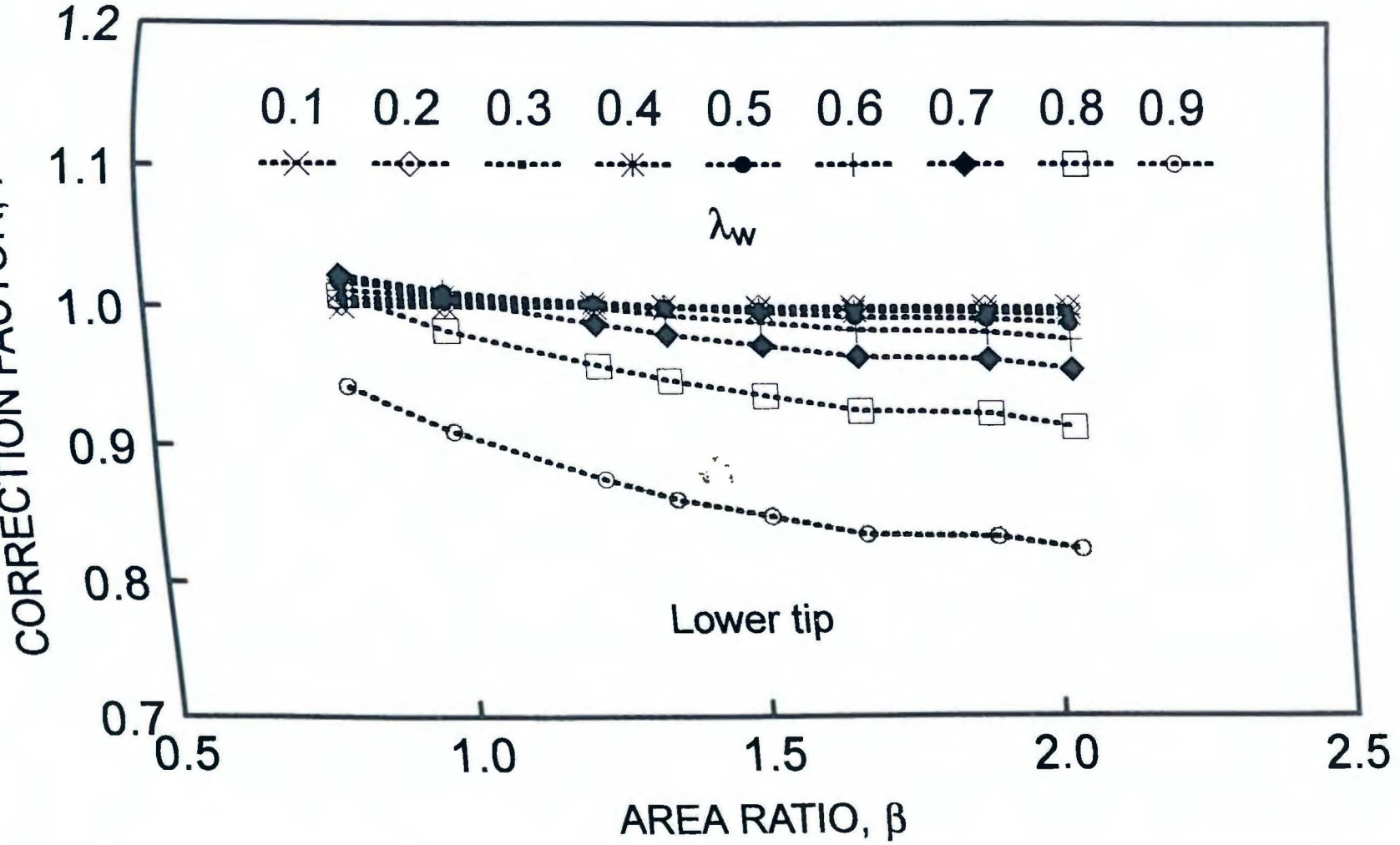

Figure 5.14. Correction factors for two-tip cracked I-beam under tension; lower tip, $\varepsilon = 0.5$.

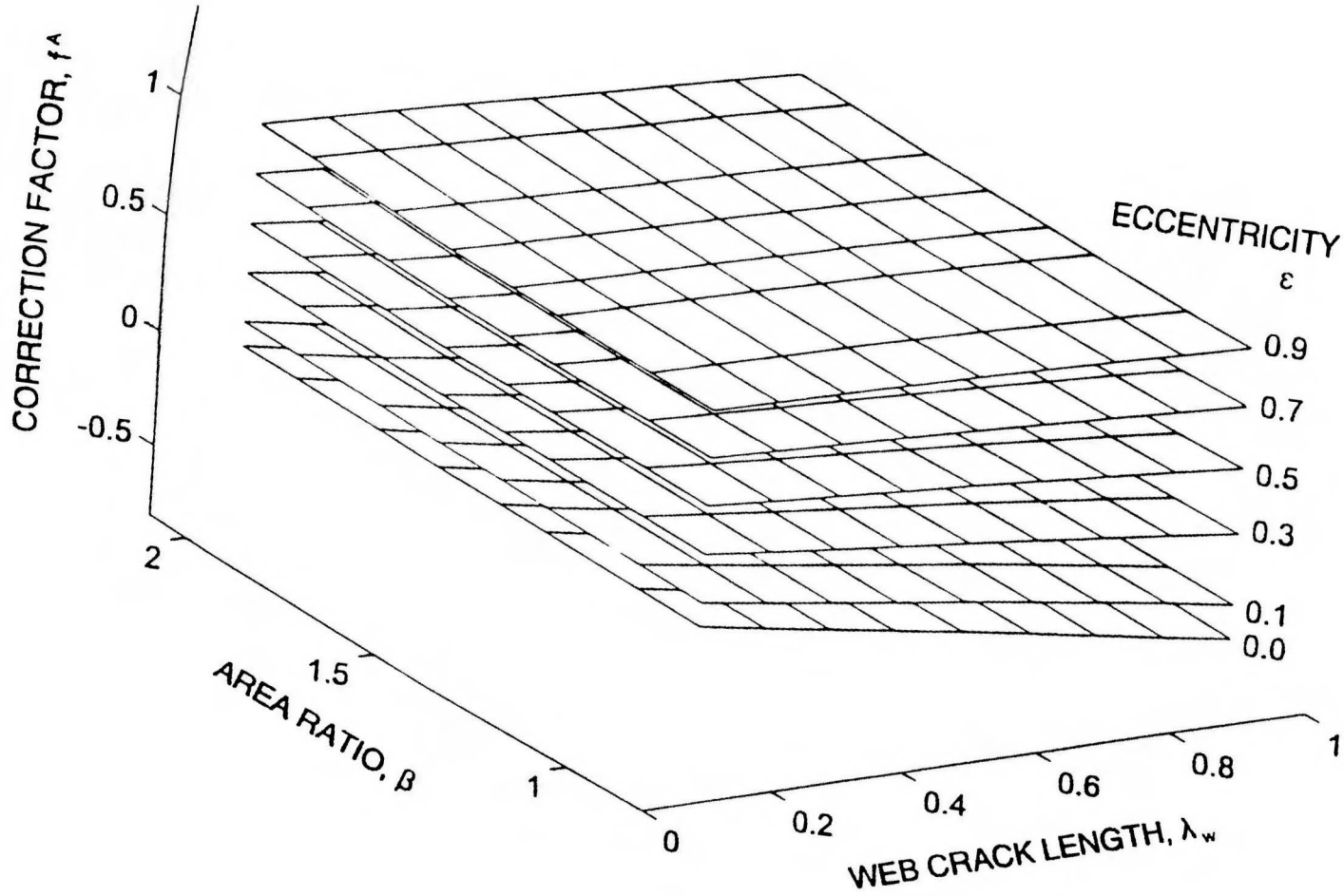

Figure 5.15. Correction factor for two-tip cracked I-beam under bending; upper tip.

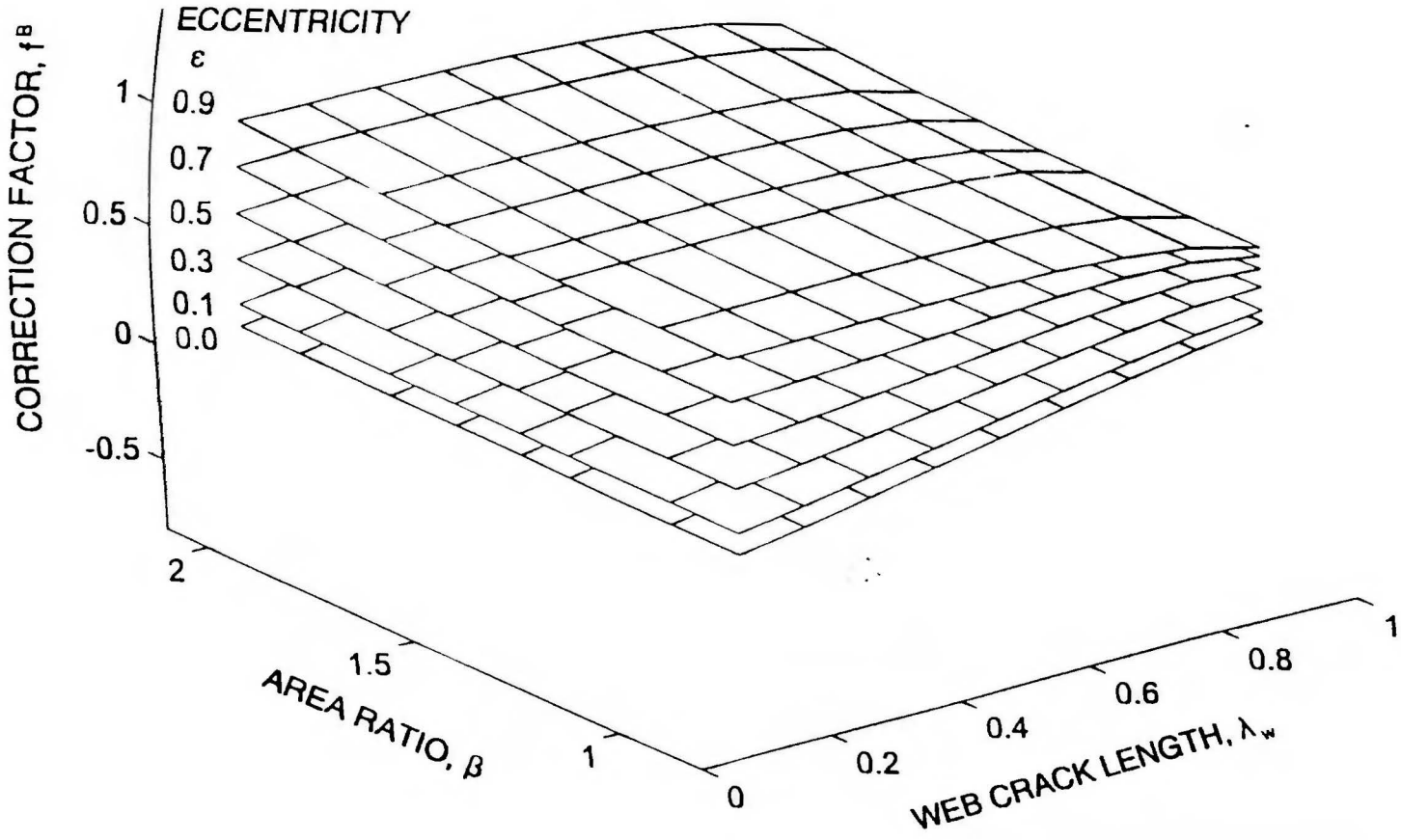

Figure 5.16. Correction factor for two-tip cracked I-beam under bending; lower tip.

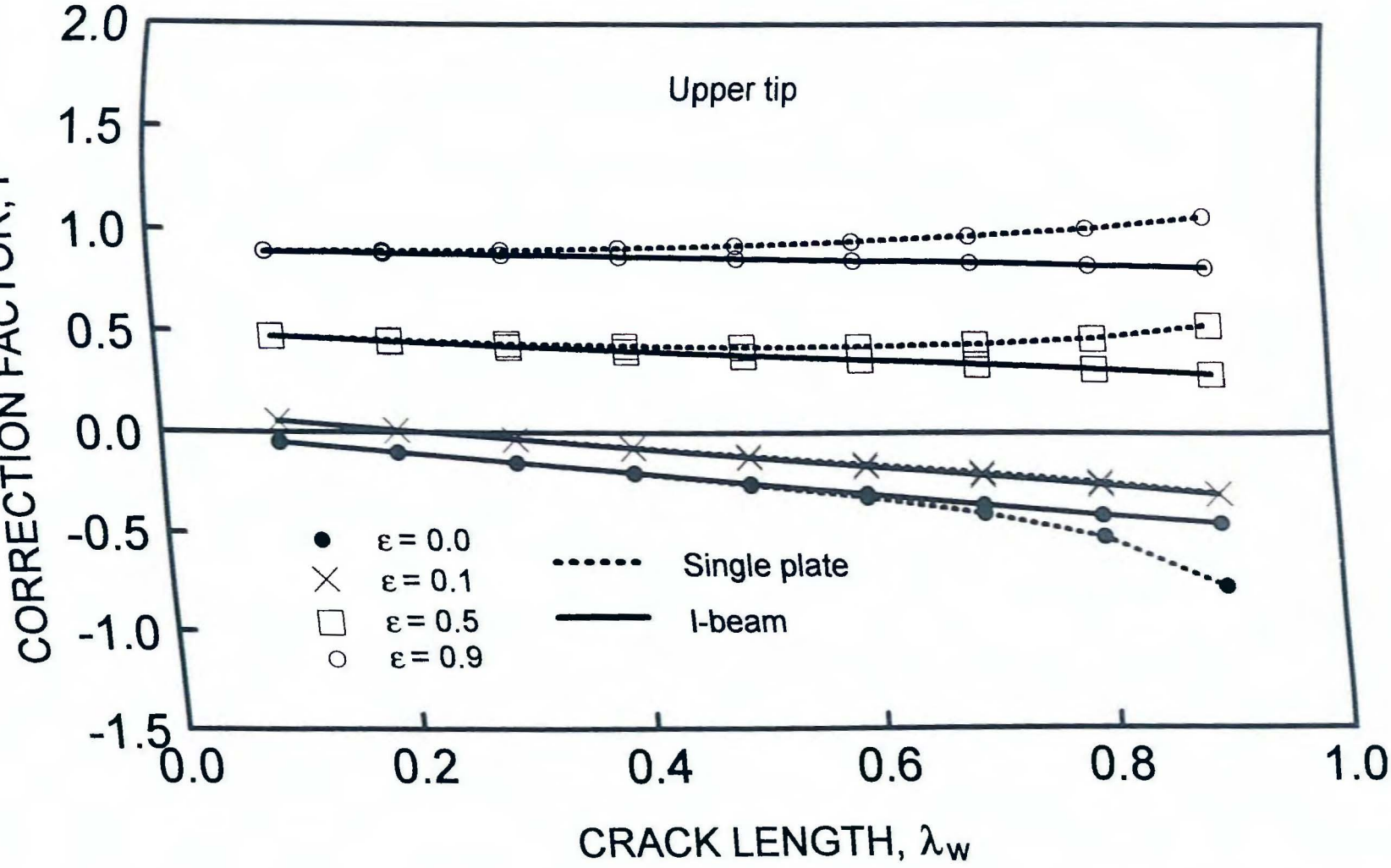

Figure 5.17. Comparison of I-beam and single web plate under bending; upper tip, $\beta = 0.83$.

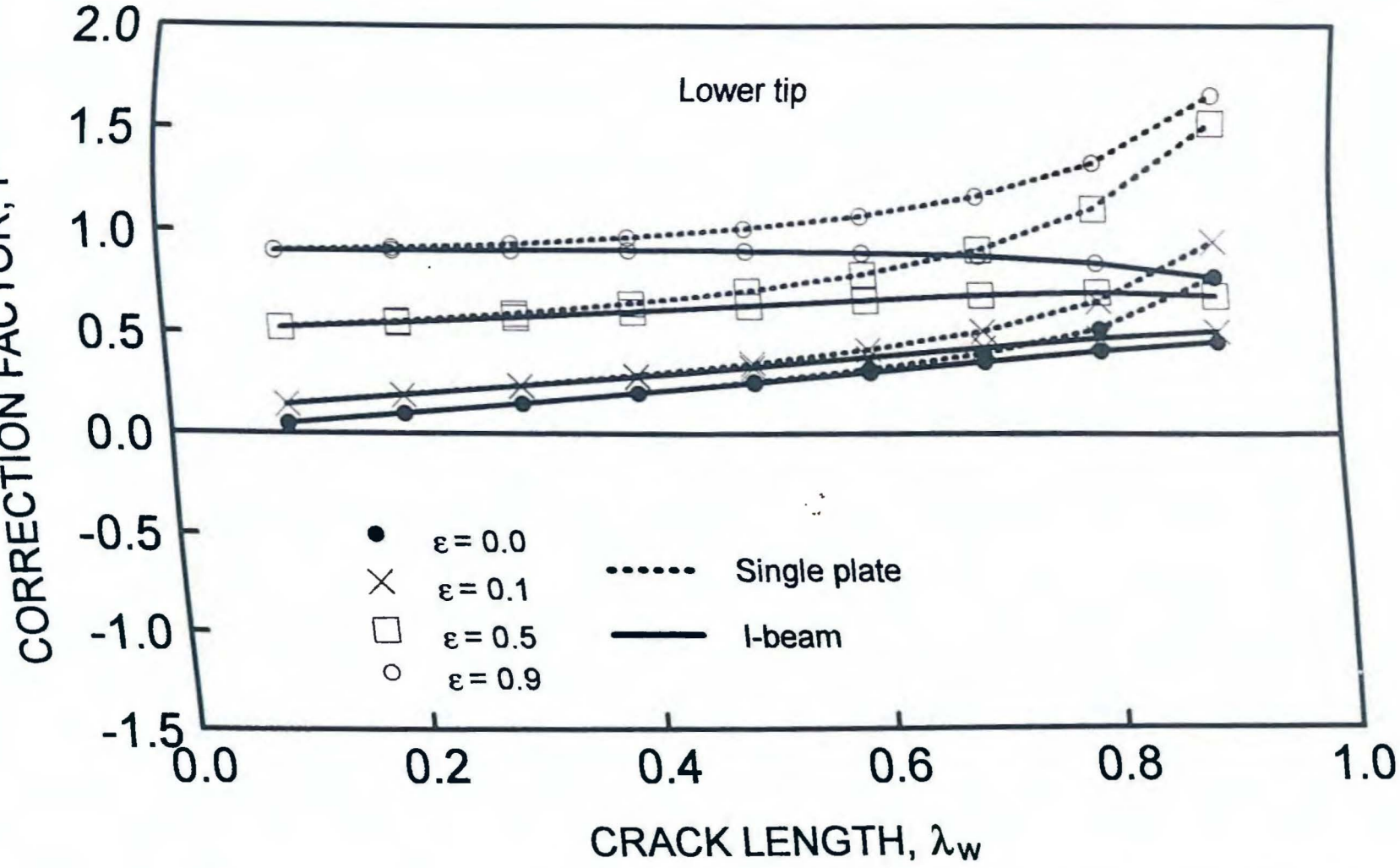

Figure 5.18. Comparison of I-beam and single web plate under bending; lower tip, $\beta = 0.83$.

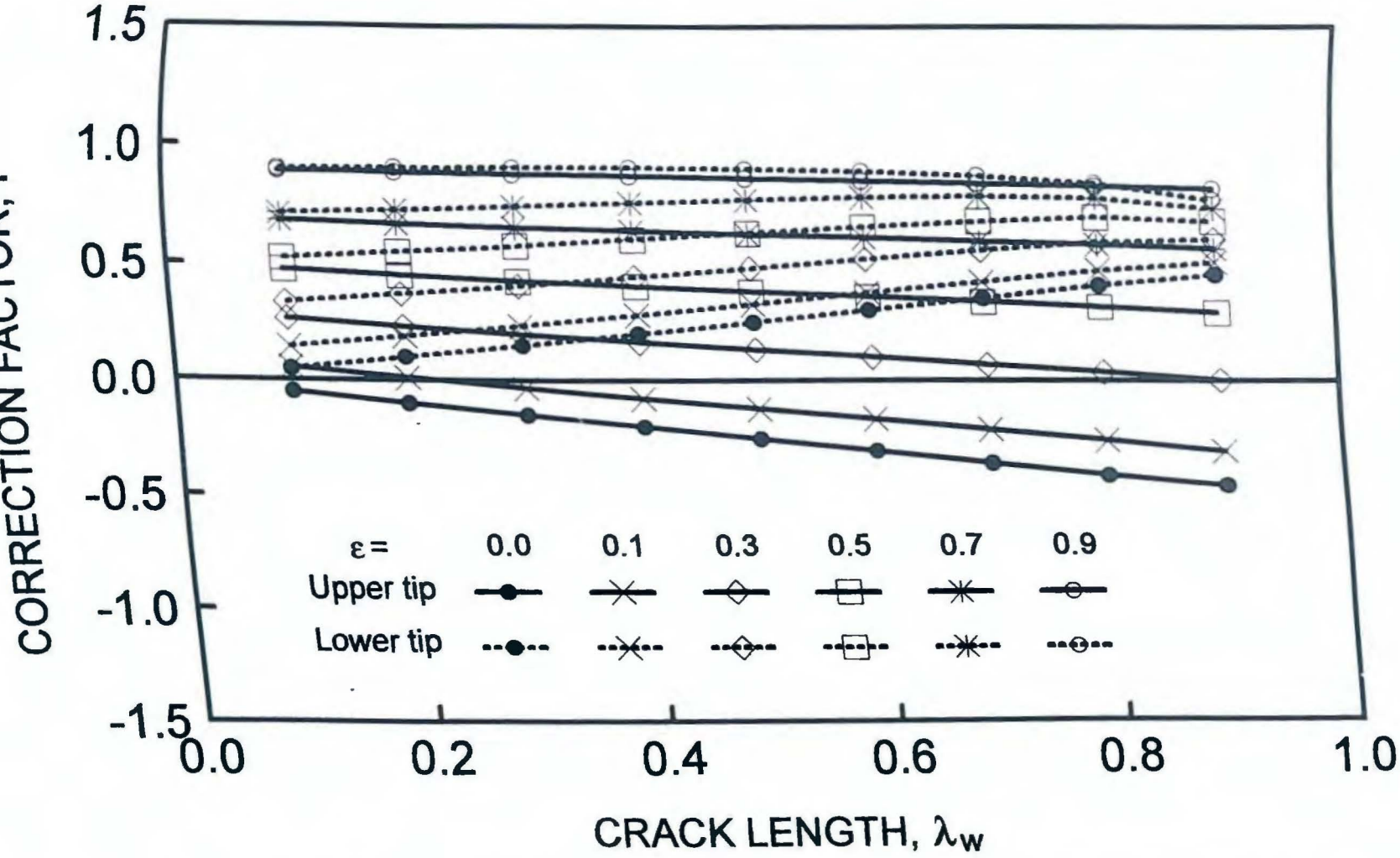

Figure 5.19. Correction factors for two-tip cracked I-beam under bending; $\beta = 0.83$.

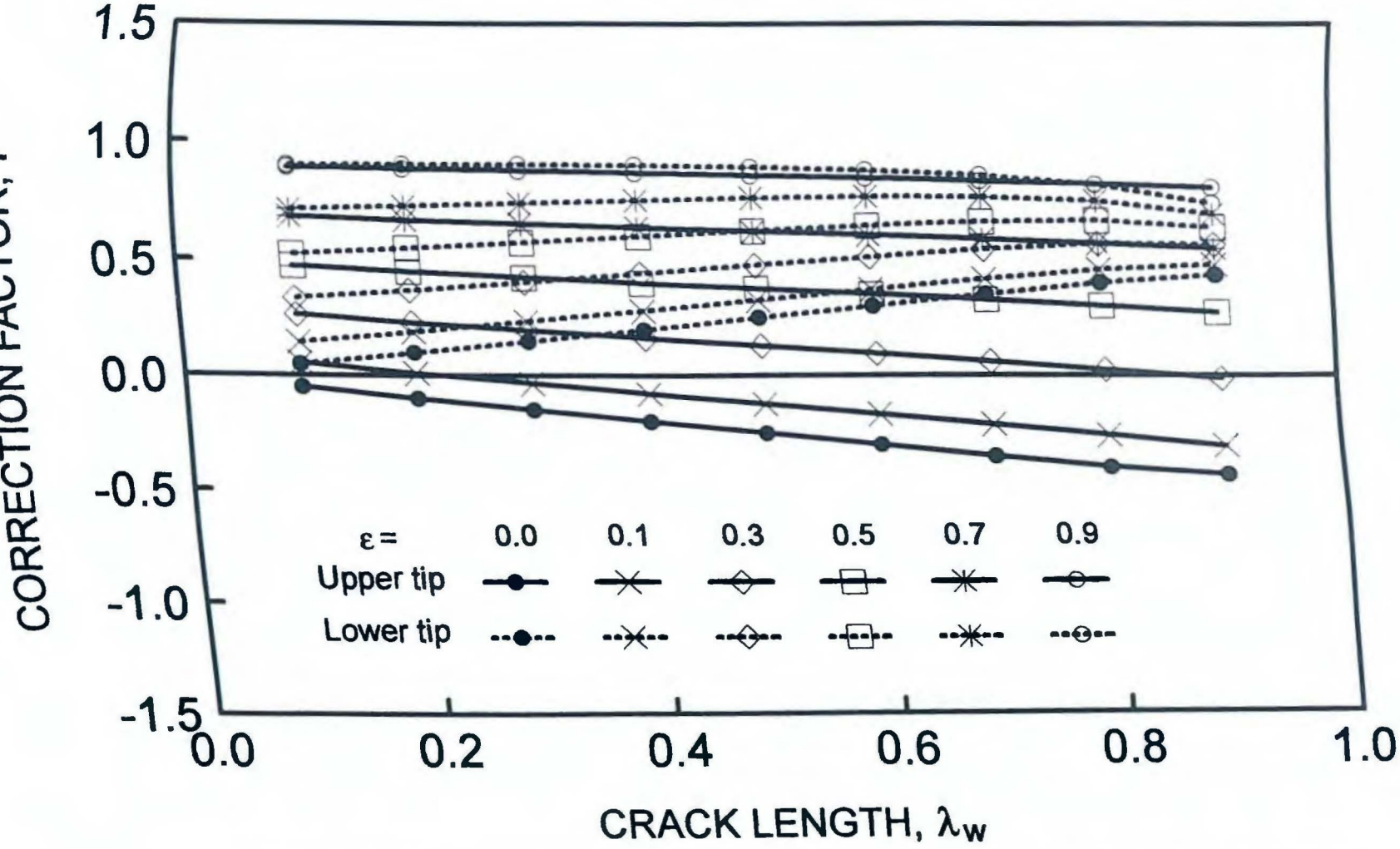

Figure 5.20. Correction factors for two-tip cracked I-beam under bending; $\beta = 1.37$.

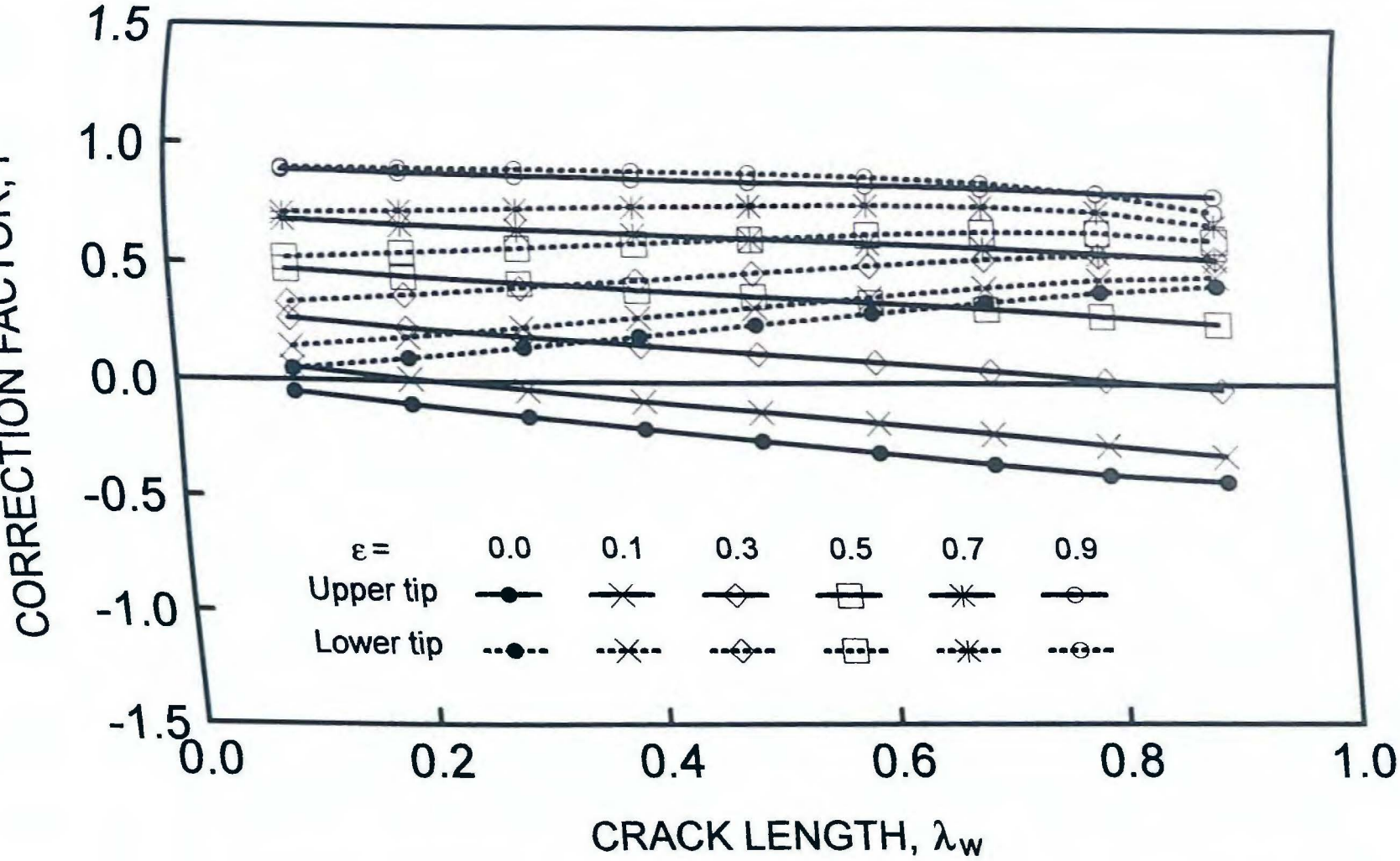

Figure 5.21. Correction factors for two-tip cracked I-beam under bending; $\beta = 2.05$.

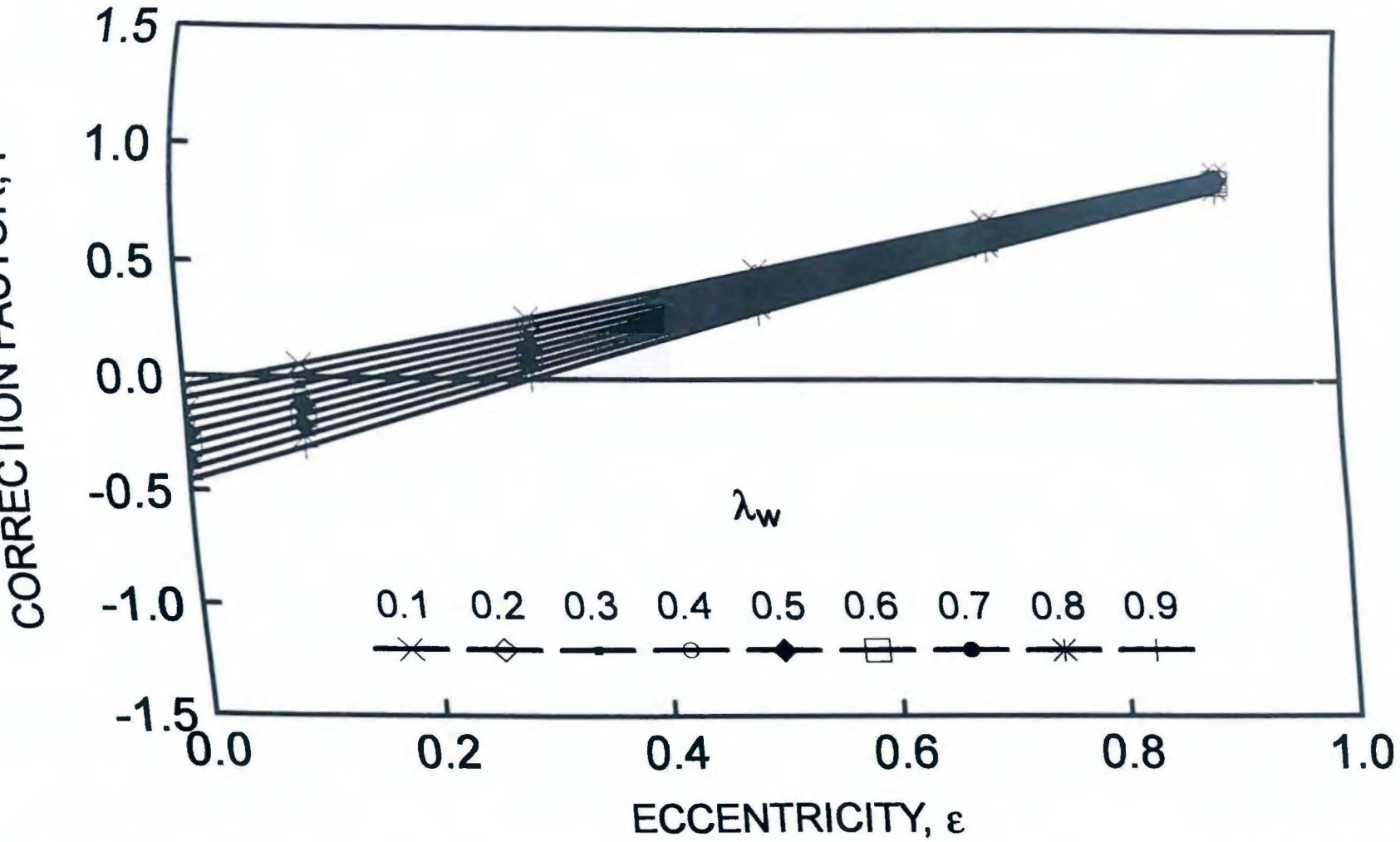

Figure 5.22. Correction factors for two-tip cracked I-beam under bending; upper tip, $\beta = 0.83$.

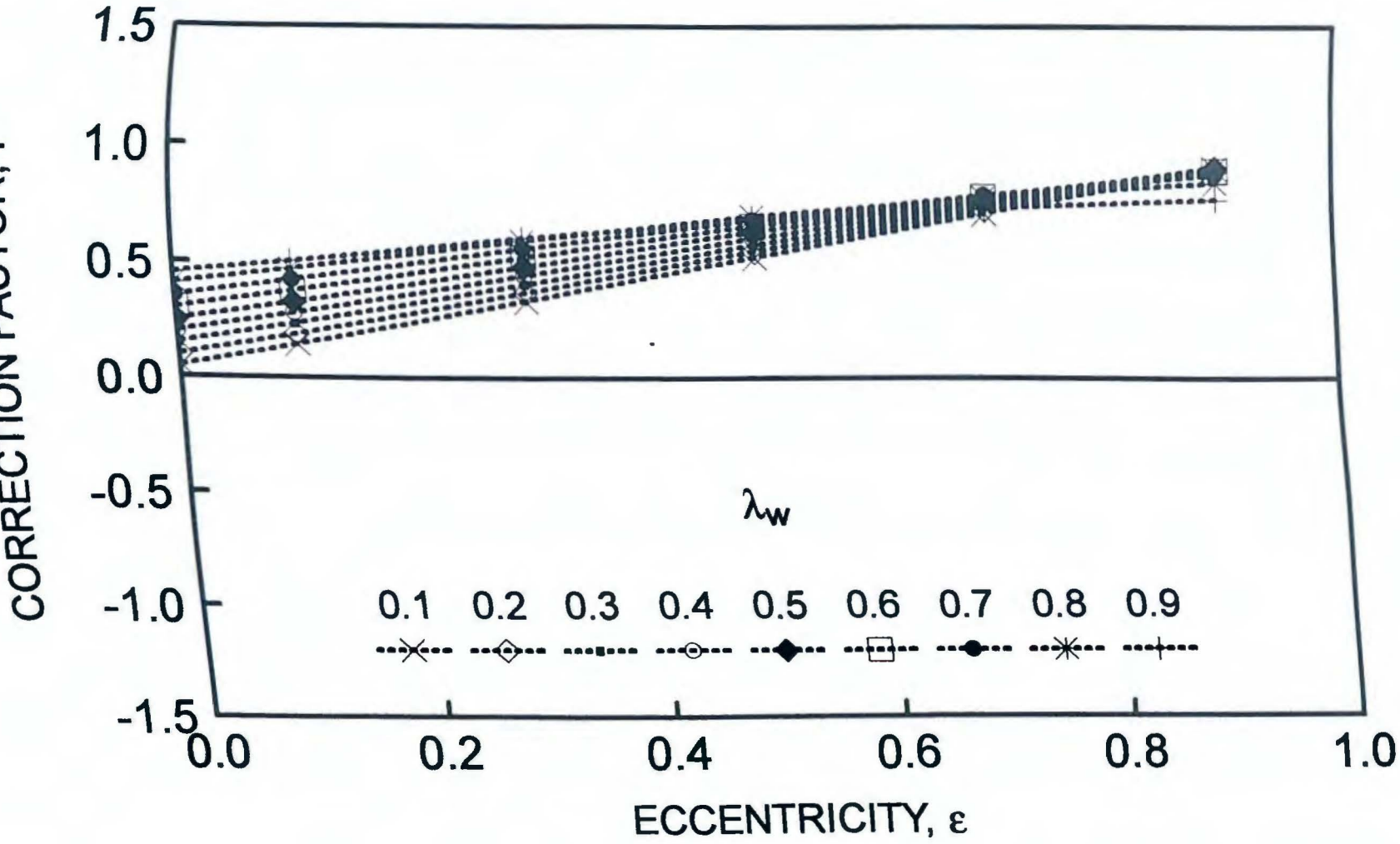

Figure 5.23. Correction factors for two-tip cracked I-beam under bending; lower tip, $\beta = 0.83$.

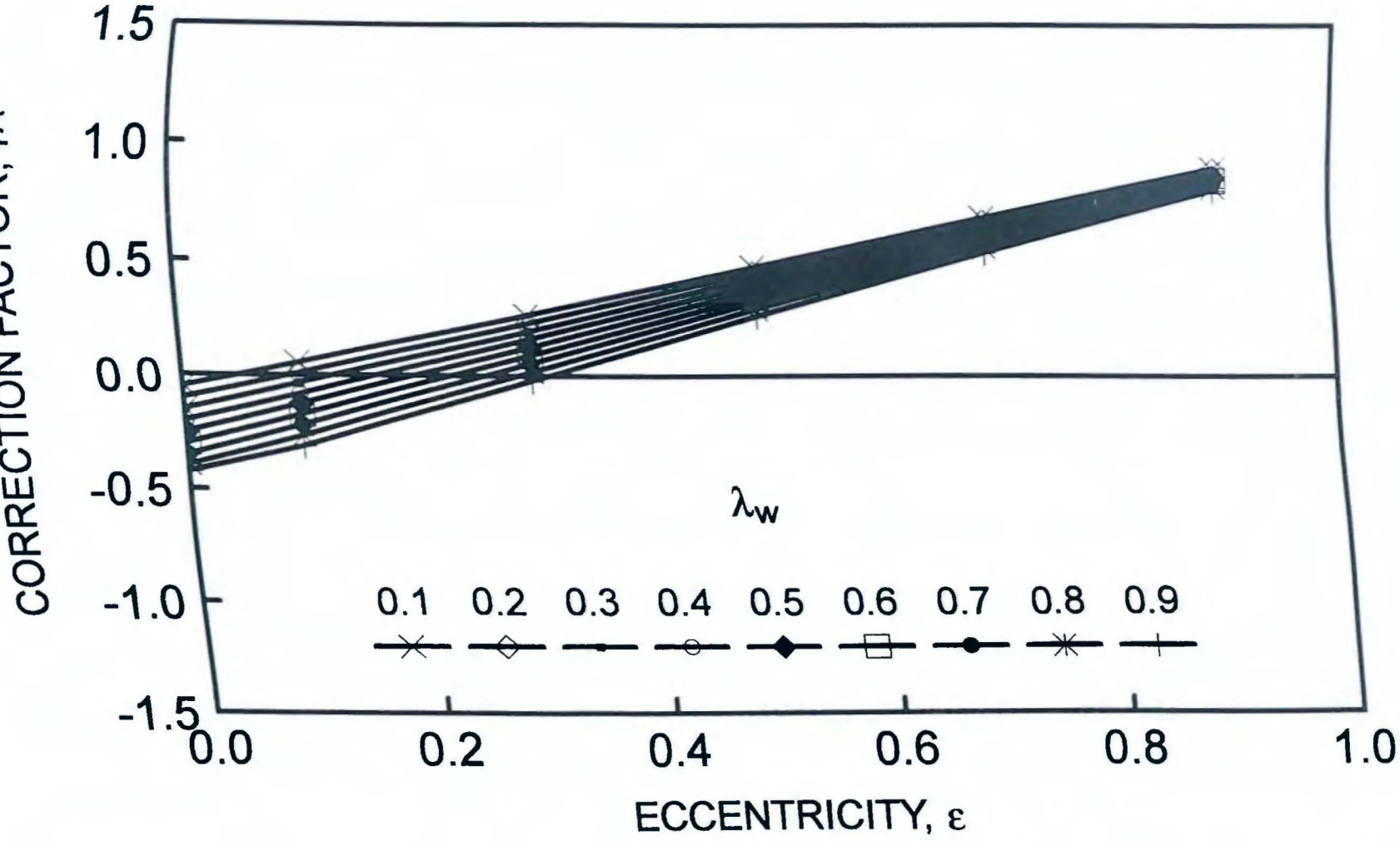

Figure 5.24. Correction factors for two-tip cracked I-beam under bending; upper tip, $\beta = 2.05$.

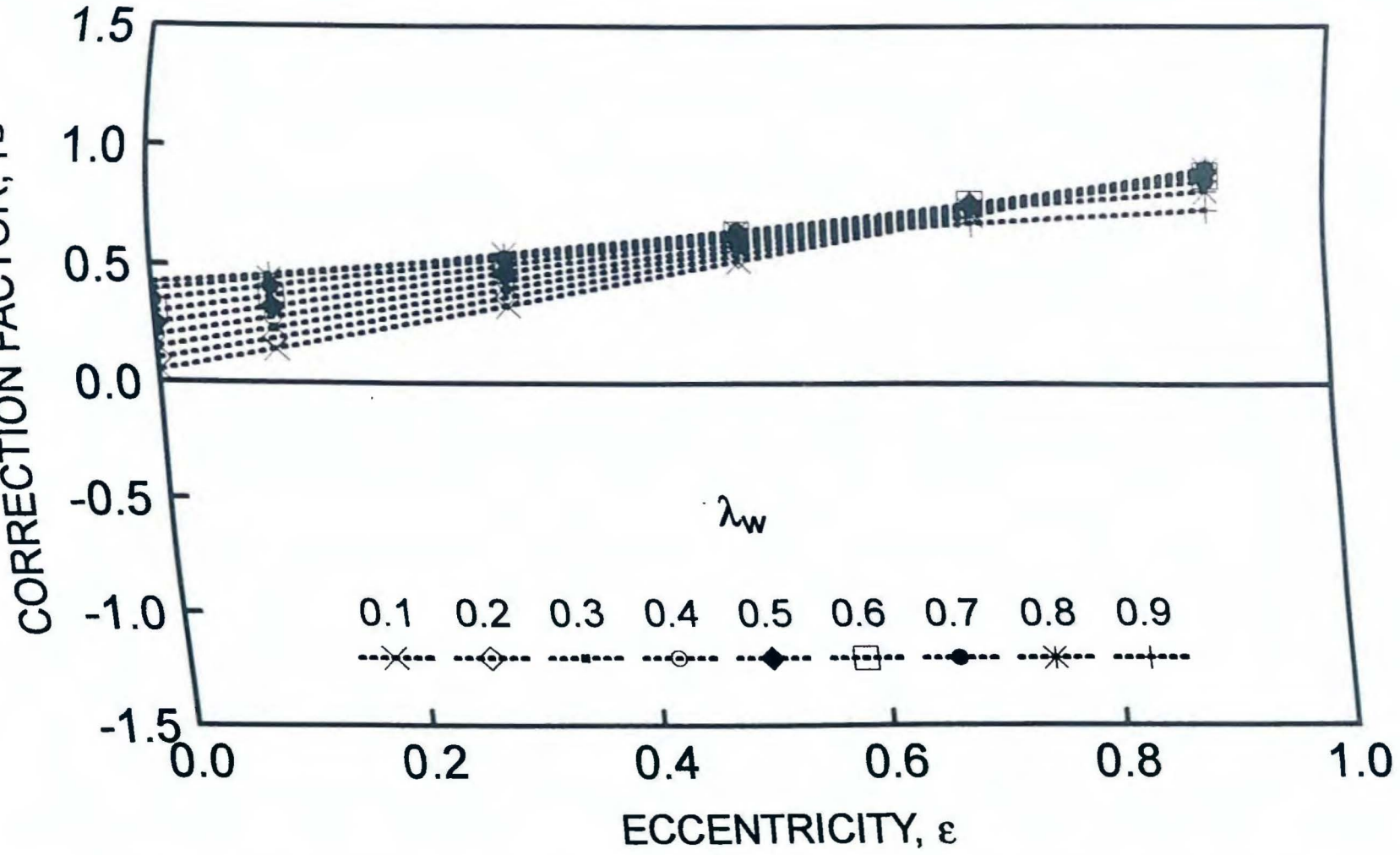

Figure 5.25. Correction factors for two-tip cracked I-beam under bending; lower tip, $\beta = 2.05$.

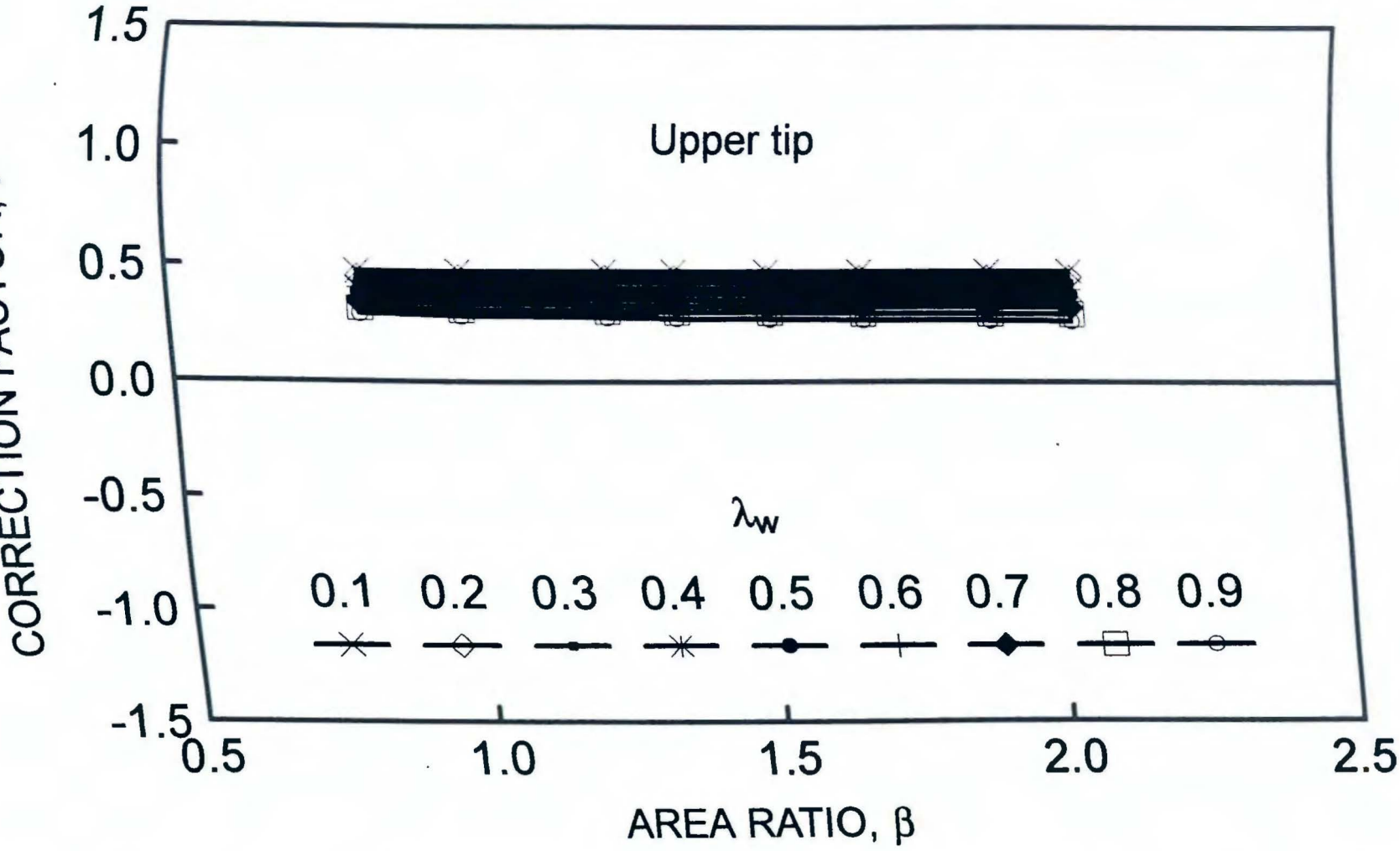

Figure 5.26. Correction factors for two-tip cracked I-beam under bending; upper tip, $\varepsilon = 0.5$.

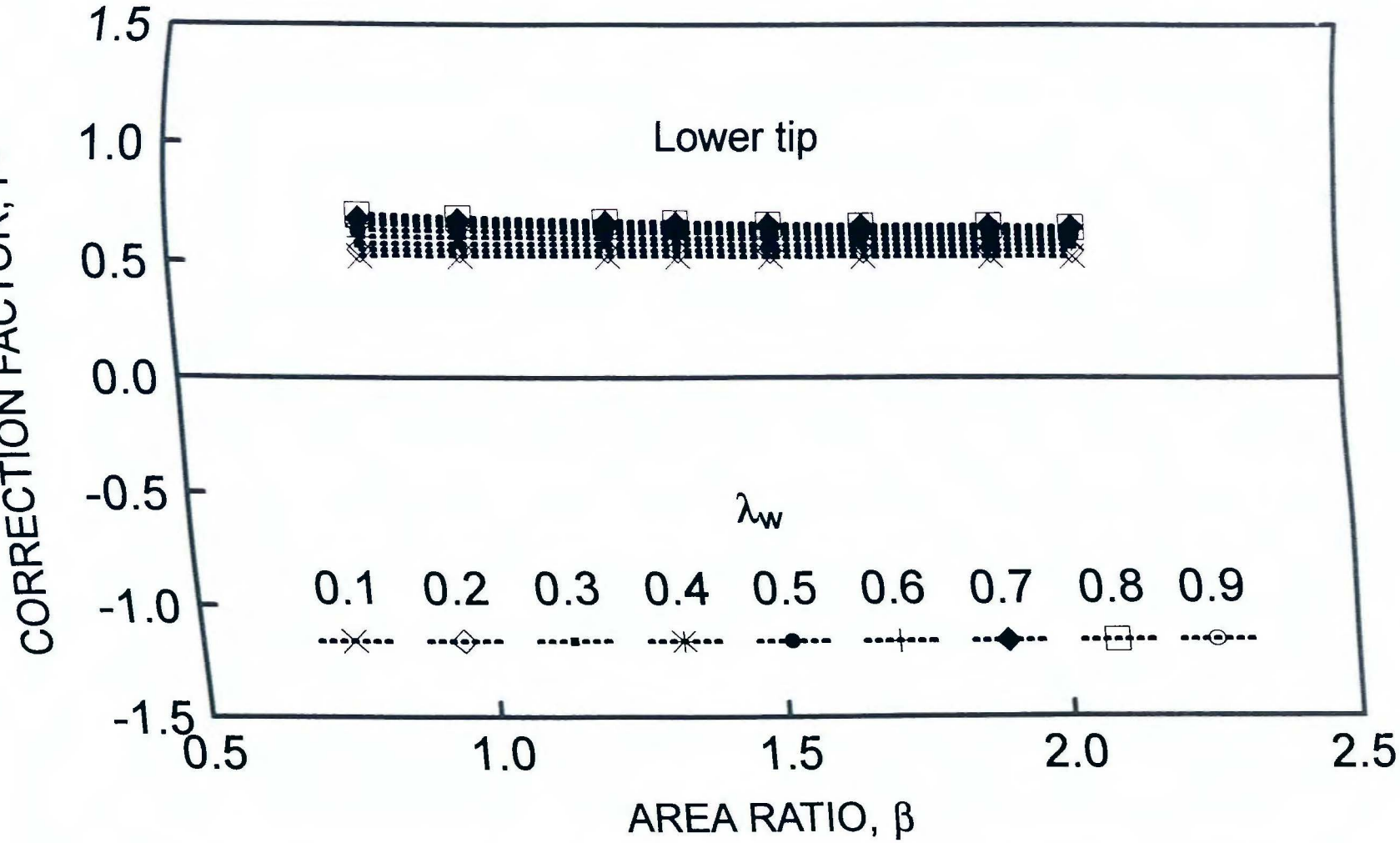

Figure 5.27. Correction factors for two-tip cracked I-beam under bending; lower tip, $\varepsilon = 0.5$.

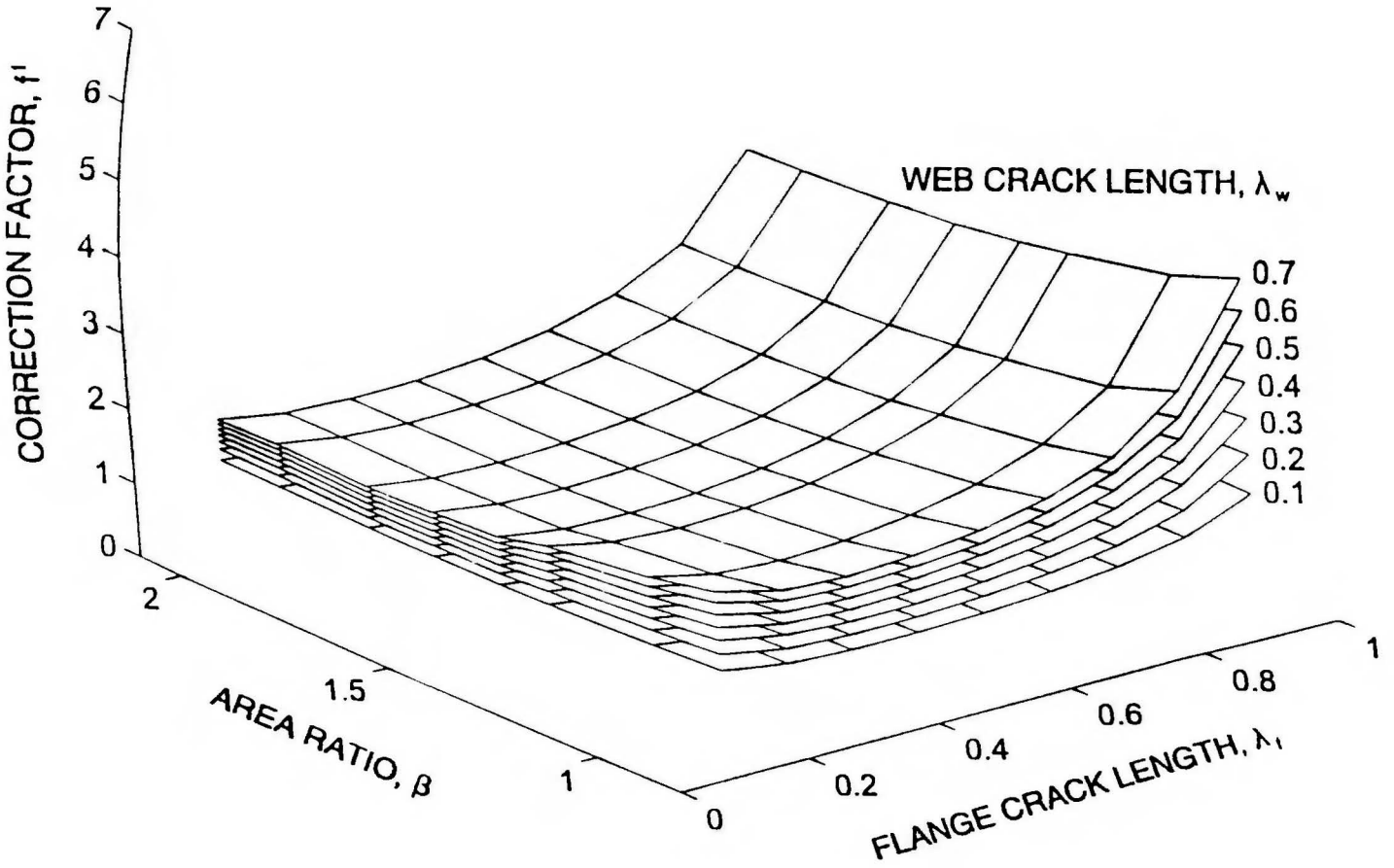

Figure 5.28. Correction factor for three-tip cracked I-beam under tension; flange crack tip.

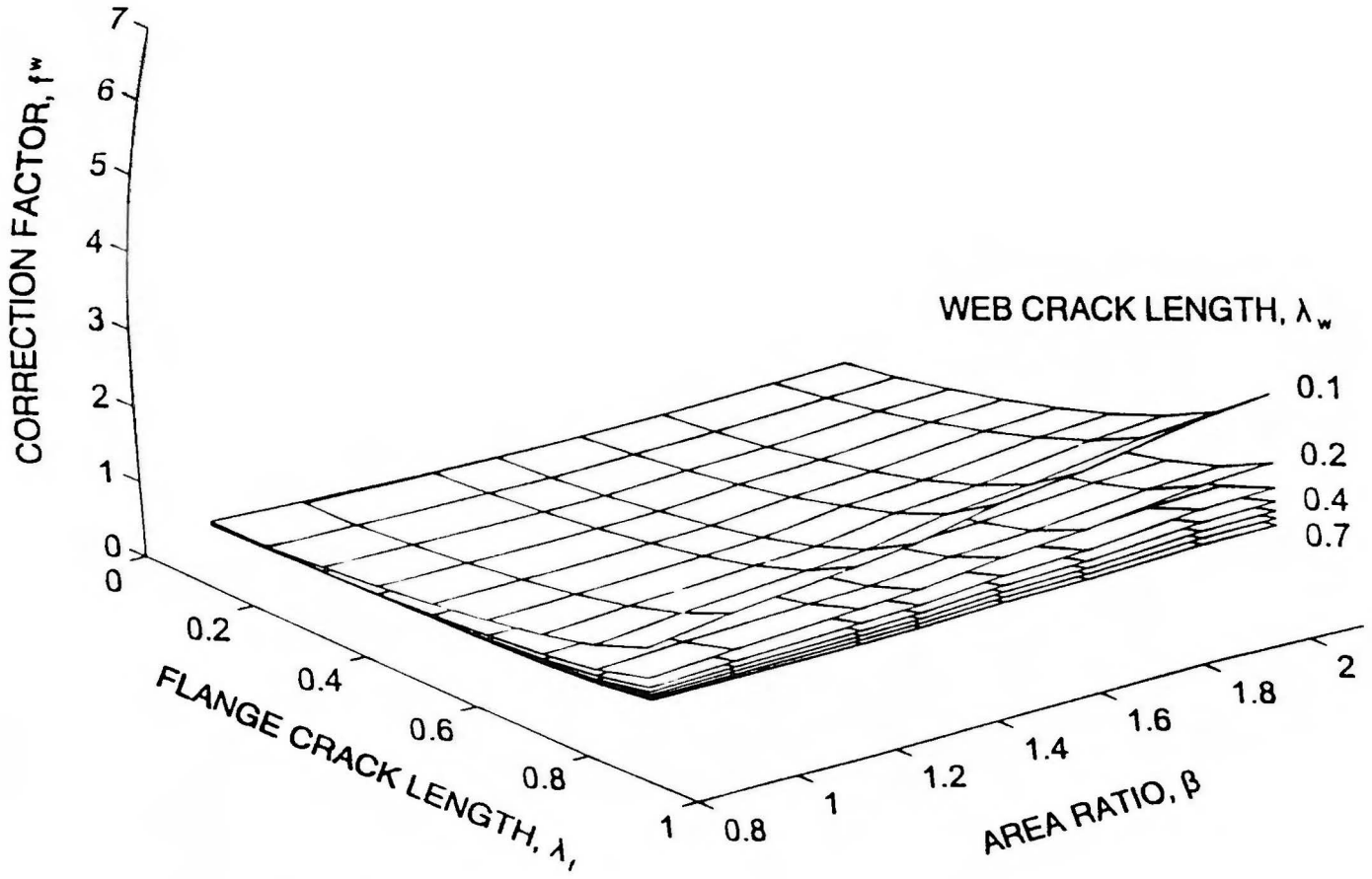

Figure 5.29. Correction factor for three-tip cracked I-beam under tension; web crack tip.

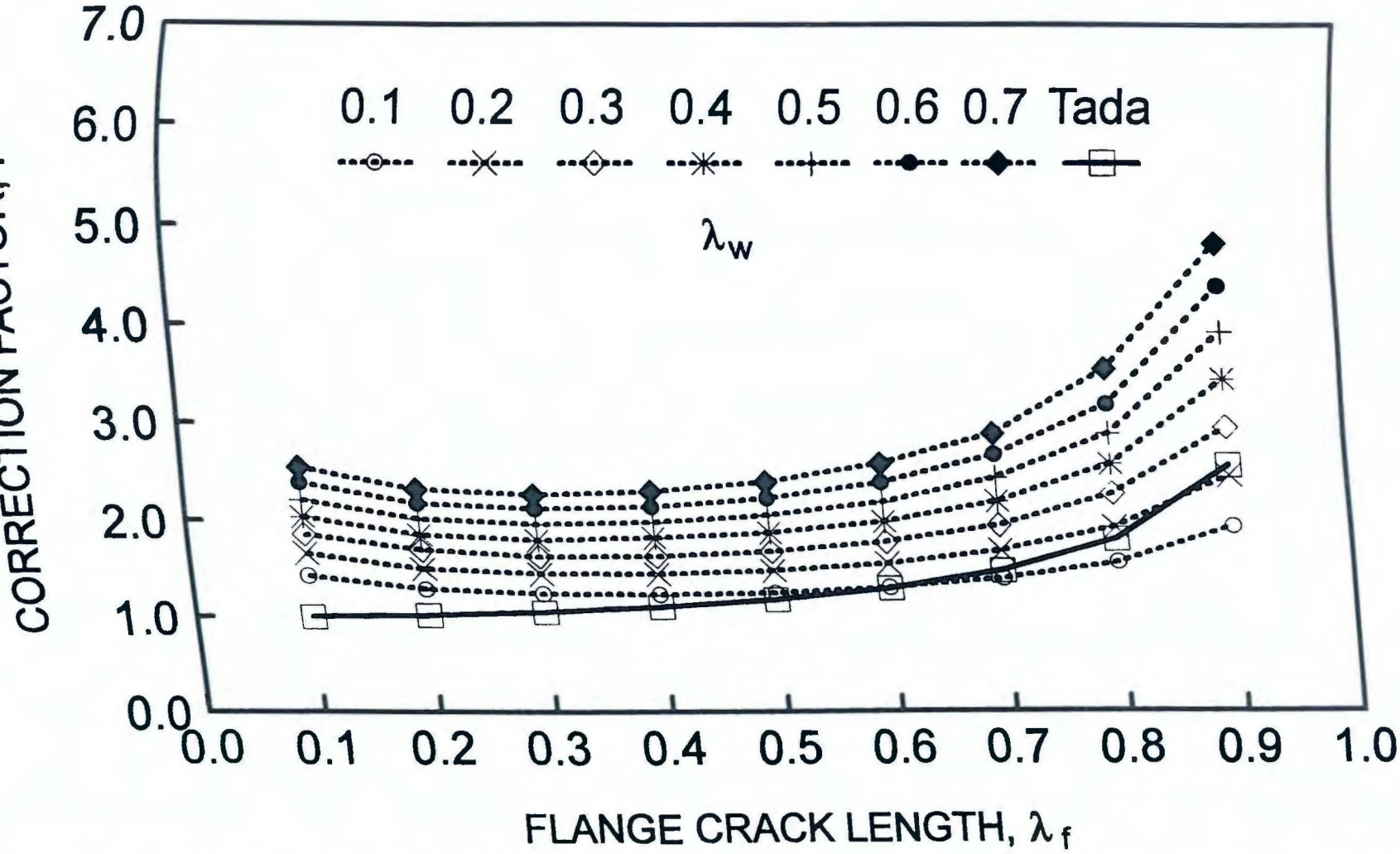

Figure 5.30. Correction factor for flange crack of three-tip cracked I-beam under tension; $\beta = 0.83$.

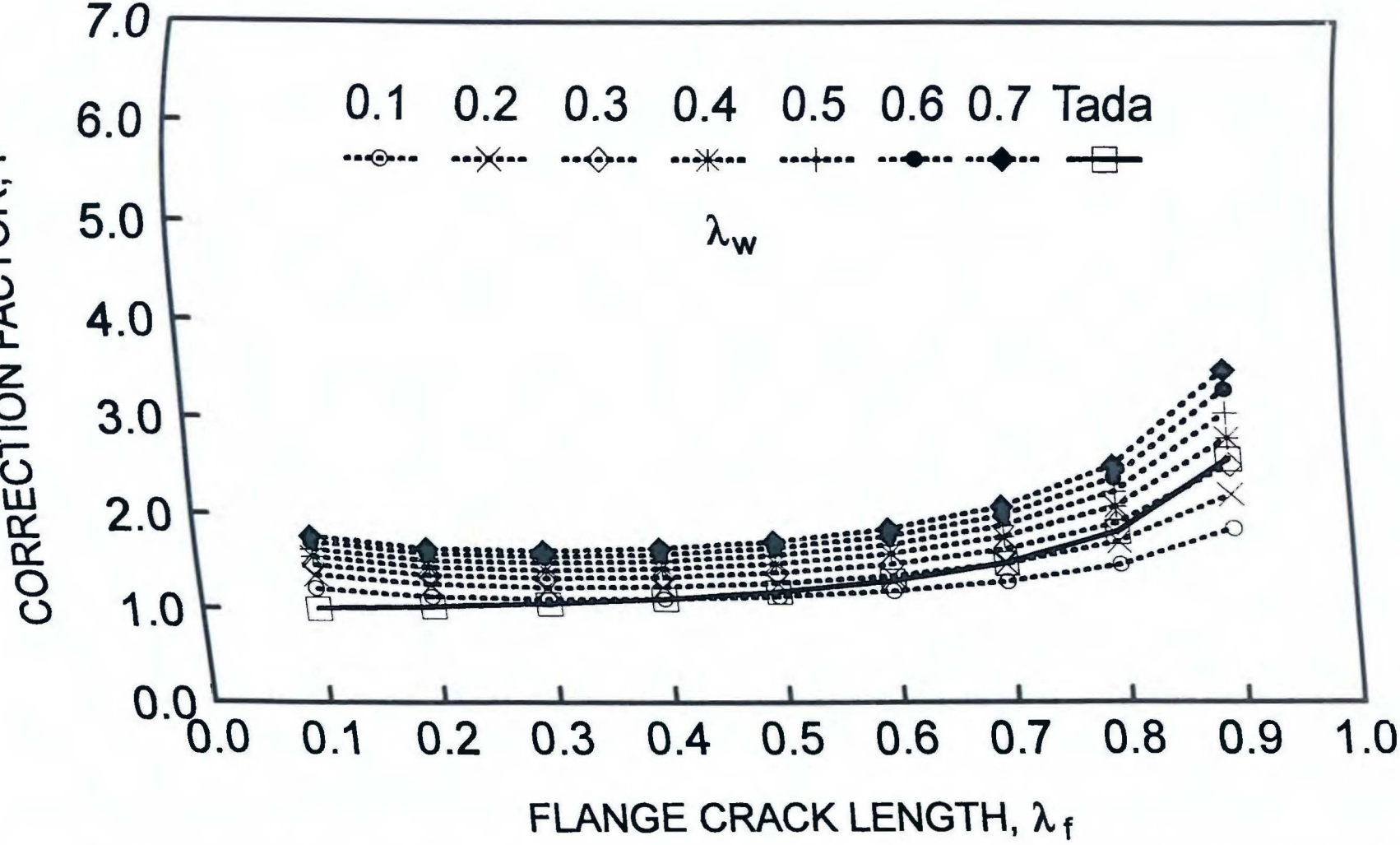

Figure 5.31. Correction factor for flange crack of three-tip cracked I-beam under tension; $\beta = 2.05$.

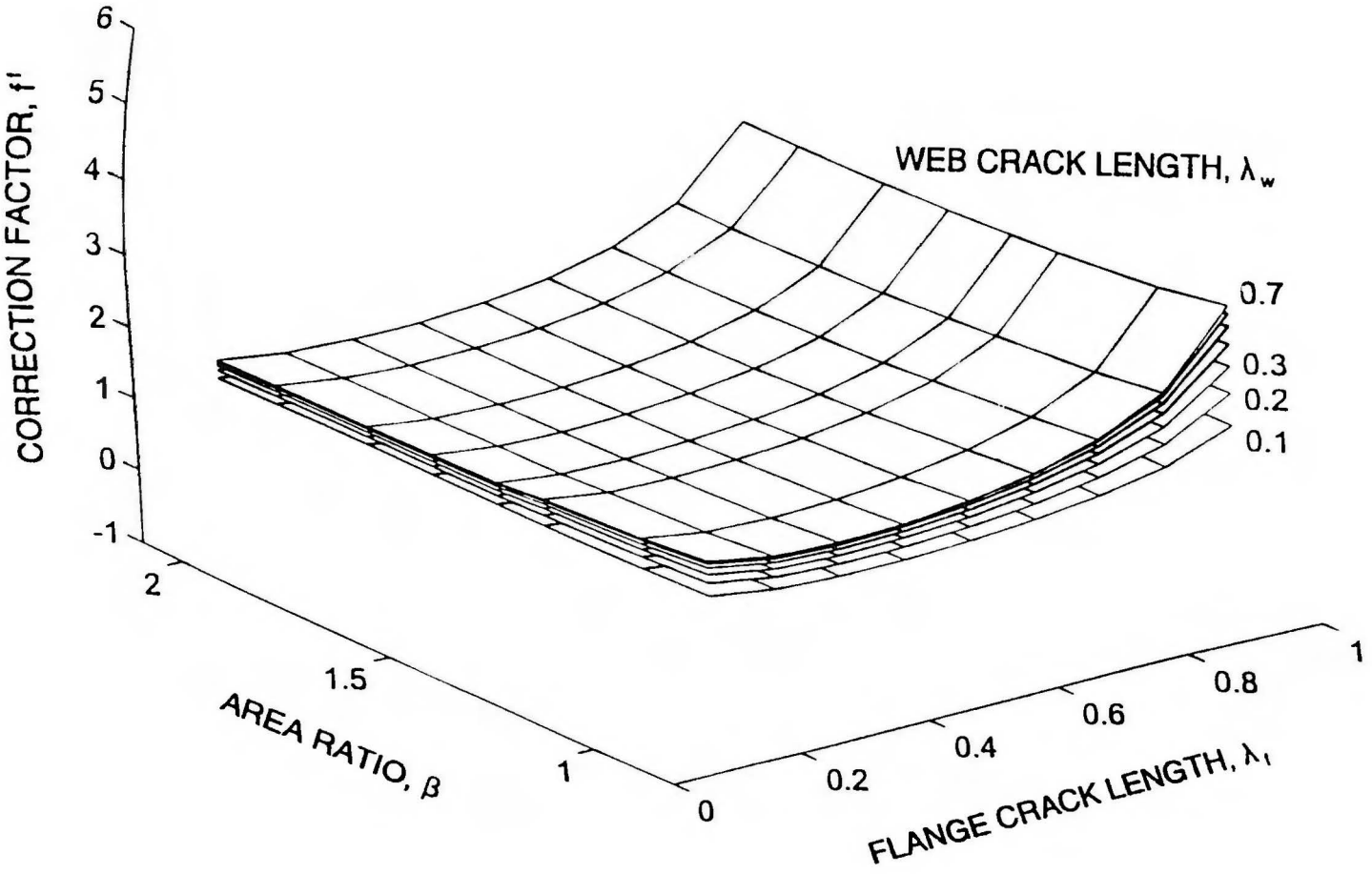

Figure 5.32. Correction factor for three-tip cracked I-beam under bending; flange crack tip.

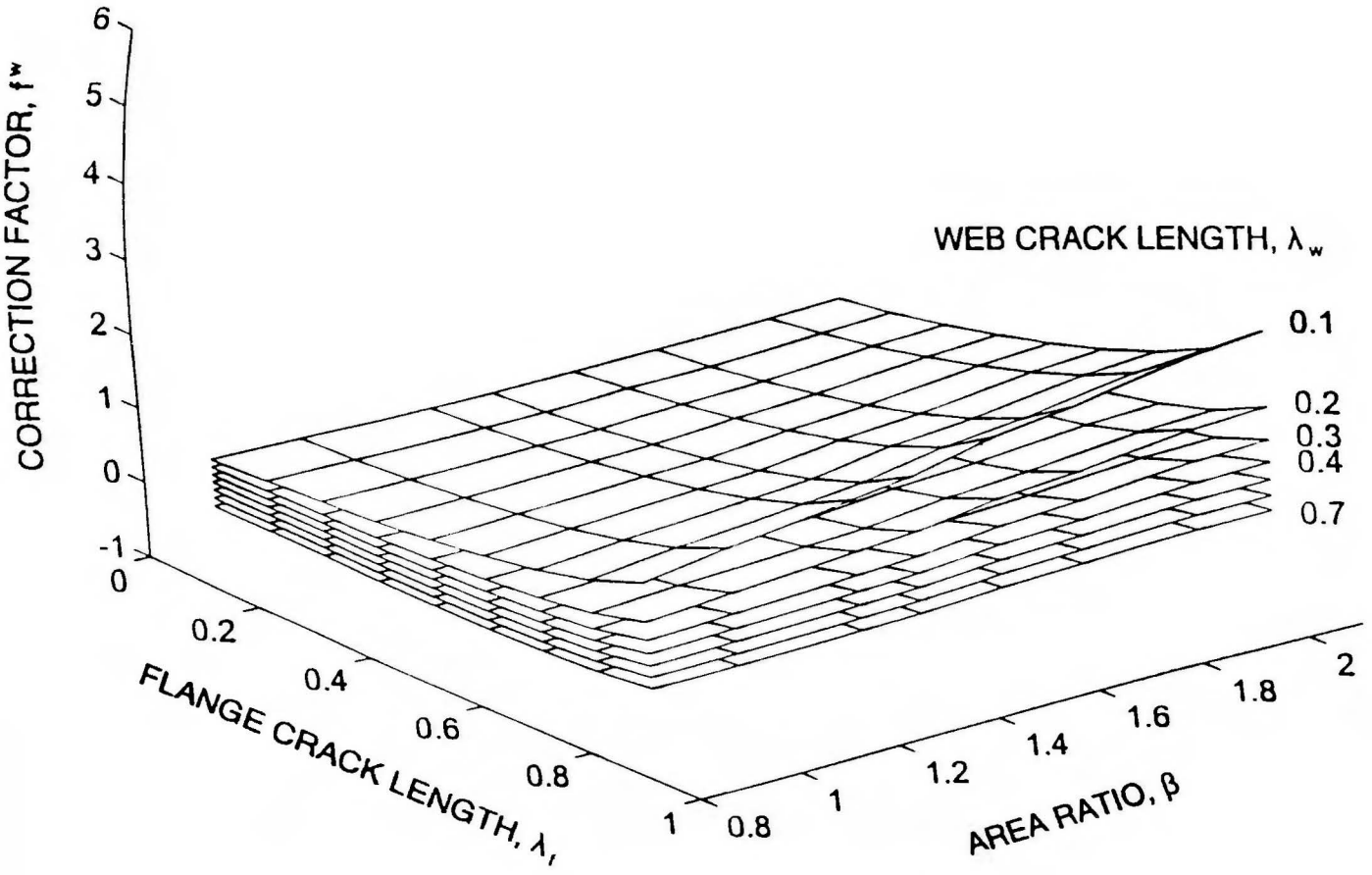

Figure 5.33. Correction factor for three-tip cracked I-beam under bending; web crack tip.

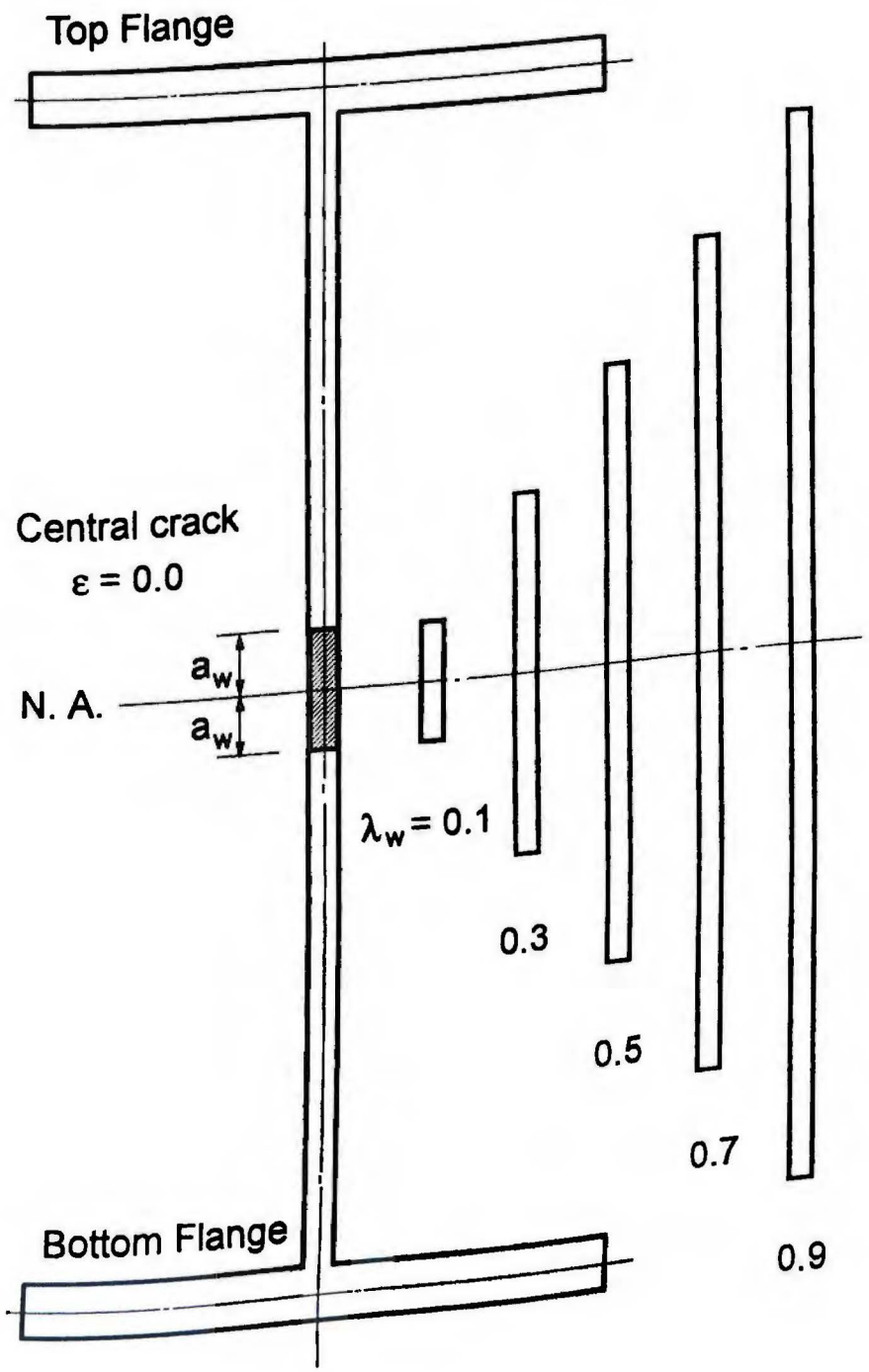

Figure 6.1. Crack tip positions for central crack in two-tip cracked I-beam.

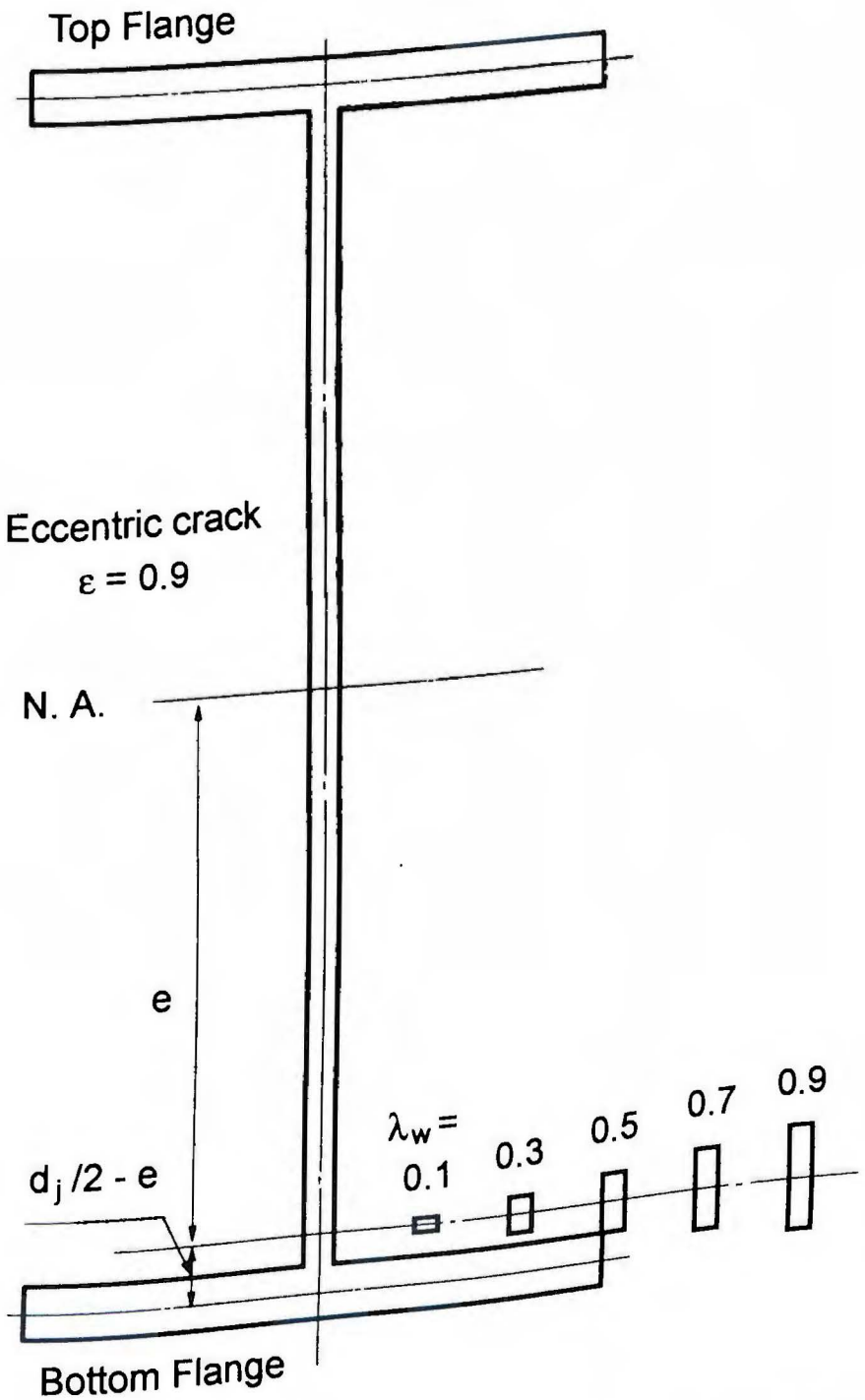

Figure 6.2. Crack tip positions for eccentric crack in two-tip cracked I-beam.

TWO-TIP CRACKED I-BEAM UNDER TENSION (β = 0.83, UPPER TIP)
Rank 2 Eqn 310 $z=a+bx+cy+dx^2+ey^2+fxy+gx^3+hy^3+ixy^2+jx^2y$
r^2=0.99644395 DF Adj r^2=0.99561696 FitStdErr=0.0017932712 Fstat=1369.9183
a=1.0012688 b=-0.033178023 c=-0.0052519952 d=0.098629911 e=0.2348546
f=-0.0055733149 g=-0.069786609 h=-0.088357688 i=-0.19196655 j=-0.022351272

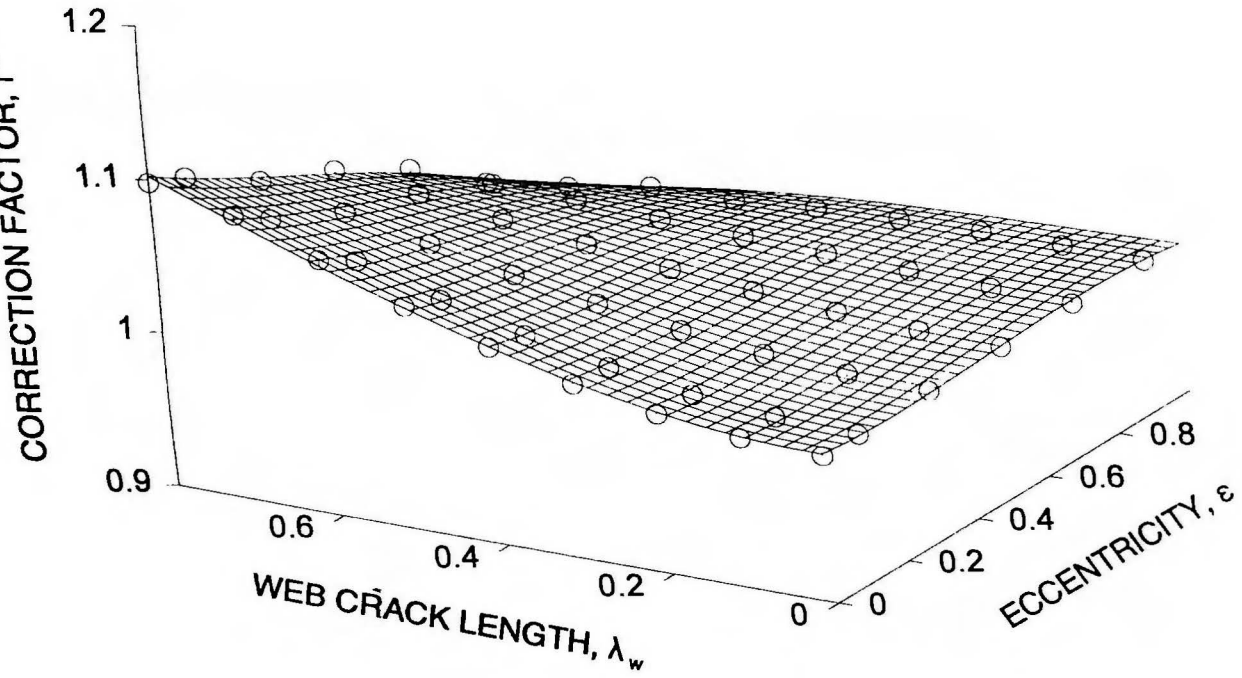

Figure 6.3. Preliminary fit for two-tip cracked I-beam under tension; W40 x 149, upper tip.

TWO-TIP CRACKED I-BEAM UNDER TENSION (β = 2.05, UPPER TIP)
Rank 1 Eqn 310 $z=a+bx+cy+dx^2+ey^2+fxy+gx^3+hy^3+ixy^2+jx^2y$
r^2=0.8872528 DF Adj r^2=0.86103253 FitStdErr=0.0044121576 Fstat=38.472623
a=1.0001551 b=0.0041146541 c=0.00095247605 d=-0.051742828 e=0.047985352
f=0.089452254 g=0.062369869 h=-0.11957134 i=0.070260188 j=-0.20039998

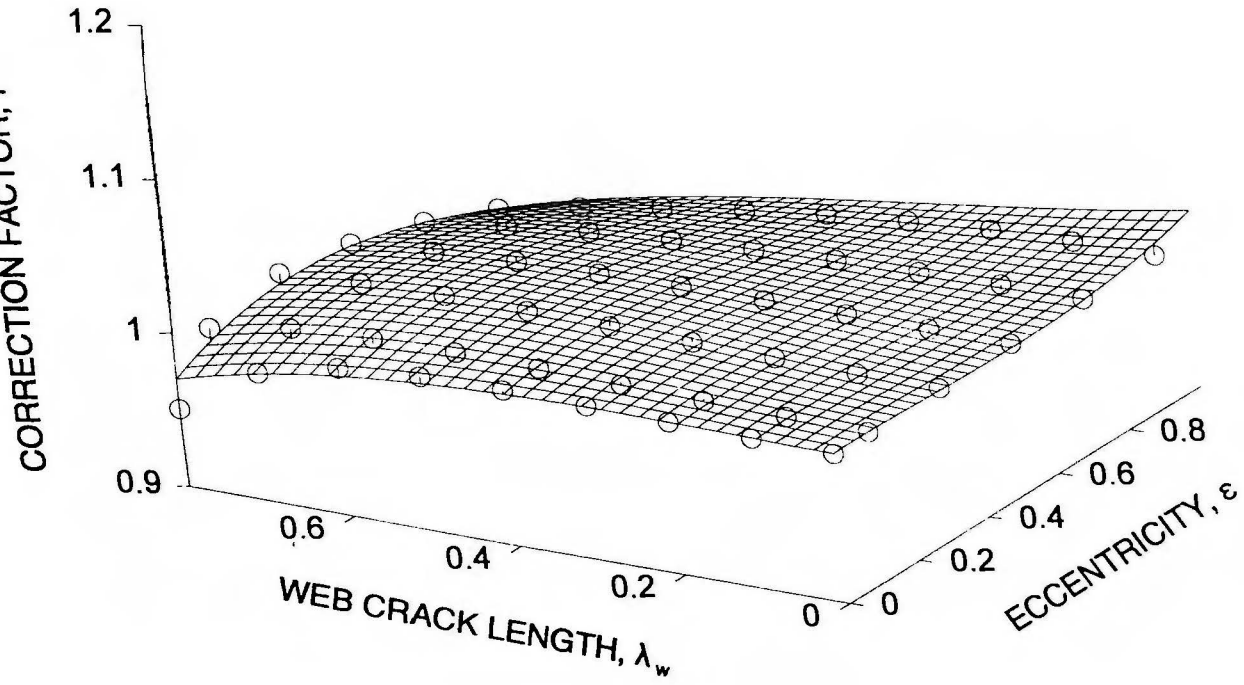

Figure 6.4. Preliminary fit for two-tip cracked I-beam under tension; W18 x 9 7, upper tip.

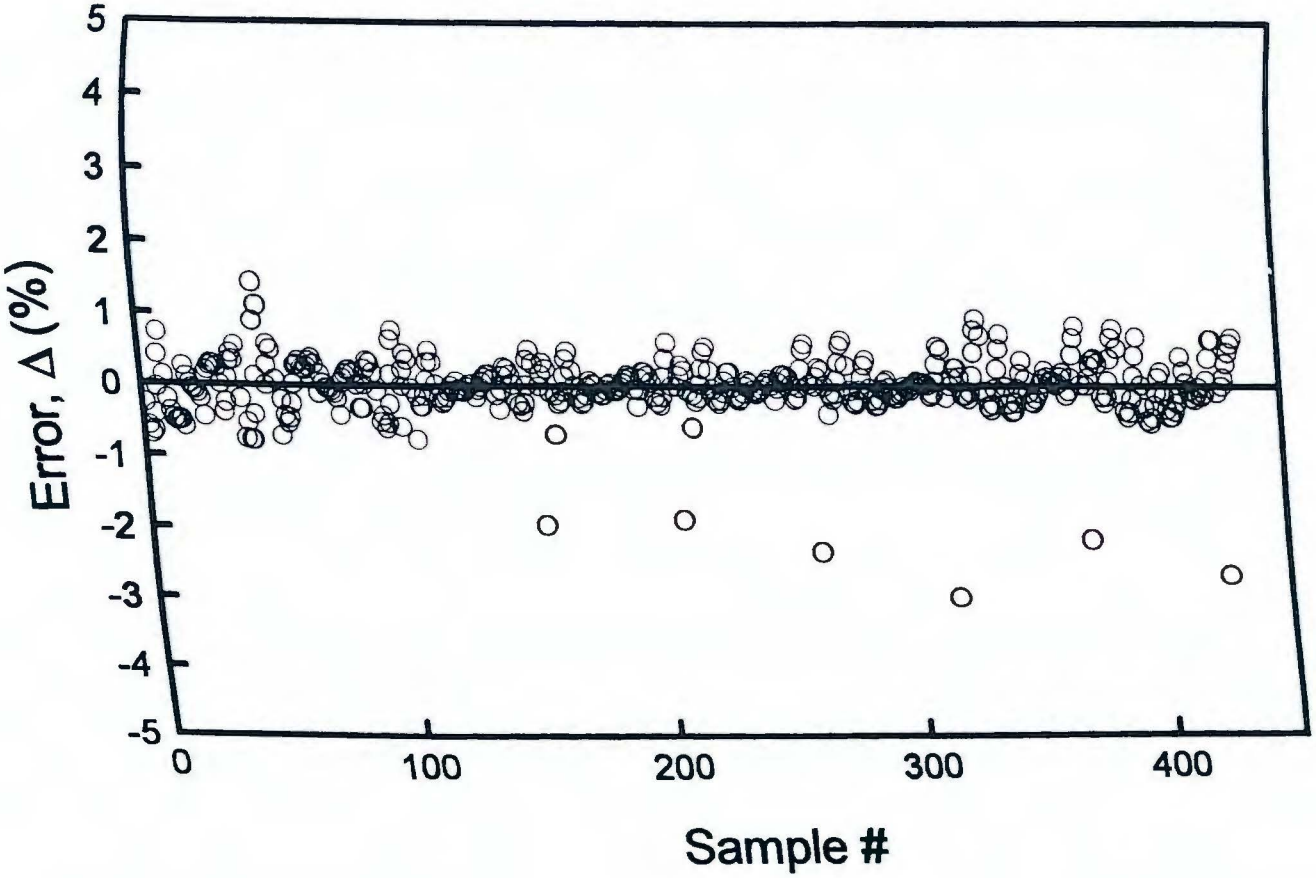

Figure 6.5. Error in predicting correction factor for two-tip cracked I-beam under tension; upper crack tip.

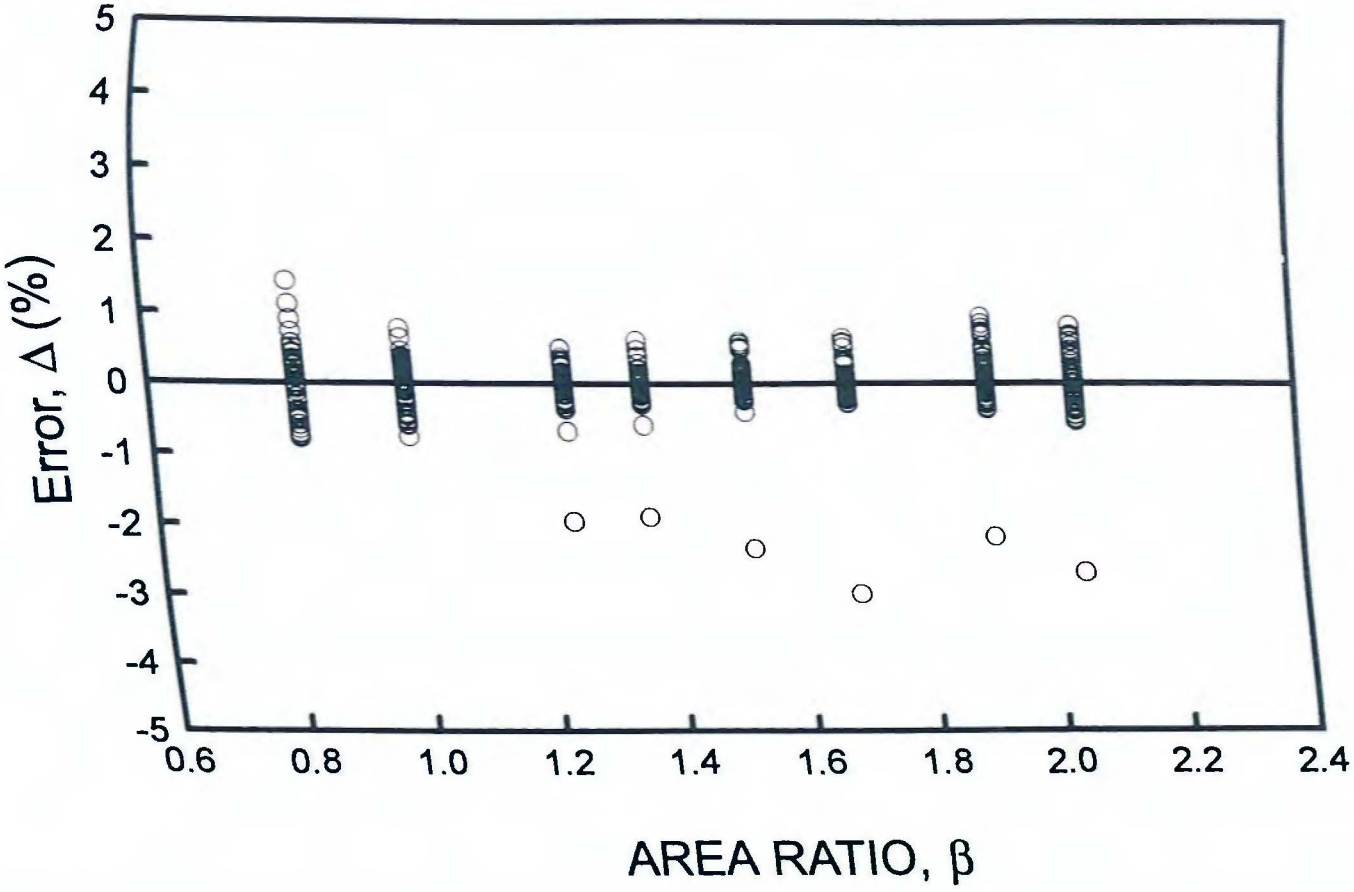

Figure 6.6. Variation in prediction error with area ratio; two-tip cracked I-beam under tension, upper crack tip.

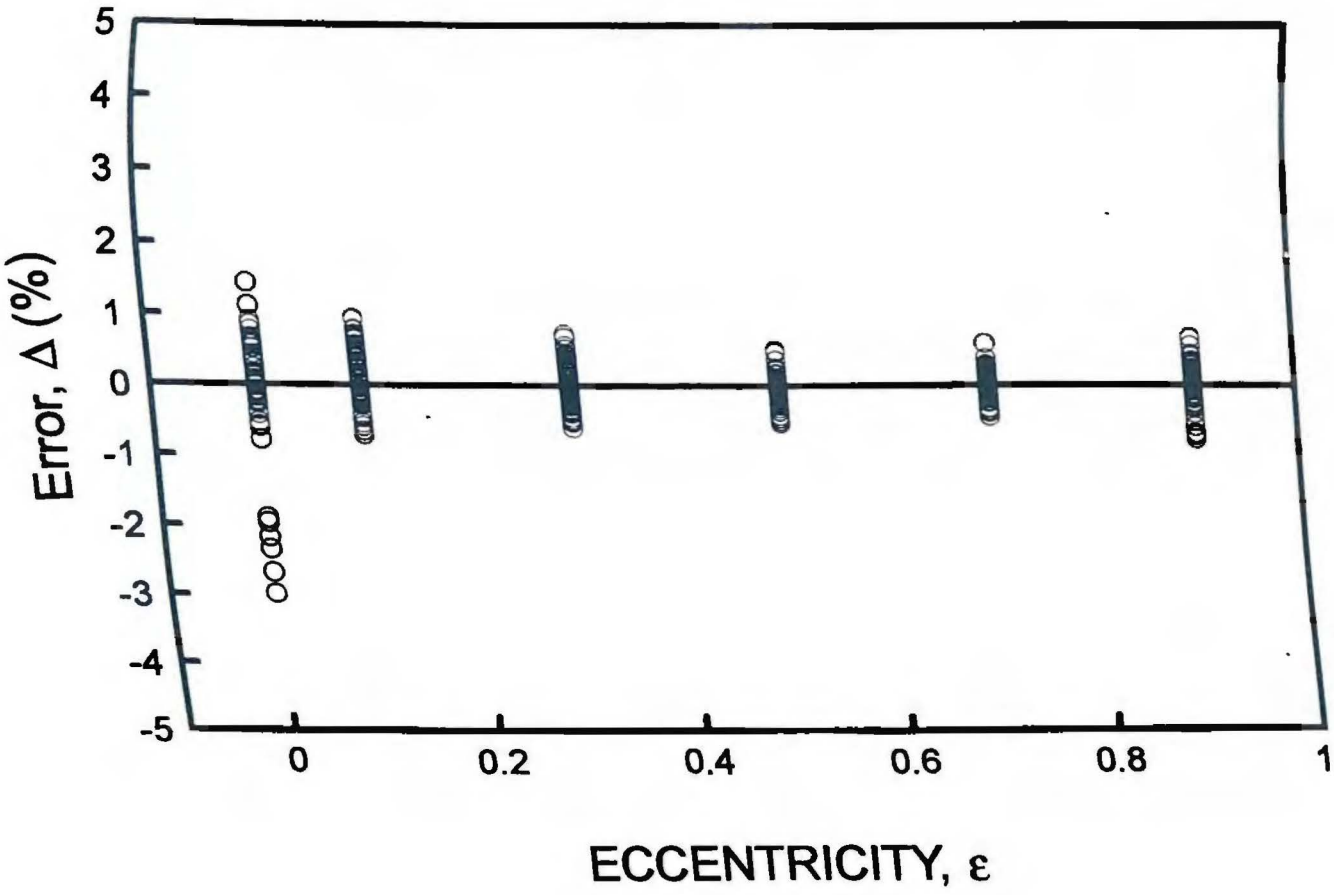

Figure 6.7. Variation in prediction error with eccentricity; two-tip cracked I-beam under tension, upper crack tip.

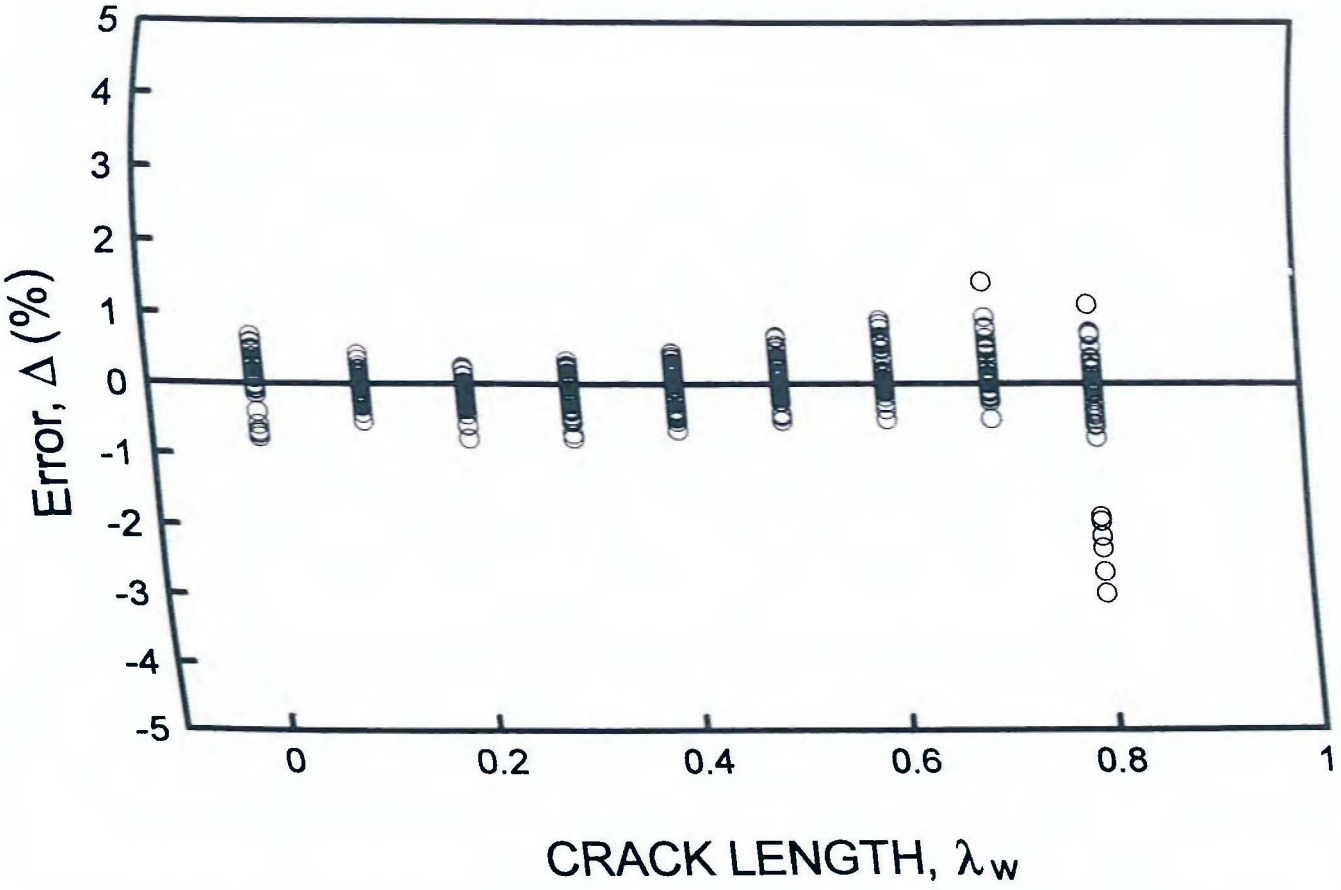

Figure 6.8. Variation in prediction error with web crack length; two-tip cracked I-beam under tension, upper crack tip.

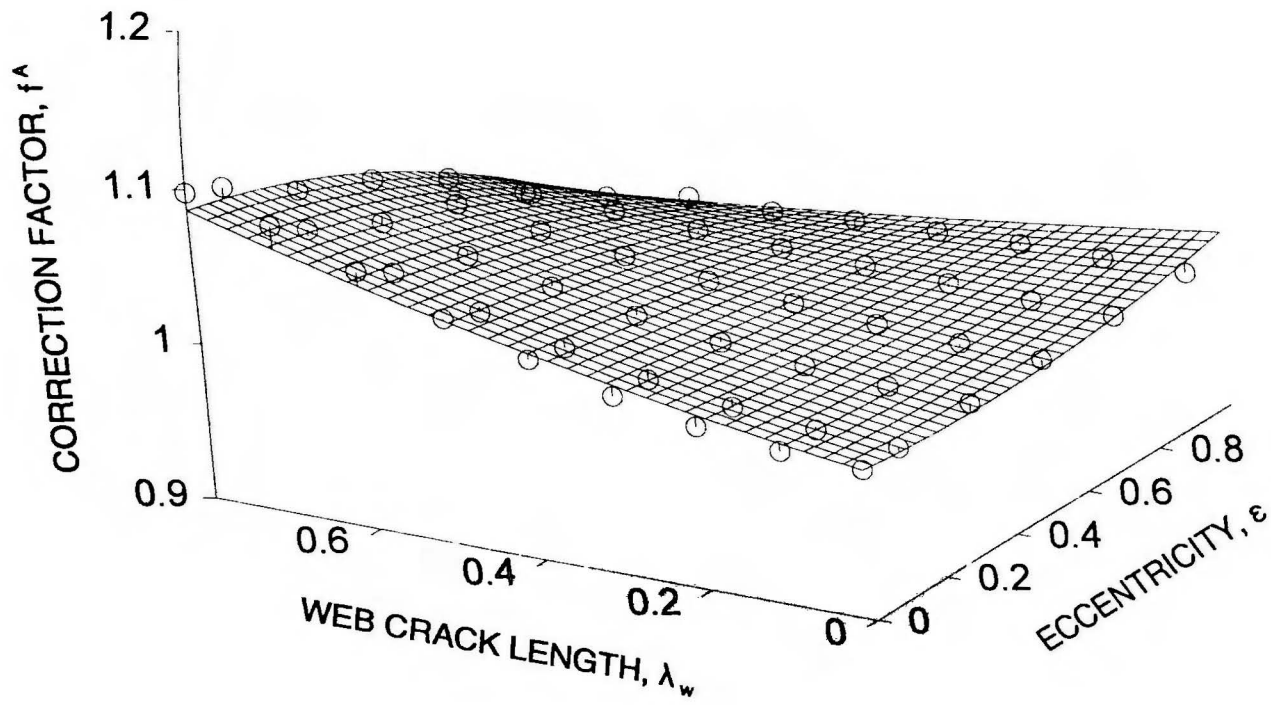

Figure 6.9. Comparison of predicted and calculated correction factors for two-tip cracked I-beam under tension; W40 x 149, upper tip.

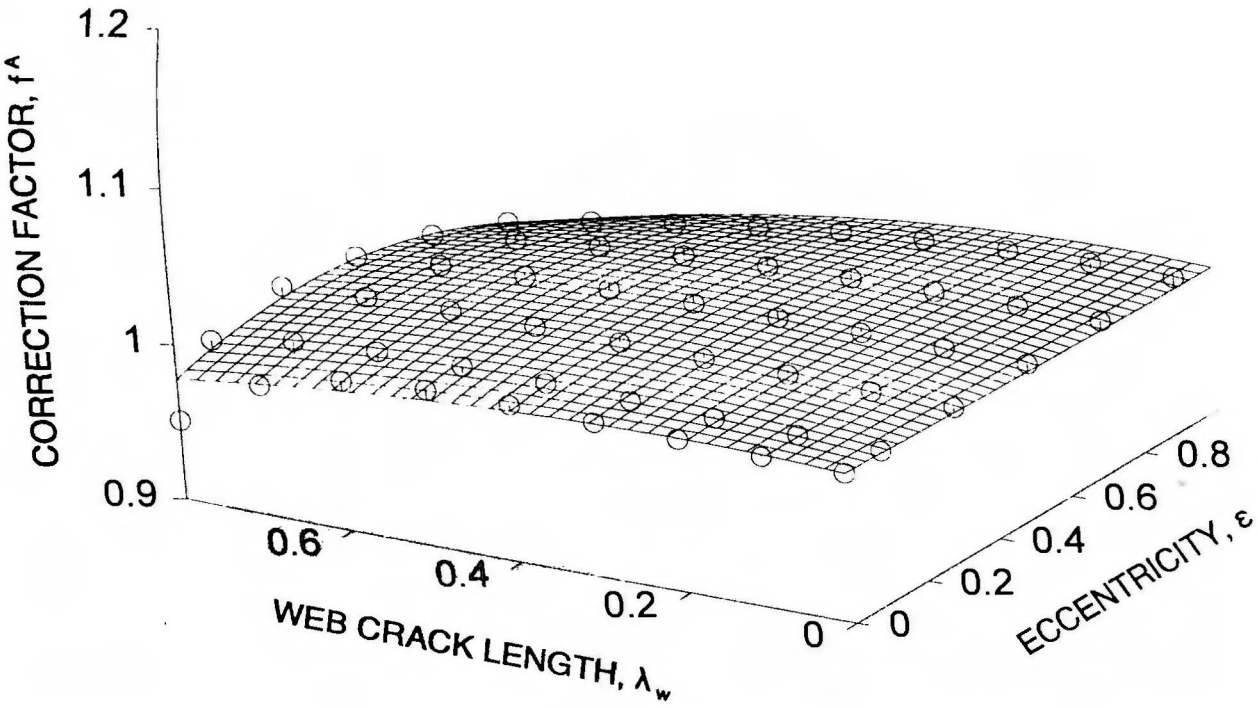

Figure 6.10. Comparison of predicted and calculated correction factors for two-tip cracked I-beam under tension; W18 x 9 7, upper tip.

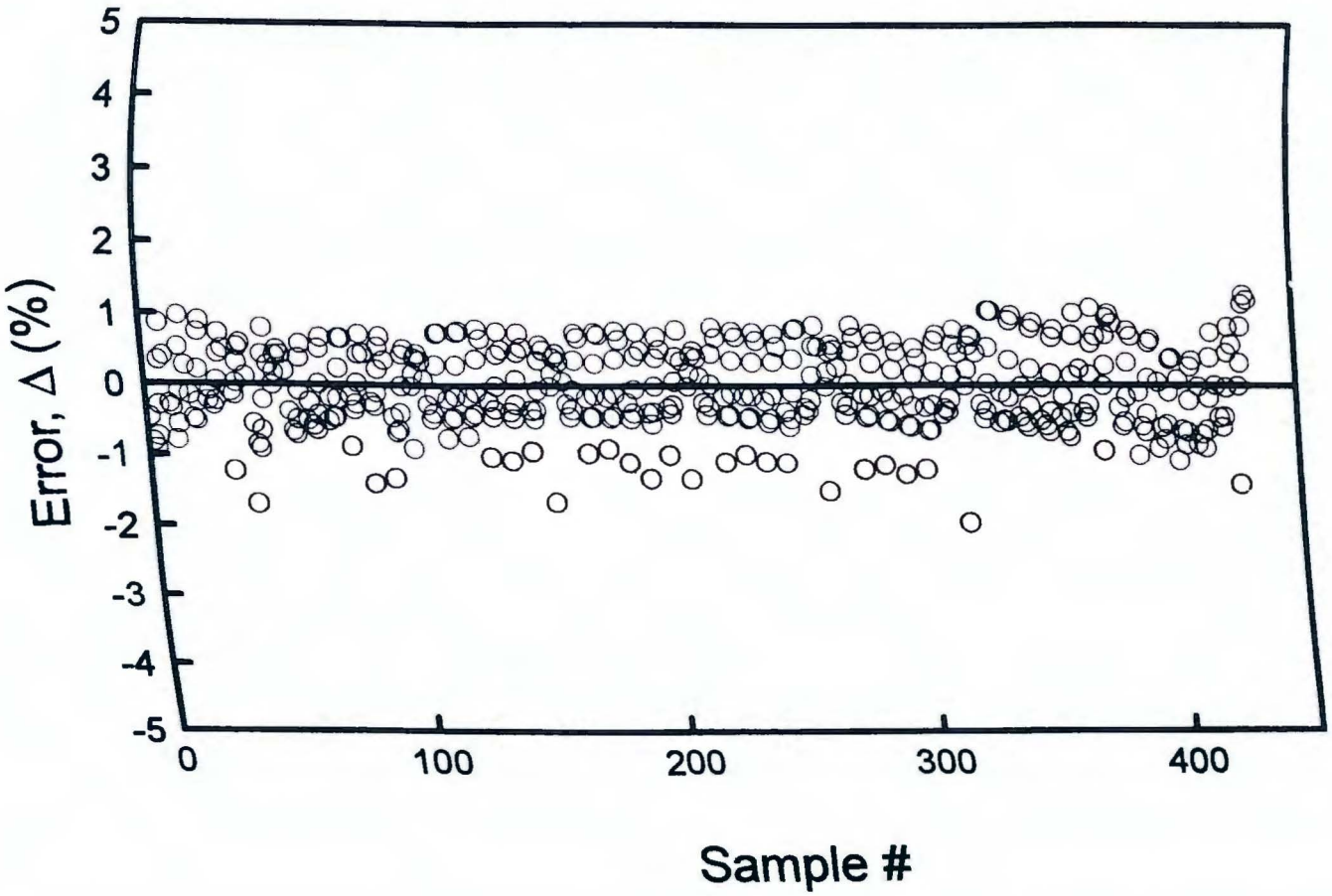

Figure 6.11. Error in predicting correction factor for two-tip cracked I-beam under tension; lower crack tip.

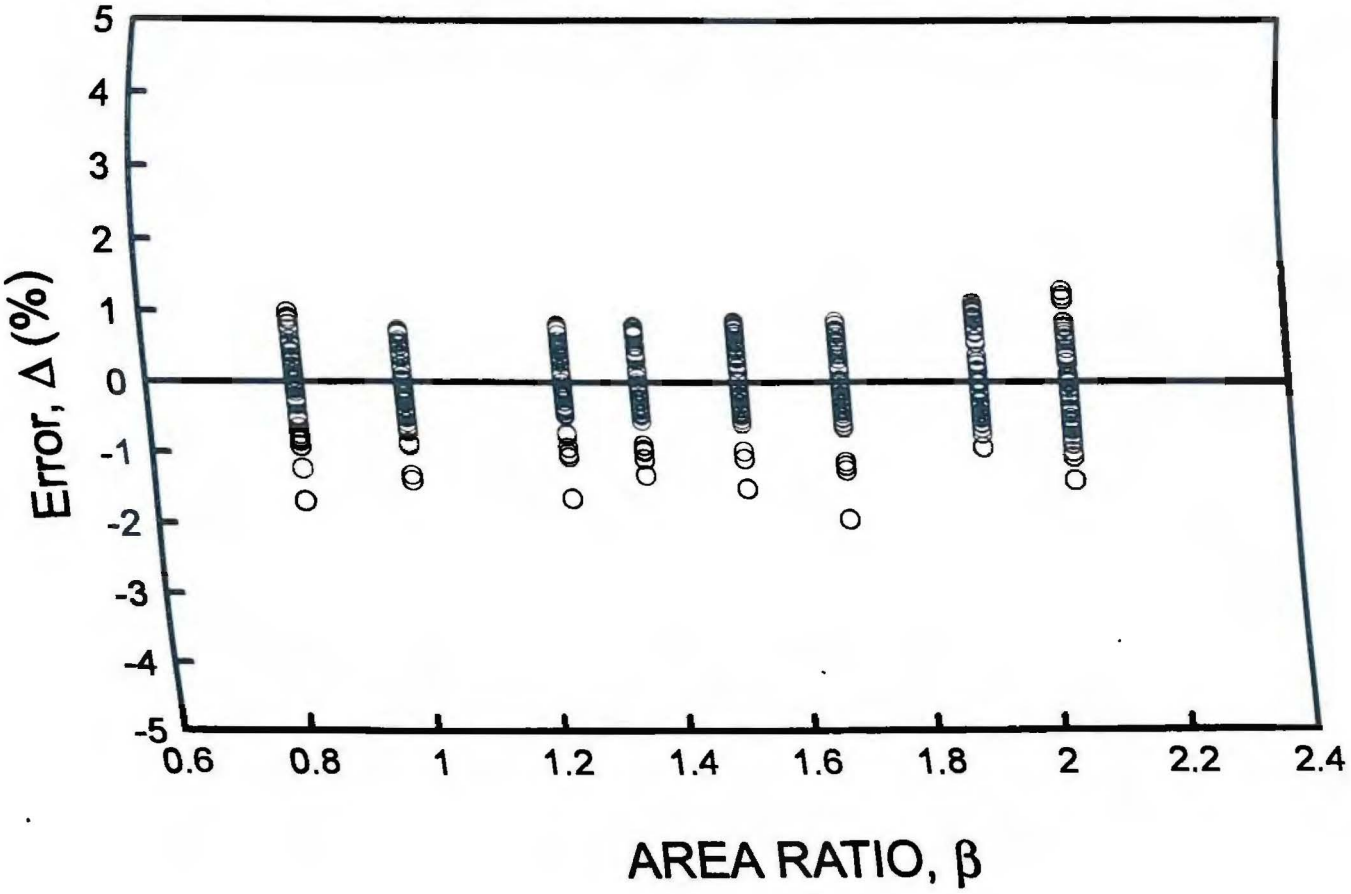

Figure 6.12. Variation in prediction error with area ratio; two-tip cracked I-beam under tension, lower crack tip.

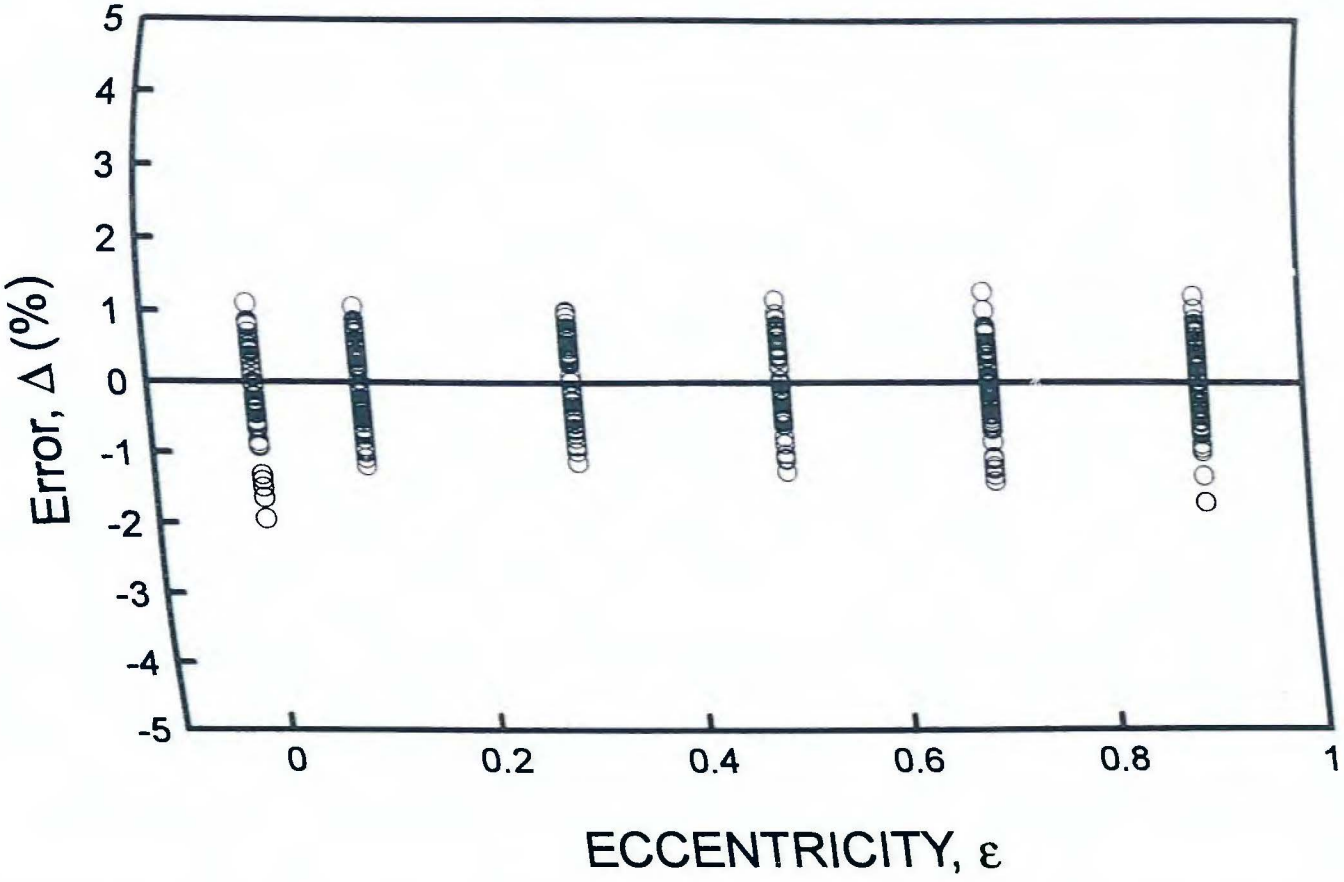

Figure 6.13. Variation in prediction error with eccentricity; two-tip cracked I-beam under tension, lower crack tip.

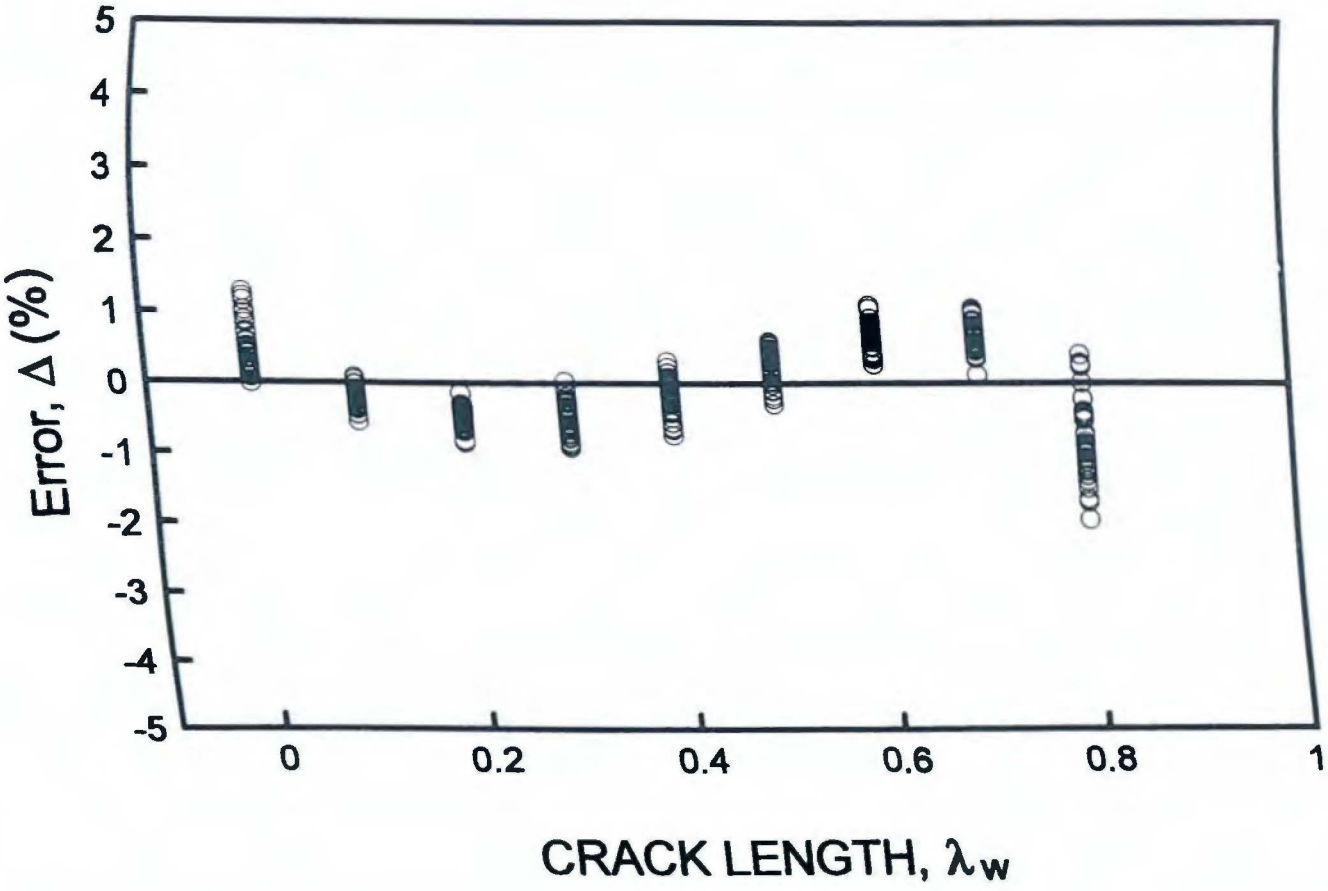

Figure 6.14. Variation in prediction error with web crack length; two-tip cracked I-beam under tension, lower crack tip.

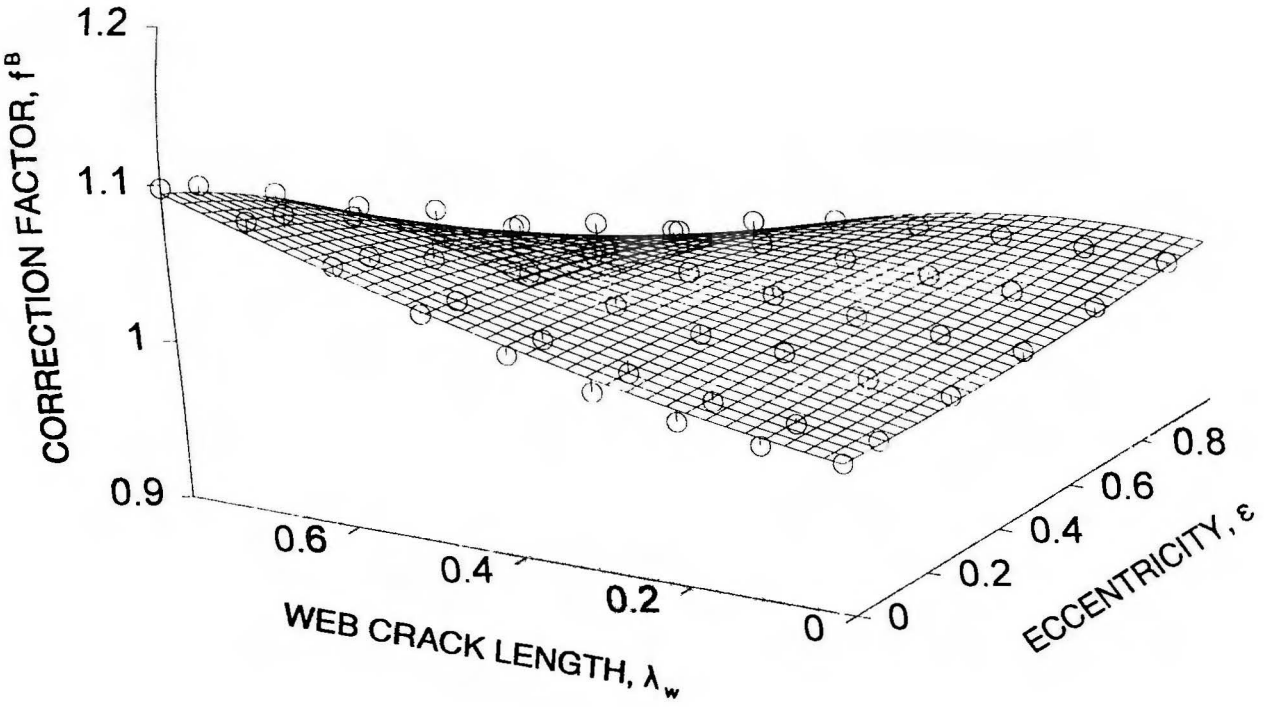

Figure 6.15. Comparison of predicted and calculated correction factors for two-tip cracked I-beam under tension; W40 x 149, lower tip.

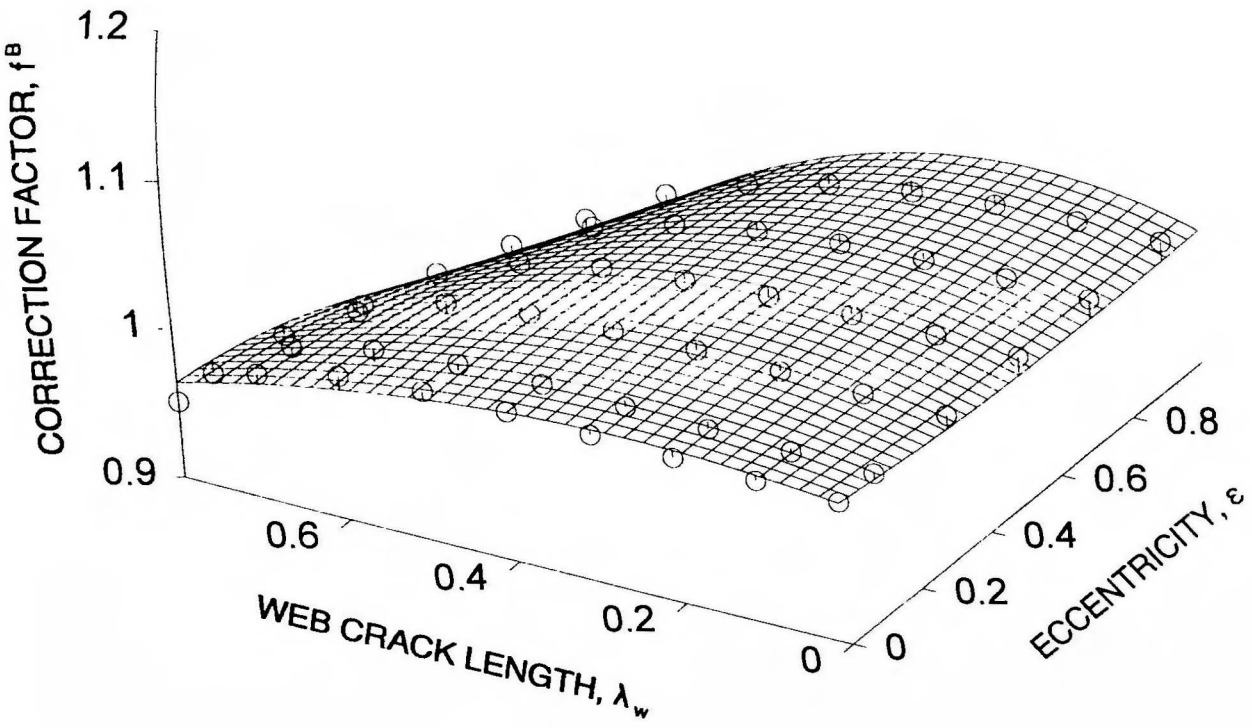

Figure 6.16. Comparison of predicted and calculated correction factors for two-tip cracked I-beam under tension; W18 x 9 7, lower tip.

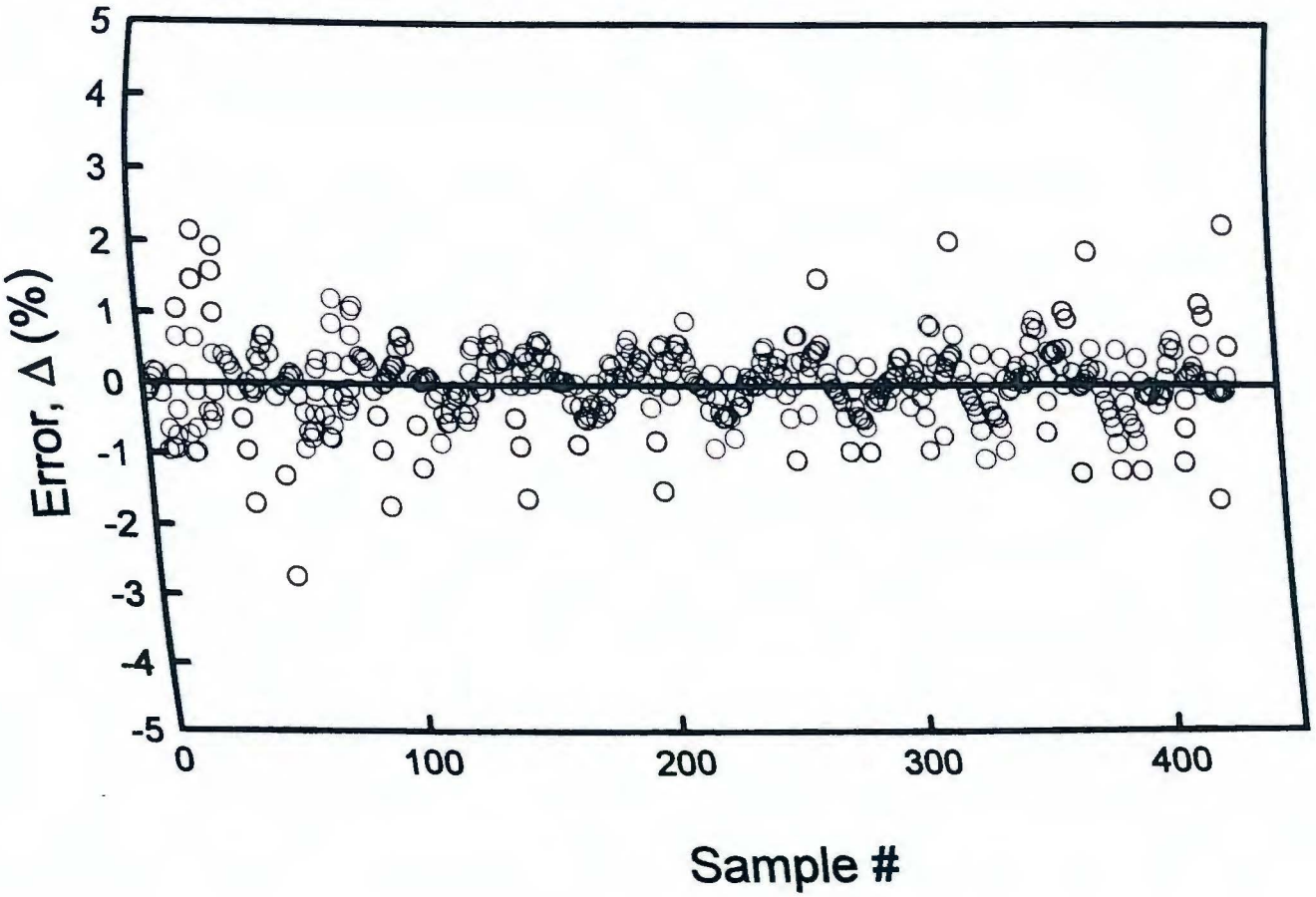

Figure 6.17. Error in predicting correction factor for two-tip cracked I-beam under bending; upper crack tip.

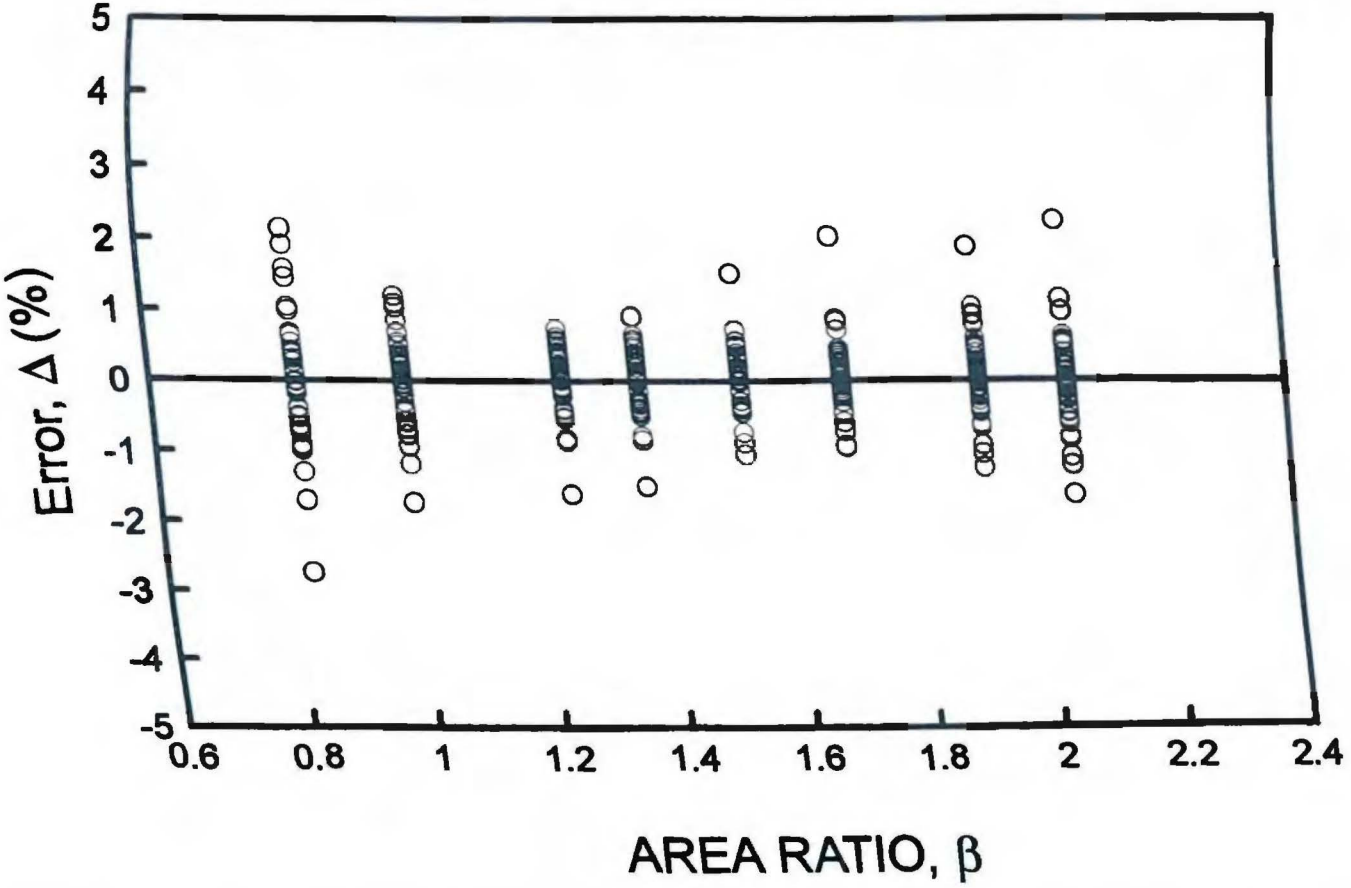

Figure 6.18. Variation in prediction error with area ratio; two-tip cracked I-beam under bending, upper crack tip.

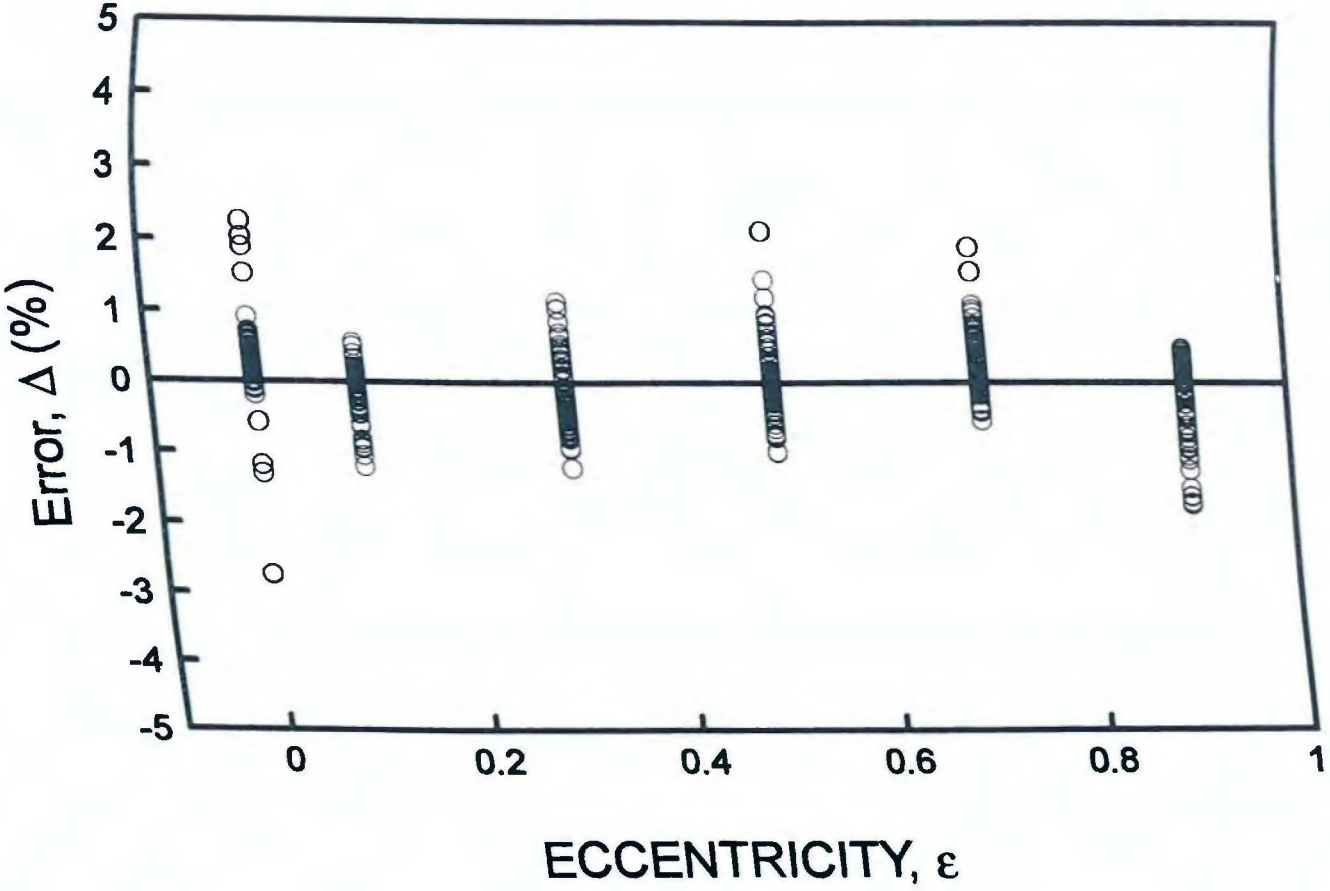

Figure 6.19. Variation in prediction error with eccentricity; two-tip cracked I-beam under bending, upper crack tip.

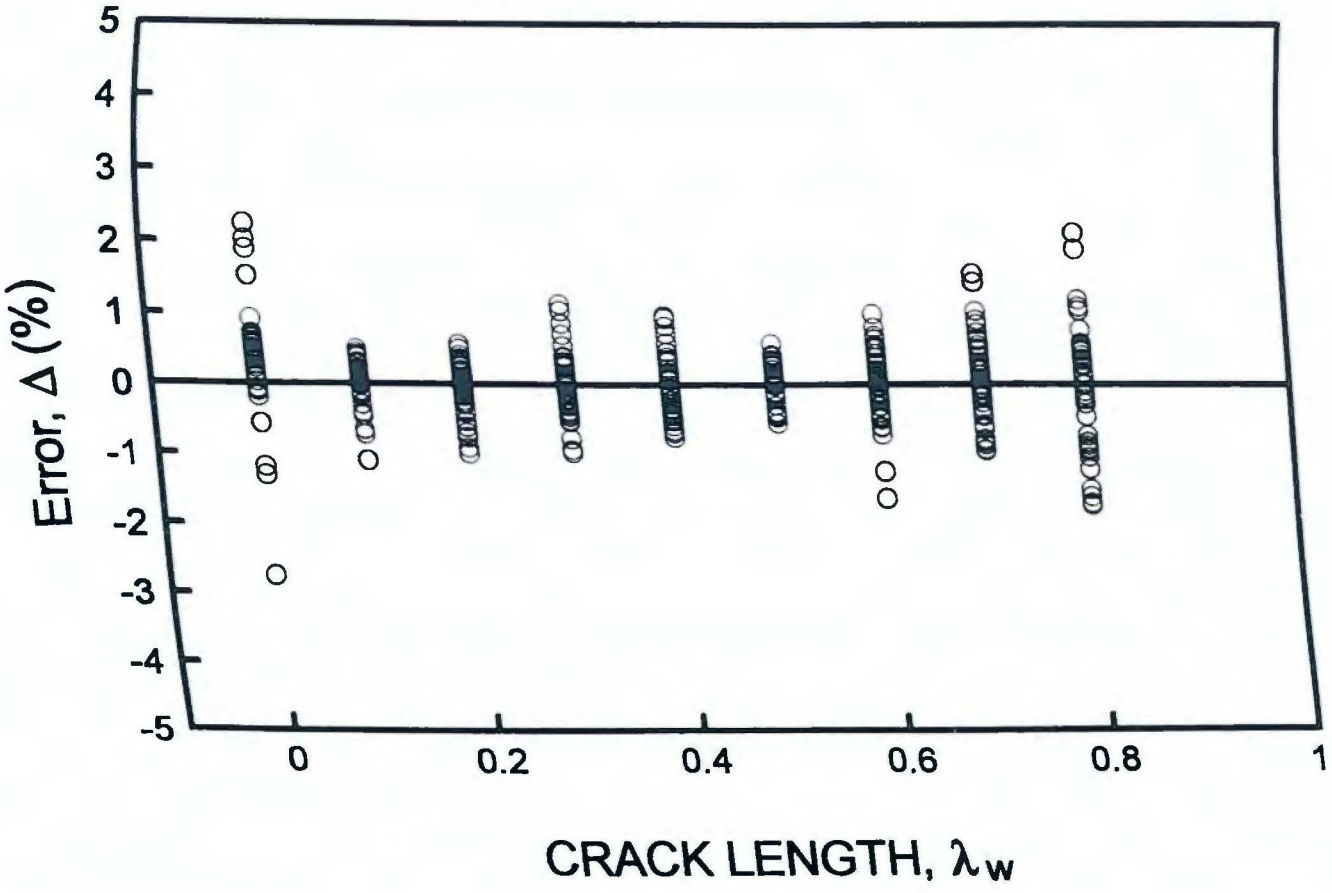

Figure 6.20. Variation in prediction error with web crack length; two-tip cracked I-beam under bending, upper crack tip.

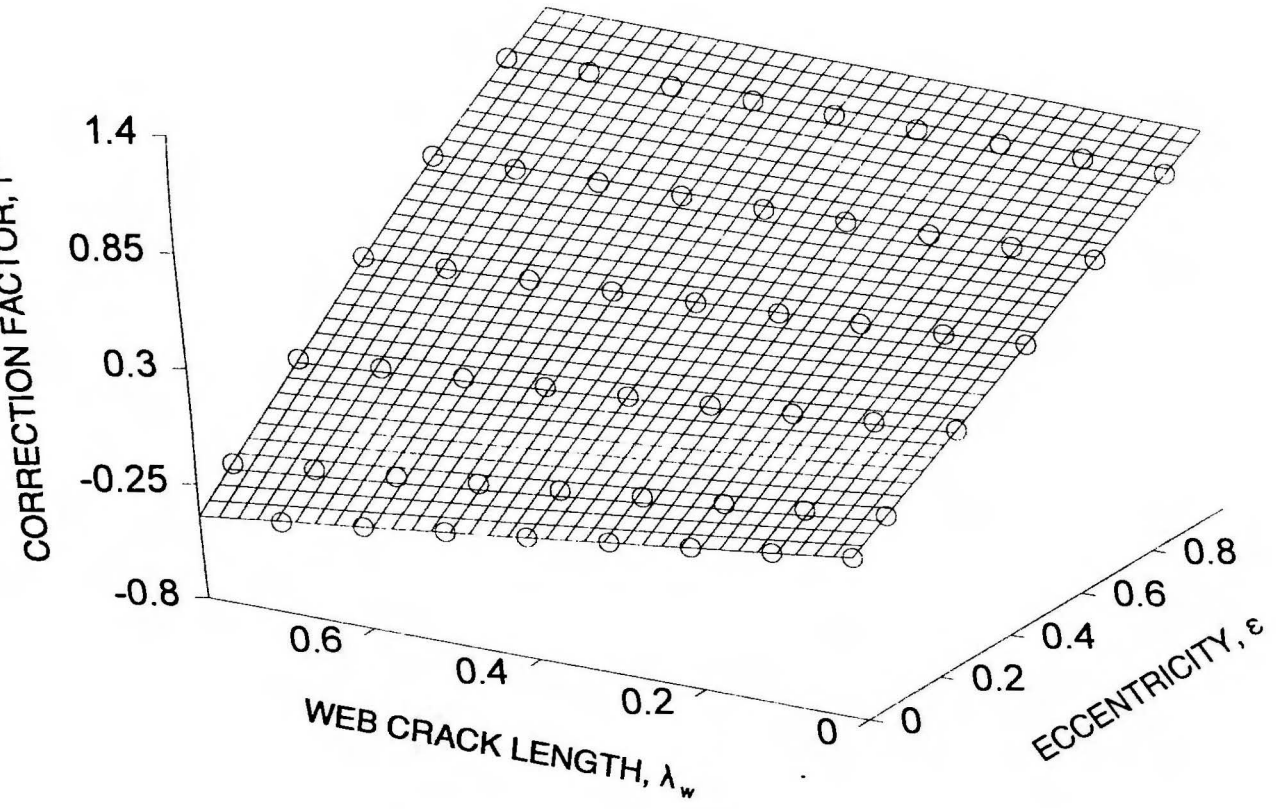

Figure 6.21. Comparison of predicted and calculated correction factors for two-tip cracked I-beam under bending; W40 x 149, upper tip.

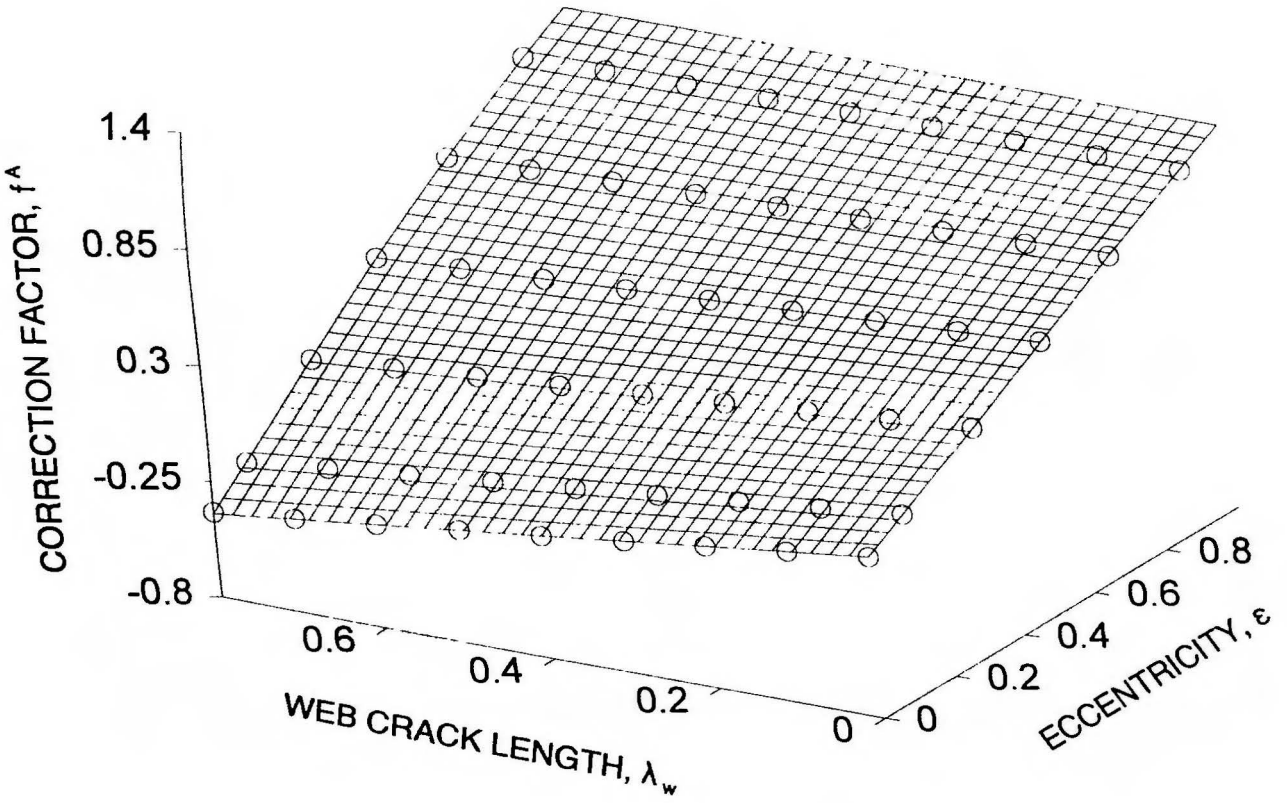

Figure 6.22. Comparison of predicted and calculated correction factors for two-tip cracked I-beam under bending; W18 x 9 7, upper tip.

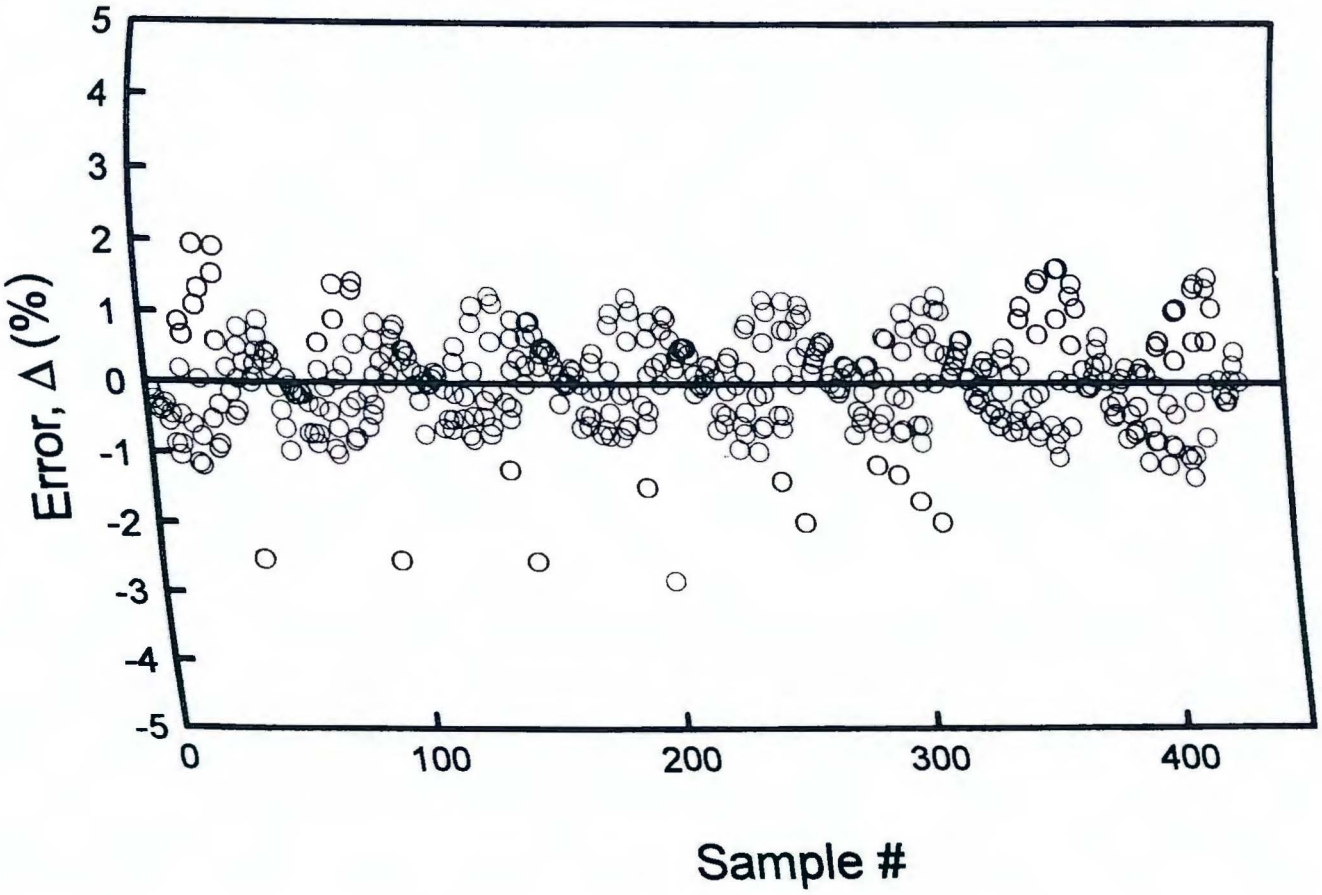

Figure 6.23. Error in predicting correction factor for two-tip cracked I-beam under bending; lower crack tip.

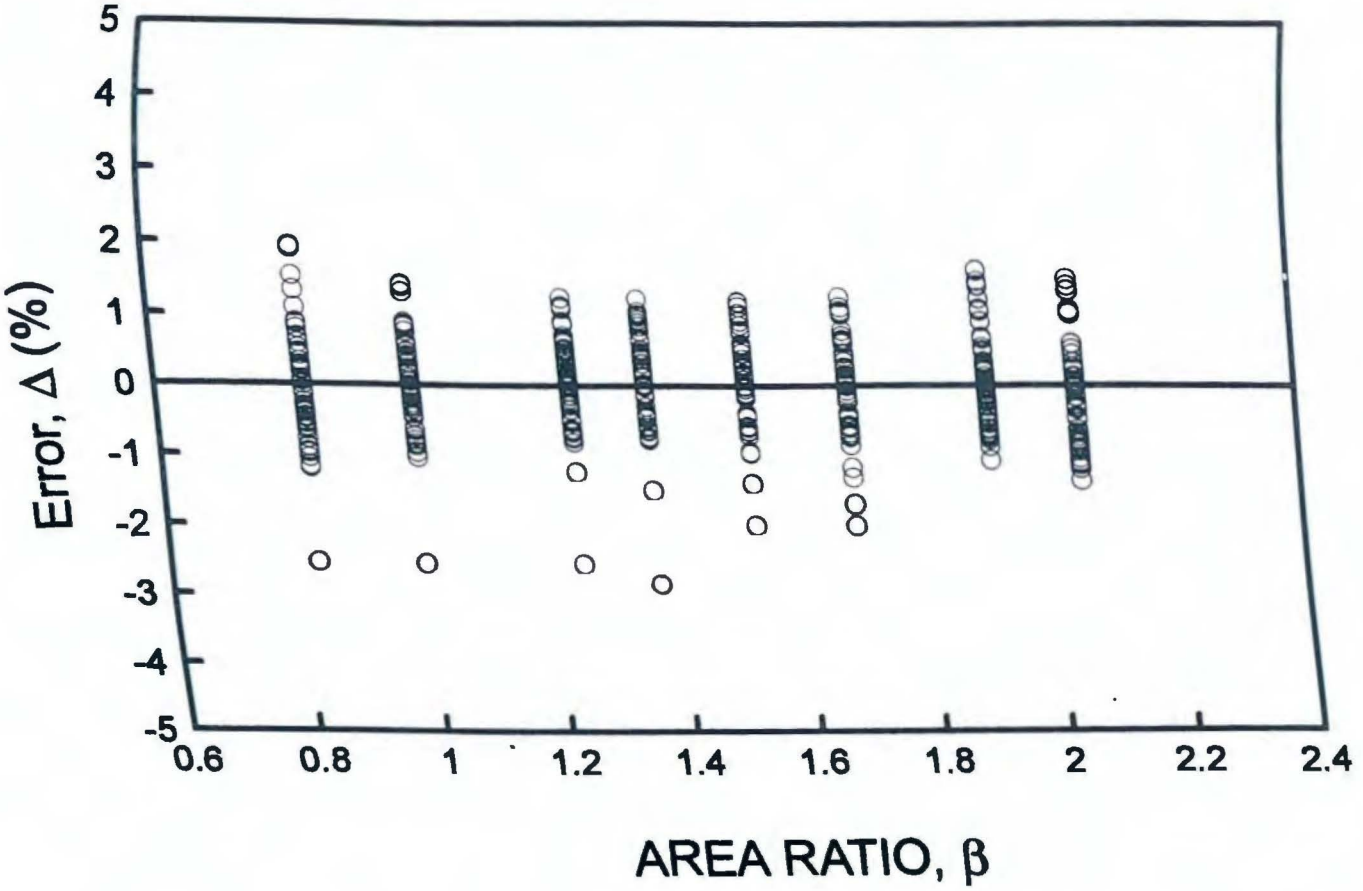

Figure 6.24. Variation in prediction error with web crack length; two-tip cracked I-beam under bending, lower crack tip.

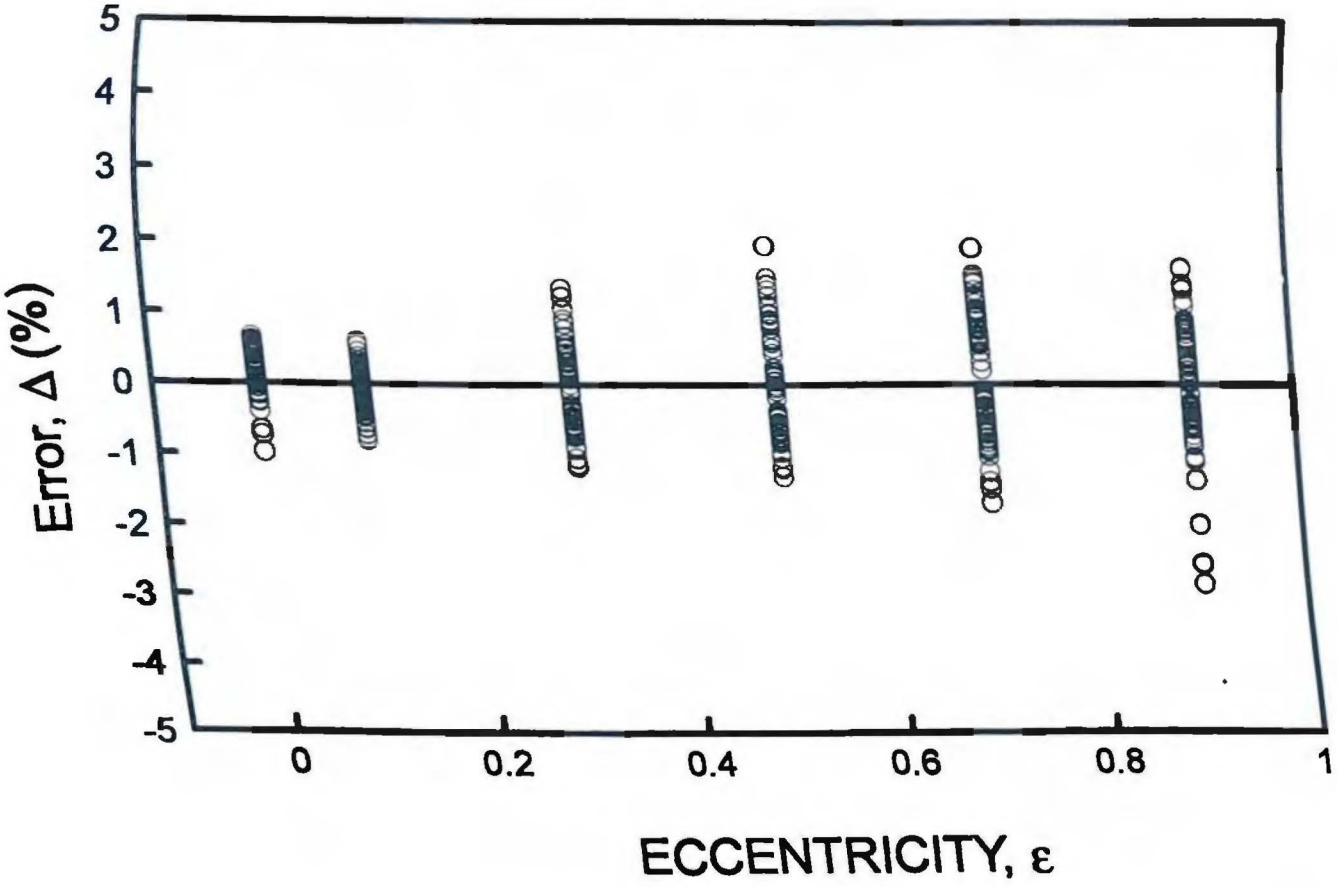

Figure 6.25. Variation in prediction error with eccentricity; two-tip cracked I-beam under bending, lower crack tip.

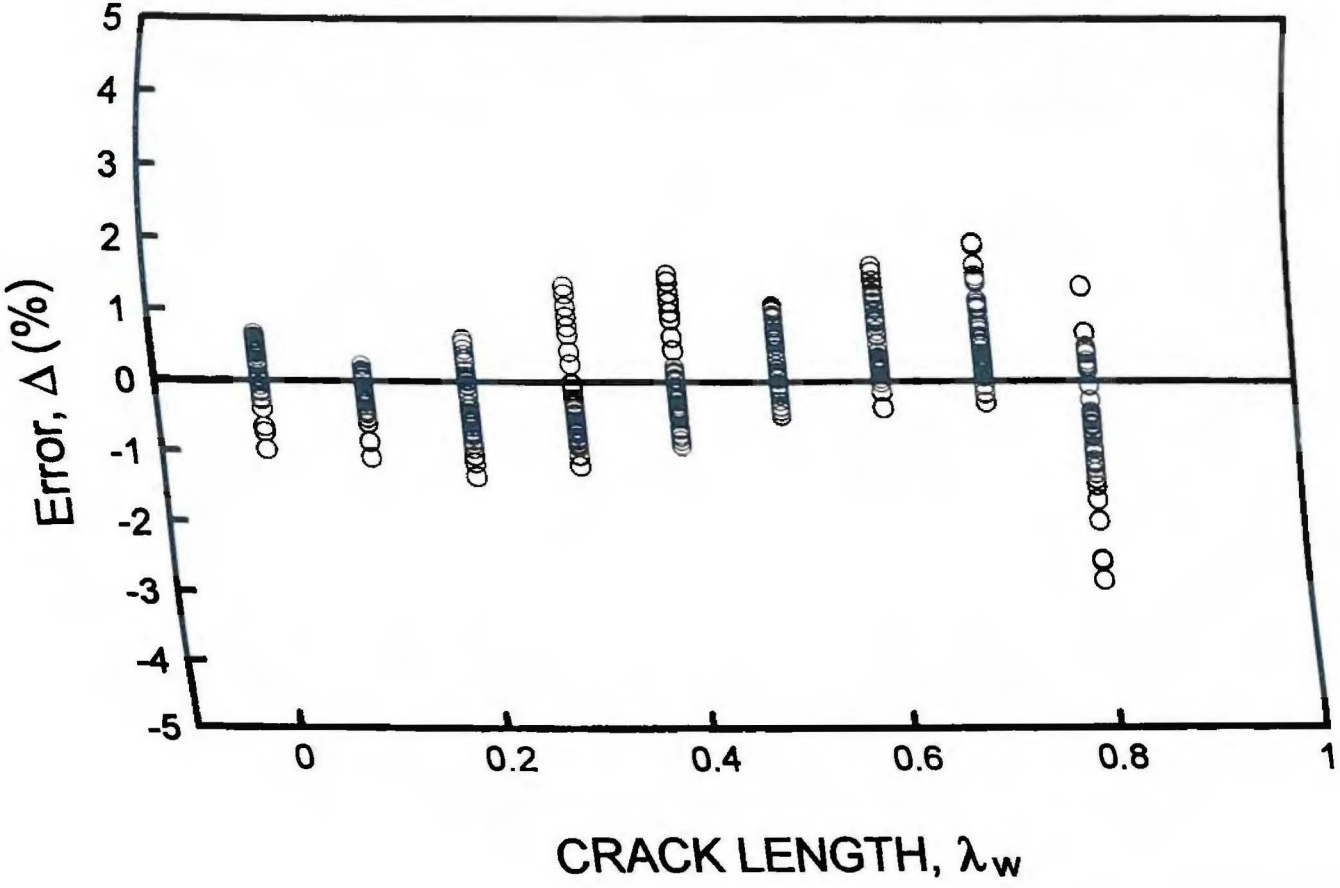

Figure 6.26. Variation in prediction error with web crack length; two-tip cracked I-beam under bending, lower crack tip.

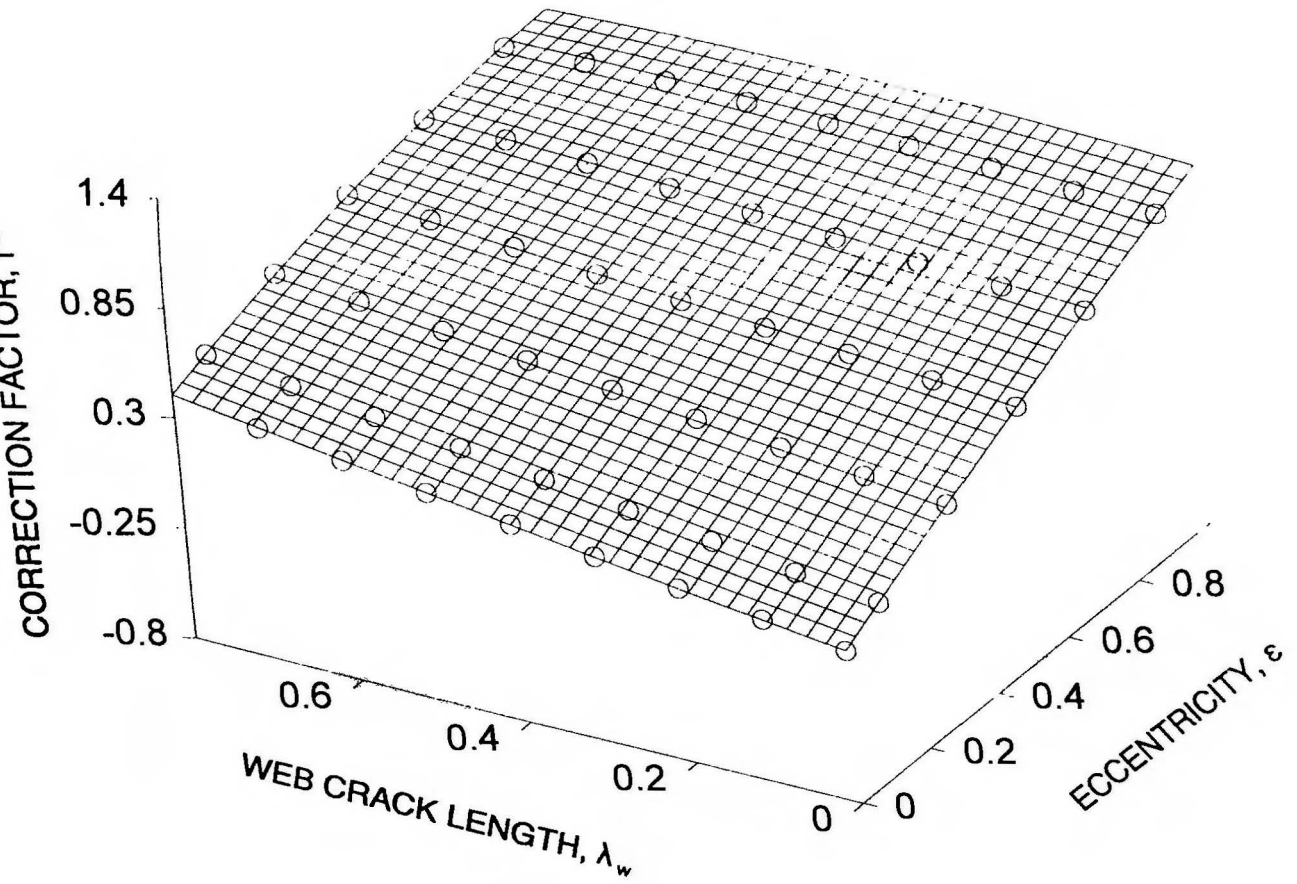

Figure 6.27. Comparison of predicted and calculated correction factors for two-tip cracked I-beam under bending; W40 x 149, lower tip.

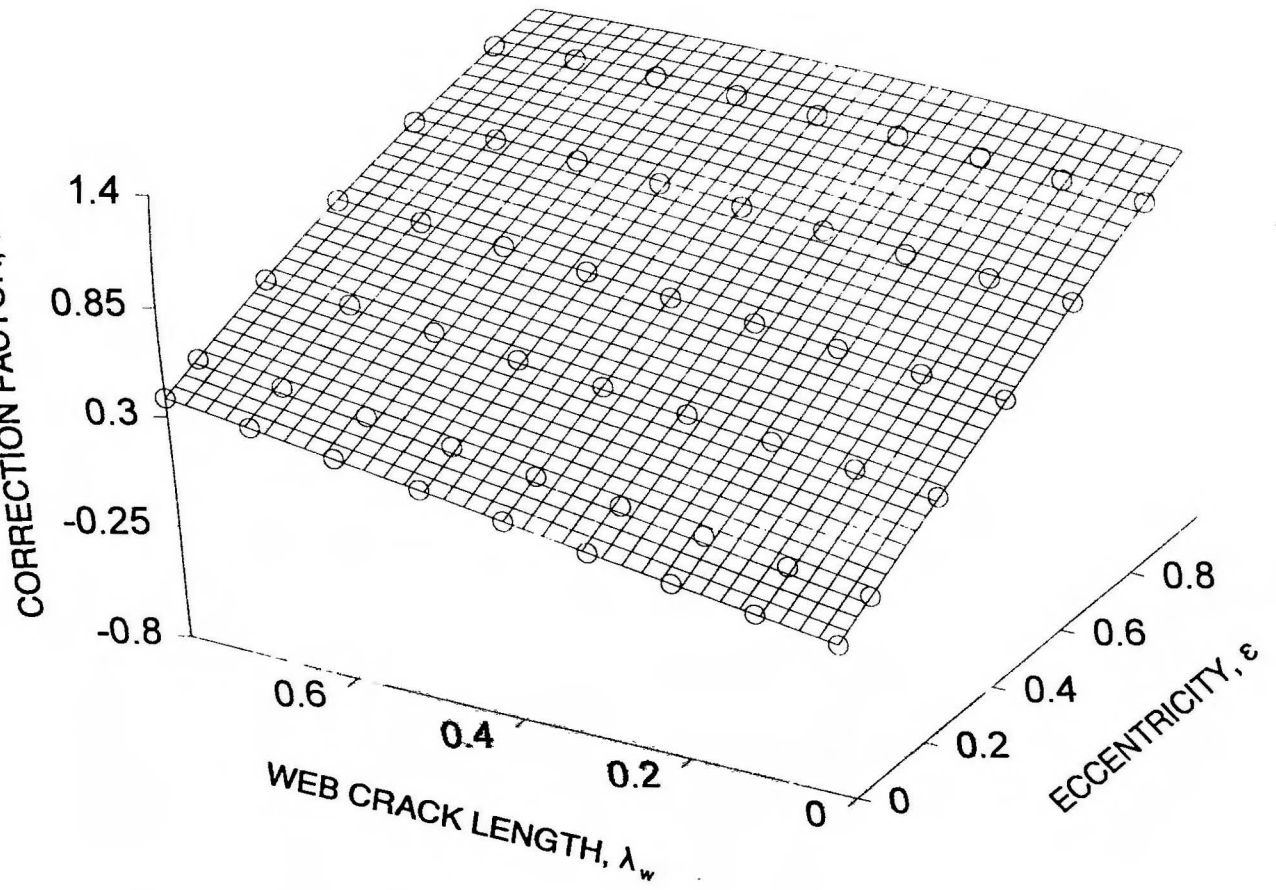

Figure 6.28. Comparison of predicted and calculated correction factors for two-tip cracked I-beam under bending; W18 x 9 7, lower tip.

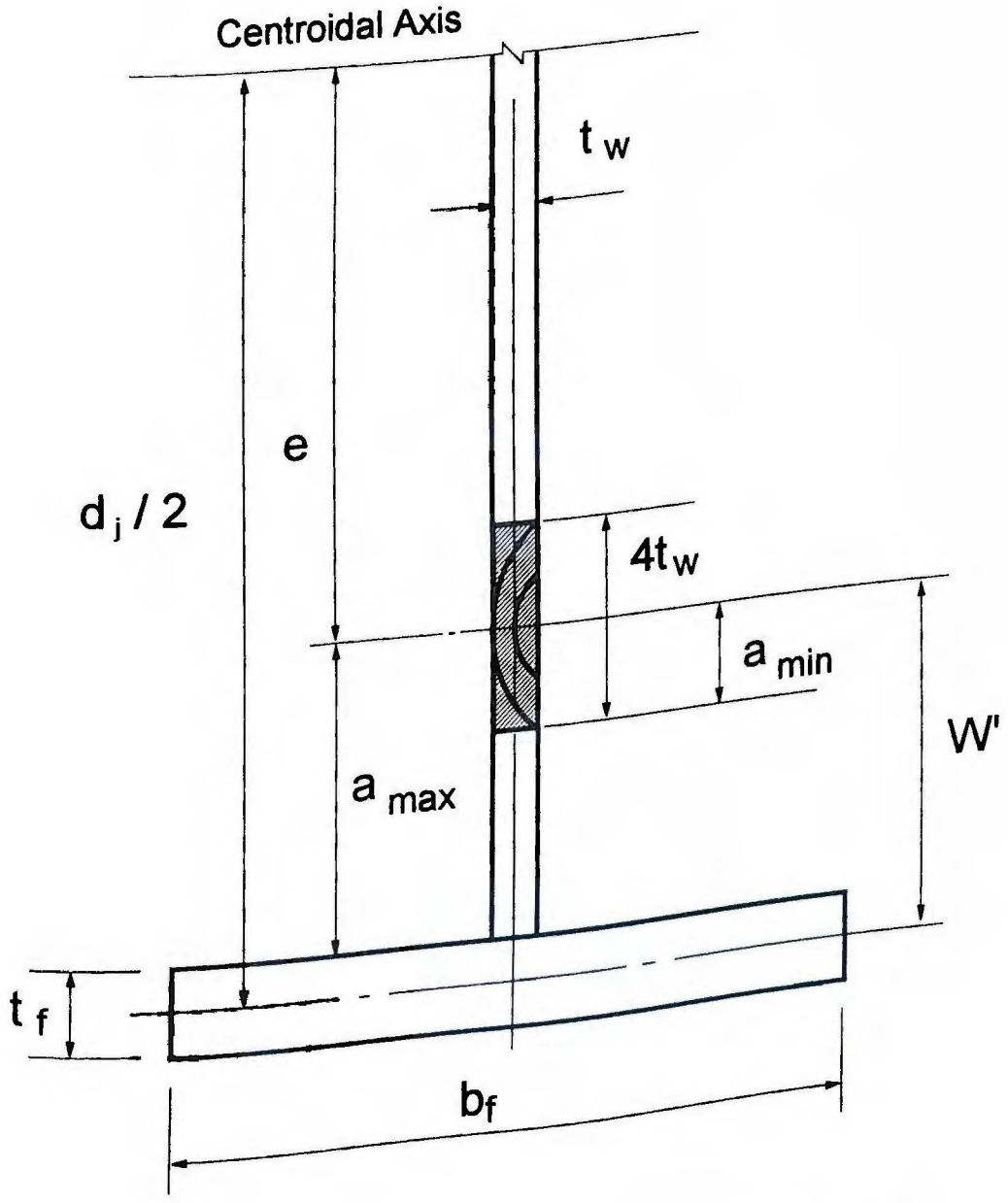

$a_{min} = 2t_w$ $\quad a_{max} = W' - t_f/2 = d_j/2 - e - t_f/2$

$W' = d_j/2 - e$

Figure 6.29. Maximum and minimum web crack lengths for two-tip cracked I-beam.

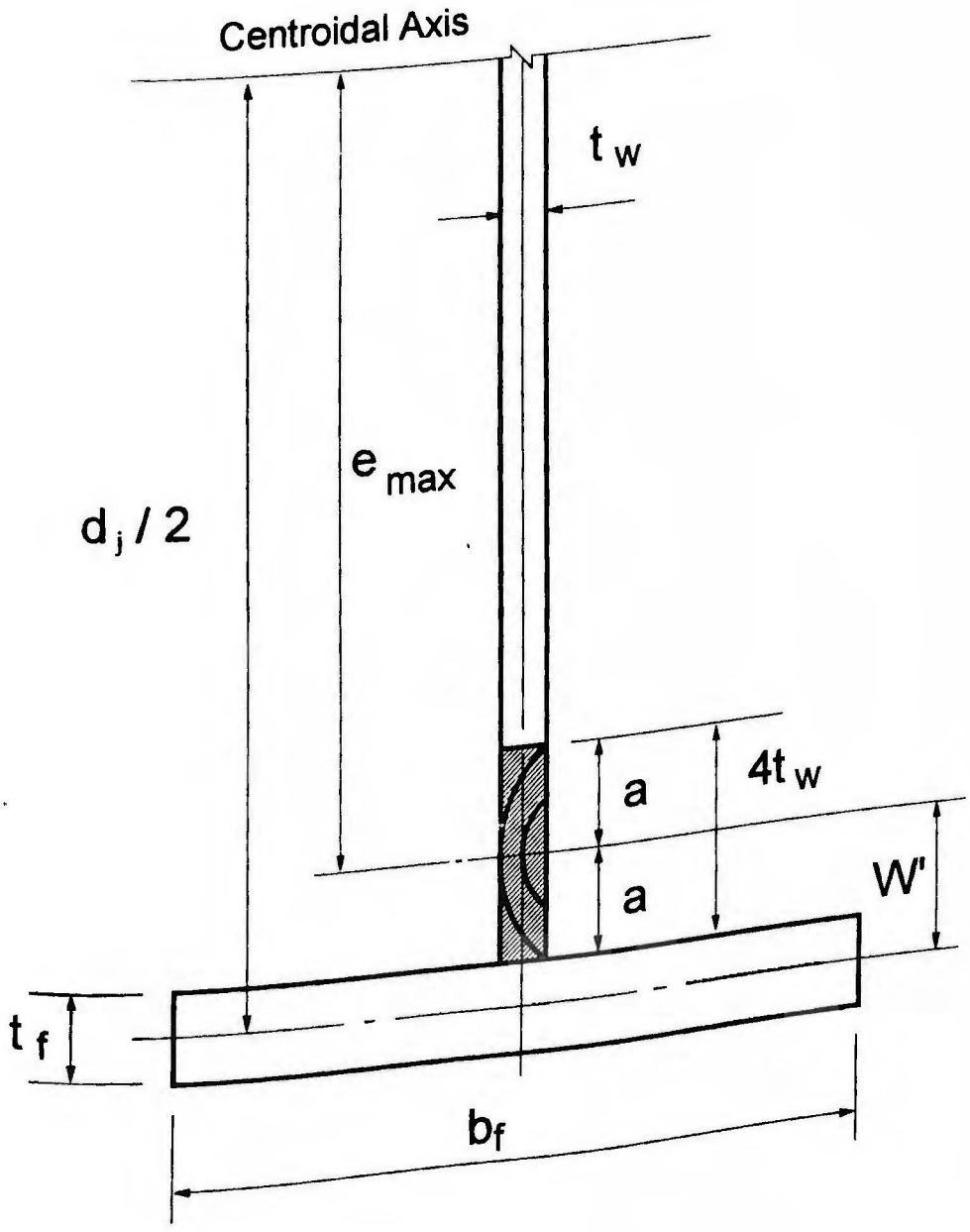

$$e_{max} = d_j/2 - t_f/2 - 2t_w$$

$$a_{min} = a_{Max.} = 2t_w$$

$$W' = d_j/2 - e = t_f/2 + 2t_w$$

Figure 6.30. Maximum eccentricity in two-tip cracked I-beam.

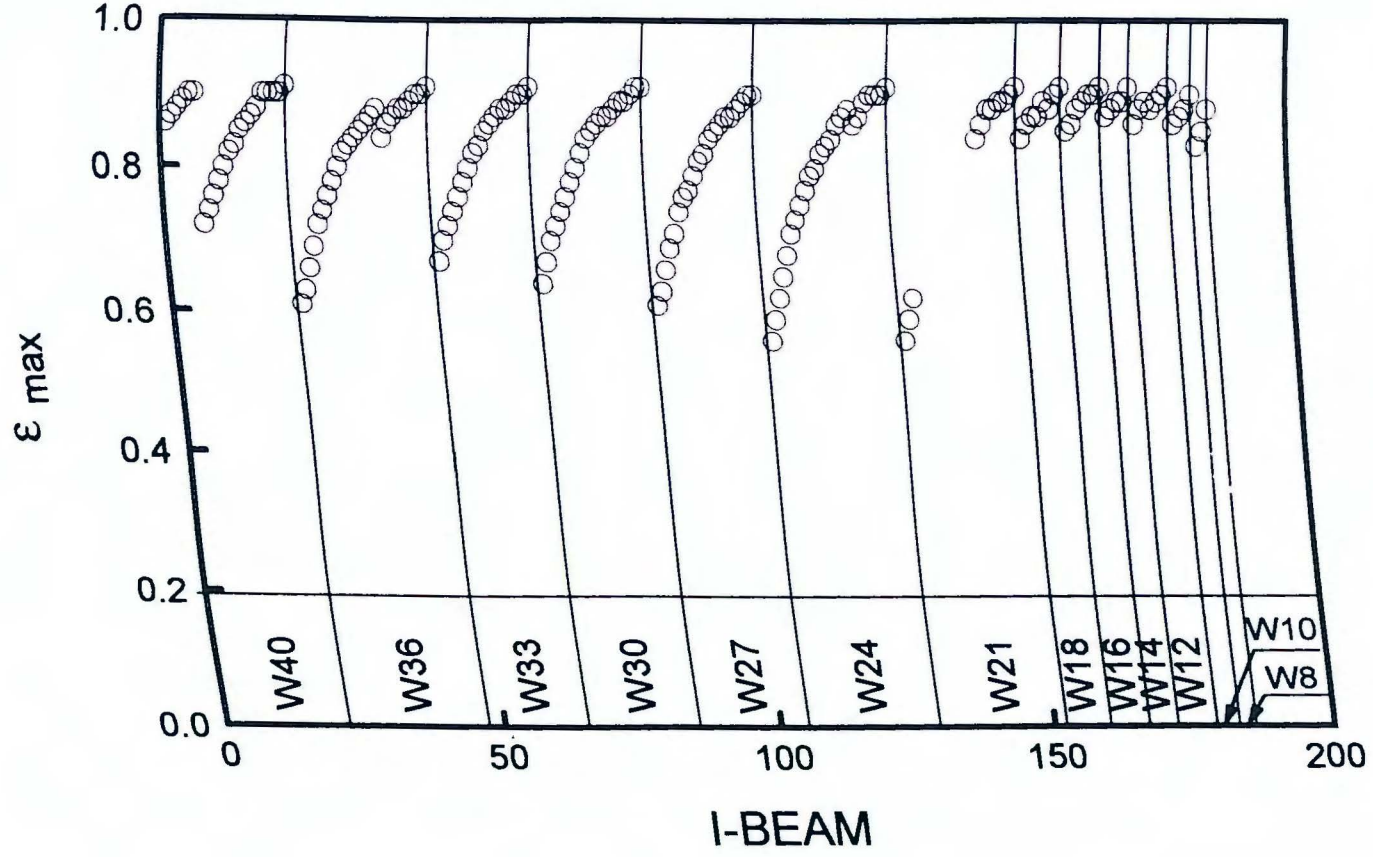

Figure 6.31. Maximum eccentricity for rolled I-beams used in engineering.

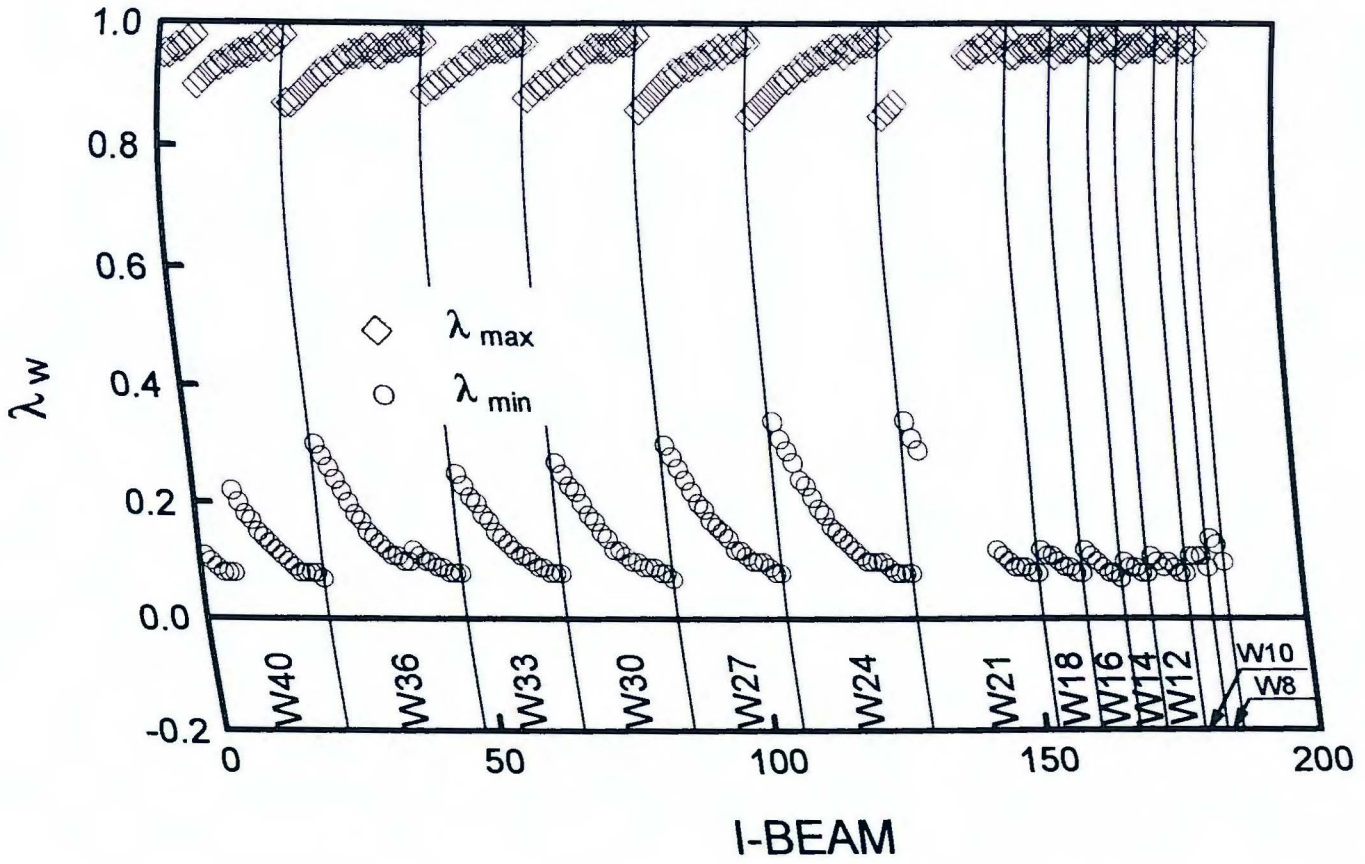

Figure 6.32. Maximum and minimum crack lengths for two-tip eccentrically cracked I-beams; $\varepsilon = 0.1$.

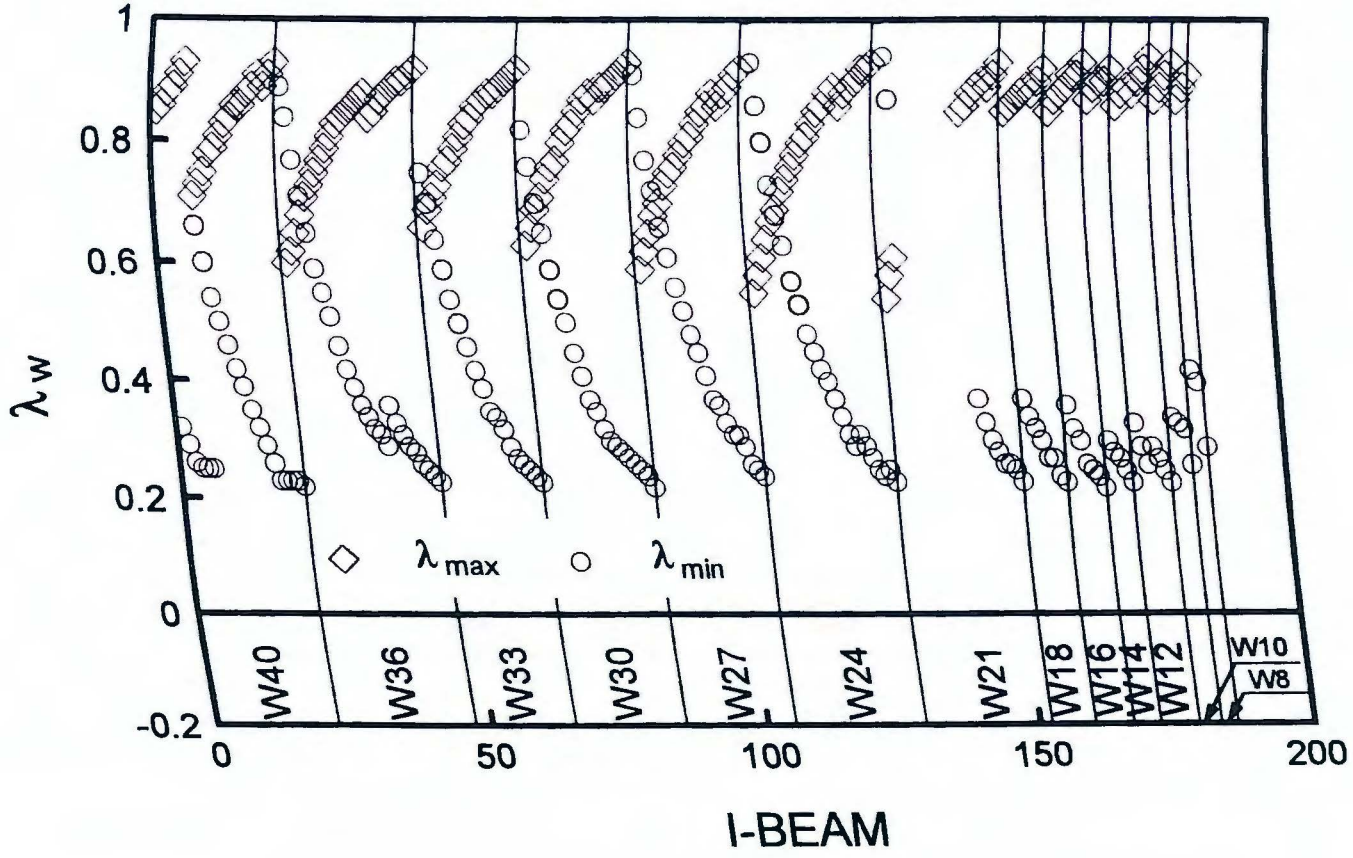

Figure 6.33. Maximum and minimum crack lengths for two-tip eccentrically cracked I-beams; $\varepsilon = 0.7$.

THREE-TIP CRACK UNDER TENSION (β = 0.83, FLANGE CRACK TIP)
Rank 2 Eqn 1069 $z=(a+bx+cx^2+dy+ey^2+fy^3)/(1+gx+hx^2+iy+jy^2)$
r^2=0.99959764 DF Adj r^2=0.99952026 FitStdErr=0.015843707 Fstat=14629.955
a=1.4491295 b=2.7079453 c=-0.93669006 d=-1.5246754 e=2.6792026
f=-2.3704207 g=0.12536049 h=-0.17643216 i=1.0164406 j=-1.8710641

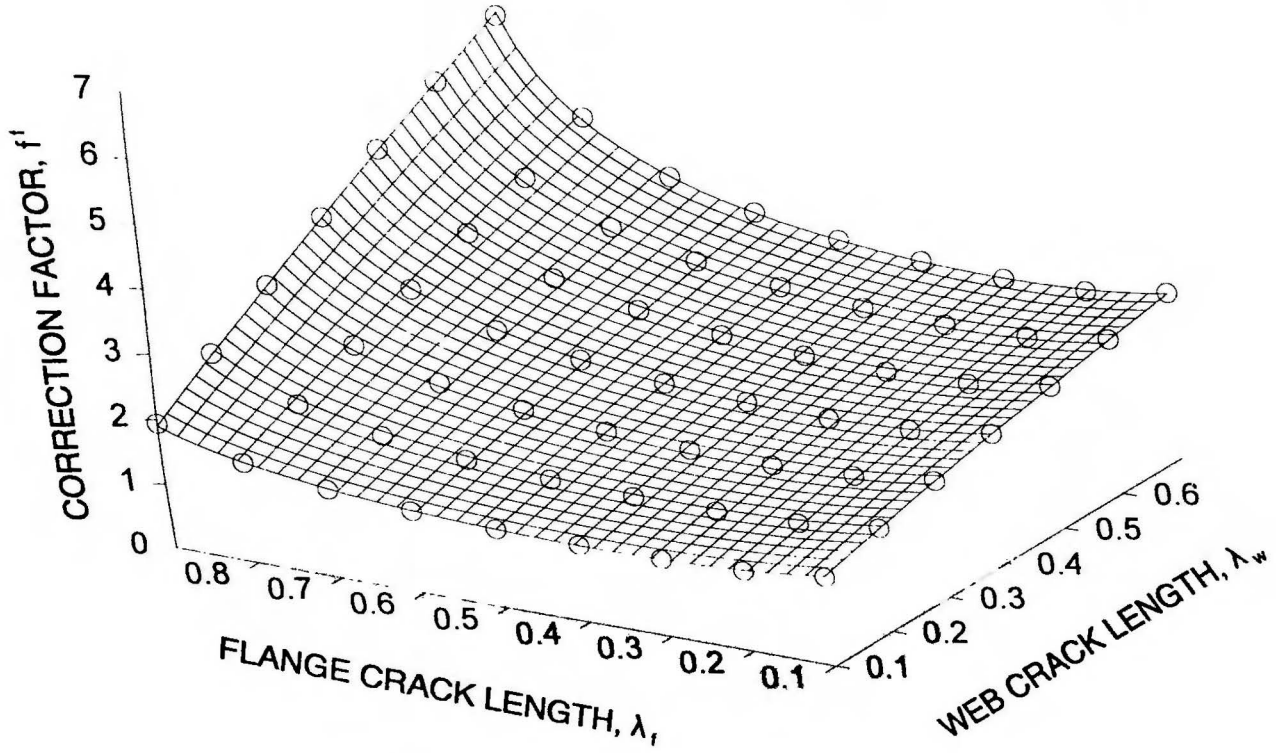

Figure 6.34. Preliminary fit for three-tip cracked I-beam under tension; W40 x 149, flange crack tip.

THREE-TIP CRACK UNDER TENSION (β = 2.05, FLANGE CRACK TIP)
Rank 1 Eqn 1197 $z=(a+b\ln x+c(\ln x)^2+dy+ey^2+fy^3)/(1+g\ln x+h(\ln x)^2+iy+jy^2)$
r^2=0.99984934 DF Adj r^2=0.99982036 FitStdErr=0.0067189534 Fstat=39080.386
a=2.1546174 b=0.44997565 c=0.052775671 d=-1.1518982 e=2.2402615
f=-2.2113989 g=-0.041007561 h=-0.019990034 i=0.88022965 j=-1.8180909

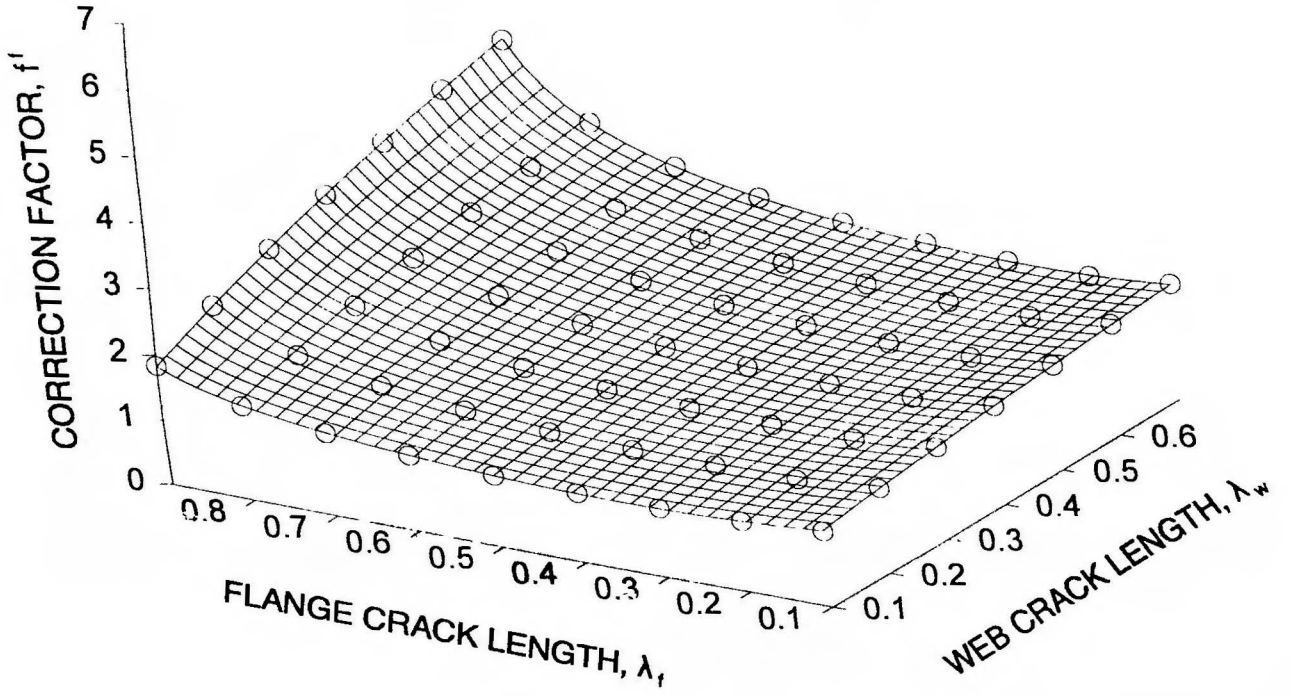

Figure 6.35. Preliminary fit for three-tip cracked I-beam under tension; W18 x 9 7, flange crack tip.

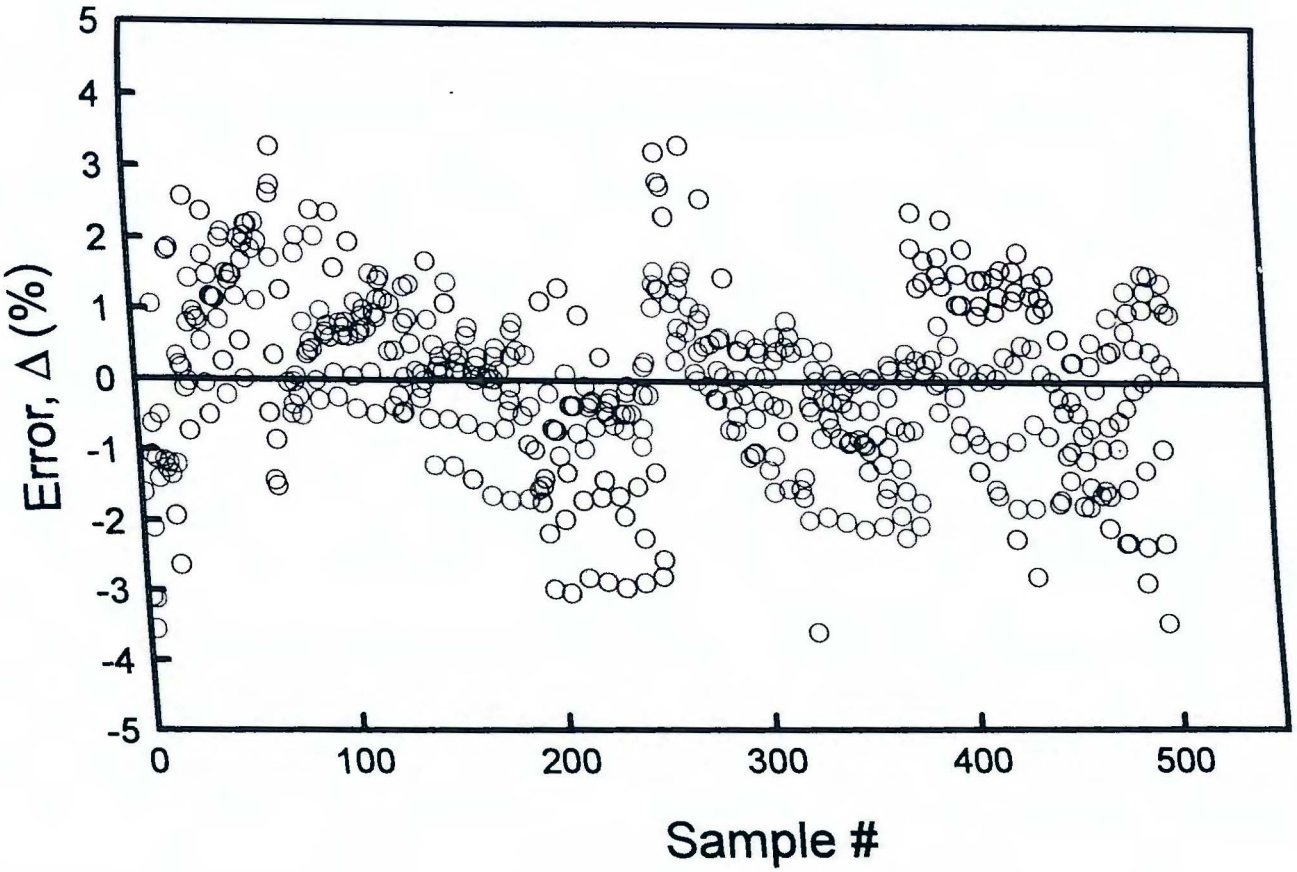

Figure 6.36. Error in predicting correction factor for three-tip cracked I-beam under tension; web crack tip.

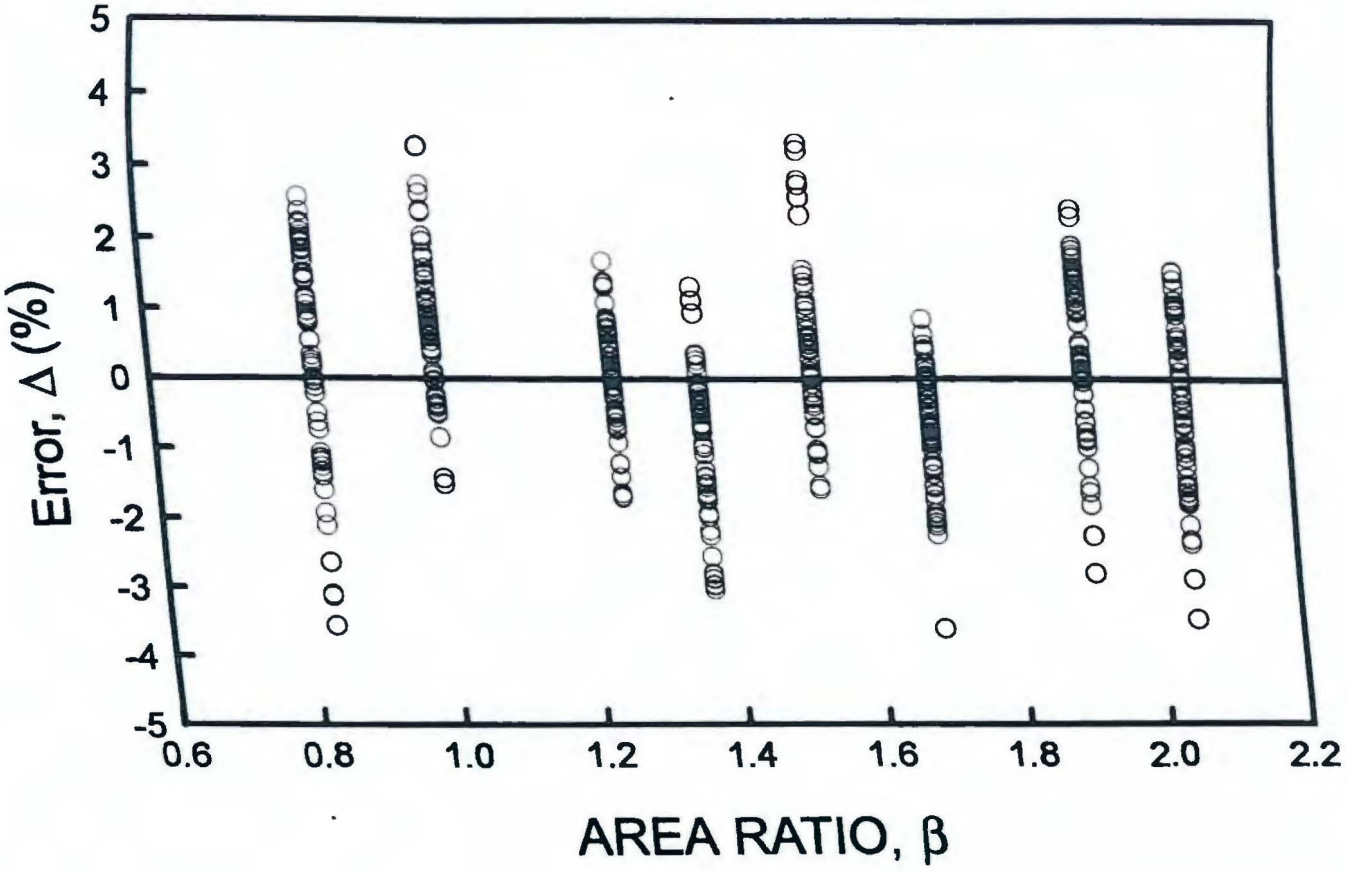

Figure 6.37. Variation in prediction error with area ratio; three-tip cracked I-beam under tension, web crack tip.

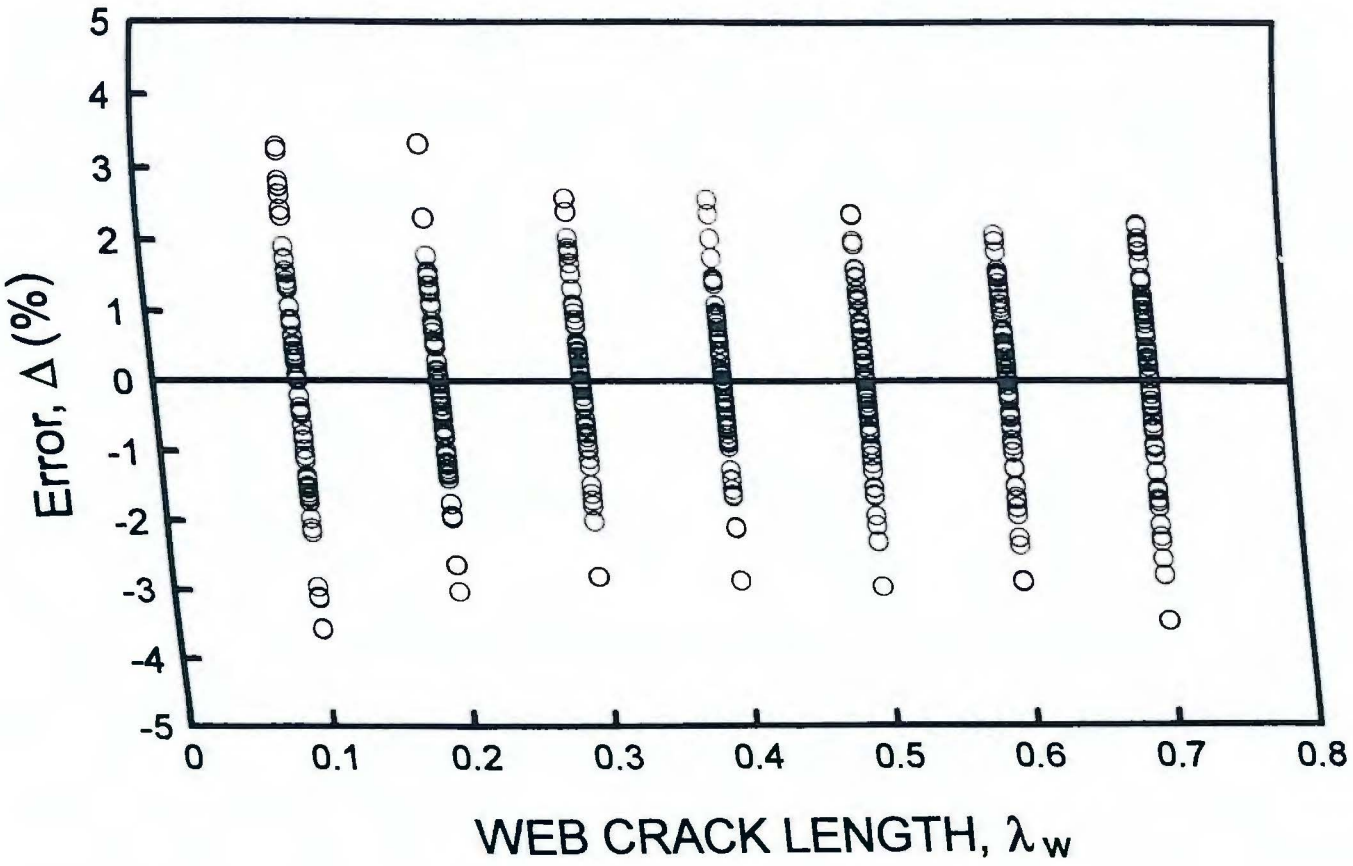

Figure 6.38. Variation in prediction error with web crack length; three-tip cracked I-beam under tension, web crack tip.

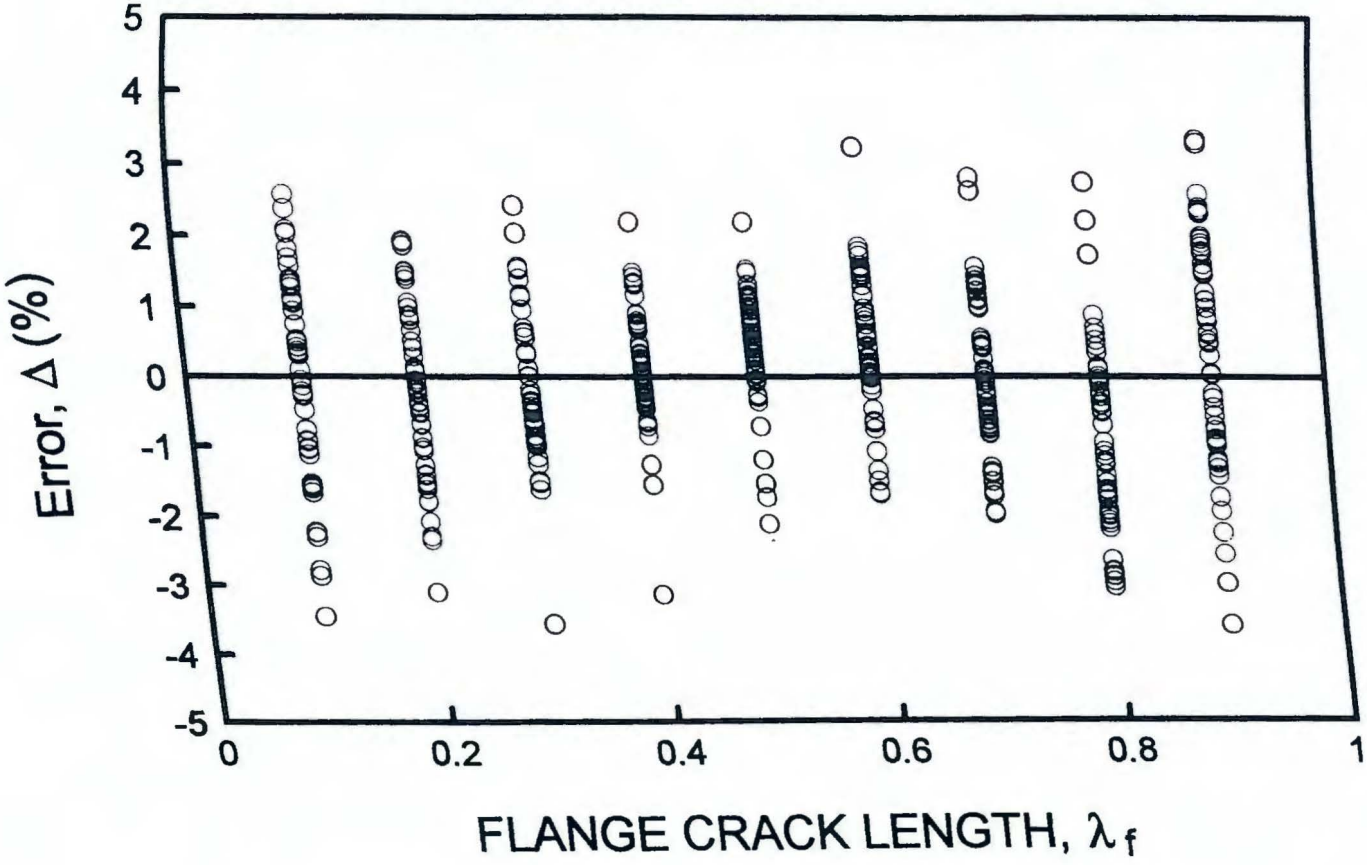

Figure 6.39. Variation in prediction error with flange crack length; three-tip cracked I-beam under tension, web crack tip.

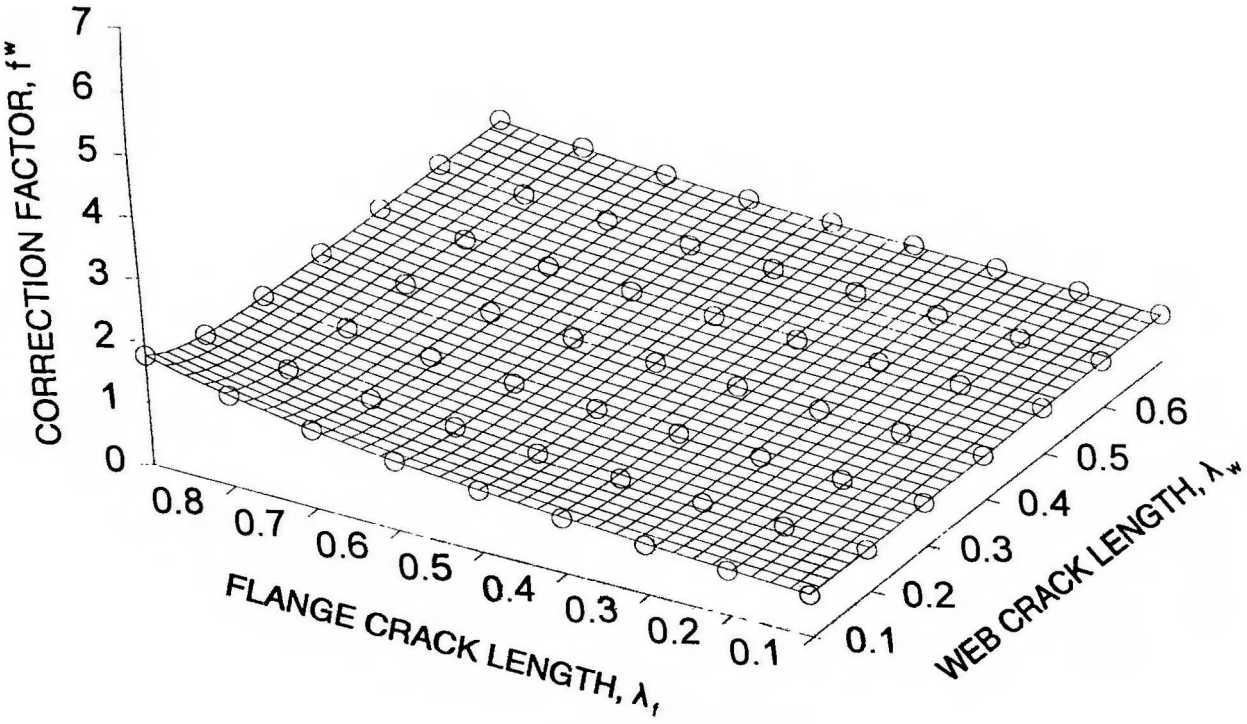

Figure 6.40. Comparison of predicted and calculated correction factors for three-tip cracked I-beam under tension; W40 x 149, web crack tip.

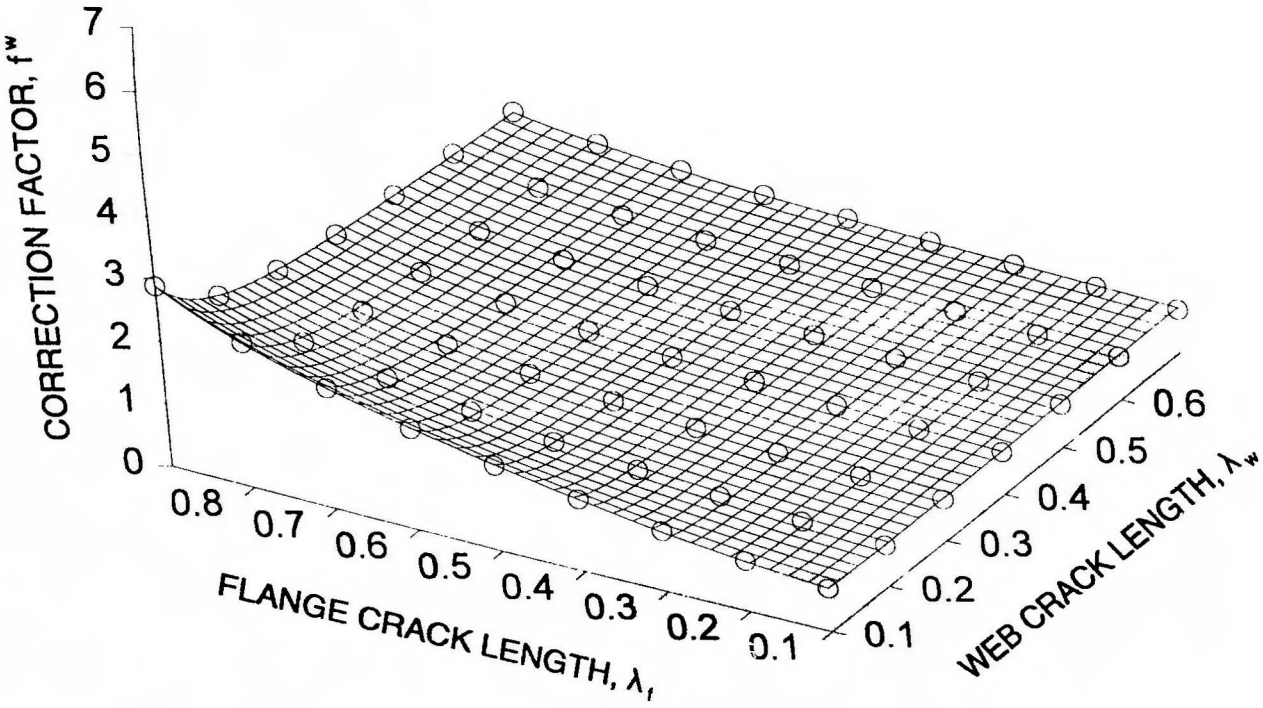

Figure 6.41. Comparison of predicted and calculated correction factors for three-tip cracked I-beam under tension; W18 x 9 7, web crack tip.

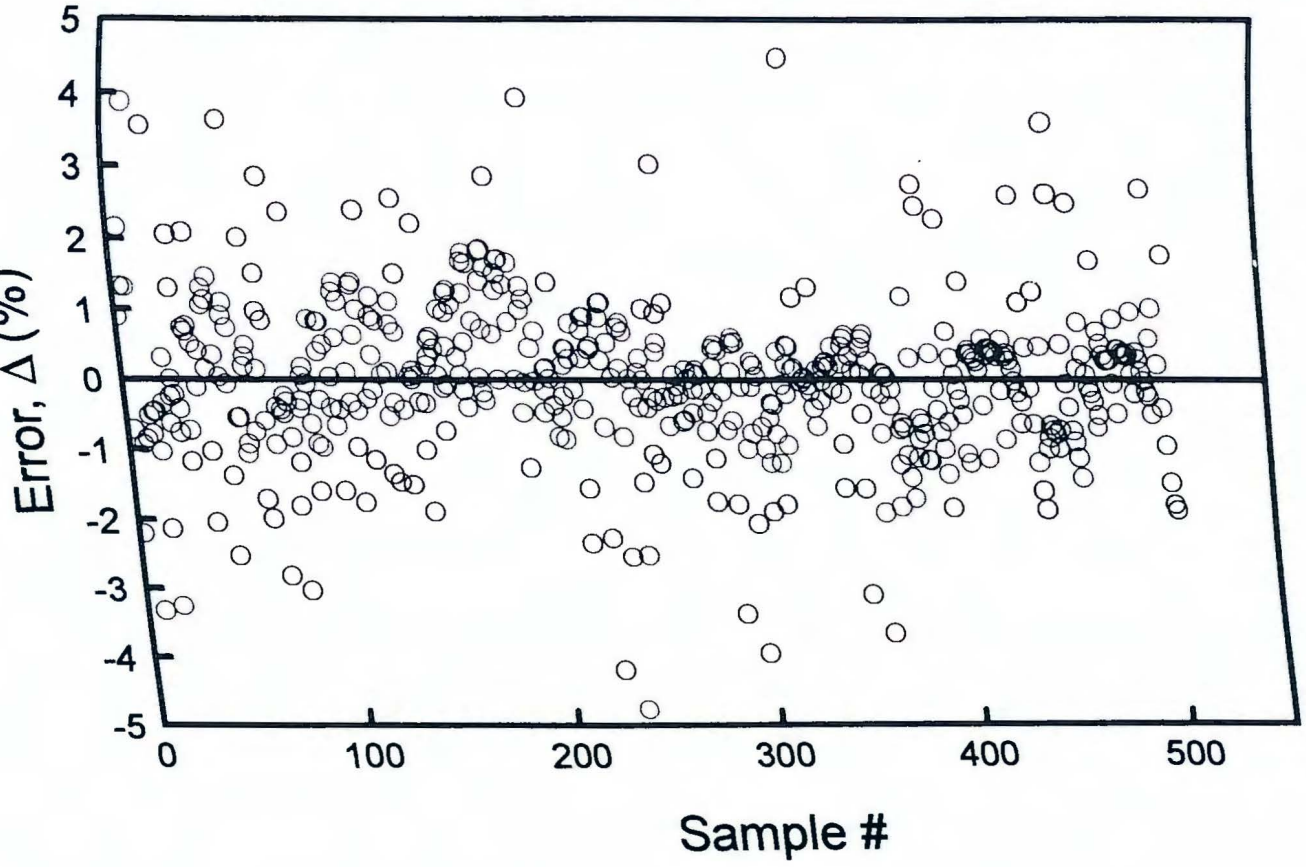

Figure 6.42. Error in predicting correction factor for three-tip cracked I-beam under tension; flange crack tip.

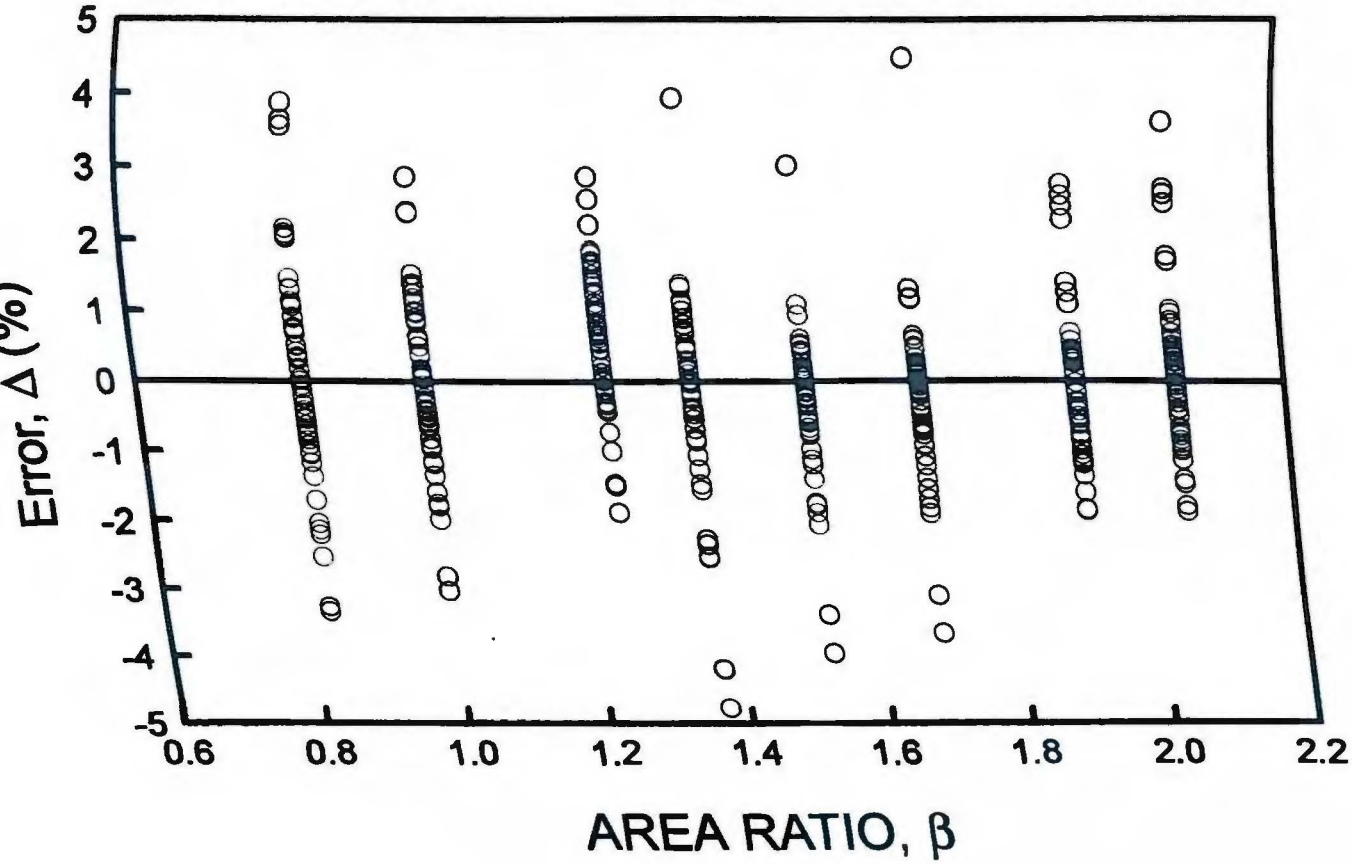

Figure 6.43. Variation in prediction error with area ratio; three-tip cracked I-beam under tension, flange crack tip.

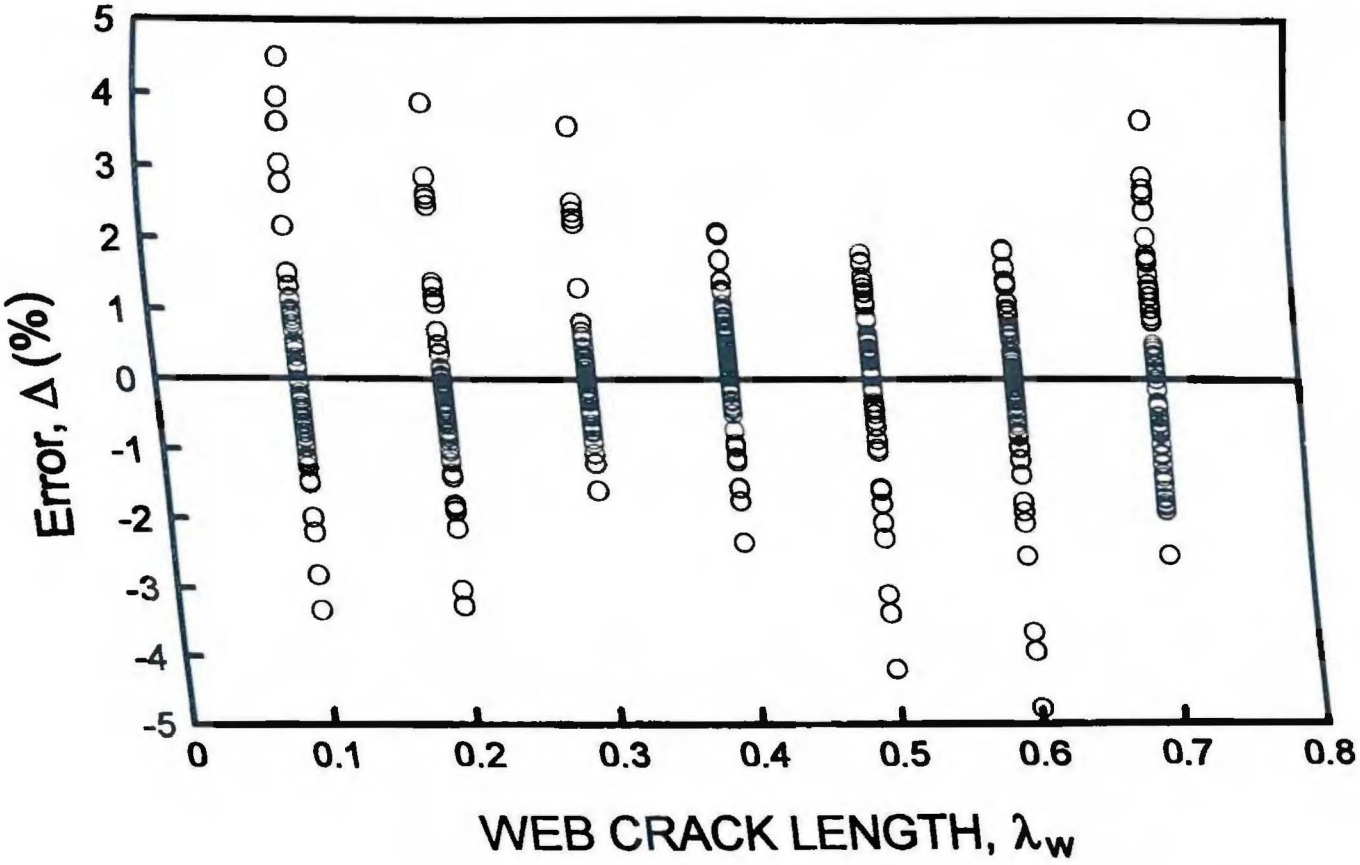

Figure 6.44. Variation in prediction error with web crack length; three-tip cracked I-beam under tension, flange crack tip.

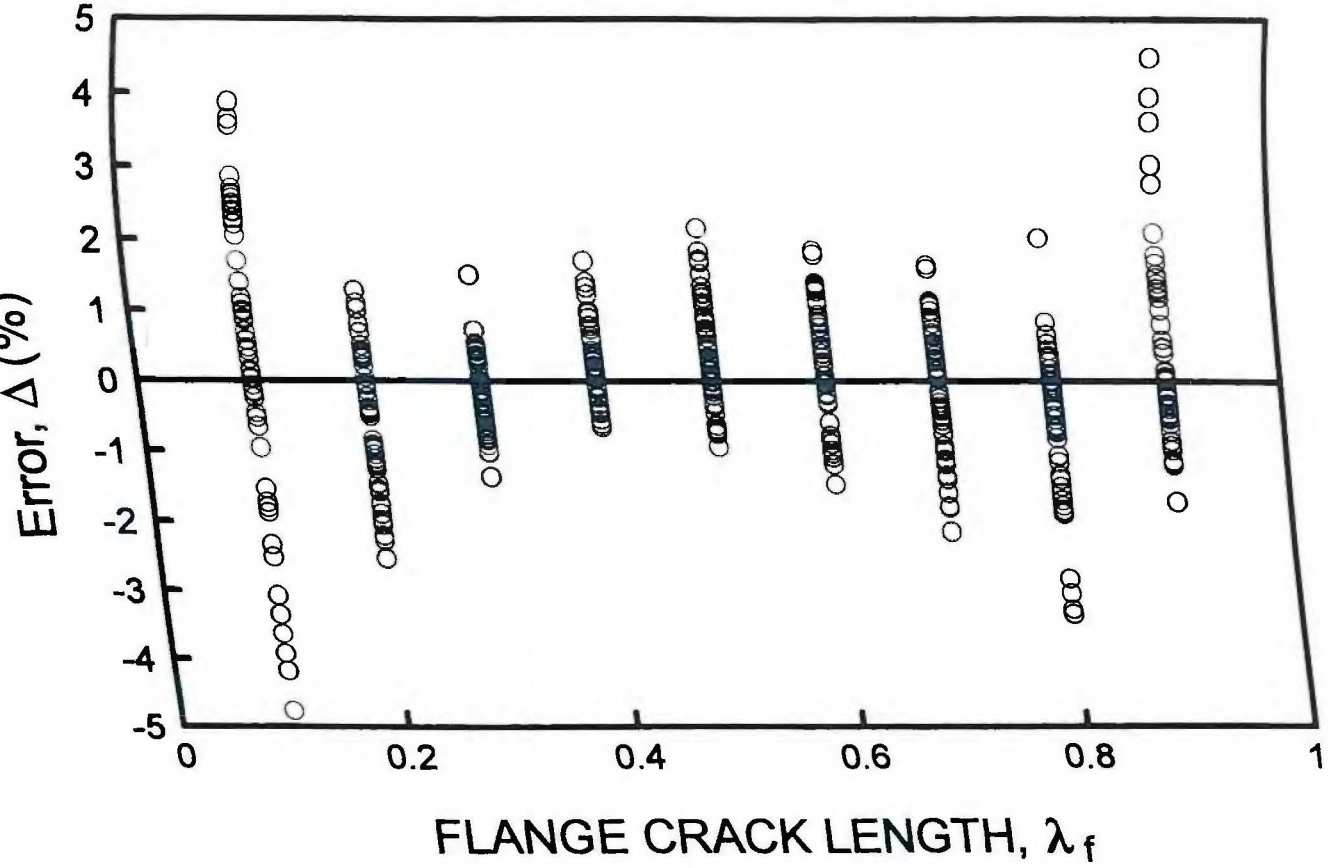

Figure 6.45. Variation in prediction error with flange crack length; three-tip cracked I-beam under tension, flange crack tip.

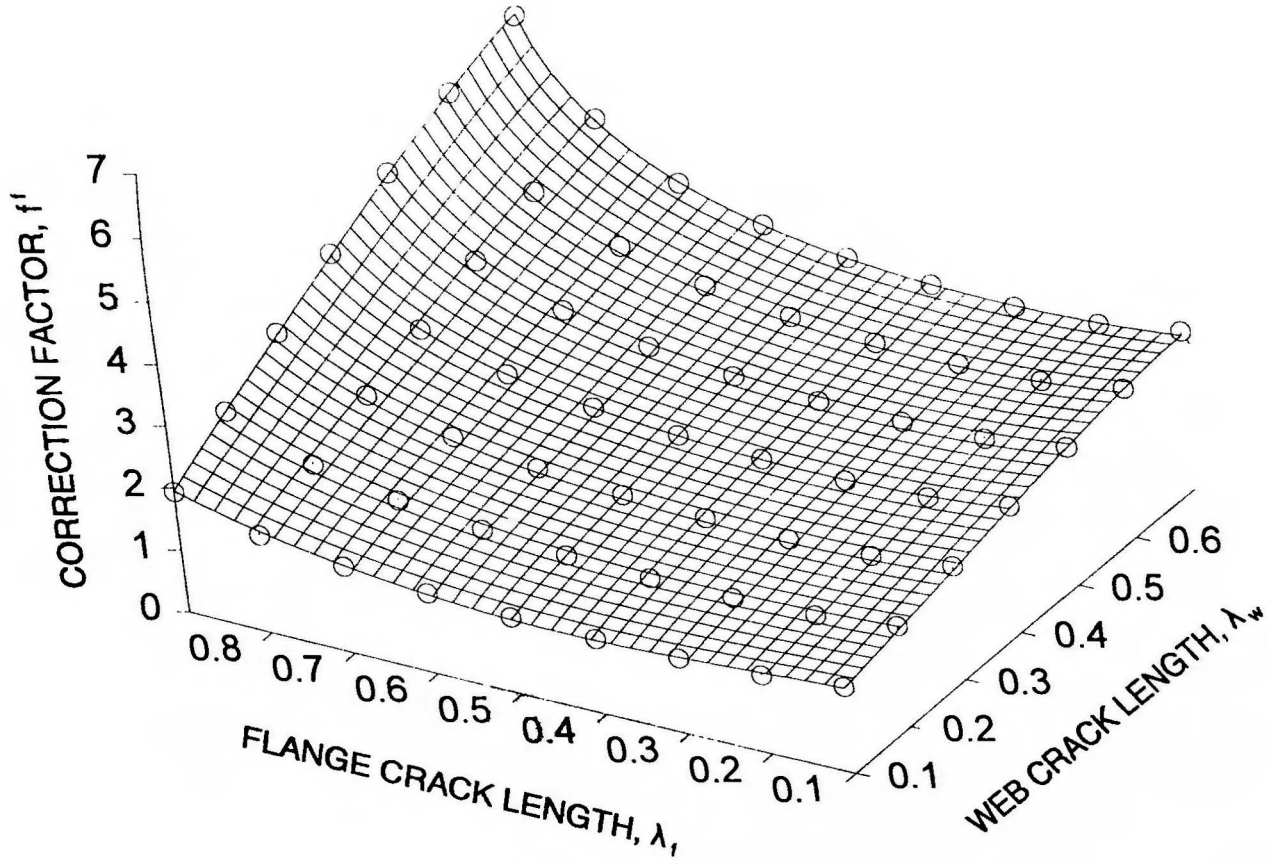

Figure 6.46. Comparison of predicted and calculated correction factors for three-tip cracked I-beam under tension; W40 x 149, flange crack tip.

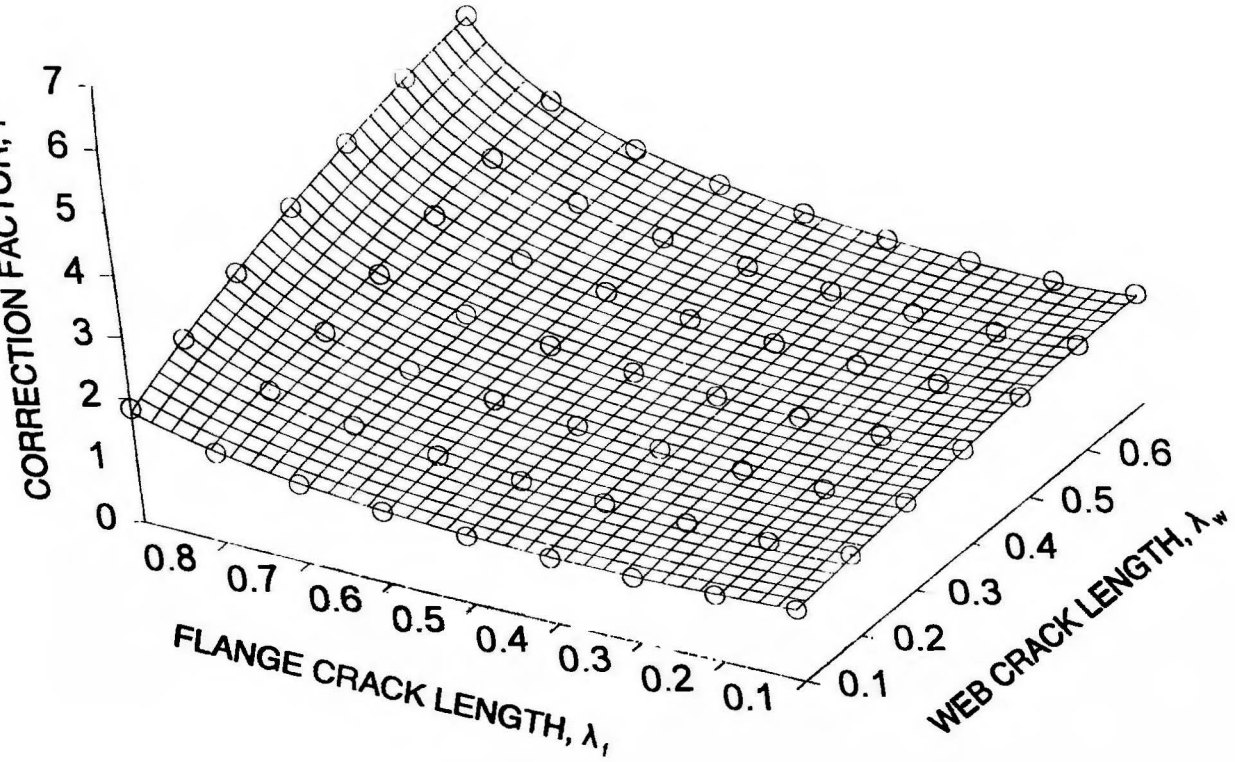

Figure 6.47. Comparison of predicted and calculated correction factors for three-tip cracked I-beam under tension; W18 x 9 7, flange crack tip.

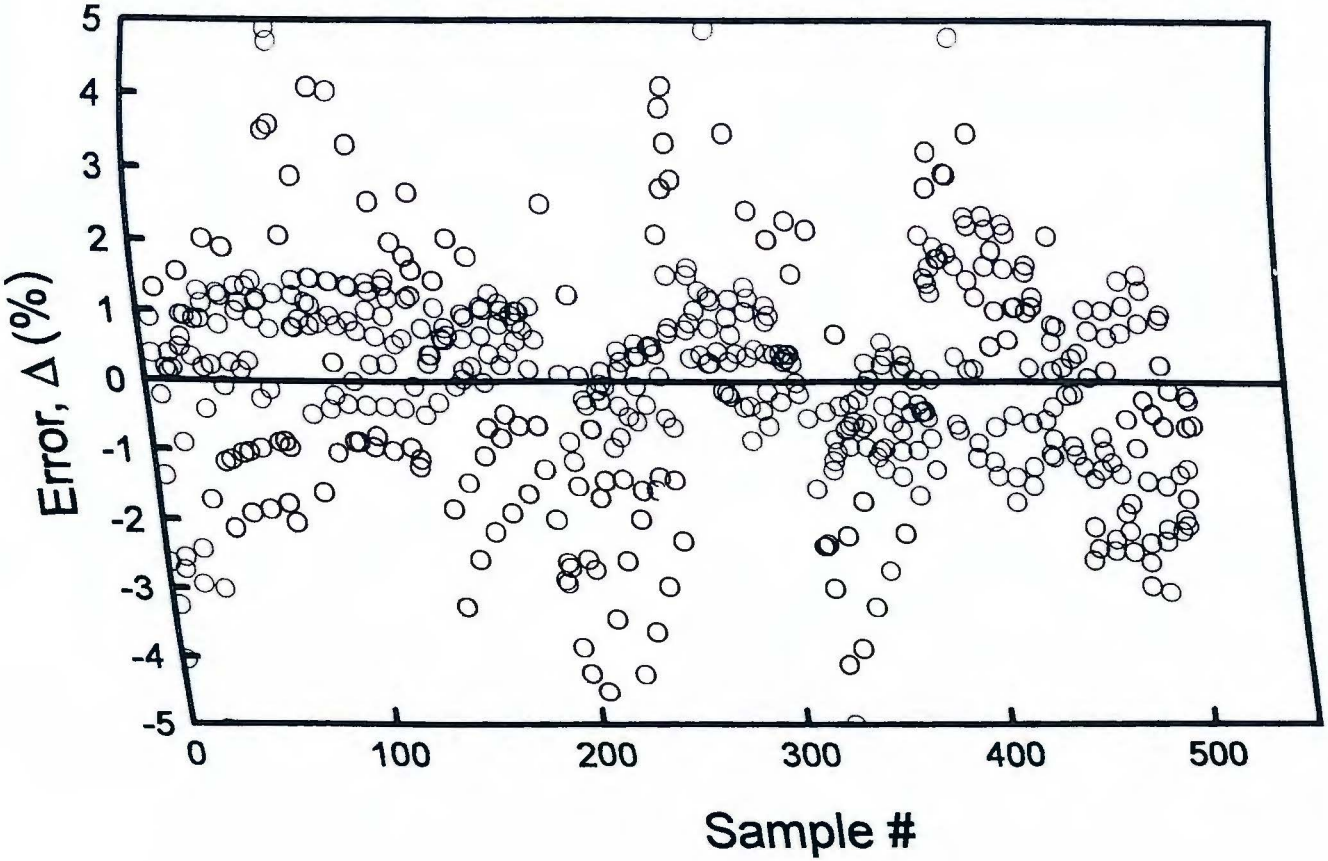

Figure 6.48. Error in predicting correction factor for three-tip cracked I-beam under bending; web crack tip.

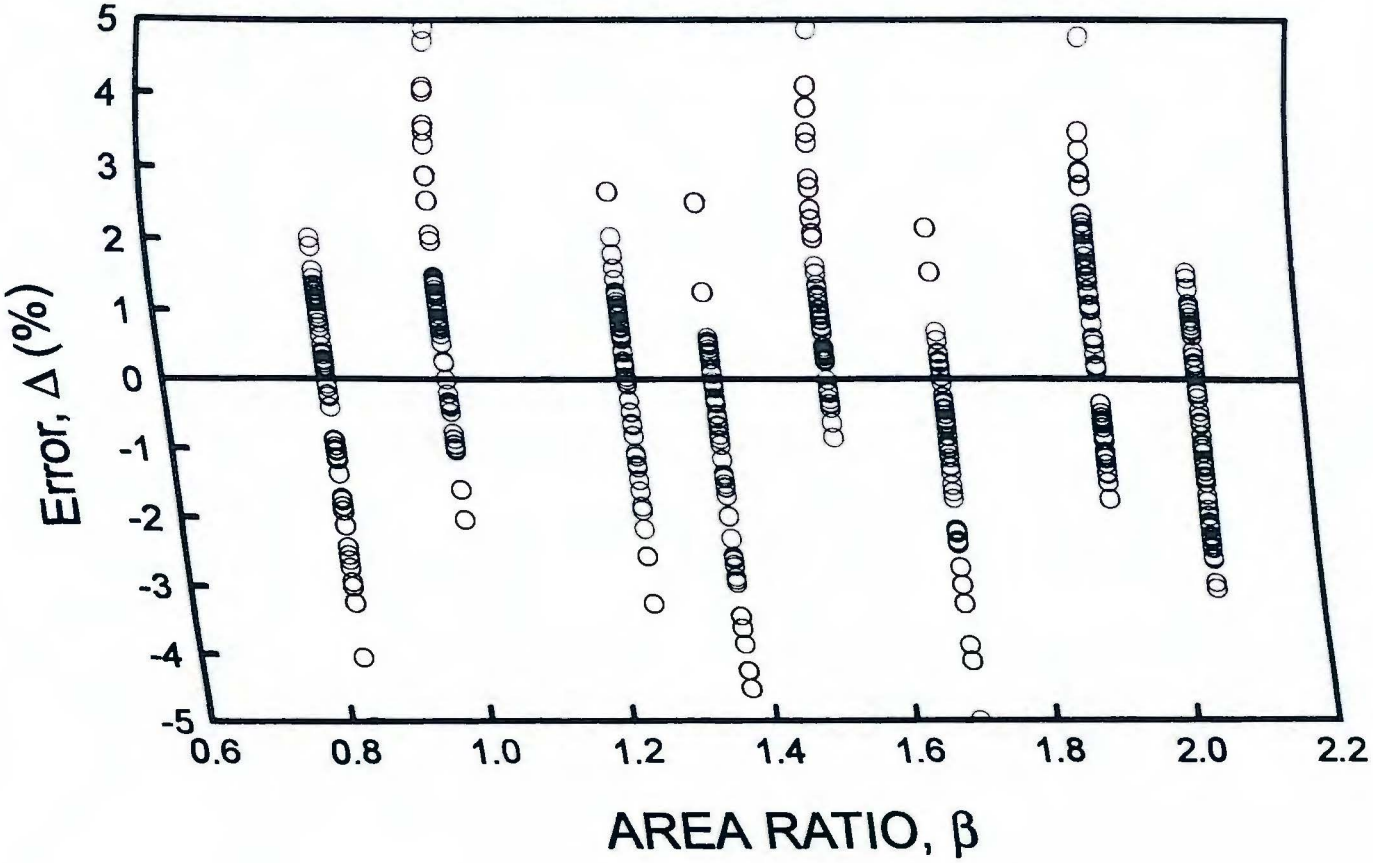

Figure 6.49. Variation in prediction error with area ratio; three-tip cracked I-beam under bending, web crack tip.

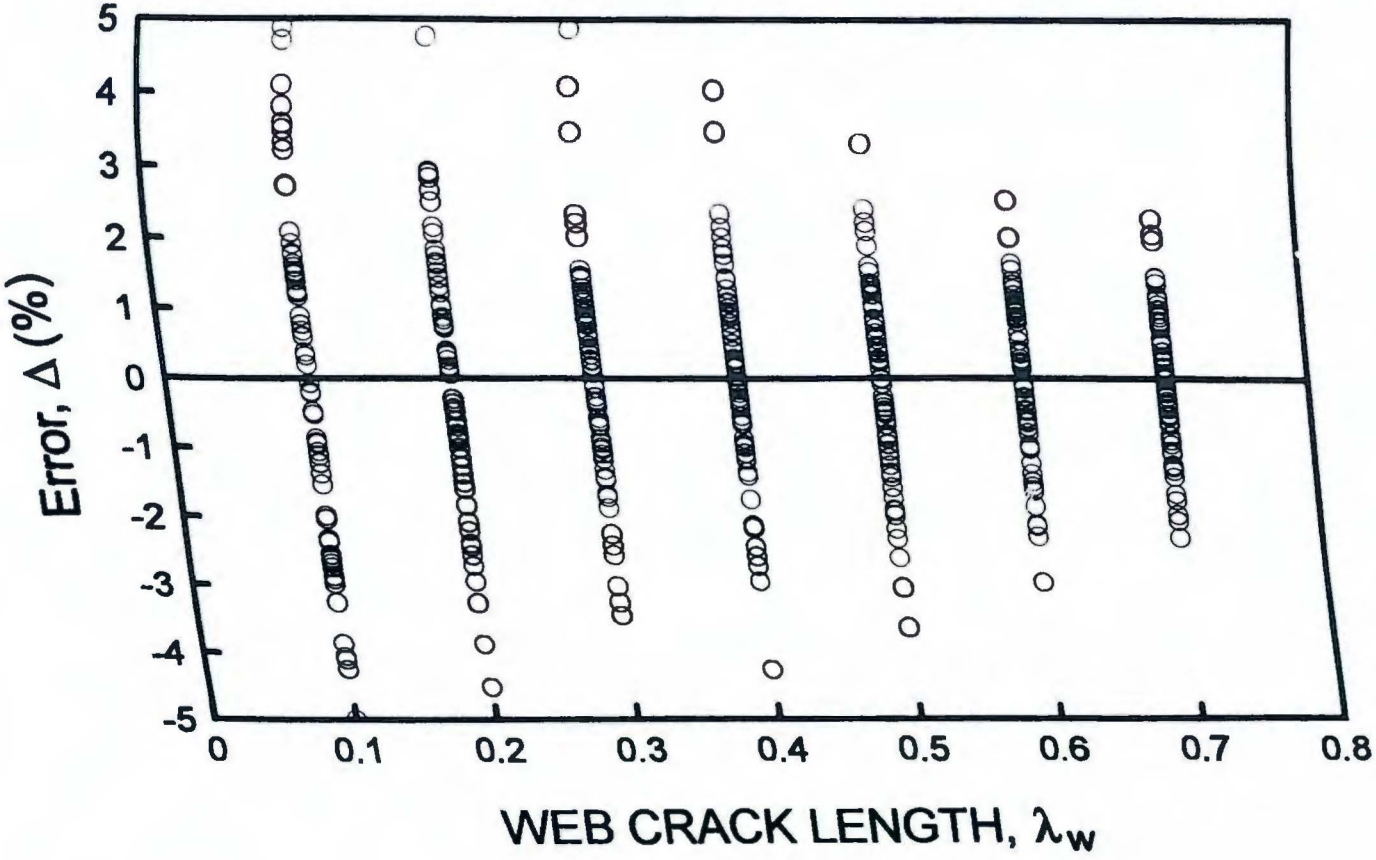

Figure 6.50. Variation in prediction error with web crack length; three-tip cracked I-beam under bending, web crack tip.

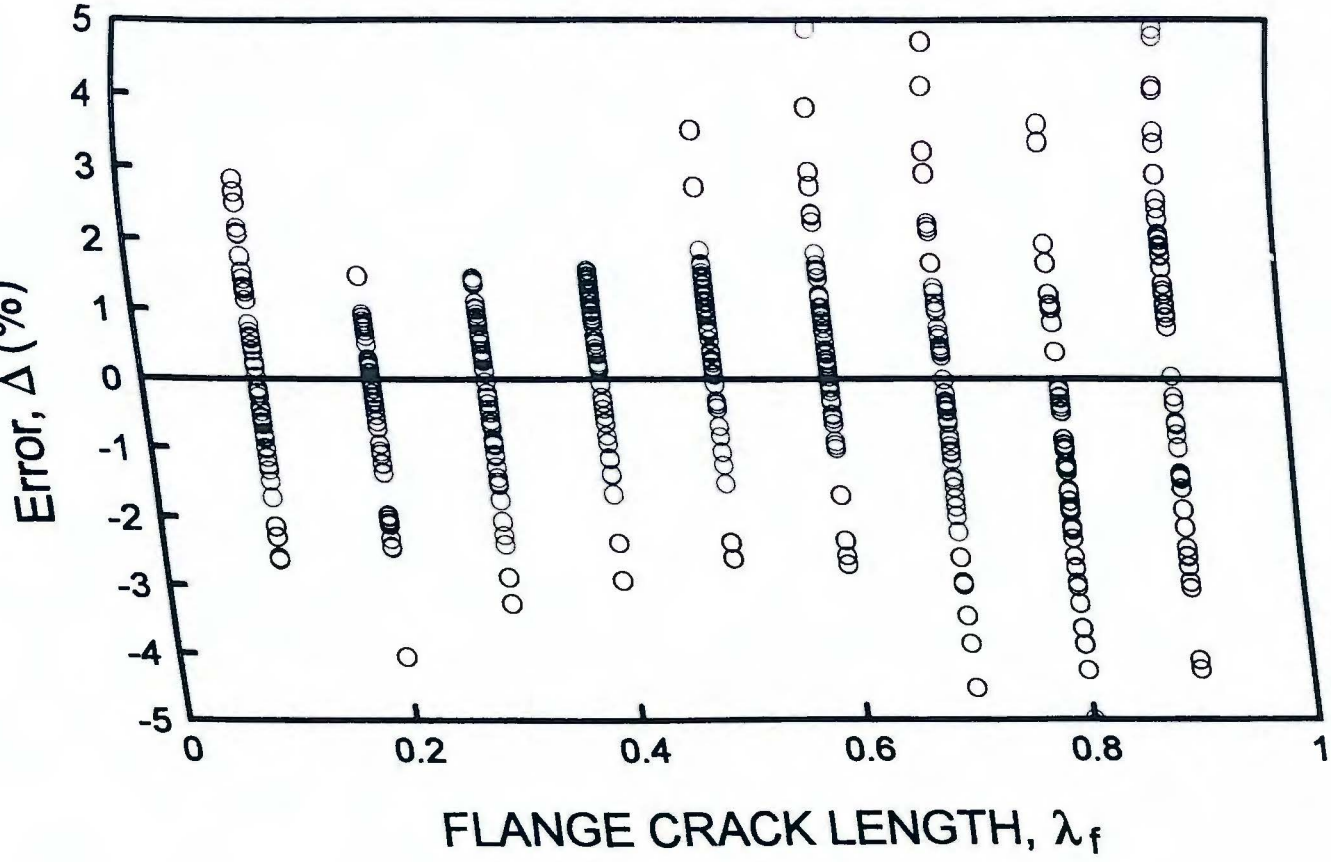

Figure 6.51. Variation in prediction error with flange crack length; three-tip cracked I-beam under bending, web crack tip.

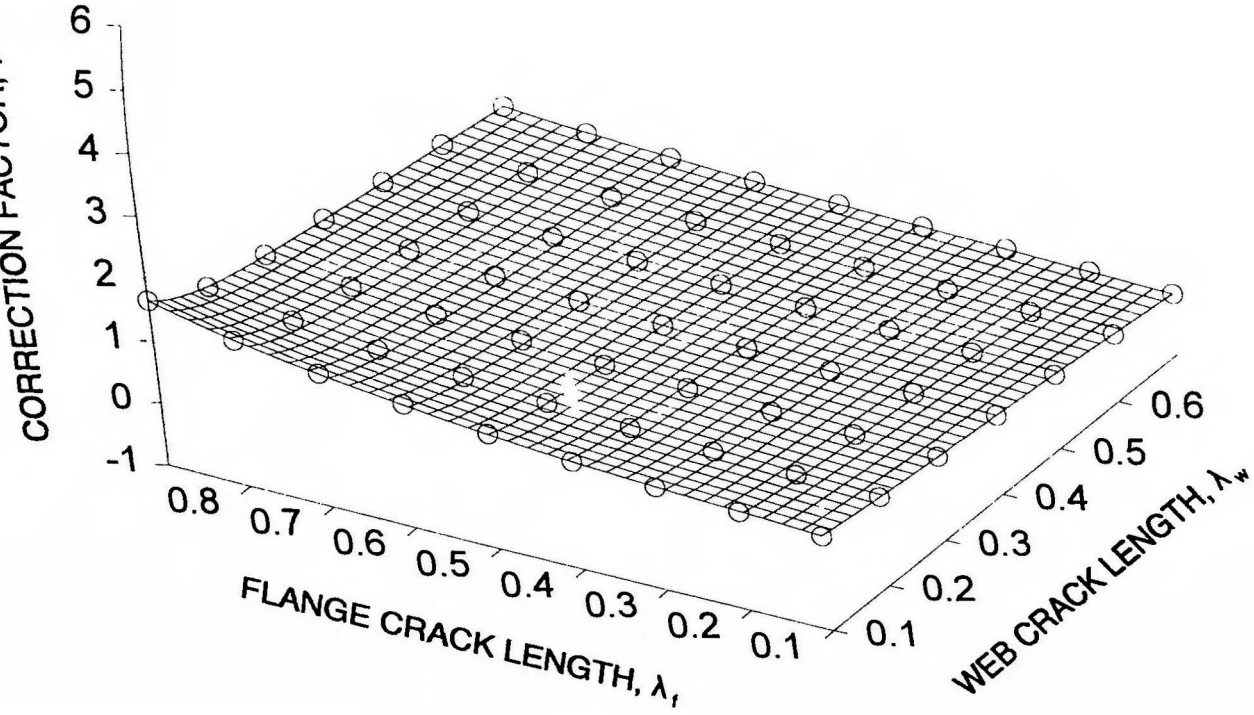

Figure 6.52. Comparison of predicted and calculated correction factors for three-tip cracked I-beam under bending; W40 x 149, web crack tip.

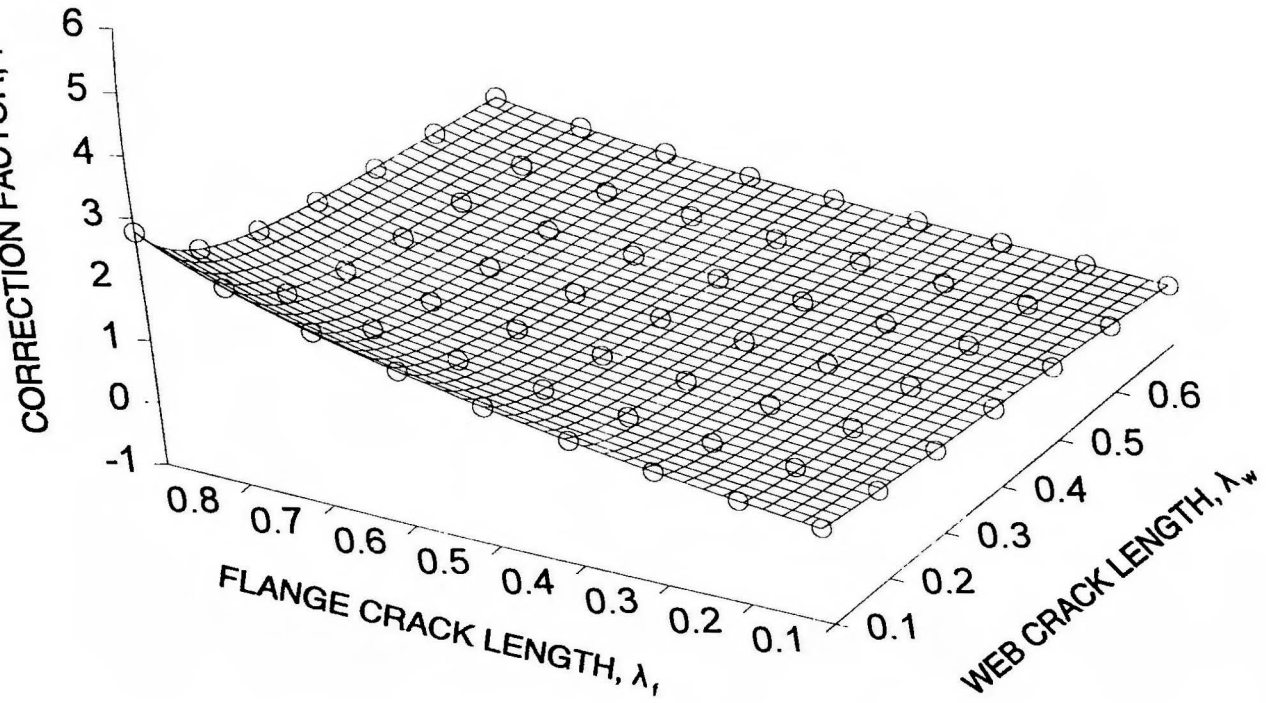

Figure 6.53. Comparison of predicted and calculated correction factors for three-tip cracked I-beam under bending; W18 x 9 7, web crack tip.

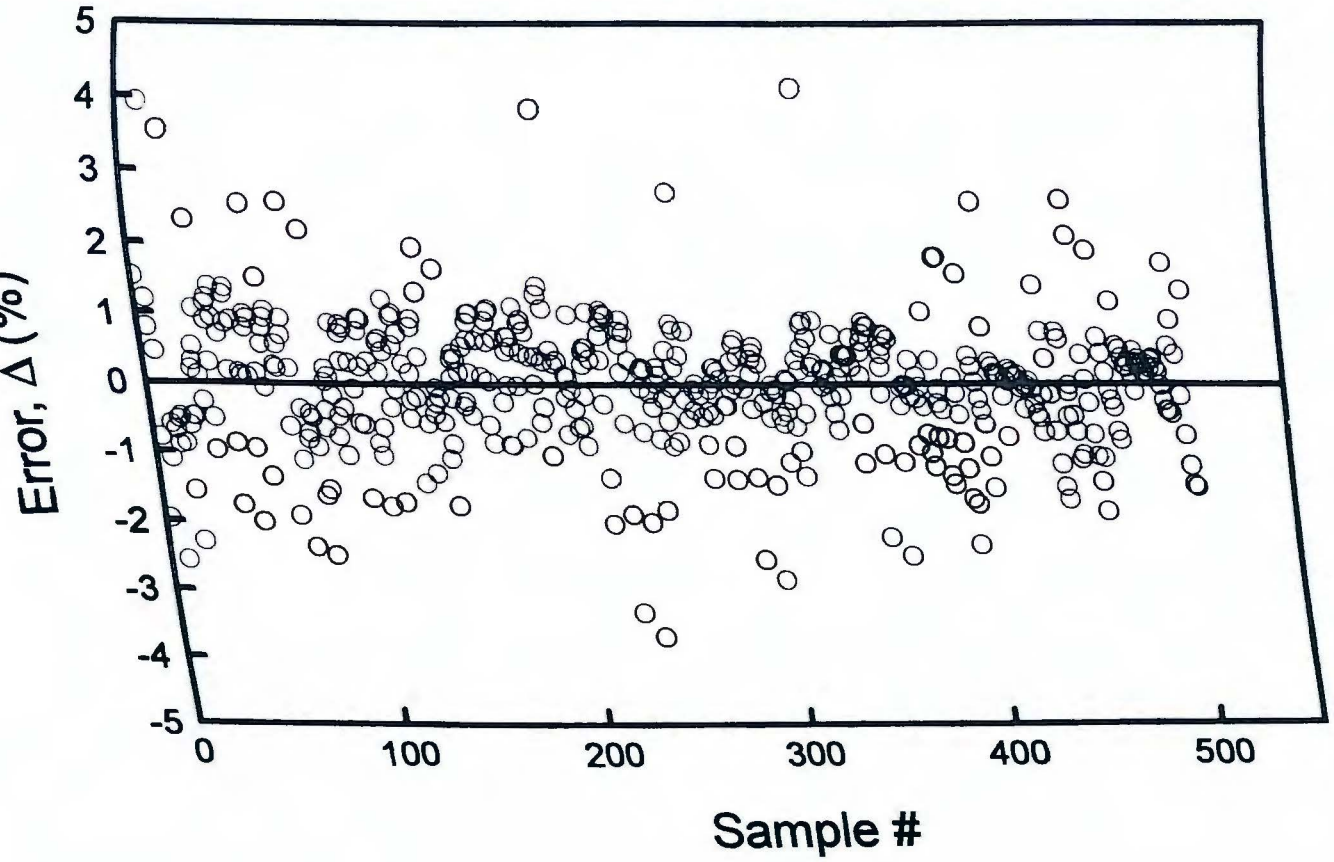

Figure 6.54. Error in predicting correction factor for three-tip cracked I-beam under bending; flange crack tip.

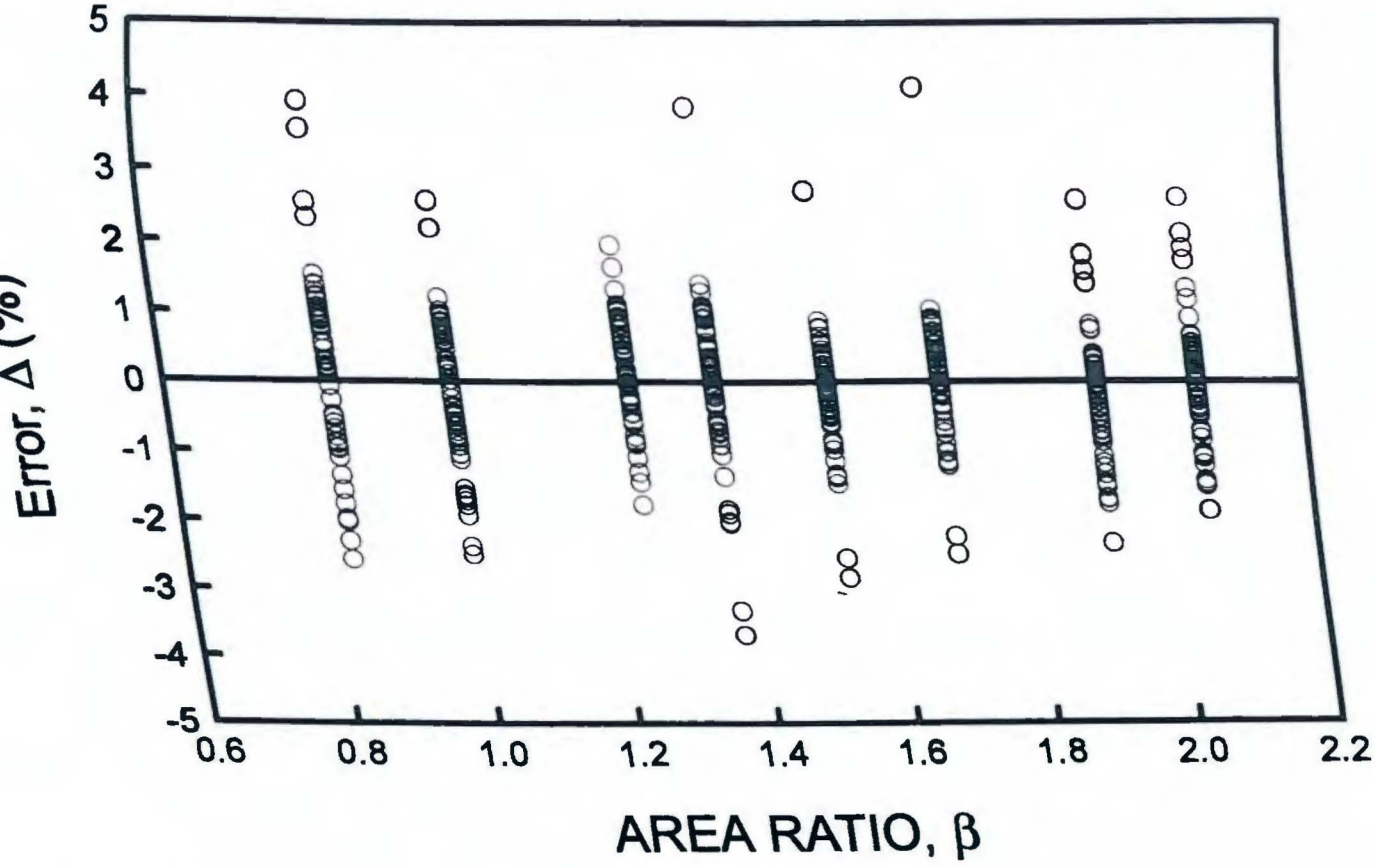

Figure 6.55. Variation in prediction error with area ratio; three-tip cracked I-beam under bending, flange crack tip.

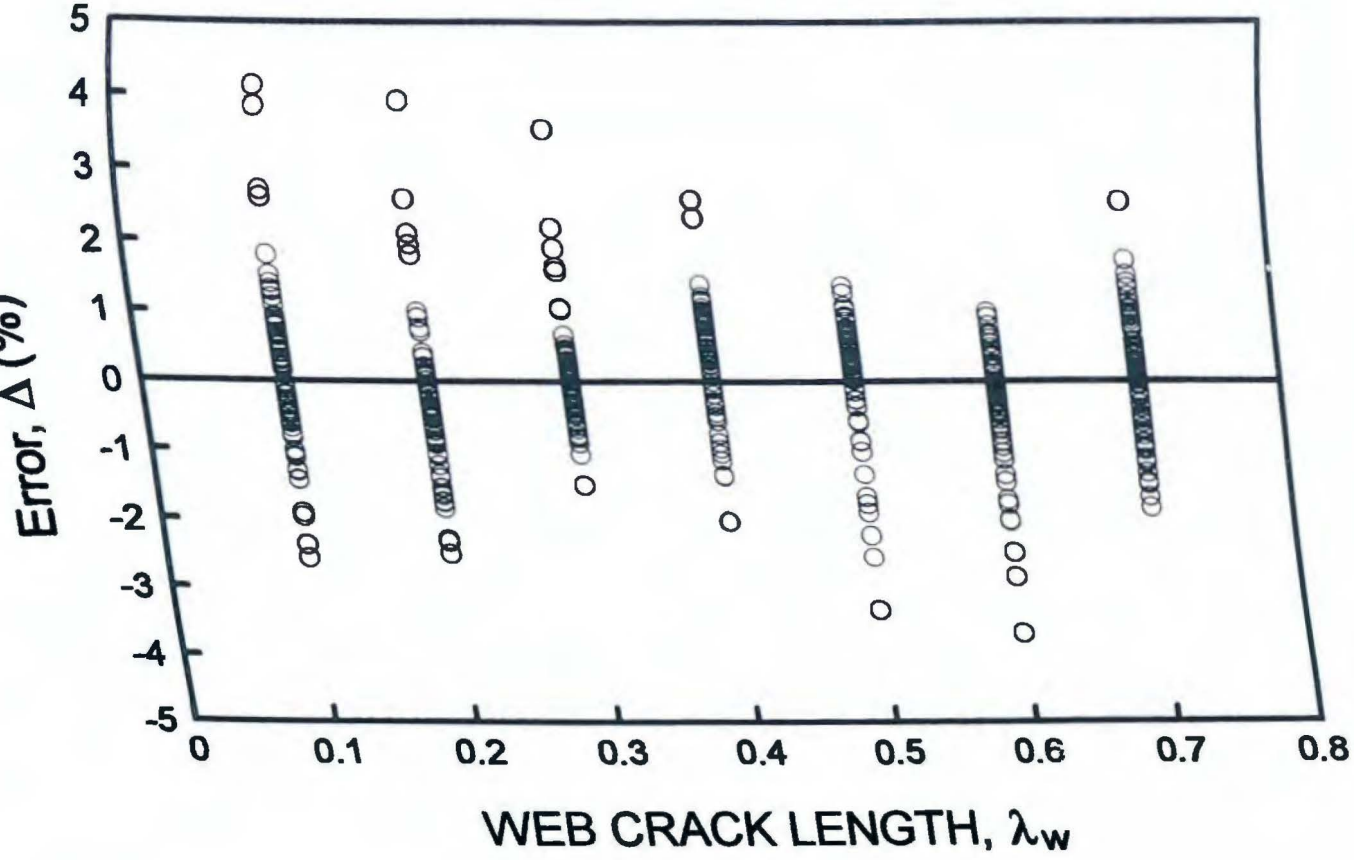

Figure 6.56. Variation in prediction error with web crack length; three-tip cracked I-beam under bending, flange crack tip.

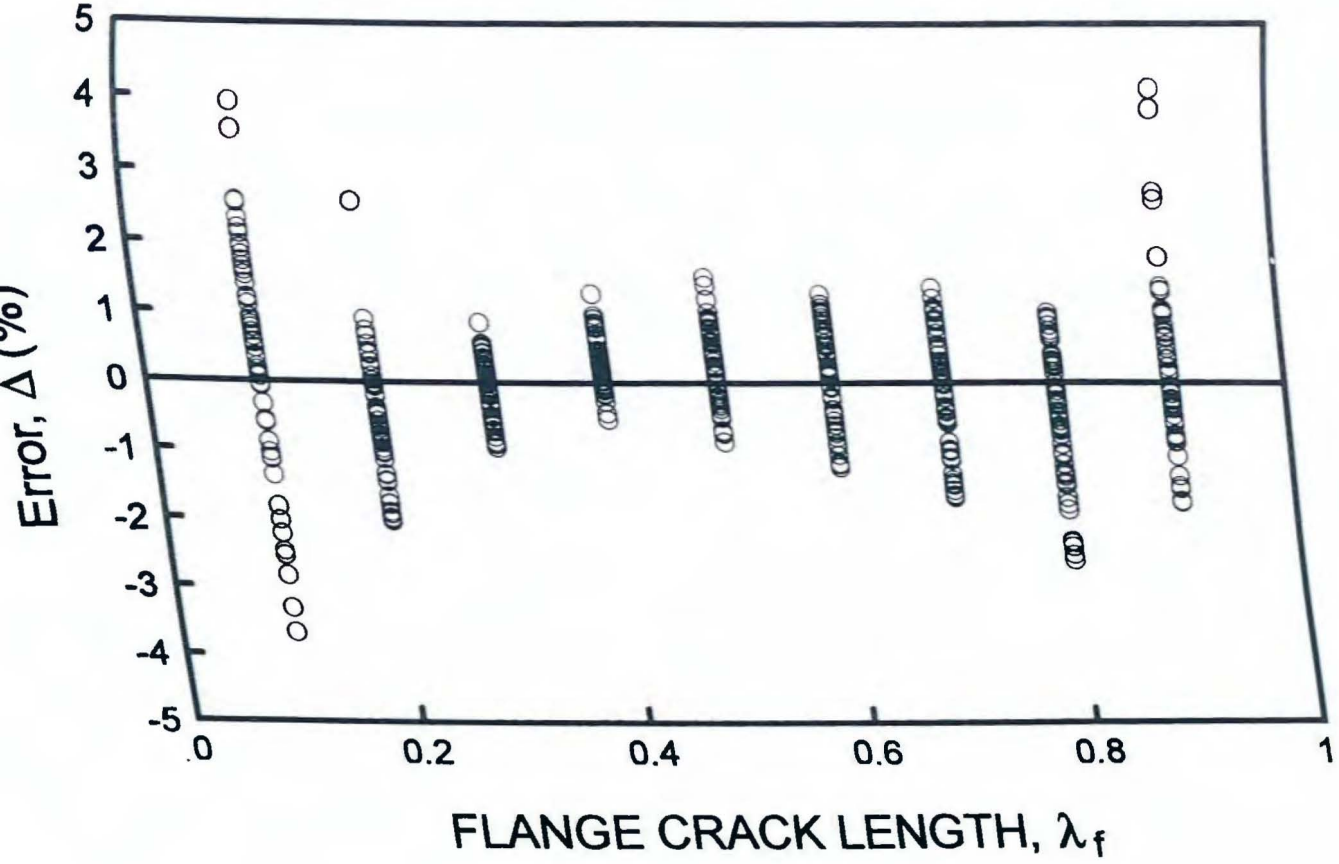

Figure 6.57. Variation in prediction error with flange crack length; three-tip cracked I-beam under bending, flange crack tip.

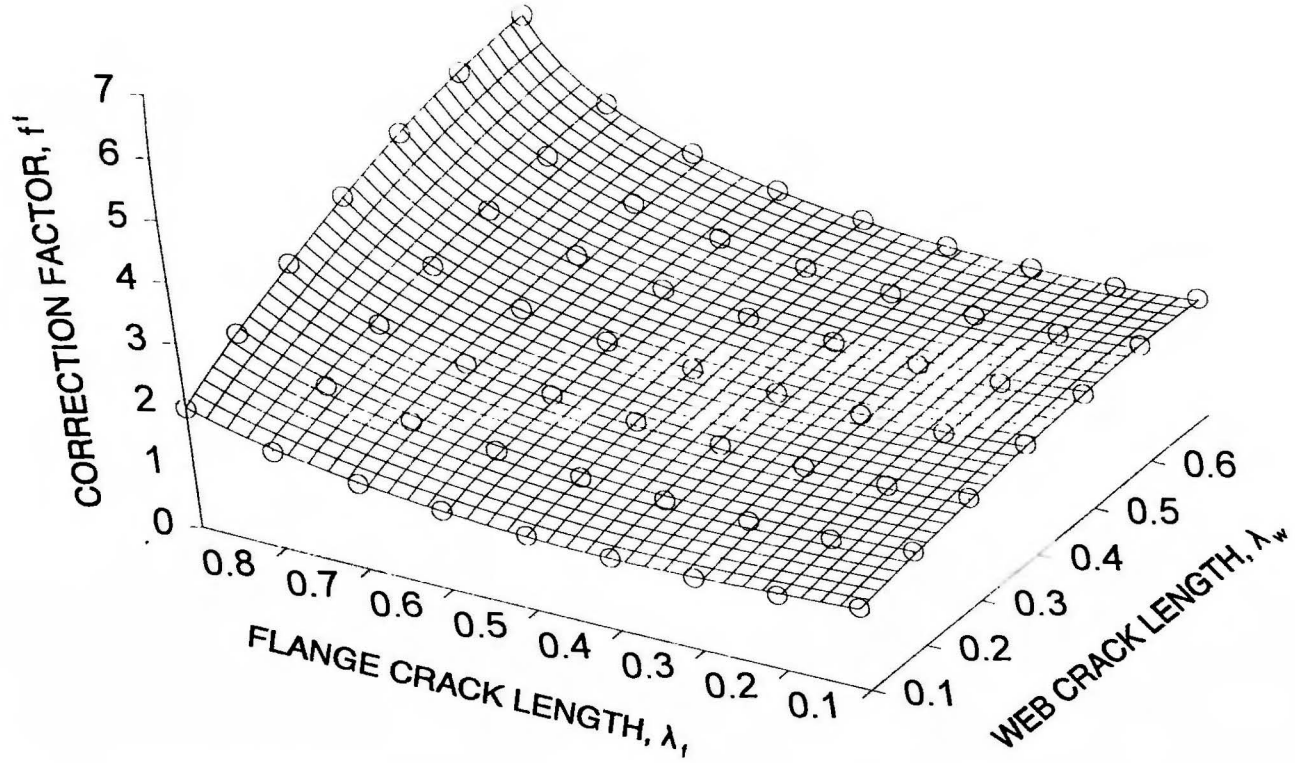

Figure 6.58. Comparison of predicted and calculated correction factors for three-tip cracked I-beam under bending; W40 x 149, flange crack tip.

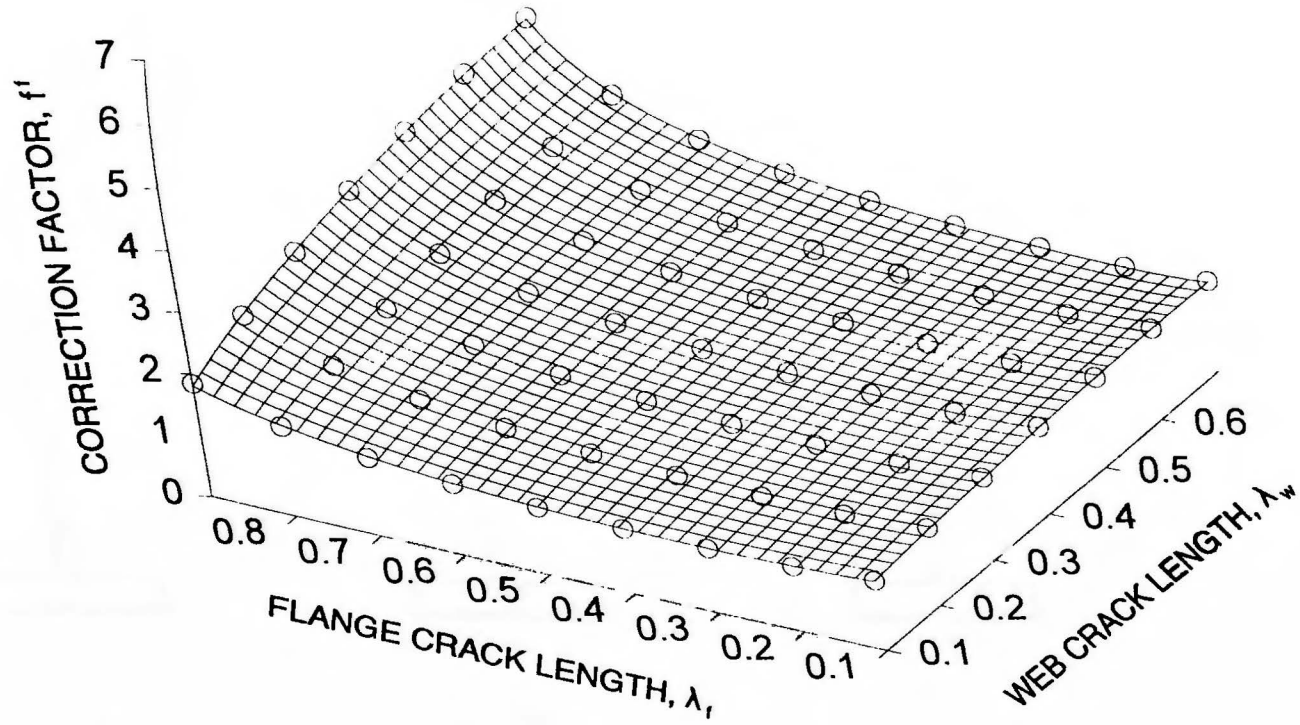

Figure 6.59. Comparison of predicted and calculated correction factors for three-tip cracked I-beam under bending; W18 x 9 7, flange crack tip.

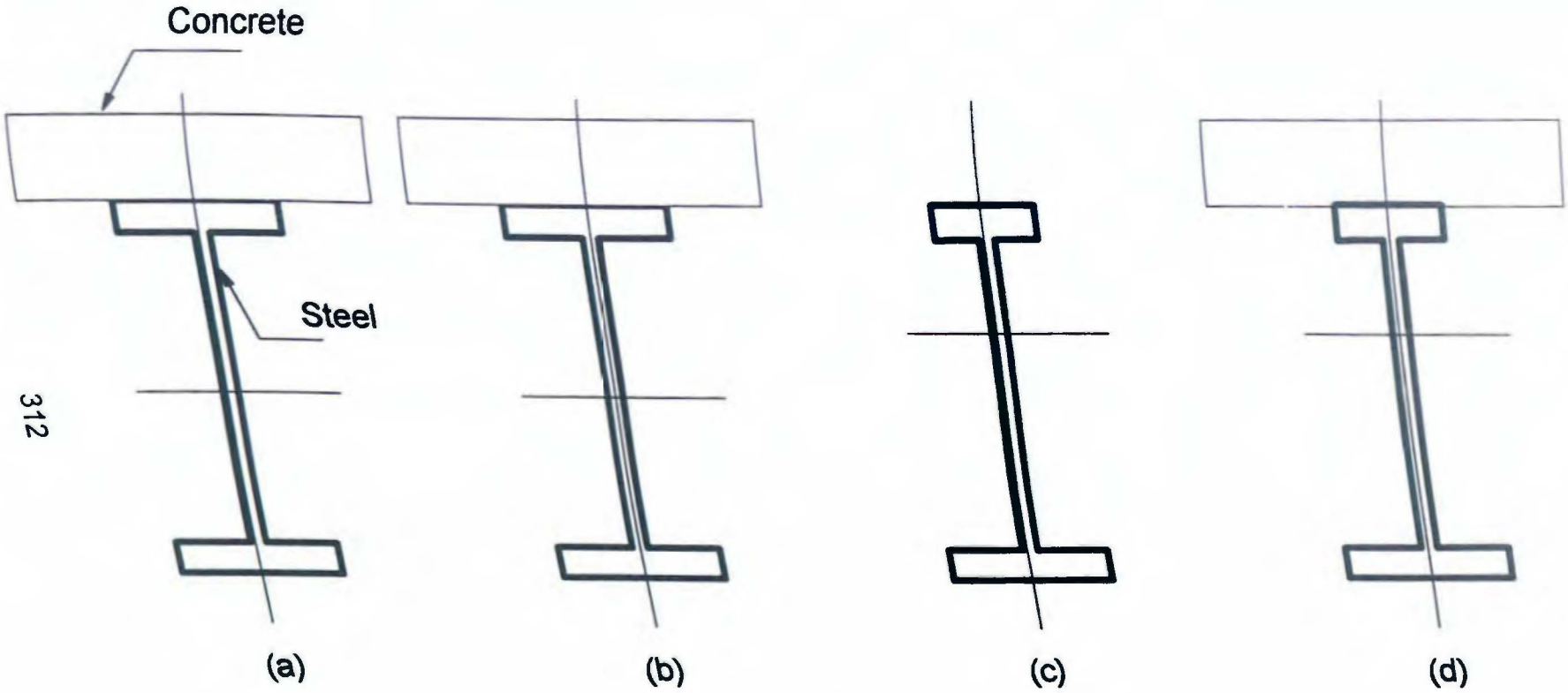

Figure 6.60. (a) Composite rolled beam; (b) composite plate girder with doubly symmetric section; (c) noncomposite singly symmetric section; (d) composite plate girder with singly symmetric section.

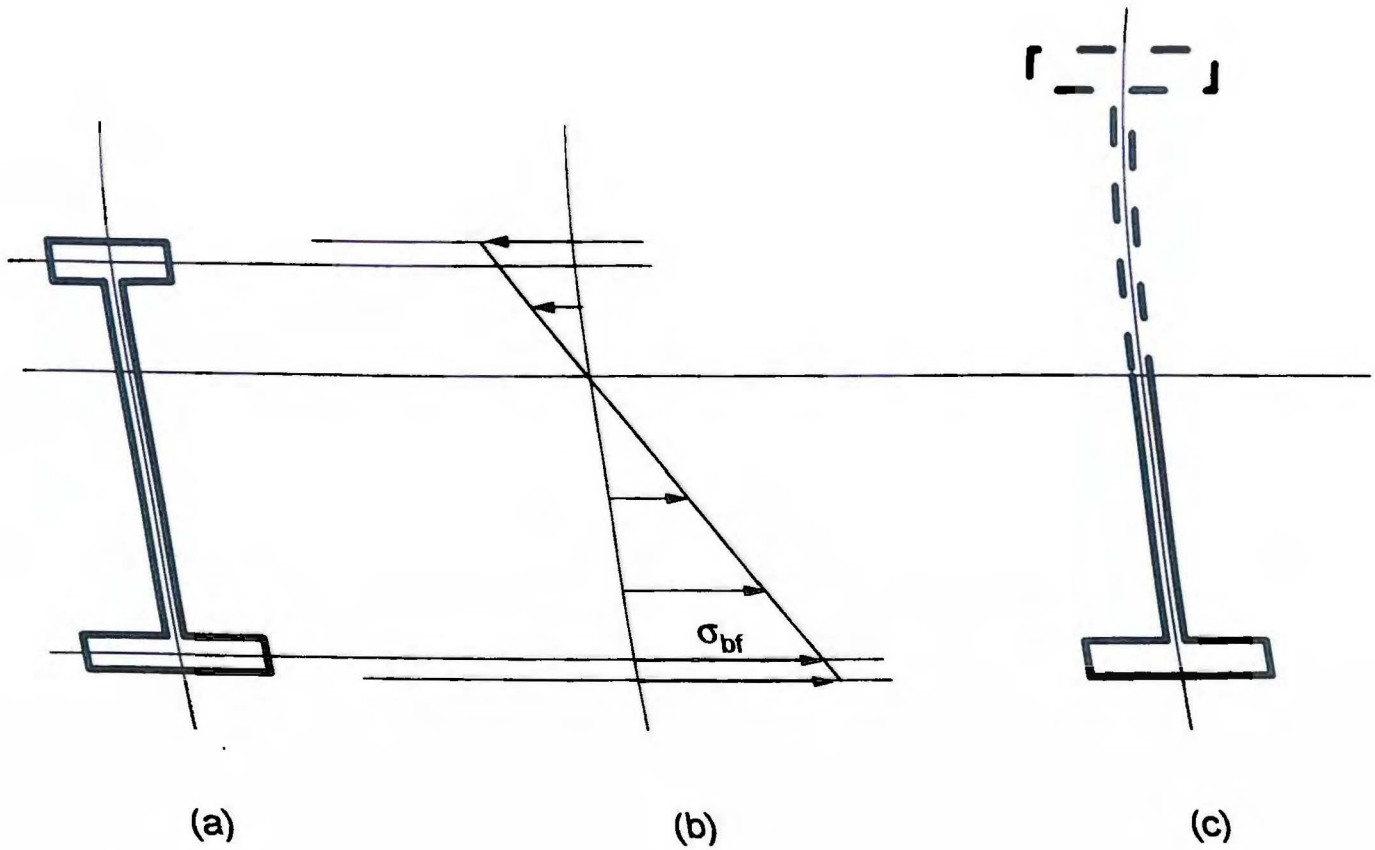

Figure 6.61. (a) Noncomposite singly symmetric section; (b) stress distribution; and (c) equivalent doubly symmetric section.

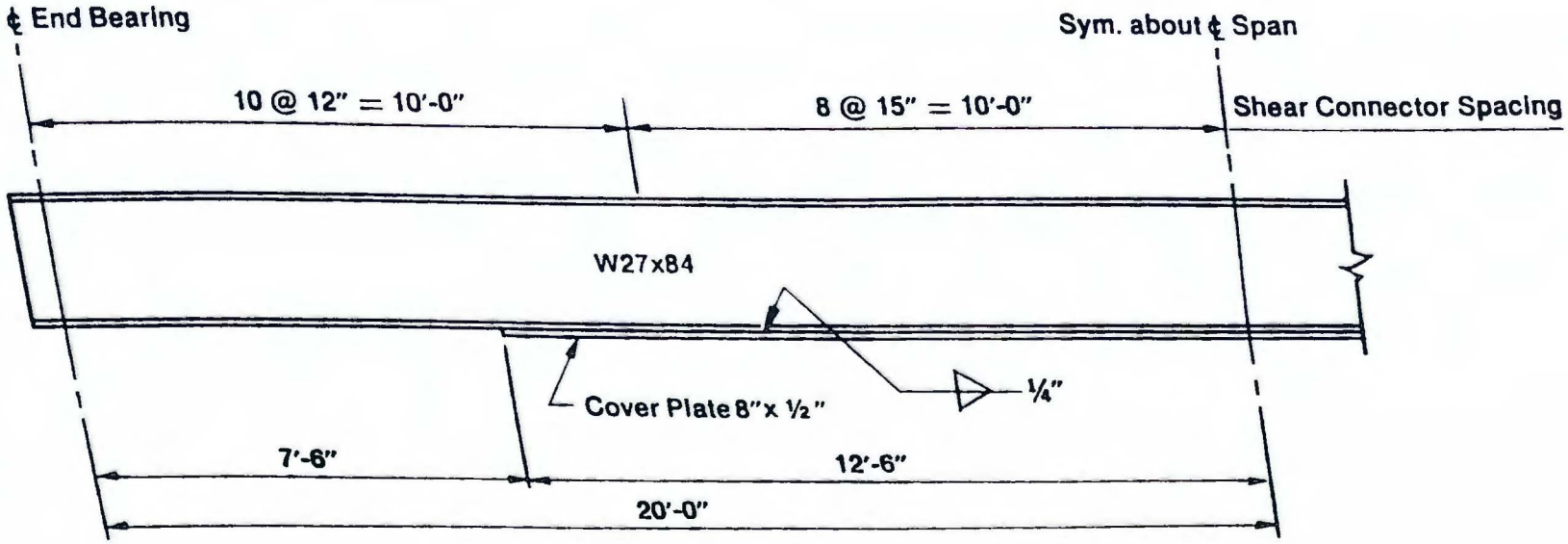

Figure 6.62. Composite, simple supported, rolled beam.

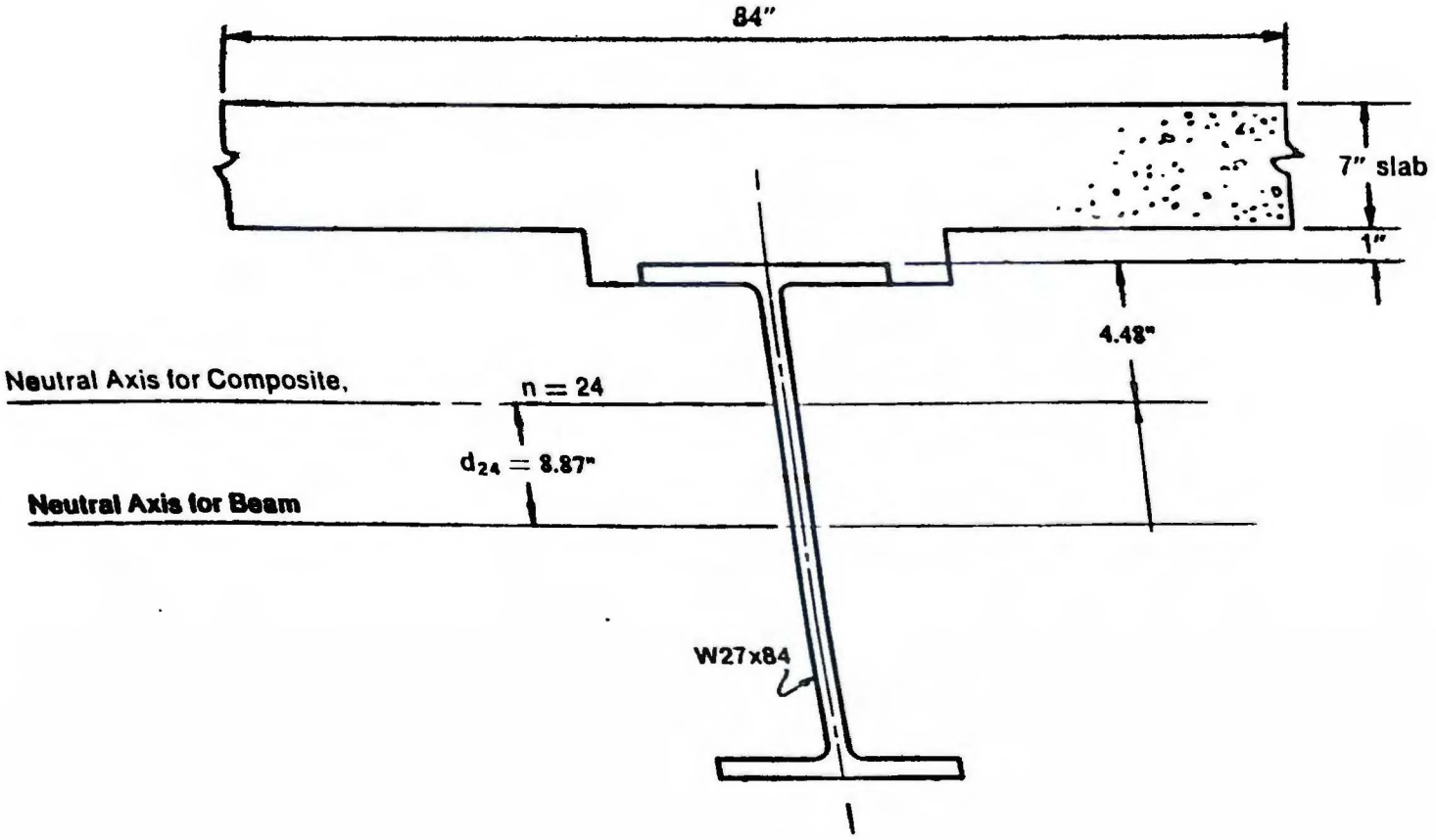

Figure 6.63. Composite section.

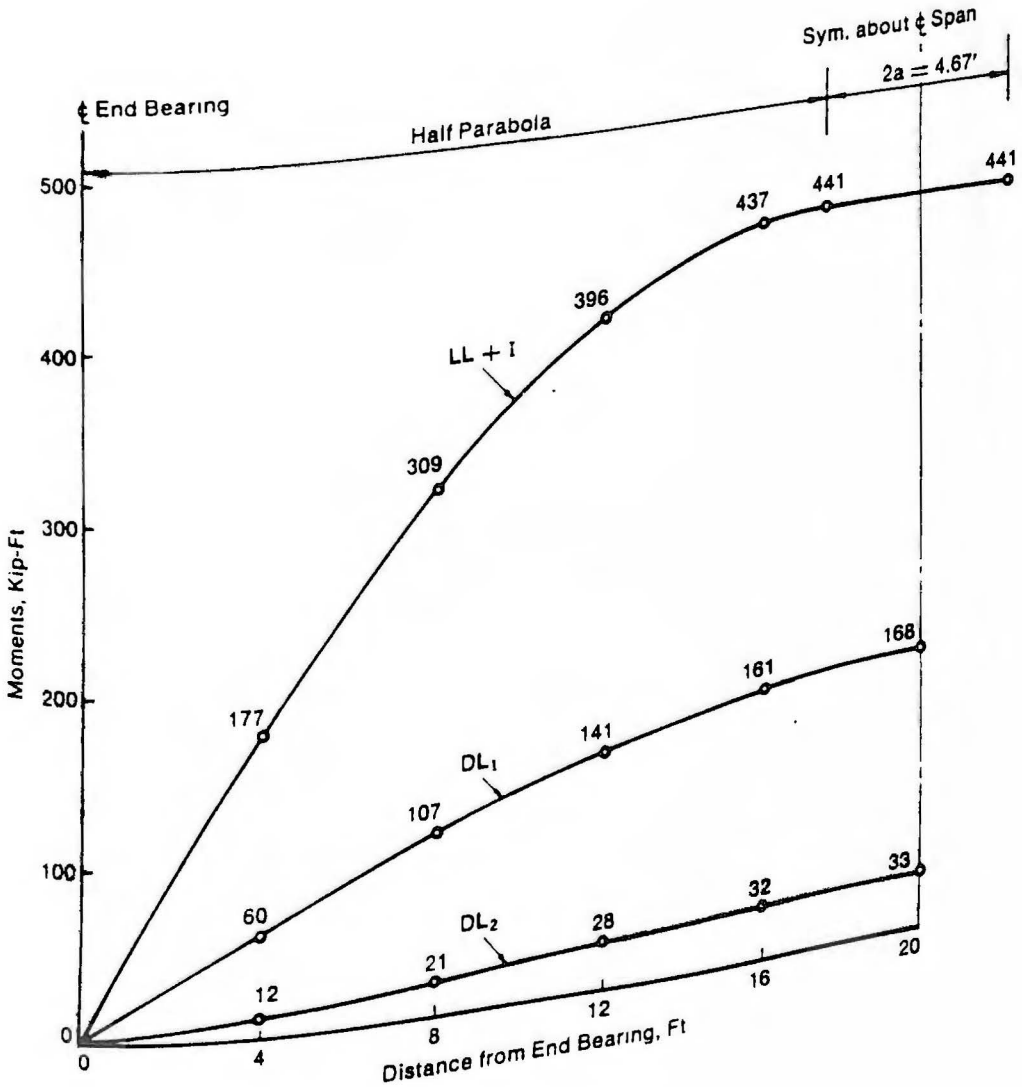

Figure 6.64. Bending moment diagrams.

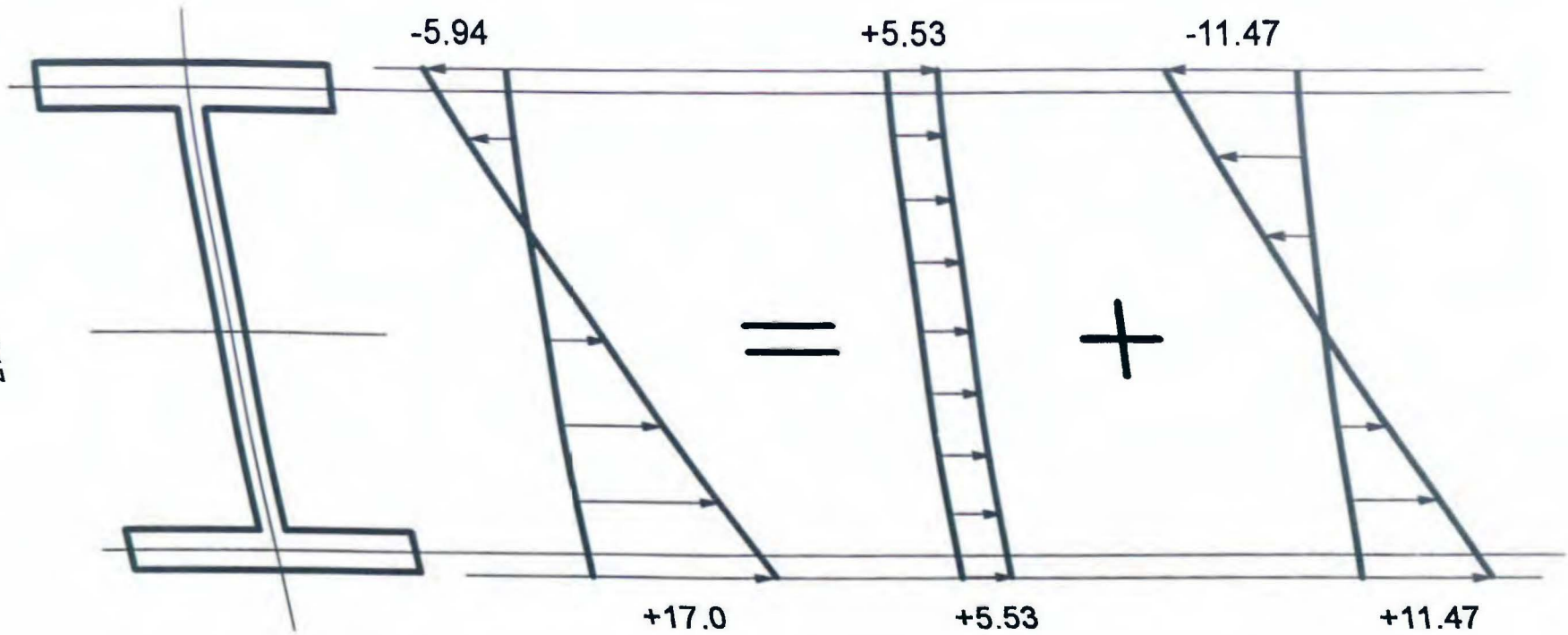

Figure 6.65. Decomposition of linearly distributed loading into axial tension and pure bending.

Note: All dimensions are in mm.

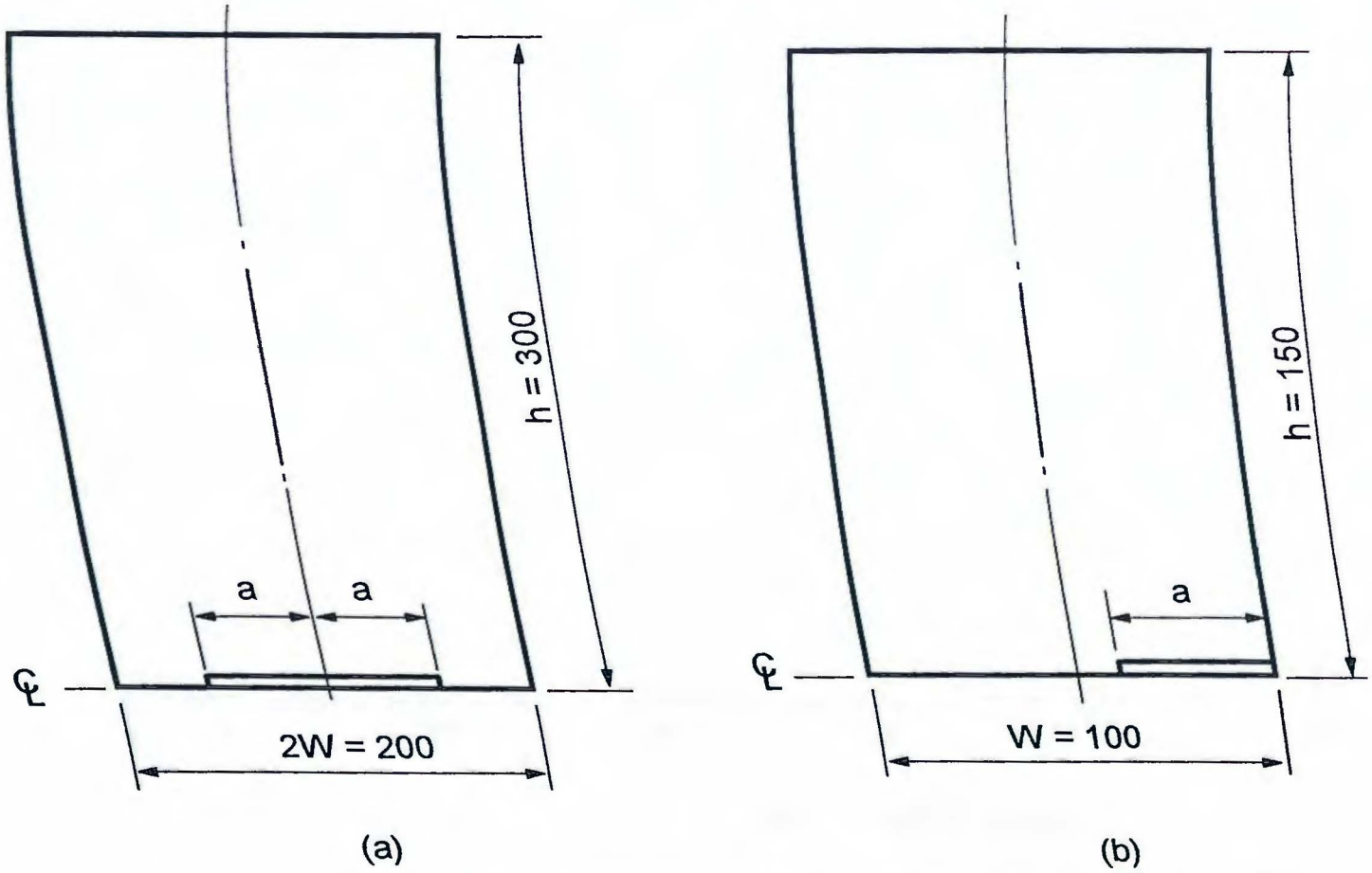

(a) (b)

Figure A.1. (a) Center-cracked plate; (b) edge-cracked plate.

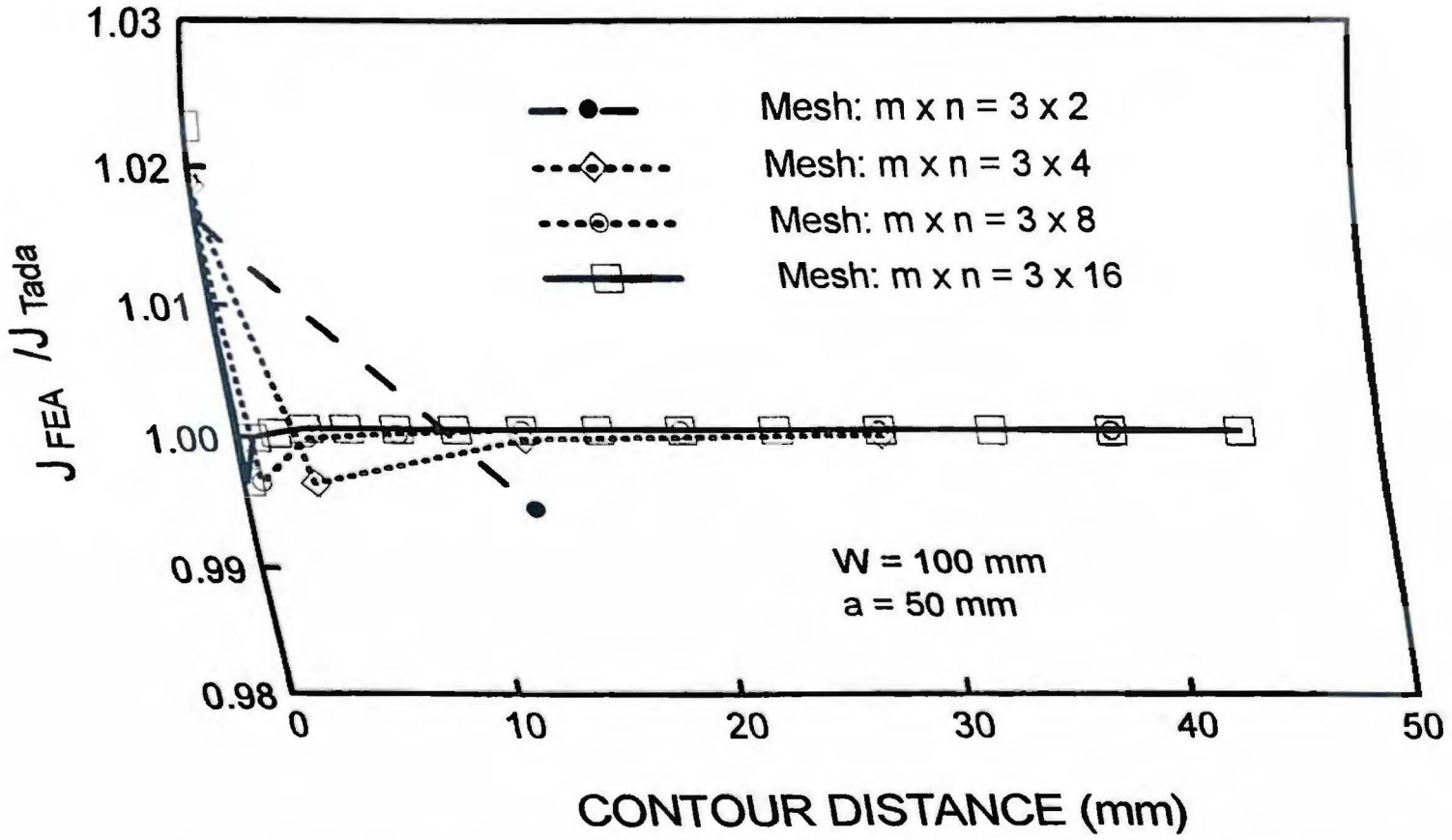

Figure A.2. J-integral versus contour distance from crack tip within inner region for center-cracked plate under tension; a/W = 0.5.

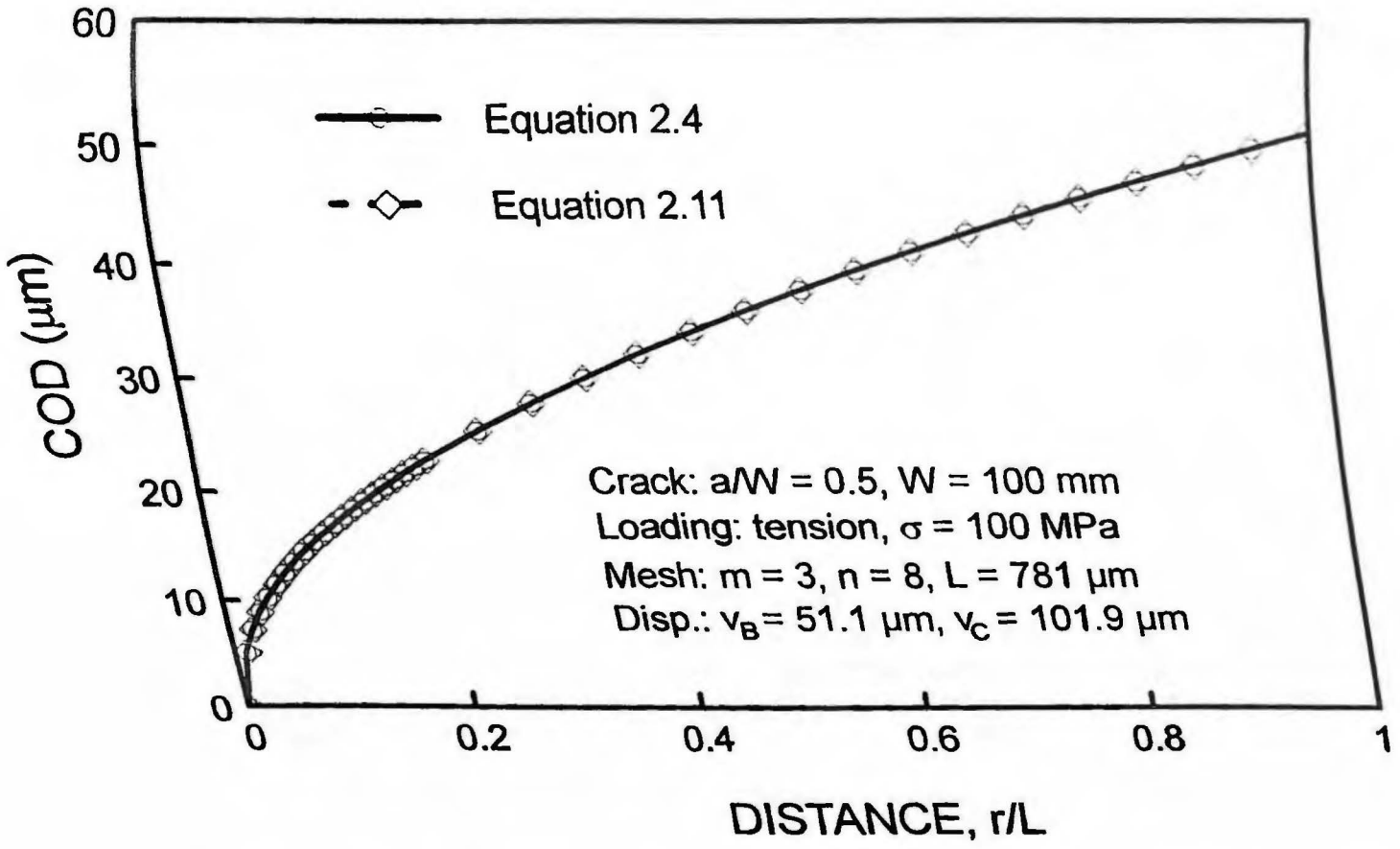

Figure A.3. COD profiles within crack tip element for center-cracked plate under tension, a/W = 0.5.

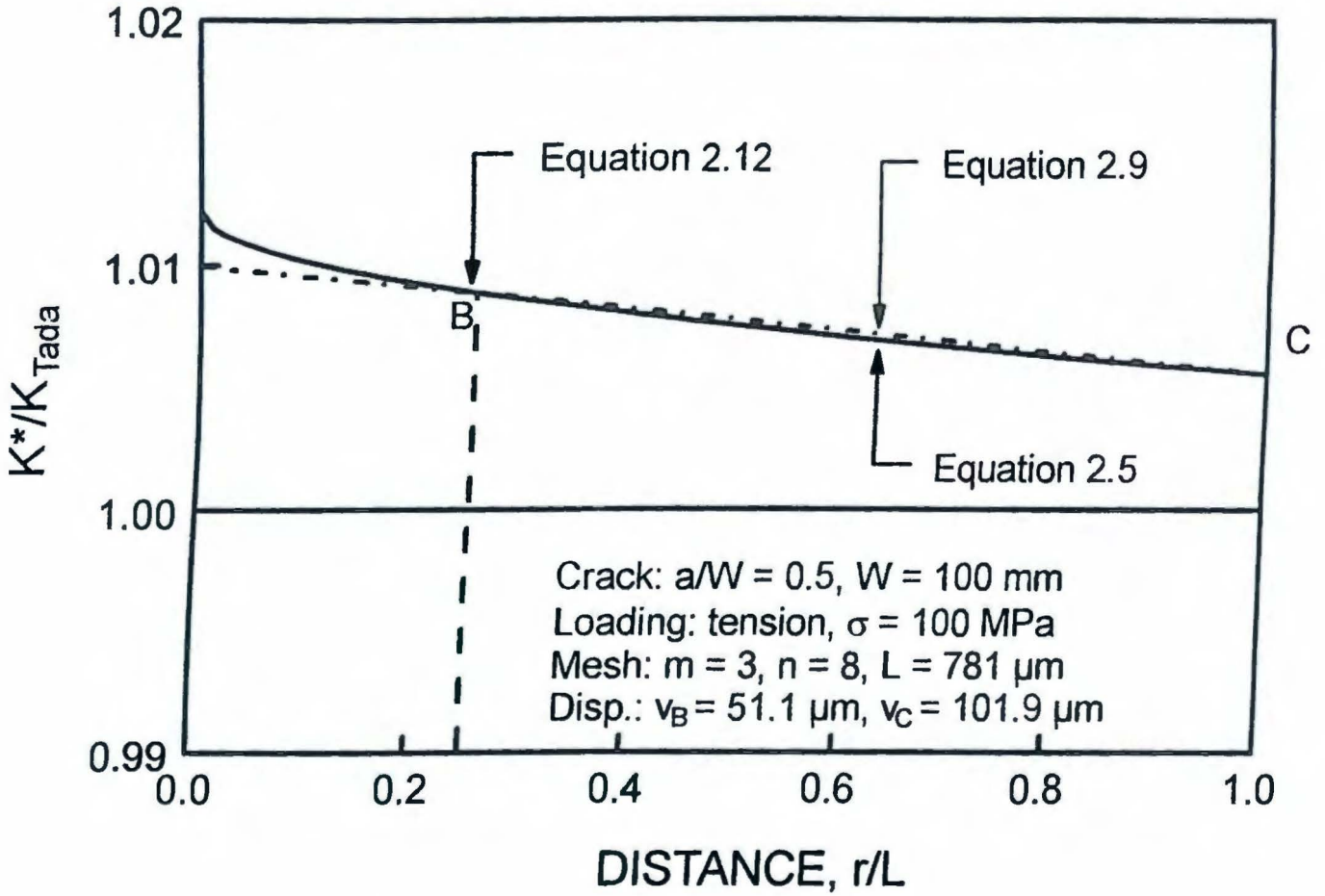

Figure A.4. Normalized apparent SIF within crack tip element for center-cracked plate under tension; a/W = 0.5.

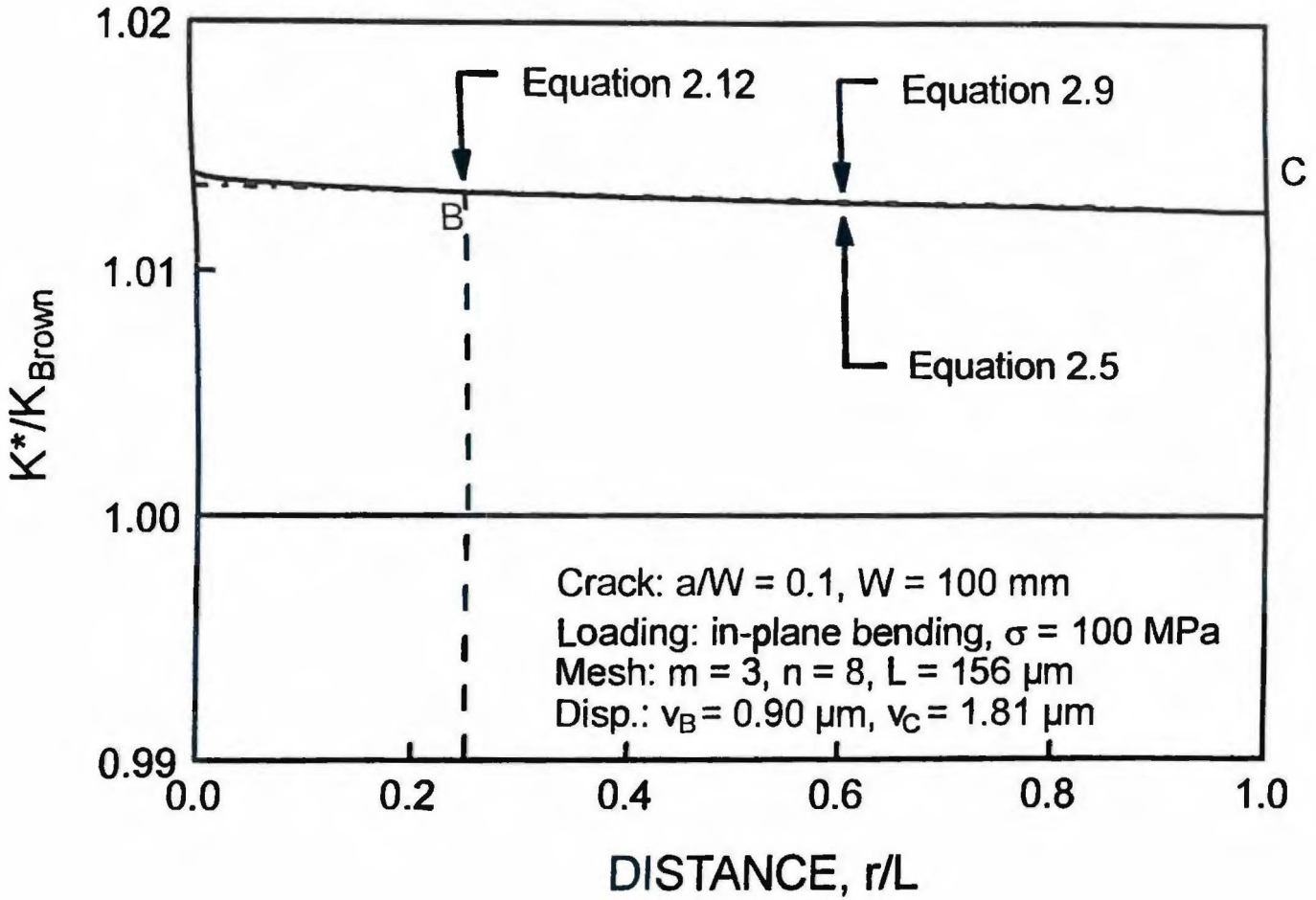

Figure A.5. Normalized apparent SIF within crack tip element for edge-cracked plate under bending; a/W = 0.1.

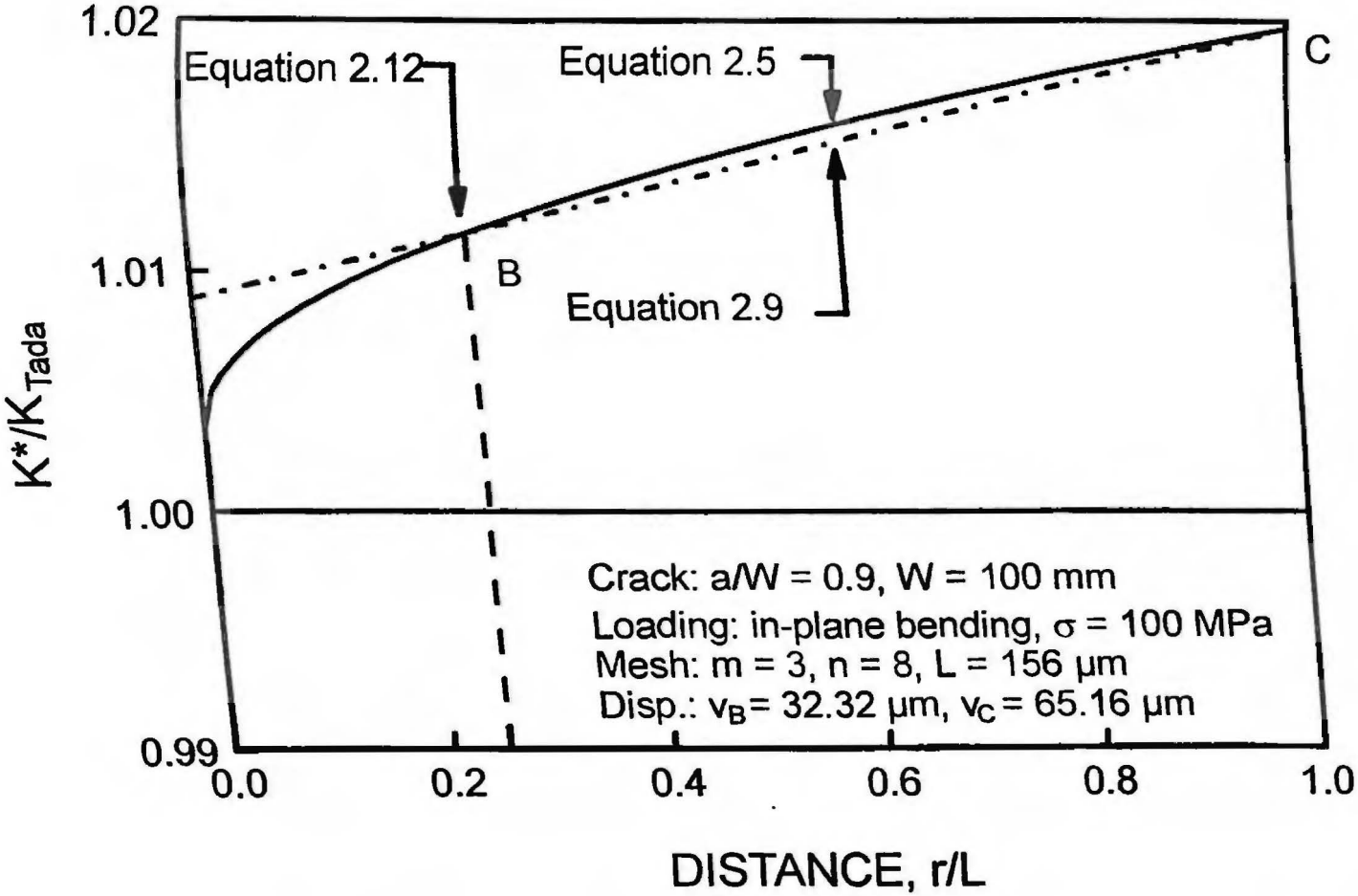

Figure A.6. Normalized apparent SIF within crack tip element for edge-cracked plate under bending; a/W = 0.9.

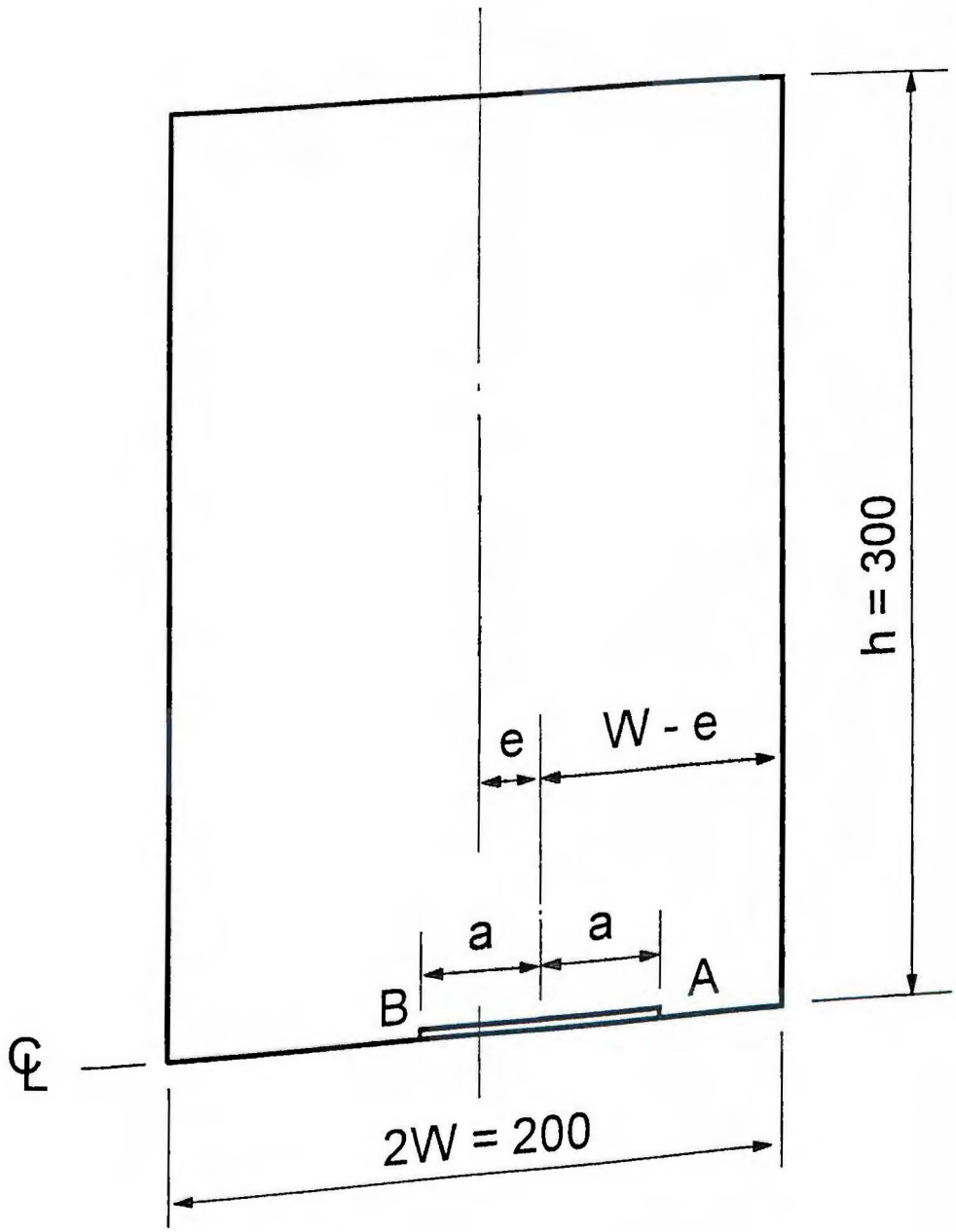

Note: All dimensions in mm

Figure A.7. Plate with eccentric crack.

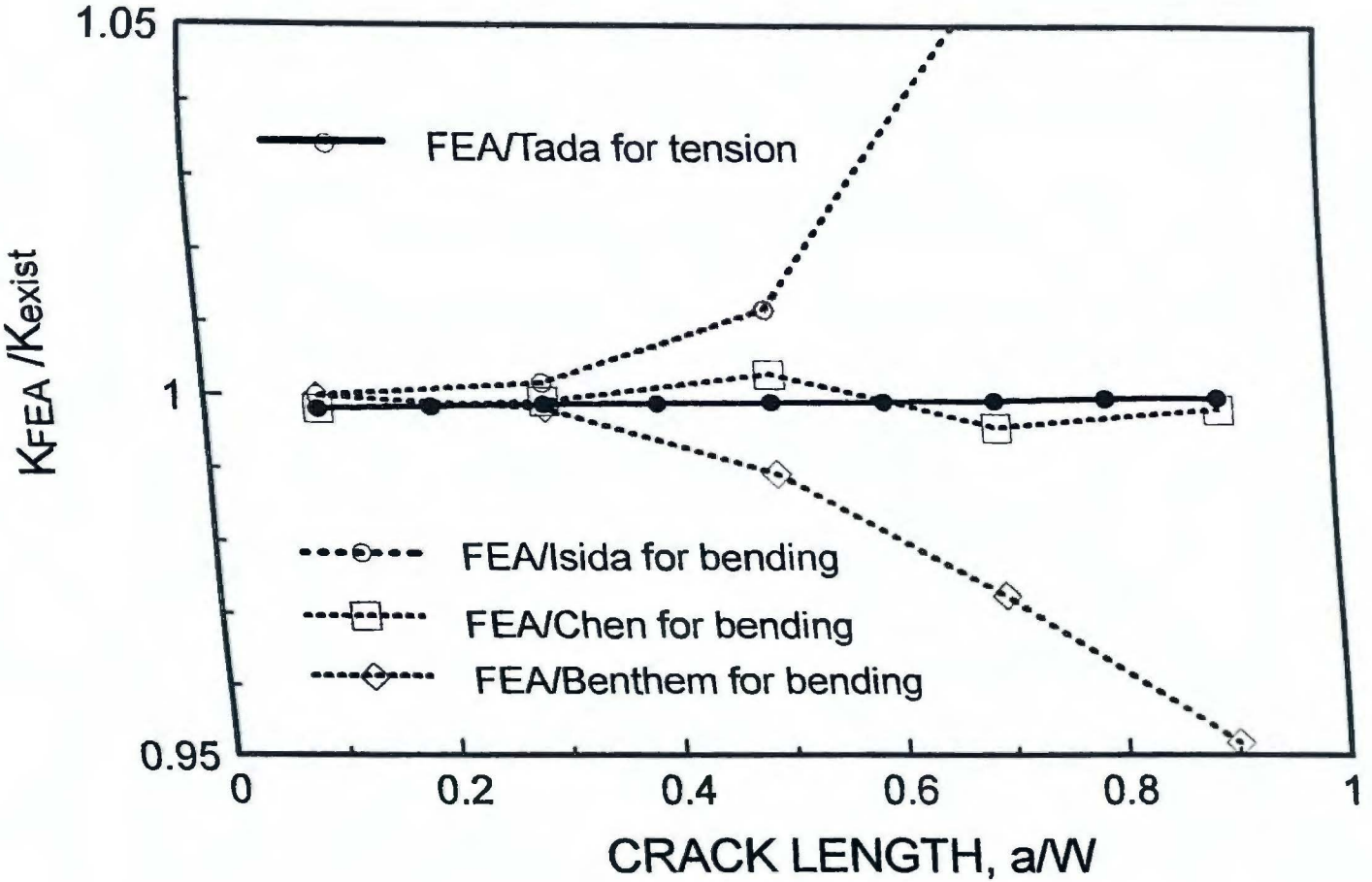

Figure A.8. Comparison of FEA and existing solutions for center-cracked plate under tension or bending.

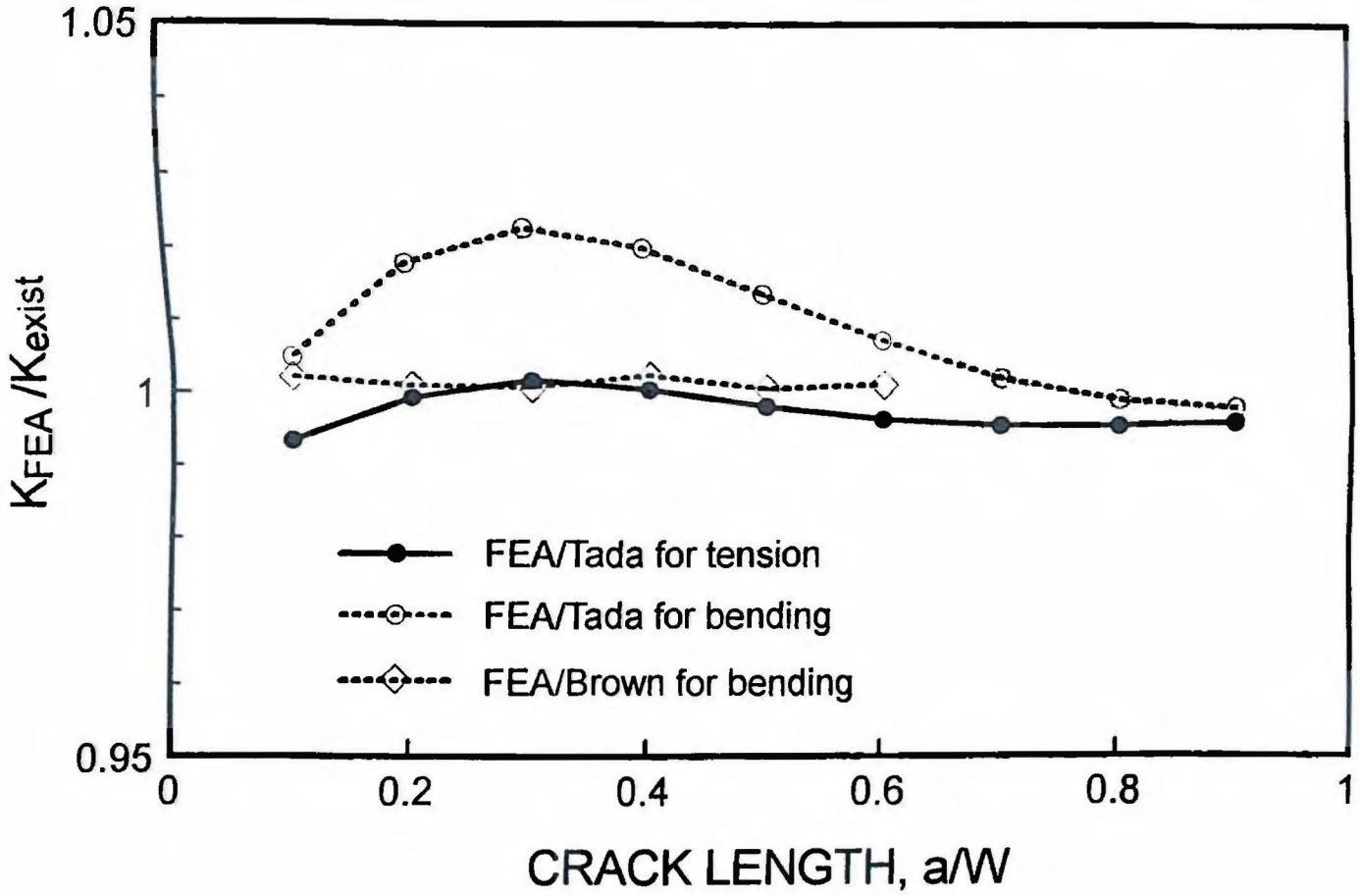

Figure A.9. Comparison of FEA and existing solutions for edge-cracked plate under tension or bending.

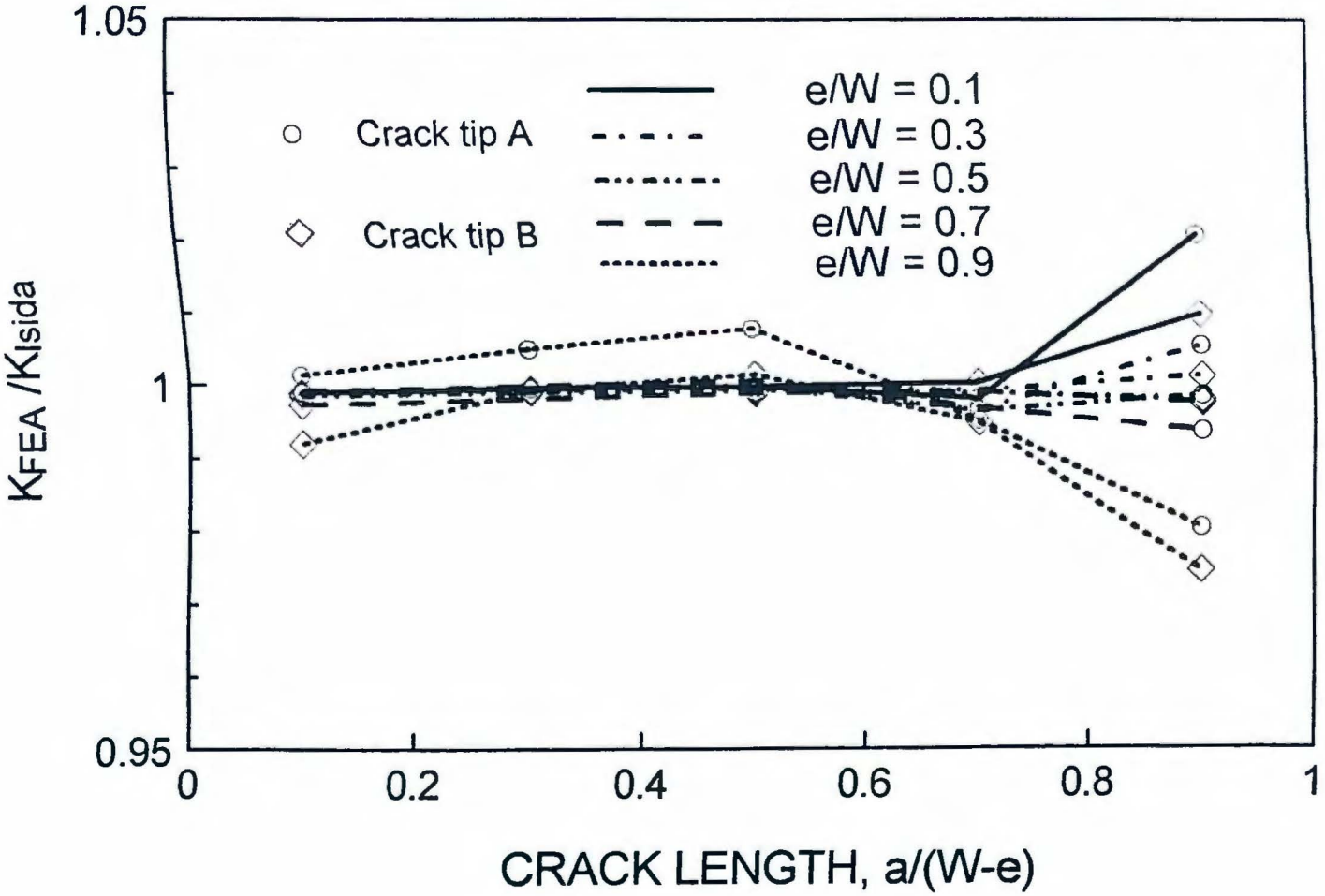

Figure A.10. Comparison of FEA and Isida's solution (1965) for plate with eccentric crack under tension.

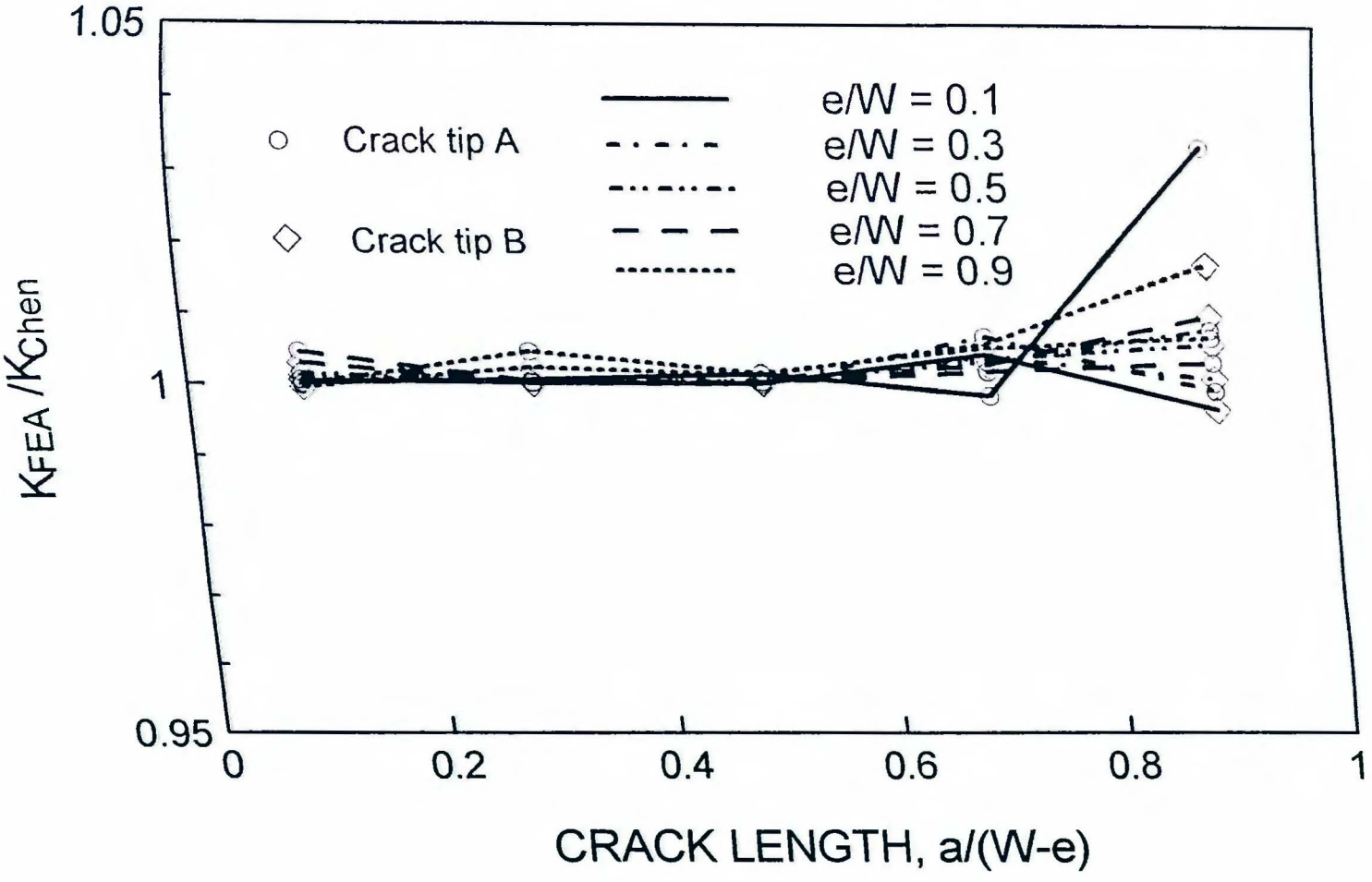

Figure A.11. Comparison of FEA and Chen and Albrecht's (1994) solution for plate with eccentric crack under bending.

REFERENCE

ABAQUS/Standard User's Manual, (1993). Version 5.3, Hibbitt, Karlsson & Sorensen, Inc., Rhode Island.

Aliabadi, M. H., and Rooke, D. P. (1991). *Numerical Fracture Mechanics*. Kluwer Academic Publishers.

Banks-Sills, L., and Sherman, D. (1992). "On the Computation of Stress Intensity Factors for Three-Dimensional Geometries by Means of the Stiffness Derivative and J-integral Methods." *International Journal of Fracture*, Vol. 53, pp. 1-20.

Barsoum, R. S. (1974). "Application of Quadratic Isoparametric Finite Elements in Linear Fracture Mechanics." *International Journal of Fracture*, Vol. 10, pp. 603-605.

Barsoum, R. S. (1976). "On the Use of Isoparametric Finite Elements in Linear Fracture Mechanics." *International Journal of Numerical Methods in Engineering*, Vol.10, pp. 25-37.

Benthem, J. P., and Koiter, W. T. (1972). "Asymptotic Approximations to Crack Problems." *Method of Analysis and Solutions of Crack Problems, Mechanics of Fracture 1*, by G. C. Sih, Noordhoff International Publishing, Leiden.

Bowie, O. L., and Freese, C. E. (1976). "On the 'Overlapping' Problem in Crack Analysis." *Engineering Fracture Mechanics*, Vol. 8, pp. 373-379.

Brown, W. F., and Srawley, J. E. (1966). "Plane Strain Crack Toughness Testing of High Strength Metallic Materials." American Society for Testing and Materials, ASTM STP 410.

Bueckner, H. F. (1970). "A Novel Principle for the Computation of Stress Intensity Factors." Zeitschrift der Angewandten Mathematik und Mechanik, Vol. 50, pp. 529-545.

Cartwright, D. J., and Miller, M. (1975). "Stress Intensity Factors for a Crack in a Sheet with a Partially Debonded Stiffener." *International Journal of Fracture*, Vol. 11, pp. 925-932.

Chan, S. K., Tuba, I. S., and Wilson, W. K. (1970). "On the Finite Element Methods in Linear Fracture Mechanics." *Engineering Fracture Mechanics*, Vol. 2, pp. 1-17.

Chen, L. S., and Kuang, J. H. (1992). "A Modified Linear Extrapolation Formula for Determination of Stress Intensity Factors." *International Journal of Fracture*, Vol. 54, R3-R8.

Chen, X. G. (1992). "Application of Fracture Mechanics to Highway Bridges." Ph.D. Dissertation, Department of Civil Engineering, University of Maryland, College Park, MD.

Chen, X. G., and Albrecht, P. (1994). "Weight Functions for Eccentric Cracks." *Fracture Mechanics: Twenty-Fourth Volume*, ASTM STP 1207, American Society for Testing and Materials, Philadelphia, pp. 581-614

Fisher, J. W., Frank, K. H., Hirt, M. A., and McNamee, B. M. (1970). "Effect of Weldments on the Fatigue Strength of Steel Beams." *NCHRP Report* 102, Transportation Research Board, Washington, D. C.

Fisher, J. W., Albrecht, P., Yen, B. T., Klingerman, D. J., and McNamee, B. M. (1974). "Fatigue Strength of Steel Beams with Welded Stiffeners and Attachments." *NCHRP Report* 147, Transportation Research Board, Washington, D. C..

Freese, C. E., and Tracy, D. M. (1976). " The Natural Isoparametric Triangular Verse Collapsed Quadrilateral for Elastic Crack Analysis." Vol. 12, pp. 768-770.

Greif, R., and Sanders, J. L. (1965). "The Effect of a Stringer on the Stress in a Cracked Sheet." *Journal of Applied Mechanics*, pp. 59-66.

Henshell, R. D., and Shaw, K. G. (1975). "Crack Tip Finite Elements Are Unnecessary." *Journal of Numerical Methods in Engineering*. Vol. 9, pp. 495-509.

Irwin, G. R. (1957). "Analysis of Stresses and Strains Near the End of a Crack Traversing a Plate." *Journal of Applied Mechanics*, Transactions, American Society of Mechanical Engineers, Vol. 24, pp. 361-364.

Isida, M. (1956). "On the In-plane Bending of a strip with a Central Elliptical Hole." Transactions, Japanese Society for Mechanical Engineers, Vol. 22, pp. 809-812.

Isida, M. (1965). "Stress Intensity Factors for the Tension of an Eccentrically Cracked Strip." *Journal of Applied Mechanics*, Vol. 33, pp. 674-675.

Isida, M. (1973a). "Method of Laurent Series Expansion for Internal Crack Problems." *Method of Analysis and Solutions of Crack Problems, Mechanics of Fracture 1*, by G. C. Sih, Noordhoff International Publishing, Leiden.

Isida, M. A. (1973). "Analysis of Stress Intensity Factors for the Tension of a Centrally Cracked Strip with Stiffened Edges." *Engineering Fracture Mechanics*, Vol. 5, pp. 647-665.

Lim, I. L., Johnston, I. W., and Choi, S. K. (1992). " Comparison Between Various Displacement-Based Stress Intensity Factor Computation Techniques." *International Journal of Fracture*, Vol. 58, pp. 193-210.

Manual of Steel Construction. (1986). Load & Resistance Factor Design, American Institute of steel Construction, Chicago, Illinois.

Murakami, H. (1986). *Stress Intensity Factor Handbook*. Pergamon.

Nishimura, T. (1991). "Stress Intensity Factors for a Cracked Stiffened Sheet with Cracked Stiffeners." *Journal of Applied Mechanics*, Vol. 113, pp. 219-224.

Parks, D. M. (1974). "A stiffness Derivative Finite Element Technique for Determination of Crack Tip Stress Intensity Factors." *International Journal of Fracture*, Vol. 10, No. 4, pp. 487-502.

Pang, H. L. J. (1993). "Linear Elastic Fracture Mechanics Benchmarks: 2D Finite Element Test Cases." *Engineering Fracture Mechanics*, Vol. 44, No. 5, pp. 741-751.

Paris, P. C. (1957). "The Mechanics of Fracture Propagation and Solutions to Fracture Arrester Problems." Document D2-2195, The Boeing Company.

Petroski, H. J., and Achenbach, J. D. (1978). "Computation of Weight Function from a Stress Intensity Factor." *Engineering Fracture Mechanics*, Vol. 10, pp. 257-266.

Rice, J. R. (1968). "A Path Independent Integral and the Approximate Analysis of Strain Concentration by Notches and Cracks." *Journal of Applied Mechanics*, Transactions, American Society of Mechanical Engineers, Vol. 35, pp. 379-386.

Rice, J. R. (1972). "Some Remarks on Elastic Crack-tip Stress Fields." *International Journal of Solid and Structure*, Vol. 8, pp. 751-758.

Rooke, D. P., and Cartwright, D. J. (1976). *Compendium of Stress Intensity Factors*. HMSO, London, England.

Saouma, V. E., and Schwemmer, D. (1984). "Numerical Evaluation of the Quarter-point Crack Tip Element." *Journal of Numerical Methods in Engineering*, Vol. 20, pp. 1629-1641.

Shih, C. F., DeLorenzi, H. G., and German, M. D. (1976). "Crack Extension Modeling with Singular Quadratic Isoparametric Elements." *International Journal of Fracture*, Vol. 12, pp. 647-651.

SigmaPlot for Windows User's Manual. (1994). Jandel Scientific Software, U. S. A.

Sih, G. C. (1973). *Handbook of Stress Intensity Factors*. Lehigh University, Bethlehem, Pennsylvania.

TableCurve3D for Windows User's Manual. (1993). AISN Software, Jandel Scientific Software, U. S. A.

Tada, H., Paris, P., and Irwin, G. R. (1973). *The Stress Analysis of Cracks Handbook*. Del Research Corporation, Hellertown, Pennsylvania.

Tracey, D. M. (1977). "Discussion of 'On the Use of Isoparametric Finite Element in Linear Fracture Mechanics,' by R. S. Barsoum." *International Journal of Numerical Methods in Engineering*, Vol. 11, pp. 401-402.

Woo, C. W., Cheung, Y. K., Chen, Y. Z., and Wang, Y. H. (1988). "A Simple Model for the Contact Problem of a Finite Cracked Plate in Bending." *Engineering Fracture Mechanics*, Vol. 29, No. 2, pp. 227-231.

Wu, X. R., and Carlsson, J. (1983). "The Generalized Weight Function Method for Crack Problems with Mixed Boundary Conditions." *Journal of the Mechanics and Physics of Solids*, Vol. 31, pp. 485-497.

Wu, X. R. (1984). "Approximate Weight Functions for Center and Edge Cracks in Finite Bodies." *Engineering Fracture Mechanics*, Vol. 20, pp. 35-49.

Yehia, N. A. B., and Shephard, M. S. (1985). "On the Effect of Quarter-point Element Size on Fracture Criteria." *International Journal of Numerical Methods in Engineering*, Vol. 21, pp. 1911-1924.